Finite-temperature transport in one-dimensional quantum lattice models

B. Bertini

Department of Physics, Faculty of Mathematics and Physics, University of Ljubljana, Ljubljana SI-1000, Slovenia

F. Heidrich-Meisner

Institute for Theoretical Physics, Georg-August-Universität Göttingen, D-37077 Göttingen, Germany

C. Karrasch

Institut für Mathematische Physik, Technische Universität Braunschweig, Mendelssohnstraße 3, D-38106 Braunschweig, Germany

T. Prosen

Department of Physics, Faculty of Mathematics and Physics, University of Ljubljana, Ljubljana SI-1000, Slovenia

R. Steinigeweg

Department of Physics, University of Osnabrück, D-49076 Osnabrück, Germany

M. Žnidarič

Department of Physics, Faculty of Mathematics and Physics, University of Ljubljana, Ljubljana SI-1000, Slovenia

(published 5 May 2021)

Over the last decade impressive progress has been made in the theoretical understanding of transport properties of clean, one-dimensional quantum lattice systems. Many physically relevant models in one dimension are Bethe-ansatz integrable, including the anisotropic spin-$1/2$ Heisenberg (also called the spin-$1/2$ XXZ chain) and the Fermi-Hubbard model. Nevertheless, practical computations of correlation functions and transport coefficients pose hard problems from both the conceptual and technical points of view. Only because of recent progress in the theory of integrable systems, on the one hand, and the development of numerical methods, on the other hand, has it become possible to compute their finite-temperature and nonequilibrium transport properties quantitatively. Owing to the discovery of a novel class of quasilocal conserved quantities, there is now a qualitative understanding of the origin of ballistic finite-temperature transport, and even diffusive or superdiffusive subleading corrections, in integrable lattice models. The current understanding of transport in one-dimensional lattice models, in particular, in the paradigmatic example of the spin-$1/2$ XXZ and Fermi-Hubbard models, is reviewed, as well as state-of-the-art theoretical methods, including both analytical and computational approaches. Among other novel techniques, matrix-product-state-based simulation methods, dynamical typicality, and, in particular, generalized hydrodynamics are covered. The close and fruitful connection between theoretical models and recent experiments is discussed, with examples given from the realms of both quantum magnets and ultracold quantum gases in optical lattices.

DOI: 10.1103/RevModPhys.93.025003

CONTENTS

I. INTRODUCTION

The physics of strongly correlated quantum systems in one dimension has long attracted the interest of theoreticians (Giamarchi, 2004; Schönhammer, 2004; Cazalilla *et al.*, 2011; Guan, Batchelor, and Lee, 2013) because of its intriguing properties. For instance, quantum fluctuations can have a particularly pronounced effect in one dimension, leading to the absence of finite-temperature phase transitions and to the breakdown of Landau's Fermi liquid theory, rendering one dimension unique in many regards. A particularly appealing aspect of many-body physics in one dimension is the existence of exact solutions for a subset of microscopic models, including both systems in the continuum such as the Gaudin-Yang model (Gaudin, 1967; Yang, 1967) and the Lieb-Liniger gas (Lieb and Liniger, 1963) and lattice models such as the spin-1/2 *XXZ* and the Fermi-Hubbard chain. For the aforementioned models, versions of the Bethe ansatz are exploited in order to arrive at such solutions, and these are considered instances of integrable quantum models.[1]

Because of the wide range of available theoretical approaches, there is the appealing ambition of developing a full theoretical understanding of these systems, both quantitative and qualitative. Moreover, many quasi-one-dimensional (quasi-1D) materials from quantum magnetism, are, to a good approximation, described by relatives of the integrable spin-1/2 Heisenberg or the Fermi-Hubbard chain. Ultracold quantum gases (Bloch, Dalibard, and Zwerger, 2008) provide another avenue for the experimental study of 1D systems, ranging from degenerate quantum gases in the continuum [see Kinoshita, Wenger, and Weiss (2004, 2006), Paredes *et al.* (2004), Hofferberth *et al.* (2007), Liao *et al.* (2010), and Langen *et al.* (2015)] to fermionic or bosonic lattice gases [see Cheneau *et al.* (2012), Ronzheimer *et al.* (2013), Xia *et al.* (2015), Kaufman *et al.* (2016), Salomon *et al.* (2019), and Vijayan *et al.* (2020)], including realizations of Heisenberg Hamiltonians (Fukuhara *et al.*, 2013; Fukuhara, Schauß *et al.*, 2013; Hild *et al.*, 2014). A renewed interest in 1D systems originates from the fields of nonequilibrium dynamics in closed quantum systems [for reviews, see Polkovnikov *et al.* (2011), Eisert, Friesdorf, and Gogolin (2015), Calabrese, Essler, and Mussardo (2016), D'Alessio *et al.* (2016), and Gogolin and Eisert (2016)] and many-body localization [for reviews, see Altman and Vosk (2015), Nandkishore and Huse (2015), and Abanin *et al.* (2019)], where 1D systems are the playground and testing ground for new concepts, novel phase transitions, or far-from-equilibrium dynamics. Because of the integrability of some 1D systems, one can systematically study the transition between integrability and quantum-chaotic behavior; see D'Alessio *et al.* (2016), Essler and Fagotti (2016), and Vidmar and Rigol (2016) and references therein.

One of the most generic nonequilibrium situations is steady-state transport. This concept has a rich history. It was Joseph Fourier who in 1807 presented his manuscript to the French Academy describing heat transport in terms of the diffusion equation (Fourier, 1822). The work was groundbreaking in several ways (Narasimhan, 1999). Prior to its publication, physicists were trying to understand heat conduction in terms of the complicated motion of the constituent particles, but Fourier changed that mindset by suggesting

[1]The notion of integrability in quantum systems is commented upon later.

an effective continuum description in terms of a partial differential equation. Fourier's law (or its extensions to other conserved quantities such as Fick's law and Ohm's law) states that the energy current $j^{(E)}$ is proportional to the temperature difference and to the inverse of the system's length[2] L. Empirically, it holds in real materials. However, the microscopic origin of such normal, i.e., diffusive, transport is even today not entirely understood. Particularly in low-dimensional systems, one often finds that simple Hamiltonian systems do not obey Fourier's law: instead, transport is anomalous with a nontrivial power-law scaling of the current $j^{(E)} \sim 1/L^{\gamma}$ with $\gamma \neq 1$. Understanding under which conditions one gets normal transport is one of the main challenges of theoretical physics (Bonetto, Lebowitz, and Rey-Bellet, 2000; Buchanan, 2005).

In classical systems, this question has been studied since Fermi, Pasta, Ulam, and Tsingou's work on equilibration in anharmonic chains (Fermi, Pasta, and Ulam, 1955; Dauxois, 2008), which eventually led to the birth of the theory of classical Hamiltonian chaos. One would naively expect integrable systems to be ballistic conductors, i.e., that they would exhibit a zero bulk resistivity, while chaotic ones should display diffusion; this is rooted in the existence of extra conservation laws, which may prevent currents from decaying. Such a distinction, however, is not as clear cut as one might think. While no rigorous conclusions have been reached yet [for reviews, see Lepri, Livi, and Politi (2003), Dhar (2008), and Benenti, Lepri, and Livi (2020)], explicit examples demonstrate that even systems without classical chaos can display a wide spectrum of transport types.

In the quantum domain, the situation is even more interesting. There has been significant progress in recent years in the understanding of transport in 1D quantum lattice systems, thanks to both analytical and numerical work. Because of the large number of studies since the latest overview articles appeared (Zotos, 2002; Zotos and Prelovšek, 2004; Zotos, 2005; Heidrich-Meisner, Honecker, and Brenig, 2007), there is the need for a comprehensive survey of the state of the art of this field. The aim of this review is to give an overview over the transport properties of 1D quantum lattice models at finite temperatures, to describe the established results, to identify open questions, and to point out future directions. Specifically, we are interested in lattice systems in the thermodynamic limit, including examples of integrable and nonintegrable cases.

We stress that the field was driven not only by theoretical questions but also (equally importantly) by experiments on quantum magnets (Hess, 2007, 2019; Sologubenko, Lorenz *et al.*, 2007), which show that low-dimensional quantum magnets typically feature significant contributions from magnetic excitations to the thermal conductivity. Moreover, experiments with ultracold atomic gases in optical lattices can investigate transport properties as well (Schneider *et al.*, 2012; Ronzheimer *et al.*, 2013; Hild *et al.*, 2014; Xia *et al.*, 2015; Scherg *et al.*, 2018; Brown *et al.*, 2019; Nichols *et al.*, 2019; Schemmer *et al.*, 2019; Guardado-Sanchez *et al.*, 2020; Jepsen *et al.*, 2020; Malvania *et al.*, 2020).

The universal features of 1D quantum systems at low temperatures are well captured by the Tomonaga-Luttinger low-energy theory, which can be solved using bosonization; see Giamarchi (2004) and Schönhammer (2004) for reviews. This reflects the general failure of the Landau quasiparticle description and accounts for the phenomenon of spin-charge separation. Moreover, many numerical tools work particularly well in the one-dimensional case, such as the density-matrix-renormalization group (DMRG) technique and its relatives (White, 1992; Schollwöck, 2005, 2011). As a consequence, many of the equilibrium properties of one-dimensional quantum systems are well understood. Despite the power of such methods, there are, nevertheless, open questions and limitations. In the universal low-energy theory, it is not straightforward to capture nontrivial conservation laws of the microscopic lattice models, and a description of the transport properties therefore remains a challenging task. Numerical methods often suffer from limitations in the accessible timescales and system sizes, rendering the calculation of dc transport coefficients particularly difficult.

A number of specific 1D Hamiltonians allow for exact solutions via Bethe-ansatz techniques (Bethe, 1931). These include the isotropic spin-1/2 Heisenberg, its anisotropic extension, the spin-1/2 XXZ chain (Takahashi, 1999), and the Fermi-Hubbard chain (Essler *et al.*, 2005), which serve as paradigmatic models of 1D quantum physics. For concreteness and because of its significance within the scope of the review, we now detail the Hamiltonian of the anisotropic Heisenberg chain. It can be written as $H = \sum_r h_{r,r+1}$, with

$$h_{r,r+1} = J(s_r^x s_{r+1}^x + s_r^y s_{r+1}^y + \Delta s_r^z s_{r+1}^z). \tag{1}$$

Here $s_r^{x,y,z}$ are spin-1/2 operators at site r ($\hbar = 1$), J is the exchange coupling constant, and Δ parametrizes the exchange anisotropy. We choose $J > 0$, i.e., an antiferromagnetic coupling, unless stated otherwise. The spin-1/2 XXZ chain is gapless for $|\Delta| \leq 1$ and features a gapped charge-density-wave phase for $\Delta > 1$. By using a Jordan-Wigner transformation (Giamarchi, 2004), the model can be mapped to the following system of spinless lattice fermions $c_r^{(\dagger)}$:

$$h_{r,r+1} = \frac{J}{2} c_r^{\dagger} c_{r+1} + \text{H.c.} + J\Delta\left(n_r - \frac{1}{2}\right)\left(n_{r+1} - \frac{1}{2}\right). \tag{2}$$

The limit $\Delta = 0$ corresponds to free fermions and can thus be solved analytically by a simple Fourier transform from real to (quasi)momentum space. Because of this mapping, the spin-1/2 XXZ chain is often considered to be one of the simplest models of interacting spinless fermions.

While the aforementioned Bethe-ansatz methods provide access to the eigenenergies (Orbach, 1958; Essler *et al.*, 2005), thermodynamics [see Gaudin (1971), Takahashi (1971, 1973), Klümper (1993), Takahashi (1999), and Klümper and Johnston (2000)], and even the response functions [see Caux and Maillet (2005) and Klauser *et al.* (2011)] of such Hamiltonians (Schollwöck *et al.*, 2004),

[2]As we deal in the review with lattice Hamiltonians, we use L for denoting the number of sites as well, with the understanding that the lattice spacing is set to unity.

calculating exactly their transport coefficients is difficult and has remained an open problem for decades.

The notion of integrability is not unambiguously defined in quantum physics (Caux and Mossel, 2011). Within the scope of this review, we deal exclusively with examples of Bethe-ansatz integrable models that possess an infinite number of local conservation laws. These are primarily the spin-$1/2$ XXZ chain and the 1D Fermi-Hubbard model. The nonintegrable models covered here emerge from these integrable models by adding perturbations that are expected to break all nontrivial conservation laws, such as generic spin-$1/2$ ladders, chains with a staggered magnetic field, frustrated spin chains, and dimerized spin chains.

The following discussion is based on the description of transport within linear-response theory, which relates transport coefficients to current autocorrelation functions via Kubo formulas. At zero temperature ($T = 0$), the transport coefficients of clean systems are well understood (Kohn, 1964; Shastry and Sutherland, 1990; Scalapino, White, and Zhang, 1993): in gapless phases, we deal with ideal metals and hence a divergent dc conductivity. This divergence is captured via the so-called Drude weight, the prefactor of a δ singularity in the real part of the conductivity. At $T = 0$, the presence or absence, respectively, of such a singularity simply distinguishes metallic behavior from insulators and, therefore, in this limit integrability of the microscopic model is not relevant for the existence of nonzero Drude weights.

An intriguing property of integrable models with regard to their transport properties is that they can be *ideal finite-temperature* conductors despite the presence of two-body interactions. This connection was comprehensively worked out in seminal papers (Castella, Zotos, and Prelovšek, 1995; Zotos and Prelovšek, 1996; Zotos, Naef, and Prelovšek, 1997) and is explained by the presence of nontrivial conservation laws preventing current autocorrelation functions from decaying to zero. This is reflected by a nonzero finite-temperature Drude weight in the corresponding transport coefficient.[3] Similarly, one can view this as a quantum-quench problem: Imagine a current is induced in a ring at finite temperature by applying and then turning off a force. If there is an overlap with conserved quantities, then the induced current will never decay, even in the thermodynamic limit (Mierzejewski, Prelovšek, and Prosen, 2014). Therefore, there is an intimate connection to the intensely debated topic of thermalization and relaxation in closed quantum many-body systems (Polkovnikov *et al.*, 2011; Eisert, Friesdorf, and Gogolin, 2015; D'Alessio *et al.*, 2016; Essler and Fagotti, 2016; Gogolin and Eisert, 2016; Vidmar and Rigol, 2016).

The existence of a finite-temperature Drude weight is trivial in a system of free fermions (or bosons) such as the spin-$1/2$ XX chain. In an ordinary metal and in the Drude model, a finite Drude weight arises in the limit of a diverging relaxation time. In a Fermi liquid, this occurs in the limit of $T \to 0$, where the quasiparticle lifetime becomes infinite provided that there are no impurities.

In some famous cases of integrable interacting models, the conservation laws relevant for ballistic transport properties are easy to identify (Grabowski and Mathieu, 1995): For thermal transport in the spin-$1/2$ XXZ chain, the total energy current $\mathcal{J}^{(\mathrm{E})}$ itself is conserved, rendering the transport coefficients for thermal (or energy) transport divergent. The conservation of $\mathcal{J}^{(\mathrm{E})}$ is also sufficient to prove that *spin transport* is ballistic at any finite magnetization $m_z = 2\langle S^z\rangle/L \neq 0$ where $S^z = \sum_r s_r^z$ (Zotos, Naef, and Prelovšek, 1997). For thermal transport in spin-$1/2$ XXZ chains at zero magnetization, the energy Drude weight[4] was computed from Bethe-ansatz methods (Klümper and Sakai, 2002; Sakai and Klümper, 2003; Zotos, 2017).

For spin transport and at *zero magnetization* (in either the canonical or the grand-canonical ensemble), the problem turned out to be much harder and has evolved into one of the key open questions in the theory of low-dimensional quantum systems. While a first Bethe-ansatz calculation (Zotos, 1999) indicated nonzero spin Drude weights in a wide parameter range, which is consistent with exact diagonalization (Zotos and Prelovšek, 1996; Narozhny, Millis, and Andrei, 1998; Heidrich-Meisner *et al.*, 2003), the actual relevant conservation laws were not known until 2011. Exact diagonalization was often argued to be inconclusive due to the small accessible system sizes (Sirker, Pereira, and Affleck, 2009, 2011), while the Bethe-ansatz results from Zotos (1999) were challenged as well: The calculation of the spin Drude weight cannot be done in the same rigorous manner as that of the energy Drude weight, and qualitatively different results were obtained from another Bethe-ansatz calculation using different assumptions (Benz *et al.*, 2005). Therefore, the question as to whether the spin Drude weight is finite in the spin-$1/2$ XXZ chain at $m_z = 0$ and how to compute it quantitatively attracted the attention of theoreticians using a range of methods such as quantum Monte Carlo (Alvarez and Gros, 2002c; Heidarian and Sorella, 2007; Grossjohann and Brenig, 2010), field theory (Fujimoto and Kawakami, 2003; Sirker, Pereira, and Affleck, 2009, 2011), DMRG simulations at finite temperatures (Karrasch, Bardarson, and Moore, 2012; Karrasch *et al.*, 2013), dynamical typicality (Steinigeweg, Gemmer, and Brenig, 2014), DMRG simulations of open quantum systems (Prosen and Žnidarič, 2009; Žnidarič, 2011a), and more recently generalized hydrodynamics (GHD) (Ilievski and De Nardis, 2017b; Bulchandani *et al.*, 2018). GHD is a hydrodynamic description valid for general Bethe-ansatz integrable models that was developed by Bertini *et al.* (2016) and Castro-Alvaredo, Doyon, and Yoshimura (2016); see also the recent review by Doyon (2020).

The question of the finiteness of the finite-temperature spin Drude weight in the gapless regime ($|\Delta| < 1$) of the spin-$1/2$ XXZ chain was resolved in 2011 (Prosen, 2011b; Prosen and

[3]We note that in this review the term "transport coefficient" refers to the entire frequency-dependent object, including potential zero-frequency singularities such as the Drude weight. Note further that a nonzero Drude weight does not exclude the existence of nonzero and nondivergent zero-frequency contributions stemming from the regular part; see Spohn (2012) for a review and references therein. This is, in fact, a generic situation in normal fluids in the continuum.

[4]Throughout this review, we use the term energy Drude weight instead of thermal Drude weight.

TABLE I. Overview of the different finite-temperature Drude weights of the antiferromagnetic spin-1/2 XXZ chain whose differing behaviors are covered in this review: the spin Drude weight $\mathcal{D}_{\mathrm{w}}^{(\mathrm{S})}$ and the energy Drude weight $\mathcal{D}_{\mathrm{w}}^{(\mathrm{E})}$ as a function of magnetization $m_z = 2\langle S^z\rangle/L$ and the model parameters, where Δ is the exchange anisotropy. The actual definitions for the Drude weights are given in Sec. II and the theoretical predictions are covered in Secs. III and VI.

Transport channel	m_z	$0 \le \Delta < 1$	$\Delta = 1$	$\Delta > 1$
Energy Drude weight $\mathcal{D}_{\mathrm{w}}^{(\mathrm{E})}$	$0, \neq 0$	> 0	> 0	> 0
Spin Drude weight $\mathcal{D}_{\mathrm{w}}^{(\mathrm{S})}$	0	> 0	0	0
Spin Drude weight $\mathcal{D}_{\mathrm{w}}^{(\mathrm{S})}$	$\neq 0$	> 0	> 0	> 0

Ilievski, 2013) upon the discovery of so-called quasilocal charges, which were derived, quite unexpectedly, from an exact solution of a boundary-driven many-body Lindblad master equation. These conserved quantities are fundamentally different from the previously known local conserved charges derived from the algebraic Bethe ansatz since they break spin-reversal symmetry. This can be interpreted as a consequence of the dissipative, non-time-reversal invariant setup that they are derived from. Soon after the quasilocal charges were extended to periodic (or, more generally, twisted) boundary conditions (Pereira *et al.*, 2014; Prosen, 2014c), and generalized to a one-parameter family (Prosen and Ilievski, 2013). The existence of these hitherto unknown quasilocal charges quantitatively explains the results of numerical simulations and qualitatively confirms the thermodynamic Bethe-ansatz (TBA) result (Zotos, 1999). The lower bound to the spin Drude weight agrees exactly with recent analytical results for the spin Drude weight based on GHD (Ilievski and De Nardis, 2017b) and the thermodynamic Bethe ansatz (Zotos, 1999; Urichuk *et al.*, 2019). Table I summarizes the Drude weights covered in this review for the spin-1/2 XXZ chain.

Along with the issue of Drude weights, there are equally interesting questions concerning diffusion and finite-frequency behavior.[5] In the gapless regime of the spin-1/2 XXZ chain ($|\Delta| < 1$), a regular diffusive subleading contribution to transport was advocated for by Sirker, Pereira, and Affleck (2009, 2011), while a pseudogap structure in the low-frequency window was suggested by Herbrych, Steinigeweg, and Prelovšek (2012). In the regime $|\Delta| > 1$, anomalous low-frequency properties were observed on finite systems (Prelovšek *et al.*, 2004), while most studies indicate a nonzero dc spin conductivity and thus a finite diffusion constant (Prosen and Žnidarič, 2009; Steinigeweg and Gemmer, 2009; Steinigeweg and Brenig, 2011; Žnidarič, 2011a; Karrasch, Moore, and Heidrich-Meisner, 2014). Diffusion in integrable systems was recently explained within the GHD framework and also yielded a quantitative prediction for the diffusion constant (De Nardis, Bernard, and Doyon, 2018; Gopalakrishnan and Vasseur, 2019). Moreover, numerical evidence for superdiffusive spin transport with a dynamical exponent of $z = 3/2$ at the Heisenberg point $\Delta = 1$ was found by Ljubotina, Žnidarič, and Prosen (2017, 2019) and self-consistently explained within GHD (De Nardis *et al.*, 2019; Gopalakrishnan and Vasseur, 2019; De Nardis, Medenjak *et al.*, 2020). This is the same exponent as in the Kardar-Parisi-Zhang universality class (Kardar, Parisi, and Zhang, 1986), which leads to the actively investigated question as to whether this scenario is realized in the spin-1/2 Heisenberg chain and possibly other systems with SU(2)-symmetric exchange (Ljubotina, Žnidarič, and Prosen, 2017, 2019; De Nardis *et al.*, 2019; De Nardis, Medenjak *et al.*, 2020; Dupont and Moore, 2020; Spohn, 2020a; Weiner *et al.*, 2020).

While much of the research has concentrated on the linear-response regime of the spin-1/2 XXZ chain, current activities have evolved in a number of interesting directions. An immediate goal (Karrasch, Kennes, and Moore, 2014; Jin *et al.*, 2015; Karrasch, Kennes, and Heidrich-Meisner, 2016; Karrasch, 2017b; Karrasch, Prosen, and Heidrich-Meisner, 2017) is to establish a complete picture for the linear-response transport in the Fermi-Hubbard chain, which is perhaps the other equally important integrable lattice model with regard to experimental realizations. Significant theoretical progress has recently been made by using the GHD framework; see Ilievski and De Nardis (2017a), Ilievski *et al.* (2018), and Fava *et al.* (2020).

Next, having real materials in mind, we see that another important question asks how robust transport properties are against perturbations. This has triggered much research involving nonintegrable models; see Saito, Takesue, and Miyashita (1996), Zotos and Prelovšek (1996), Prosen (1999), Alvarez and Gros (2002a), Heidrich-Meisner *et al.* (2002, 2003, 2004b), Rabson, Narozhny, and Millis (2004), Zotos (2004), Jung, Helmes, and Rosch (2006), Jung and Rosch (2007), Huang, Karrasch, and Moore (2013), Steinigeweg, Gemmer, and Brenig (2015), and Steinigeweg, Herbrych, Zotos, and Brenig (2016) and further references mentioned in Sec. VIII. In this regime, numerical methods play a crucial role. While the expectation is that nonintegrable models should exhibit diffusive transport at finite temperature, demonstrating this in an exact manner or in numerical simulations is a challenging task. Significant progress has been made with modern computational methods that allow one to obtain diffusion constants at least at high temperatures (Žnidarič, 2011a; Karrasch, Moore, and Heidrich-Meisner, 2014; Steinigeweg, Gemmer, and Brenig, 2015; Steinigeweg, Herbrych, Zotos, and Brenig, 2016). The generic description of nonintegrable models at low temperatures results from extensions of Tomonaga-Luttinger low-energy theories for gapless systems (Sirker, Pereira, and Affleck, 2009, 2011) or field theories for gapped situations (Sachdev and Damle, 1997; Damle and Sachdev, 2005). Moreover, nonintegrable models in one dimension may still possess long-lived dynamics and hydrodynamic tails, and it is by no means obvious that diffusion is the only possible scenario; see De Nardis, Medenjak *et al.* (2020) and Medenjak, De Nardis, and Yoshimura (2020) for recent work.

In the discussion of nonintegrable models, we exclude systems with disorder (Altman and Vosk, 2015; Nandkishore and Huse, 2015; Luitz and Lev, 2017; Abanin *et al.*, 2019; Gopalakrishnan and Parameswaran, 2020). Many-body lattice systems with disorder are believed to host both ergodic and many-body localized phases; see also the recent discussions by Panda *et al.* (2019), Sierant, Delande, and Zakrzewski

[5]The range of possible transport types (ballistic, diffusive, superdiffusive, subdiffusive) is introduced in Sec. II.B; see also Fig. 1.

(2020), Šuntajs *et al.* (2020), and Abanin *et al.* (2021). The transport properties of the ergodic phase are interesting and there are a number of studies (Agarwal *et al.*, 2015; Žnidarič, Scardicchio, and Varma, 2016) that claim the existence of a subdiffusive regime within the ergodic phase. This result, however, is still controversial (Barišić *et al.*, 2016; Steinigeweg, Herbrych, Pollmann, and Brenig, 2016; Bera *et al.*, 2017). Nevertheless, the ergodic phase of disordered models is often considered a generic example of a thermalizing phase with diffusive transport (then obviously excluding the putative subdiffusive regime).

Moreover, there has been fervent activity concerning the studies of more general forms of transport. For instance, manifestly nonequilibrium situations with inhomogeneous density profiles have been investigated (Ruelle, 2000; Aschbacher and Pillet, 2003; Gobert *et al.*, 2005; Langer *et al.*, 2009, 2011; Lancaster and Mitra, 2010; Jesenko and Žnidarič, 2011; Karrasch, Ilan, and Moore, 2013; Bertini *et al.*, 2016; Castro-Alvaredo, Doyon, and Yoshimura, 2016; Ljubotina, Žnidarič, and Prosen, 2017; Steinigeweg, Jin, Schmidtke *et al.*, 2017), partially because such initial conditions can be realized with both quantum magnets (Otter *et al.*, 2009; Montagnese *et al.*, 2013) and quantum gases (Schneider *et al.*, 2012; Fukuhara *et al.*, 2013; Fukuhara, Schauß *et al.*, 2013; Ronzheimer *et al.*, 2013). In addition, there is growing interest in using insights from conformal field theory (CFT) and AdS/CFT correspondence for the description of such nonequilibrium situations (Bernard and Doyon, 2012; Bhaseen *et al.*, 2015; Dubail *et al.*, 2017).

For the description of both transport in the linear-response regime and nonequilibrium situations, GHD has been established as a powerful theoretical framework for Bethe-ansatz integrable quantum lattice models (Bertini *et al.*, 2016; Castro-Alvaredo, Doyon, and Yoshimura, 2016). The approach allows one to compute Drude weights (Ilievski and De Nardis, 2017b) and diffusion constants (De Nardis, Bernard, and Doyon, 2018) and can provide the full temperature dependence of both quantities. Moreover, subleading corrections to transport coefficients such as diffusive or superdiffusive corrections can be extracted in the presence of a Drude weight (Agrawal *et al.*, 2020). GHD often allows for developing an intuition and interpretation, as it is based on a kinetic theory of the characteristic excitations of integrable models. While GHD is a recent development, it is prominently featured throughout the review.

Furthermore, we complement the picture emerging from linear-response theory or closed quantum system simulations with insights from studies of open quantum systems. In our context, these are long pieces of spin or Fermi-Hubbard chains coupled to an environment via boundary driving. The theoretical description is based on quantum master equations, and the Lindblad equation is the most commonly employed starting point. The boundary-driving terms can be used to induce a temperature or magnetization difference across the region of interest. The focus is on the steady state that can be close to or far away from equilibrium and is referred to as a nonequilibrium steady state (NESS). While there are methods to solve such setups exactly for free systems (Prosen, 2008, 2010) and statements about the existence and uniqueness of the steady state (Evans, 1977; Frigerio, 1977; Spohn, 1977), one frequently needs to resort to numerical methods, particularly when dealing with interacting systems. Time-dependent DMRG has emerged as a useful solver and comparably large systems sizes have been studied (Prosen and Žnidarič, 2009). The scaling behavior of the NESS current with system size allows one to characterize transport as diffusive, ballistic, or superdiffusive (or subdiffusive) and is therefore a valuable complementary approach. For instance, the notion of superdiffusive dynamics in the spin-1/2 Heisenberg chain was first established using open quantum system simulations (Žnidarič, 2011a). One can also extract diffusion constants that in certain limiting cases should agree with the results from linear-response theory (Žnidarič, 2019). Open quantum system simulations were extensively used to investigate transport in spin-1/2 XXZ chains, the Fermi-Hubbard chain, and spin ladders, to name a few examples; see Michel *et al.*, 2003, 2008; Mejia-Monasterio and Wichterich, 2007; Prosen and Žnidarič, 2012; Mendoza-Arenas, Grujic *et al.*, 2013; Mendoza-Arenas, Clark, and Jaksch, 2015; Katzer *et al.*, 2020.

As in any review, choices regarding the scope, topics, and focus need to be made. This review will not discuss transport in mesoscopic systems, systems with disorder, or continuum models. Out of the wide range of transport theory in lattice models, here we emphasize certain Hamiltonians, results from the Bethe ansatz, the role of newly discovered quasilocal charges, results from GHD and a range of numerical methods, and a comparison between linear-response theory and open quantum systems. Field-theoretical approaches are important, but complete coverage of the technical aspects and its predictions are beyond the scope of this work; the interested reader is referred to recent reviews (Sirker, 2020) and the original literature for more details. The same goes for a wide range of results for nonintegrable models, Floquet systems [see Lange, Lenarčič, and Rosch (2018), Lenarčič, Altman, and Rosch (2018), and Lenarčič, Lange, and Rosch (2018)], transport in disordered systems, and many nonequilibrium studies that are not covered here in full detail.

This review is organized as follows. First, we introduce the calculations of transport coefficients within linear-response theory in Sec. II. Then we discuss how nontrivial conservation laws can constrain the dynamics of current correlations, approaches based on the Bethe ansatz, and generalized hydrodynamics in Sec. III. In Sec. IV, we cover recent developments in theoretical and numerical methods, which are intimately intertwined with the progress in the theory of finite-temperature transport. The introductory sections are concluded in Sec. V, which discusses open quantum systems. After discussing the theoretical background and the methods, in Secs. VI–X we cover specific models and results.

We extensively discuss the properties of the spin-1/2 XXZ chain and stress the importance of local and quasilocal conservation laws in Sec. VI. We provide an overview of the established results and open questions for the Hubbard chain in Sec. VII, while Sec. VIII is devoted to transport in nonintegrable systems. Section IX covers examples of far-from-equilibrium transport.

Finally, we provide a brief overview of key experimental results in Sec. X. Besides experiments investigating the steady-state thermal conductivity in quantum magnets, these

also include measuring spin diffusion using NMR methods and a more recent approach, namely, the driving of spin currents in quantum magnets via the Seebeck effect (Hirobe *et al.*, 2017). In parallel, ultracold quantum gases have emerged as an additional platform to investigate transport in 1D lattice models; see Ronzheimer *et al.* (2013), Hild *et al.* (2014), Xia *et al.* (2015), and Vijayan *et al.* (2020). A major result is the first observation of ballistic nonequilibrium mass transport in a 1D integrable model of strongly interacting bosons (Ronzheimer *et al.*, 2013).

The theoretical progress in characterizing the different spin-transport regimes in the spin-1/2 XXZ chain that include ballistic transport (i.e., finite Drude weights) and diffusive and superdiffusive dynamics have stimulated recent experiments with both quantum magnets and quantum gases. A neutron-scattering study carried out in the high-temperature regime on $KCuF_3$ reports evidence for superdiffusive spin dynamics that is consistent with the Kardar-Parisi-Zhang behavior (Scheie *et al.*, 2021). A nonequilibrium optical-lattice experiment using ^{7}Li atoms has investigated the crossover from ballistic transport to superdiffusion and diffusion in the same model as a function of Δ (Jepsen *et al.*, 2020).

II. LINEAR-RESPONSE THEORY

In most studies of transport in interacting 1D lattice quantum systems, the linear response is the dominant approach. In the context of this review, one reason is that much of the focus has been on ballistic transport in integrable models, which in linear-response theory is conveniently characterized by the Drude weight. One appealing aspect of linear-response theory is that correlation functions, in terms of which transport coefficients are expressed, and specifically their Fourier transformations (i.e., spectral functions) are readily accessible in various scattering experiments.

A. Framework

We are interested in the transport of conserved quantities. Specifically, we consider extensive quantities Q that (i) are conserved ($[Q,H]=0$), and (ii) are expressed as a sum of local terms q_r whose support is localized around the site r, $Q=\sum_r q_r$. These quantities are often referred to as "conserved charges." If Q is not conserved, one cannot, in the strict sense, speak about transport because Q is not just transported from one place to another but also locally generated. To be concrete, in the review we often refer to a specific example of a local Hamiltonian, i.e., the spin-1/2 XXZ model with $H=\sum_r h_{r,r+1}$ and $h_{r,r+1}$ given in Eq. (1). We focus on the two most local conserved quantities that are connected to global symmetries of the model: energy $q_r=h_{r,r+1}$ stems from the invariance under time translations, while conservation of magnetization or spin $q_r=s^z_r$ is due to the U(1) symmetry associated with rotations around the z axis. For spin and energy, we have $Q=S^z=\sum_r s^z_r$ and $Q=H$, respectively.

The definition of the corresponding local current $j^{(Q)}_r$, where the superscript labels the conserved quantity Q,[6] follows from requiring the validity of a continuity equation and Heisenberg's equation of motion. For instance, take the total magnetization $S^z_{[l,l']}\coloneqq\sum_{r=l}^{l'} s^z_r$ of a chain subsection with indices $\{l,l+1,\ldots,l'\}$. The time derivative of $S^z_{[l,l']}$ should be given by the difference of local spin currents $j^{(\mathrm{S})}_r$ flowing at the section's edge,

$$\frac{dS^z_{[l,l']}}{dt}+j^{(\mathrm{S})}_{l'}-j^{(\mathrm{S})}_{l-1}=0, \tag{3}$$

which together with Heisenberg's equation of motion $\dot{S}^z_{[l,l']}=i[H,S^z_{[l,l']}]$ naturally leads to the identification

$$\begin{aligned} j^{(\mathrm{S})}_r &\coloneqq i[s^z_r,h_{r,r+1}] \\ &= J(s^x_r s^y_{r+1}-s^y_r s^x_{r+1}). \end{aligned} \tag{4}$$

Similarly, energy conservation leads to the energy current $j^{(\mathrm{E})}_r$, defined as

$$\begin{aligned} j^{(\mathrm{E})}_r &\coloneqq i[h_{r-1,r},h_{r,r+1}] \\ &= J[\Delta(j^{(\mathrm{S})}_{r-1}s^z_{r+1}+s^z_{r-1}j^{(\mathrm{S})}_r)-j^{(\mathrm{S})}_{r-1,r+1}s^z_r], \end{aligned} \tag{5}$$

where the explicit expression is again written for the XXZ model (1), and a two-index spin current is $j^{(\mathrm{S})}_{r-1,r+1}\coloneqq J(s^x_{r-1}s^y_{r+1}-s^y_{r-1}s^x_{r+1})$. We note that the continuity equation (3) does not uniquely define the current; one can always add a divergence-free operator (such as a constant). This ambiguity does not affect the dc conductivity, yet it may affect the finite-frequency behavior. While energy and spin currents can be defined microscopically, a definition of heat requires an excursion into thermodynamics [see Ashcroft and Mermin (1976)], which is beyond the scope of this review.

Before writing the linear-response expressions, we give a simple classical example that illustrates their general form. We assume that we are following a particle with a coordinate $x(t)$ and are interested in the variance $\Sigma^2\coloneqq\langle x^2(t)\rangle$, where the average can be taken over different realizations of the stochastic trajectory $x(t)$ (or the distribution of positions). Kinematics gives $x(t)=\int_0^t v(t_1)dt_1$, and therefore the variance becomes $\int_0^t\int_0^t\langle v(t_1)v(t_2)\rangle dt_1dt_2$. Provided that the process becomes stationary at long times and $\langle v(t)\rangle\to 0$, the correlation function depends only on the time difference $\langle v(t_1)v(t_2)\rangle=\langle v(t_1-t_2)v(0)\rangle$, leading to $\Sigma^2\to\int_0^t 2(t-\tau)\langle v(\tau)v(0)\rangle d\tau$ in the long time limit. If in addition the correlation function decays to zero for large τ (which is assumed at this point but may not necessarily happen for a specific model), one finally gets

$$\Sigma^2\overset{t\to\infty}{\to}2Dt,\qquad D\coloneqq\int_0^\infty\langle v(\tau)v(0)\rangle d\tau. \tag{6}$$

[6]For simplicity and in order to be consistent with the bulk of the literature in the field, we use the labels S and E for spin and energy, respectively.

The interpretation is simple: the diffusion constant of the coordinate is given by an integral of an autocorrelation function of a "coordinate current": the velocity. This is the spirit of all linear-response formulas for transport coefficients and rests on simple kinematics or, equivalently, on the continuity equation for a conserved quantity. As we later see, the same type of kinematic relation (an equality of the second moment of the density autocorrelation function and the integral of the current autocorrelation function) holds also in lattice systems; see Sec. II.C.1. One remark is that the aforementioned derivation is exact because it involves the full nonequilibrium process $v(t)$, while in linear response the validity is limited to small gradients of driving fields.

Linear-response theory deals with the response of a system to an additional perturbation in the Hamiltonian. It sprouted up from studies conducted in the 1950s that connected equilibrium correlation functions and nonequilibrium properties, leading to the fluctuation-dissipation relation obtained by Callen and Welton (1951) and to Green-Kubo type formulas for the transport coefficients obtained by Green (1952, 1954) and Kubo (1957); for an early review, see Zwanzig (1965).

The frequency-dependent conductivity $\mathcal{L}_{QQ}(\omega)$ is defined via a Fourier-space proportionality $\mathcal{J}^{(Q)}(\omega)=\mathcal{L}_{QQ}(\omega)\mathcal{F}_Q(\omega)$, where $\mathcal{F}_Q(t)=(1/2\pi)\int_{-\infty}^{\infty}\mathcal{F}_Q(\omega)e^{-i\omega t}d\omega$ is the driving field and $\mathcal{J}^{(Q)}(\omega)$ is the extensive current, which in a lattice model is $\mathcal{J}^{(Q)}(\omega)\coloneqq\int_{-\infty}^{\infty}\mathcal{J}^{(Q)}(t)e^{i\omega t}dt$, with

$$\mathcal{J}^{(Q)}(t)\coloneqq\sum_r j_r^{(Q)}(t) \tag{7}$$

a sum of local currents at lattice sites r. Note that here and in the following we use the Heisenberg picture, i.e., $\mathcal{J}^{(Q)}(t)\coloneqq e^{iHt}\mathcal{J}^{(Q)}e^{-iHt}$. One can think of the spin conductivity in the XXZ chain as a concrete example. In this case, $Q=S^z=\sum_r s_r^z$, and the role of the driving field is played by the gradient of the magnetic field. For the spin conductivity, we use the following notation throughout this review:

$$\sigma(\omega)\coloneqq\mathcal{L}_{\mathrm{SS}}(\omega). \tag{8}$$

Calculating the lowest-order response of the current operator to a Hamiltonian perturbation that consists of a linearly increasing potential corresponding to a homogeneous field F or, equivalently, the linear perturbation of an equilibrium initial density operator, one gets the conductivity[7]

$$\begin{aligned}\mathcal{L}_{QQ}(\omega)&=\beta\lim_{t\to\infty}\lim_{L\to\infty}\int_0^t e^{i\omega\tau}\frac{K_{\mathcal{J}^{(Q)}\mathcal{J}^{(Q)}}(\tau)}{L}d\tau,\\ K_{AB}(t)&\coloneqq\frac{1}{\beta}\int_0^\beta\langle BA(t+i\lambda)\rangle d\lambda,\end{aligned} \tag{9}$$

where $K_{AB}(t)$ is the so-called Kubo (or canonical) correlation function, with the brackets denoting the canonical average, $\langle\bullet\rangle\coloneqq\mathrm{tr}(e^{-\beta H}\bullet)/Z$, $Z\coloneqq\mathrm{tr}(e^{-\beta H})$, and $\beta=1/T$ ($k_B=1$). The conductivity $\mathcal{L}_{QQ}(\omega)$ has a standard form, as it is a Fourier transformation of the correlation function in Eq. (9).

The Kubo correlation function $K_{AB}(t)$ is real (Kubo, 1957) for Hermitian A and B, and therefore $\mathcal{L}_{QQ}(\omega)$ is complex $\mathcal{L}_{QQ}(\omega)\coloneqq\mathcal{L}'_{QQ}(\omega)+i\mathcal{L}''_{QQ}(\omega)$, where $\mathcal{L}'_{QQ}(\omega)=\mathcal{L}'_{QQ}(-\omega)$ and $\mathcal{L}''_{QQ}(\omega)=-\mathcal{L}''_{QQ}(-\omega)$ [as well as $\mathcal{L}''_{QQ}(\omega>0)\geq 0$]. In the context of the electrical conductivity, where Q is the electrical charge, $\mathcal{L}_{QQ}(\omega)$ is often called the optical conductivity because it can be probed with light-reflectivity measurements.[8] The order of limits in Eq. (9) is important: taking the limit $t\to\infty$ first, one would probe the edge or finite-size effects instead of bulk physics.

In the classical limit $\hbar\to 0$ or in the high-temperature limit $\beta\to 0$, the Kubo correlation function goes to a classical correlation function $K_{AB}(t)\to\langle BA(t)\rangle$, and therefore one gets a classical expression for the conductivity $\mathcal{L}_{QQ}(\omega)=\lim_{t\to\infty}\lim_{L\to\infty}(\beta/L)\int_0^t e^{i\omega\tau}\langle\mathcal{J}^{(Q)}\mathcal{J}^{(Q)}(\tau)\rangle d\tau$. The zero-frequency conductivity at infinite temperature $T\to\infty$ is therefore

$$\lim_{\beta\to 0}\frac{\mathcal{L}_{QQ}(0)}{\beta}=\lim_{t\to\infty}\lim_{L\to\infty}\frac{1}{L}\int_0^t\langle\mathcal{J}^{(Q)}\mathcal{J}^{(Q)}(\tau)\rangle d\tau. \tag{10}$$

This infinite-temperature limit is frequently referred to in this review. Instead of the Kubo correlation $K_{\mathcal{J}^{(Q)}\mathcal{J}^{(Q)}}(t)$, one can express Eq. (9) in terms of other types of correlation functions. For instance, one has the relation (Pottier, 2010) $K_{AB}(\omega)=(2/\beta\omega)\xi_{AB}(\omega)$ with the spectral function $\xi_{AB}(t)\coloneqq(1/2)\langle[A(t),B]\rangle$. Because $K_{\mathcal{J}^{(Q)}\mathcal{J}^{(Q)}}(t)$ is real and even, $K_{\mathcal{J}^{(Q)}\mathcal{J}^{(Q)}}(\omega)$ is real as well and can be written as $K_{\mathcal{J}^{(Q)}\mathcal{J}^{(Q)}}(\omega)=2\int_0^\infty\cos(\omega t)K_{\mathcal{J}^{(Q)}\mathcal{J}^{(Q)}}(t)dt$. Such a "one-sided" Fourier transformation is exactly what is needed for $\mathcal{L}'_{QQ}(\omega)$ in Eq. (9) and results in the real part of the conductivity

$$\mathcal{L}'_{QQ}(\omega)=\frac{i}{\omega}\int_0^\infty\lim_{L\to\infty}\frac{\sin(\omega\tau)}{L}\langle[\mathcal{J}^{(Q)}(\tau),\mathcal{J}^{(Q)}]\rangle d\tau, \tag{11}$$

where we have assumed that $\xi_{\mathcal{J}^{(Q)}\mathcal{J}^{(Q)}}(t)$ is odd and we perform the limit $t\to\infty$. Similarly, $K_{AB}(\omega)=[(1-e^{-\beta\omega})/\beta\omega]C_{AB}(\omega)$, where $C_{AB}(t)\coloneqq\langle A(t)B\rangle$, leading to the equivalent expressions

$$\begin{aligned}\mathcal{L}'_{QQ}(\omega)&=\frac{1-e^{-\beta\omega}}{\omega}\int_0^\infty\lim_{L\to\infty}\frac{\mathrm{Re}[e^{i\omega\tau}\langle\mathcal{J}^{(Q)}(\tau)\mathcal{J}^{(Q)}\rangle]}{L}d\tau\\ &=\frac{2\mathrm{th}(\beta\omega/2)}{\omega}\int_0^\infty\lim_{L\to\infty}\frac{\cos(\omega\tau)}{L}\mathrm{Re}\langle\mathcal{J}^{(Q)}(\tau)\mathcal{J}^{(Q)}\rangle d\tau.\end{aligned} \tag{12}$$

The imaginary part $\mathcal{L}''_{QQ}(\omega)$ can be obtained using Kramers-Kronig (Plemelj-Sokhotski) relations (Stone and Goldbart, 2009) or the fluctuation-dissipation theorem.

[7]For a concise derivation, see Kubo (1957), and for a more pedagogical exposition, see Kubo, Toda, and Hashitsume (1991) or Pottier (2010).

[8]Energy scales of correlated electrons in most materials are of the order of electron volts (coinciding with visible light), the magnetic-field strength is negligible, and the penetration depth of light in a conductor $\sim 1/\sqrt{\omega\mu_0\mathcal{L}_{QQ}}$ (≈2–20 nm) is larger than the lattice spacing (≈0.5 nm) such that one probes the zero-wave-vector limit of the driving field described by $\mathcal{L}_{QQ}(\omega)$.

If H conserves the total number of particles, so does the current $\mathcal{J}^{(Q)}$, and therefore the same expression also holds for a grand-canonical average with the density operator $\rho \sim e^{-\beta(H-\mu N)}$, where μ is the chemical potential and N is the particle number. In case the average current is not zero ($\langle \mathcal{J}^{(Q)} \rangle \neq 0$), which happens if the total momentum is conserved, one has to take the connected correlation function or work in an ensemble with zero total momentum. For a detailed discussion and definition of the corresponding connected correlation functions, see Bonetto, Lebowitz, and Rey-Bellet (2000) and Lepri, Livi, and Politi (2003).

The linear-response formulas for the specific case of energy transport are somewhat trickier to derive, as there is no obvious microscopic driving potential (Zwanzig, 1965) [see also Gemmer, Steinigeweg, and Michel (2006) for studies in concrete systems], such as the magnetic or electric field for magnetization or particle transport. The driving force is the gradient of the inverse temperature, which is a thermodynamic quantity and not a microscopic one. This is connected to the fact that the Hamiltonian, whose expectation value is the energy, is itself the generator of dynamics and therefore plays a special role in thermodynamics. Nevertheless, one can identify a perturbation Hamiltonian that is equivalent to a thermal perturbation, ultimately leading to the same Green-Kubo type expression (Luttinger, 1964; Pottier, 2010) as for the previously discussed generic conductivity $\mathcal{L}_{QQ}(\omega)$. Defining the energy-transport coefficient $\kappa(\omega) = \beta \mathcal{L}_{\mathrm{EE}}(\omega)$ as the proportionality factor of the energy current $\mathcal{J}^{(\mathrm{E})}(\omega) = -\kappa(\omega)\nabla T(\omega)$ (at vanishing expectation value of the particle current), one gets

$$\kappa(\omega) = \beta \mathcal{L}_{\mathrm{EE}}(\omega) = \lim_{t\to\infty} \lim_{L\to\infty} \beta^2 \int_0^t e^{i\omega\tau} \frac{K_{\mathcal{J}^{(\mathrm{E})}\mathcal{J}^{(\mathrm{E})}}(\tau)}{L} d\tau. \tag{13}$$

The difference compared to the conductivity given in Eq. (9) is an additional factor of $\beta = 1/T$ stemming from the fact that κ is the proportionality factor between the current and ∇T instead of $\nabla T/T$.

In general, one can also have nonzero cross-transport coefficients, in which case one has to deal with the entire Onsager matrix[9] $\tilde{\mathcal{L}}_{QQ'}$. To ensure that the matrix $\tilde{\mathcal{L}}$ has the correct symmetry,[10] one has to be careful (Mahan, 1990; Pottier, 2010) with the choice of driving forces $\mathcal{F}_Q$, which are equal to gradients of intensive quantities obtained by entropy derivatives. One way is to start from the entropy production rate $ds/dt = \sum_Q \mathcal{J}^{(Q)}\mathcal{F}_Q/L$, from which one can identify currents $\mathcal{J}^{(Q)}$ and corresponding forces $\mathcal{F}_Q$. To linear order, the relations between currents and forces take the form

$$\mathcal{J}^{(Q)} = \sum_{Q'} \tilde{\mathcal{L}}_{QQ'} \mathcal{F}_{Q'}. \tag{14}$$

Since the entropy production rate is $\sum_{Q,Q'} \tilde{\mathcal{L}}_{QQ'}\mathcal{F}_Q\mathcal{F}_{Q'}$, the Onsager matrix has to be positive semidefinite, $\tilde{\mathcal{L}} \geq 0$. Using Hamiltonian linear-response theory, $\tilde{\mathcal{L}}_{QQ'}$ are given by the Kubo correlation function $K_{\mathcal{J}^{(Q)}\dot{A}_Q}$, where A_Q is the operator coupled to $\mathcal{F}_Q$.[11] For instance, one has $\dot{A}_{\mathrm{E}} = T\mathcal{J}^{(\mathrm{E})}$ and $\mathcal{F}_{\mathrm{E}} = \nabla(1/T)$ for energy transport and $\dot{A}_{\mathrm{S}} = T\mathcal{J}^{(\mathrm{S})}$ and $\mathcal{F}_{\mathrm{S}} = -\nabla(b/T)$ for spin transport (b is the magnetic field), so that zero-frequency transport coefficients can be written as

$$\tilde{\mathcal{L}}_{QQ'} = \int_0^\infty \lim_{L\to\infty} \frac{K_{\mathcal{J}^{(Q)}\mathcal{J}^{(Q')}}(\tau)}{L} d\tau. \tag{15}$$

In the uncoupled case, i.e., $\tilde{\mathcal{L}}_{\mathrm{ES}} \equiv 0$, one has $\kappa = \tilde{\mathcal{L}}_{\mathrm{EE}}/T^2$ and $\sigma = \tilde{\mathcal{L}}_{\mathrm{SS}}/T$, recovering Eqs. (13) and (9).

The conductivity satisfies various sum rules: formulas expressing moments of $\mathcal{L}_{QQ}(\omega)$ in terms of correlation functions (or derivatives thereof) at $t = 0$. They are useful mostly in phenomenological theories as well as in experiments because they represent rigorous constraints on $\mathcal{L}_{QQ}(\omega)$, for instance, on the large-frequency behavior. For their form see Pottier (2010). A particularly simple example is

$$\int_{-\infty}^{\infty} d\omega \lim_{\beta\to 0} \frac{\mathcal{L}_{QQ}(\omega)}{\beta} = \pi \lim_{L\to\infty} \frac{\mathrm{tr}[\mathcal{J}^{(Q)}\mathcal{J}^{(Q)}(t=0)]}{LZ_0}, \tag{16}$$

with $Z_0 = Z(\beta \to 0)$. For sum rules for the thermal conductivity $\kappa(\omega)$ see Shastry (2006).

Linear response is limited to sufficiently small driving fields. While the range of validity of linear response is system specific, we now comment on the validity of perturbation theory used in its derivation. One can argue (Kubo, Toda, and Hashitsume, 1991) that linear response should not work since the microscopic evolution is, in general, unstable against perturbations. This applies, in particular, to the limit $t \to \infty$ needed to evaluate the conductivity. The point is rather subtle: it is true that for generic observables and initial pure states perturbation theory will fail, yet, nevertheless, in the linear-response regime we are interested in smooth observables and specific states: the equilibrium density matrices. A perturbation will change microscopic dynamics and potentially even make it chaotic, but this same chaoticity also guarantees that at long times the system will locally self-thermalize such that the density matrix will change little. In short, a generic system with good thermalization properties is microscopically unstable but macroscopically stable (Dorfman, 1999).

B. Ballistic versus diffusive transport in the context of current correlations

In this section, we discuss the small-frequency behavior of transport coefficients. This is of special importance because the limit $\omega \to 0$ probes the slowest long-wavelength modes that are often of a hydrodynamic nature (note that we also implicitly take the momentum $q \to 0$, preceding frequency $\omega \to 0$). Here and in Sec. II.C.1, we exclusively focus on the case of spin transport $\sigma(\omega) = \mathcal{L}_{\mathrm{SS}}(\omega)$.

Of particular interest is the real part of the conductivity $\sigma(\omega)$, with the imaginary part being zero [$\sigma''(0) = 0$] due to the symmetry $\sigma''(\omega) = -\sigma''(-\omega)$. $\sigma'(\omega \to 0)$ can diverge.

[9]Note that $\mathcal{L}$ and $\tilde{\mathcal{L}}$ differ by a factor of β.

[10]For a time-reversal invariant system and observables with the same parity under time reversal, $\tilde{\mathcal{L}}$ is symmetric.

[11]Note that $A_Q \neq Q$. For spin transport, $Q = S^z$ and $A_Q = \sum_r r s^z_r$.

To this end, it is useful to decompose $\sigma'(\omega)$ into a singular and a regular part

$$\sigma'(\omega) \coloneqq 2\pi \mathcal{D}_{\mathrm{w}}^{(\mathrm{S})} \delta(\omega) + \sigma_{\mathrm{reg}}(\omega), \tag{17}$$

where the prefactor $\mathcal{D}_{\mathrm{w}}^{(\mathrm{S})}$ is called the Drude weight (Kohn, 1964; Scalapino, White, and Zhang, 1992). We use the notation $\mathcal{D}_{\mathrm{w}}^{(\mathrm{S})}$ to distinguish it from the diffusion constant $D^{(\mathrm{S})}$. In older literature, it is often called spin stiffness (Shastry and Sutherland, 1990). Alternatively, using Kramers-Kronig relations, one can see that $\sigma''(\omega \to 0) = \lim_{\epsilon \to 0} [2\omega/(\omega^2 + \epsilon^2)] \mathcal{D}_{\mathrm{w}}^{(\mathrm{S})}$, and therefore $\mathcal{D}_{\mathrm{w}}^{(\mathrm{S})} = \lim_{\omega \to 0^+} (\omega/2) \sigma''(\omega)$.

To get an idea of the typical behavior of $\sigma(\omega)$, it is instructive to take a look at the simple Drude model of conduction (Ashcroft and Mermin, 1976).[12] The original Drude model consists of classical charged particles that are accelerated by the electric field and damped by a force proportional to their velocity. One gets $\sigma(\omega) = \sigma_0/(1 - i\omega\tau)$, where τ is the relaxation (damping) time and $\sigma_0 \coloneqq ne^2\tau/m$, with m the mass and n the carrier density.[13] The real part is therefore $\sigma'(\omega) = \sigma_0/(1 + \omega^2\tau^2)$, while the imaginary part is $\sigma''(\omega) = \sigma_0 \omega\tau/(1 + \omega^2\tau^2)$. At finite τ, one has diffusive transport with a Lorentzian $\sigma'(\omega)$ corresponding to an exponential decay of the autocorrelation function $C_{\mathcal{J}^{(\mathrm{S})}\mathcal{J}^{(\mathrm{S})}}(t) \sim e^{-t/\tau}$. In the limit of no relaxation $\tau \to \infty$, σ' diverges as $\sim\tau$ at its peak at $\omega = 0$, resulting in a nonzero Drude singularity $\sigma'(\omega \to 0) \to 2\pi \mathcal{D}_{\mathrm{w}}^{(\mathrm{S})} \delta(\omega)$, with $\mathcal{D}_{\mathrm{w}}^{(\mathrm{S})} = ne^2/(2m)$. In the opposite limit of fast relaxation $\tau \to 0$, where the autocorrelation function is $C_{\mathcal{J}^{(\mathrm{S})}\mathcal{J}^{(\mathrm{S})}}(t) \sim \delta(t)$, one gets a broad white noise conductivity $\sigma(\omega) = \mathrm{const}$.

The definition of the Drude weight by Eq. (17) is not unique *per se*; namely, for a physicist the Dirac delta function simply indicates a singularity without specifying its type, with different possible representations. The singularity can be characterized with a scaling exponent α as

$$\sigma'(\omega \to 0) \sim |\omega|^{\alpha}. \tag{18}$$

We use a self-consistent convention where the singularity with $\alpha = -1$ (as in the Drude model in the limit of zero relaxation) is put into the Dirac delta, while weaker integrable singularities with $-1 < \alpha < 0$ are retained in σ_{reg}. Note that in systems with a bounded local Hilbert space (or in an unbounded one at finite energy density) the singularity cannot be stronger than $1/|\omega|$. That is, if one splits the correlation function

$$C'_{\mathcal{J}^{(\mathrm{S})}\mathcal{J}^{(\mathrm{S})}}(t) \coloneqq \frac{\mathrm{Re}\langle \mathcal{J}^{(\mathrm{S})}(t) \mathcal{J}^{(\mathrm{S})} \rangle}{L} = \frac{\langle \mathcal{J}^{(\mathrm{S})}(t) \mathcal{J}^{(\mathrm{S})} \rangle + \langle \mathcal{J}^{(\mathrm{S})}(-t) \mathcal{J}^{(\mathrm{S})} \rangle}{2L} \tag{19}$$

as $C'_{\mathcal{J}^{(\mathrm{S})}\mathcal{J}^{(\mathrm{S})}}(t) \coloneqq \bar{C}'_{\mathcal{J}^{(\mathrm{S})}\mathcal{J}^{(\mathrm{S})}} + \tilde{C}'_{\mathcal{J}^{(\mathrm{S})}\mathcal{J}^{(\mathrm{S})}}(t)$ into the average $\bar{C}'_{\mathcal{J}^{(\mathrm{S})}\mathcal{J}^{(\mathrm{S})}} \coloneqq \lim_{t \to \infty} (1/t) \int_0^t C'_{\mathcal{J}^{(\mathrm{S})}\mathcal{J}^{(\mathrm{S})}}(\tau) d\tau$ and a time-dependent part $\tilde{C}'_{\mathcal{J}^{(\mathrm{S})}\mathcal{J}^{(\mathrm{S})}}(t)$, the Green-Kubo formula (11) gives

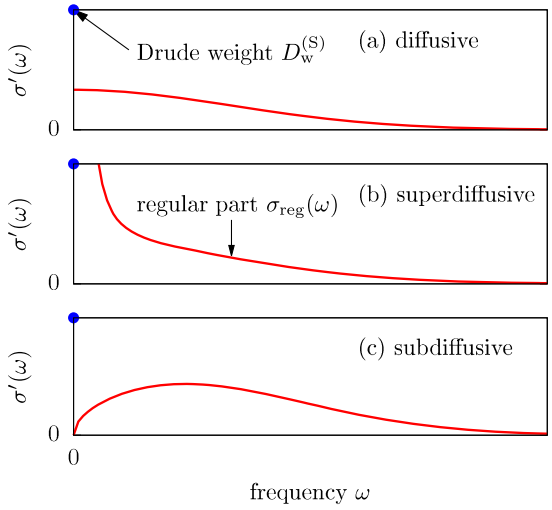

FIG. 1. The three different scenarios that one can envision for the behavior of the regular part of the optical conductivity $\sigma'(\omega)$ (solid lines) at finite temperature. The point at $\omega = 0$ indicates the Drude weight, which may coexist with a nonzero regular part.

$$\sigma'(\omega) = \beta\pi \bar{C}'_{\mathcal{J}^{(\mathrm{S})}\mathcal{J}^{(\mathrm{S})}} \delta(\omega) + \frac{2\mathrm{th}(\beta\omega/2)}{\omega} \int_0^{\infty} \cos(\omega\tau)\, \tilde{C}'_{\mathcal{J}^{(\mathrm{S})}\mathcal{J}^{(\mathrm{S})}}(\tau) d\tau. \tag{20}$$

Comparing Eq. (20) with Eq. (17), we see that

$$\mathcal{D}_{\mathrm{w}}^{(\mathrm{S})} = \frac{\beta}{2} \bar{C}'_{\mathcal{J}^{(\mathrm{S})}\mathcal{J}^{(\mathrm{S})}}. \tag{21}$$

$\mathcal{D}_{\mathrm{w}}^{(\mathrm{S})}$ can now be used to classify transport, following initial studies performed in the zero-temperature case (Shastry and Sutherland, 1990; Scalapino, White, and Zhang, 1992, 1993). Since the Drude weight $\mathcal{D}_{\mathrm{w}}^{(\mathrm{S})}$ in Eq. (21) trivially vanishes in the high-temperature limit $\beta \to 0$, a suitable quantity for the classification of transport is not $\mathcal{D}_{\mathrm{w}}^{(\mathrm{S})}$ itself but rather the quantity

$$\tilde{\mathcal{D}}_{\mathrm{w}}^{(\mathrm{S})} \coloneqq \frac{\mathcal{D}_{\mathrm{w}}^{(\mathrm{S})}}{\beta}. \tag{22}$$

If $\tilde{\mathcal{D}}_{\mathrm{w}}^{(\mathrm{S})} \neq 0$, i.e., $\alpha = -1$, one speaks of an ideal conductor, exhibiting a kind of transport that we refer to as ballistic in the review. If $\tilde{\mathcal{D}}_{\mathrm{w}}^{(\mathrm{S})} = 0$, one can distinguish among three situations (see Fig. 1): (i) if $0 < \sigma_{\mathrm{reg}}(0)/\beta < \infty$, i.e., $\alpha = 0$, the system is a normal, diffusive conductor; (ii) if $\sigma_{\mathrm{reg}}(\omega \to 0)/\beta \to \infty$, i.e., $-1 < \alpha < 0$, one has superdiffusion; and (iii) if $\sigma_{\mathrm{reg}}(0)/\beta = 0$, i.e., $\alpha > 0$, one has subdiffusive transport (including the extreme case of localization). If $\tilde{\mathcal{D}}_{\mathrm{w}}^{(\mathrm{S})} \neq 0$, the transport types (i)–(iii) must be understood as subleading corrections to ballistic transport.

In case (i) one obtains a finite diffusion constant. While $\sigma_{\mathrm{reg}}(\omega)$ is a microscopic quantity, this is not the case for the diffusion constant and one has to define it in terms of an appropriate phenomenological macroscopic relation. A common way is via Fick's law

[12]To this end, we make use of the mapping of spin-1/2 degrees of freedom to spinless fermions via the Jordan-Wigner transformation.

[13]In good conductors at room temperature, $\tau \sim 10^{-14}$ s, corresponding to a mean free path of a few lattice spacings.

$$\mathcal{J}^{(\mathrm{S})} = -D^{(\mathrm{S})}\nabla S^z, \tag{23}$$

where $D^{(\mathrm{S})}$ is the spin-diffusion constant. We can express it with $\sigma_{\mathrm{reg}}(\omega \to 0)$ using Eqs. (14) and (15). At fixed T, we also have $\mathcal{J}^{(\mathrm{S})} = -\mathcal{L}_{\mathrm{SS}}\nabla(b)/T$, which after equating it with Fick's law gives the spin-diffusion constant

$$D^{(\mathrm{S})} = \frac{\sigma_{\mathrm{reg}}(0)}{\chi}, \tag{24}$$

where b is the magnetic field. The denominator is equal to the static spin susceptibility $\chi = (\beta/L)[\langle (S^z)^2\rangle - \langle S^z\rangle^2]$, which goes as $\beta/4$ in the limit of infinite temperature. In turn, the diffusion constant at infinite T is

$$D^{(\mathrm{S})} = 4\lim_{t\to\infty}\lim_{L\to\infty}\frac{1}{L}\int_0^t \langle \mathcal{J}^{(\mathrm{S})}\mathcal{J}^{(\mathrm{S})}(\tau)\rangle d\tau. \tag{25}$$

We stress that Eq. (25) holds in the case of a vanishing Drude weight only.

The Drude weight can also be connected to the sensitivity of the spectrum to a threading flux ϕ, in essence probing the sensitivity to boundary conditions. This was originally used for the ground state (Kohn, 1964) and then extended to finite T by Castella, Zotos, and Prelovšek (1995), leading to

$$\mathcal{D}_{\mathrm{w}}^{(\mathrm{S})} = \frac{1}{L}\sum_\alpha p_\alpha \frac{1}{2}\frac{\partial^2 E_\alpha}{\partial\phi^2}\bigg|_{\phi=0}, \tag{26}$$

where E_α are eigenenergies and $p_\alpha := e^{-\beta E_\alpha}/Z$ are the Boltzmann weights. Completely analogous Drude weights can also be defined for the transport of other quantities.

A finite Drude weight implies that the current autocorrelation function exhibits a plateau at long times. Such a nonzero plateau is typically an indication of a conserved quantity. Indeed, it is intuitively clear that a conserved operator that has a nonzero overlap with the current operator causes a plateau in the current autocorrelation function. The argument can be formalized in the form of the so-called Mazur (in)equality, first studied by Mazur (1969) and Suzuki (1971), which bounds the time-averaged autocorrelation $\bar{C}'_{\mathcal{J}^{(\mathrm{S})}\mathcal{J}^{(\mathrm{S})}}$ by constants of motion. One has

$$\bar{C}'_{\mathcal{J}^{(\mathrm{S})}\mathcal{J}^{(\mathrm{S})}} \geq \sum_n \frac{1}{L}\frac{\langle \mathcal{J}^{(\mathrm{S})}Q_n\rangle^2}{\langle Q_n^2\rangle}, \tag{27}$$

where the sum runs over Hermitian constants of motion Q_n, $[Q_n,H]=0$, which are chosen to be orthogonal ($\langle Q_n Q_m\rangle \propto \delta_{nm}$). The equality in Eq. (27) holds if the sum is over a complete set of all Q_n. The bracket is a standard canonical average. However, if one wants to bound the Kubo autocorrelation function, one uses the Kubo-Mori (Mori, 1965) (also called Bogoliubov) inner product $K_{\mathcal{J}^{(\mathrm{S})}Q_n}(0)$ as defined in Eq. (9). Mazur's inequality (27), together with Eq. (21), can be used to bound the Drude weight from below (Zotos, Naef, and Prelovšek, 1997) as

$$\mathcal{D}_{\mathrm{w}}^{(\mathrm{S})} \geq \frac{\beta}{2}\lim_{L\to\infty}\sum_n \frac{1}{L}\frac{\langle \mathcal{J}^{(\mathrm{S})}Q_n\rangle^2}{\langle Q_n^2\rangle}. \tag{28}$$

We remark that using a complete set of eigenstate projectors instead of Q_n in Eq. (28) does not work because the right-hand side is zero since the sum is exponentially small in L. The important conserved quantities are (quasi)local conserved Q_n for which overlaps are not necessarily exponentially small.

For anomalous superdiffusive transport, the Drude weight is zero but the decay of the autocorrelation function is slow, resulting in a diverging diffusion constant $D^{(\mathrm{S})}$. We note that in such anomalous cases the application of the linear-response formula is in practice not straightforward (Kundu, Dhar, and Narayan, 2009; Wu and Berciu, 2010).

We previously discussed the effect of exact conservation laws, captured via Mazur's inequality. Weakly violated or approximately conserved quantities may also affect the long-time decay of current autocorrelation functions; see Rosch (2006) for a discussion.

C. Time evolution of inhomogeneous densities

1. Generalized Einstein relations

Another widely used approach to study transport (we again focus exclusively on the spin case) is to prepare a nonequilibrium initial state

$$\rho \neq \rho_{\mathrm{eq}} \tag{29}$$

and follow the dynamics of expectation values

$$\langle \delta s_r^z(t)\rangle = \mathrm{tr}[\rho(t)\delta s_r^z], \tag{30}$$

where $\rho(t) = e^{-iHt}\rho e^{iHt}$ is the unitary time evolution in an isolated quantum system governed by H and $\delta s_r^z = s_r^z - \langle s_r^z\rangle_{\mathrm{eq}}$ measures the deviation of the local density s_r^z from its value $\langle s_r^z\rangle_{\mathrm{eq}}$ at equilibrium. In such a situation, a variety of different initial states can be prepared: They can be mixed or pure, entangled or nonentangled, close to or far from equilibrium, as resulting from sudden quenches or from joining two semi-infinite chains at different equilibria; see Sec. IX.B. Various initial profiles can be realized as well: They can be spatially localized, domain walls, staggered, etc. We stress that the situations considered in this section are not necessarily limited to the linear-response regime and are therefore more general.

A general strategy for analyzing dynamical behavior is given by the spatial variance

$$\Sigma^2(t) = \sum_r \left(\frac{\langle \delta s_r^z(t)\rangle}{\langle \delta S^z\rangle} r^2 - \left[\frac{\langle \delta s_r^z(t)\rangle}{\langle \delta S^z\rangle} r\right]^2\right), \tag{31}$$

with the time-independent sum $\langle \delta S^z\rangle = \sum_r \langle \delta s_r^z(t)\rangle$ [i.e., $\sum_r \langle \delta s_r^z(t)\rangle/\langle \delta S^z\rangle = 1$ is properly normalized], and we assume that $\langle \delta s_r^z(t)\rangle > 0$. Thus, the spatial variance yields information on the overall width of the profile. In the case in which diffusive dynamics is realized at all times,

$$\frac{d}{dt}\Sigma^2(t) = 2D^{(\mathrm{S})}. \tag{32}$$

Here the quantity $D^{(\mathrm{S})}$ is a time- and space-independent diffusion constant.

In general, the spatial variance in Eq. (31) is unrelated to the previously discussed linear-response functions. However, a relation can be derived if the initial state ρ is close enough to the equilibrium state ρ_{eq}. To this end, consider the specific nonequilibrium state

$$\rho \propto \exp\left[-\beta\left(H - \varepsilon\sum_r p_r s_r^z\right)\right], \tag{33}$$

i.e., a thermal state of the Hamiltonian H, but now with an additional potential $\sum_r p_r s_r^z$ of strength ε. As shown by Kubo, Toda, and Hashitsume (1991), Eq. (33) can be expanded in ε as

$$\rho = \rho_{\mathrm{eq}}\left[1 + \varepsilon\int_0^\beta d\beta' \sum_r p_r e^{\beta' H}\delta s_r^z e^{-\beta' H} + \mathcal{O}(\varepsilon^2)\right]. \tag{34}$$

If ε is a sufficiently small parameter, the expansion can be truncated to linear order. Using this truncation, the expectation values $\langle \delta s_r^z(t)\rangle$ become

$$\langle \delta s_r^z(t)\rangle = \varepsilon\beta\sum_{r'} p_{r'} K_{\delta s_r^z \delta s_{r'}^z}(t). \tag{35}$$

Assuming that $\langle \delta s_r^z(t)\rangle$ remains negligibly small at the boundary of the lattice, the time derivative of the spatial variance can be written in the form (Bohm and Leschke, 1992; Steinigeweg, Wichterich, and Gemmer, 2009; Yan, Jiang, and Zhao, 2015)

$$\frac{d}{dt}\Sigma^2(t) = 2D^{(\mathrm{S})}(t), \tag{36}$$

where the time-dependent diffusion constant is given by

$$D^{(\mathrm{S})}(t) = \frac{\beta}{\chi}\int_0^t dt' K_{\mathcal{J}^{(\mathrm{S})}\mathcal{J}^{(\mathrm{S})}}(t') \tag{37}$$

with the static susceptibility

$$\chi = \frac{\beta}{L} K_{\delta S^z \delta S^z}. \tag{38}$$

As mentioned, one has $\chi = \beta/4$ for the specific case of high temperatures.

Equation (37) is a generalized Einstein relation as it holds for any time t. In particular, in the longtime limit $t \to \infty$, it simplifies to the usual Einstein relation if the current autocorrelation function decays sufficiently fast to zero

$$\lim_{t\to\infty} D^{(\mathrm{S})}(t) = D^{(\mathrm{S})} = \frac{\sigma_{\mathrm{dc}}}{\chi}, \tag{39}$$

where $\sigma_{\mathrm{dc}} = \sigma_{\mathrm{reg}}(0)$ is the dc conductivity as obtained from linear-response theory; i.e., Eq. (39) is identical to Eq. (24). Therefore, the existence of σ_{dc} implies a diffusive scaling of the spatial variance in time, at least for the specific initial state ρ in Eq. (33) with a small parameter ε. However, it is worth pointing out that the requirement of a strictly mixed state can be relaxed by employing the concept of typicality; see Sec. IV.C.

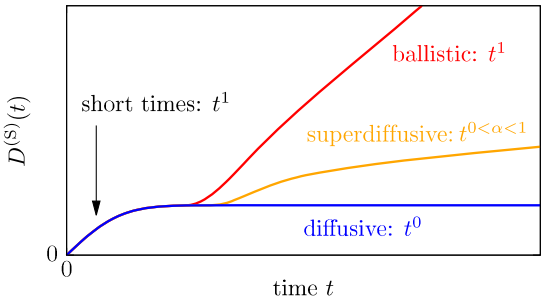

FIG. 2. Different scenarios for the time-dependent diffusion constant $D^{(\mathrm{S})}(t)$: ballistic, superdiffusive, and diffusive (top to bottom). The behavior in the short-time limit is always ballistic, and the typical exponents in the longtime dynamics are indicated as t^1, t^α $(0 < \alpha < 1)$, and t^0, respectively.

Since the generalized Einstein relation is not restricted to the limit of large times or to the case of diffusion, it allows one to investigate both different time scales and different types of transport. For example, it predicts a ballistic scaling $D^{(\mathrm{S})}(t) \propto t$ and $\Sigma^2(t) \propto t^2$ at short times $t \ll \tau$ before a diffusive scaling $D^{(\mathrm{S})}(t) = D^{(\mathrm{S})}$ and $\Sigma^2(t) \propto t$ may finally set in at intermediate times $t > \tau$. It also captures the influence of a Drude weight $\mathcal{D}_{\mathrm{w}}^{(\mathrm{S})} > 0$. A finite Drude weight $\mathcal{D}_{\mathrm{w}}^{(\mathrm{S})} > 0$ implies a ballistic scaling

$$D^{(\mathrm{S})}(t) \propto \frac{\mathcal{D}_{\mathrm{w}}^{(\mathrm{S})}}{\chi} t \tag{40}$$

and $\Sigma^2(t) \propto t^2$ at large times.

Finally, we remark that a power-law scaling of

$$\Sigma^2(t) \propto t^{\alpha'} \tag{41}$$

indicates subdiffusion for $0 < \alpha' < 1$ and superdiffusion for $1 < \alpha' < 2$; see Fig. 2. Because of the generalized Einstein relation in Eq. (37), such a power-law scaling in time also implies that the frequency dependence of the conductivity $\sigma'(\omega)$ is given by the power law (Maass *et al.*, 1991; Dyre *et al.*, 2009; Stachura and Kneller, 2015; Luitz and Lev, 2017)

$$\sigma'(\omega) \propto \int_0^\infty dt\, e^{i\omega t} t^{\alpha'-2} \propto |\omega|^{1-\alpha'}, \tag{42}$$

i.e., Eq. (18) with $\alpha = 1 - \alpha'$.

2. Diffusion

While the spatial variance in Eq. (31) is a useful quantity for studying transport, it yields no information beyond the overall width of a profile. In particular, to draw reliable conclusions on the existence of diffusion it is necessary to require the full spatial dependence of a profile to be described by the diffusion equation. In one dimension and for a discrete lattice, the diffusion equation reads

$$\frac{d\langle \delta s_r^z(t)\rangle}{dt} = D^{(\mathrm{S})}[\langle \delta s_{r-1}^z(t)\rangle - 2\langle \delta s_r^z(t)\rangle + \langle \delta s_{r+1}^z(t)\rangle], \tag{43}$$

where $D^{(\mathrm{S})}$ again denotes a time- and space-independent diffusion constant and the right-hand side can be viewed as a discretized version of the Laplacian $\partial^2/\partial r^2$. It is important to note that Eq. (43) is a phenomenological description for the expectation values $\langle s_r^z(t)\rangle$ and their irreversible relaxation toward equilibrium. A rigorous justification is still a challenge to theory (Casati *et al.*, 1984; Bonetto, Lebowitz, and Rey-Bellet, 2000; Lepri, Livi, and Politi, 2003; Buchanan, 2005; Michel, Mahler, and Gemmer, 2005; Dhar, 2008; Ljubotina, Žnidarič, and Prosen, 2017). For such a description and in the following discussion, one does not need to specify the initial state in detail; however, note that this statistical description is often discussed in the context of correlation functions (Kadanoff and Martin, 1963; Steiner, Villain, and Windsor, 1976; Forster, 1990). We stress that the diffusion in Eq. (43) is a statistical process starting at time $t=0$ and occurring between individual lattice sites; i.e., it implicitly assumes a mean free time $\tau=0$ and a mean free path $l=0$. Since $\tau>0$ and $l>0$ in specific models, it holds only when the density profile has become sufficiently broad. In terms of the density modes discussed later, statistical behavior is thus restricted to sufficiently small momenta.

For a local injection at some site r', i.e., $\langle \delta s^z_{r=r'}(0)\rangle \neq 0$ and $\langle \delta s^z_{r\neq r'}(0)\rangle = 0$, the solution of Eq. (43) reads

$$\frac{\langle \delta s_r^z(t)\rangle}{\langle \delta S^z\rangle} = \exp(-2D^{(\mathrm{S})}t) I_{r-r'}(2D^{(\mathrm{S})}t), \tag{44}$$

where $I_r(t)$ is the modified Bessel function of the first kind and of the order of r. This lattice solution is well approximated by the corresponding continuum solution

$$\frac{\langle \delta s_r^z(t)\rangle}{\langle \delta S^z\rangle} = \frac{1}{\sqrt{2\pi}\Sigma(t)} \exp\left[-\frac{(r-r')^2}{2\Sigma^2(t)}\right], \tag{45}$$

where the spatial variance $\Sigma^2(t) = 2D^{(\mathrm{S})}t$ was introduced in Sec. II.C.1. Thus,

$$\langle \delta s^z_{r=r'}(t)\rangle \propto \frac{1}{\Sigma(t)} \propto \frac{1}{\sqrt{t}}. \tag{46}$$

Since the diffusion equation is a linear differential equation, the general solution can be constructed as a superposition of δ injections at different positions.

At this point, it is instructive to provide a link to correlation functions. To this end, consider the specific initial state ρ in Eq. (33) with coefficients $p_{r=r'} \neq 0$ and $p_{r\neq r'} = 0$. For sufficiently small ε, the expectation values $\langle \delta s_r^z(t)\rangle$ become

$$\langle \delta s_r^z(t)\rangle = \varepsilon\beta p_{r'} K_{\delta s^z_{r'}\delta s^z_r}(t). \tag{47}$$

For high temperatures, $K_{\delta s^z_{r'}\delta s^z_r}(0) \propto \delta_{r,r'}$, and in the case of diffusion $\langle \delta s_r^z(t)\rangle$ satisfies Eqs. (44) and (45) (Steinigeweg, Jin, Schmidtke *et al.*, 2017).

Returning to the general case, we find that it is often convenient to study diffusion not only in real space but also in the space of lattice momenta (reciprocal space)

$$q = \frac{2\pi k}{L}, \quad k = 0, \ldots, L-1. \tag{48}$$

Note that the lattice spacing is set to 1. The quasimomentum representation is particularly useful since a discrete Fourier transform

$$\langle \delta s_q^z(t)\rangle = \frac{1}{\sqrt{L}} \sum_r e^{iqr} \langle \delta s_r^z(t)\rangle \tag{49}$$

decouples the diffusion equation in Eq. (43). Hence, after this transformation it becomes the simple rate equation

$$\frac{d\langle \delta s_q^z(t)\rangle}{dt} = -\tilde{q}^2 D^{(\mathrm{S})} \langle \delta s_q^z(t)\rangle, \tag{50}$$

where the momentum dependence $\tilde{q}^2 = 2(1-\cos q)$ may be given as $\tilde{q}^2 \approx q^2$ for sufficiently small q. The solution of Eq. (50) is an exponential decay of the form (Steiner, Villain, and Windsor, 1976)

$$\frac{\langle \delta s_q^z(t)\rangle}{\langle \delta s_q^z(t=0)\rangle} = e^{-\tilde{q}^2 D^{(\mathrm{S})} t}. \tag{51}$$

Thus, the general solution of the diffusion equation can also be written as a superposition of exponential decays at different momenta. For instance, the Bessel solution in Eq. (44) can be written in the form

$$\frac{\langle \delta s_r^z(t)\rangle}{\langle \delta S^z\rangle} = \frac{1}{L} \sum_q e^{-iq(r-r')} e^{-\tilde{q}^2 D^{(\mathrm{S})} t}. \tag{52}$$

This form makes it particularly clear when the Gaussian in Eq. (45) is a good approximation: The quasimomentum q must be sufficiently dense; i.e., L must be sufficiently large and, in addition, time t must be sufficiently long.

As the Fourier modes $\langle \delta s_q^z(t)\rangle$ decay exponentially in the case of diffusion, their spectral representation

$$\langle \delta s_q^z(\omega)\rangle = \int_0^\infty dt\, e^{i\omega t} \langle \delta s_q^z(t)\rangle \tag{53}$$

becomes a Lorentzian of the form (Kadanoff and Martin, 1963)

$$\mathrm{Re}\left[\frac{\langle \delta s_q^z(\omega)\rangle}{\langle \delta s_q^z(t=0)\rangle}\right] = \frac{\tilde{q}^2 D^{(\mathrm{S})}}{(\tilde{q}^2 D^{(\mathrm{S})})^2 + \omega^2}, \tag{54}$$

with the sum rule

$$\int_{-\infty}^{\infty} d\omega\, \mathrm{Re}\left[\frac{\langle \delta s_q^z(\omega)\rangle}{\langle \delta s_q^z(t=0)\rangle}\right] = \pi. \tag{55}$$

This Lorentzian line shape occurs for all momenta and frequencies, which reflects the fact that the diffusion equation (43) assumes a mean free path $l=0$ (and mean free time $\tau=0$). However, if l and τ are finite, a Lorentzian line shape can occur only in the hydrodynamic limit where momentum and frequency are both sufficiently small.

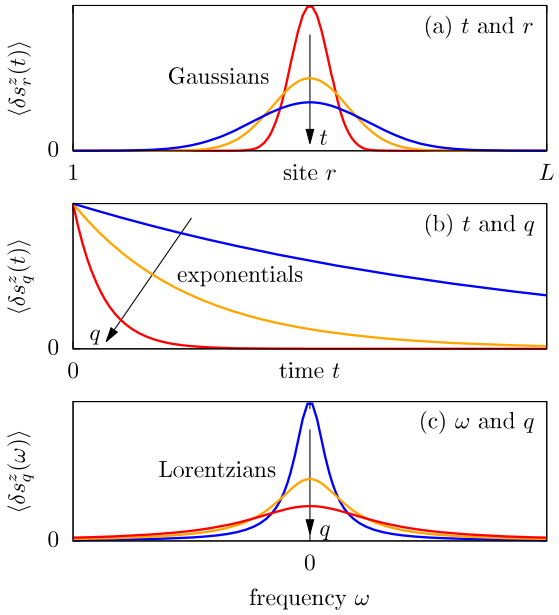

FIG. 3. Diffusive spreading of a spin-density perturbation as a function of (a) time t and real space r, (b) time t and momentum space q, and (c) frequency ω and momentum space q.

Finally, it is instructive to discuss correlation functions again. Focusing on the specific initial state ρ in Eq. (33), starting from Eq. (47) and assuming translation invariance of H, it is straightforward to show that

$$\langle \delta s^z_q(t) \rangle = \varepsilon p_{r'} \chi_q(t), \tag{56}$$

with the correlation function

$$\chi_q(t) = \beta K_{\delta s^z_q \delta s^z_{-q}}(t). \tag{57}$$

Therefore, in the case of diffusion the correlation function $\chi_q(t)$ is an exponential and the real part of its Fourier transform $\chi_q(\omega)$ is a Lorentzian.

The continuity equation in momentum space

$$\frac{d\delta s^z_q(t)}{dt} = (e^{iq} - 1) j^{(S)}_q(t) \tag{58}$$

allows one to relate $\chi_q(t)$ to the correlation function

$$\sigma_q(t) = \beta K_{j^{(S)}_q j^{(S)}_{-q}}(t). \tag{59}$$

In the time domain, this relation reads

$$\sigma_q(t) = -\frac{1}{\tilde{q}^2} \frac{d^2 \chi_q(t)}{dt^2} \tag{60}$$

and as a function of frequency it becomes

$$\mathrm{Re}\, \sigma_q(\omega) = \frac{\omega^2}{\tilde{q}^2} \mathrm{Re}\, \chi_q(\omega). \tag{61}$$

Therefore, if the dynamics is diffusive, the Lorentzian in Eq. (54) implies that

$$\mathrm{Re}\left[\frac{\sigma_q(\omega)}{\chi_q(t=0)}\right] = \frac{D^{(S)} \omega^2}{(\tilde{q}^2 D^{(S)})^2 + \omega^2}. \tag{62}$$

In the limit of small momentum, one thus obtains the Einstein relation

$$\lim_{q \to 0} \mathrm{Re}\left[\frac{\sigma_q(\omega)}{\chi_q(t=0)}\right] = D^{(S)}. \tag{63}$$

Note that no frequency dependence is left as the mean free time is assumed to be $\tau = 0$. This broad conductivity also arises in the Drude model of conduction discussed earlier.

To summarize this section, Fig. 3 sketches diffusion in (a) time t and real space r, (b) time t and momentum space q, and (c) frequency ω and momentum space q.

III. EXPLOITING INTEGRABILITY

In this section, we see how integrability affects the finite-temperature transport properties. Here we emphasize the important role played by local and quasilocal conservation laws, showing that they can lead to ballistic transport. Specifically, in Sec. III.A we show that a systematic construction of quasilocal charges provides lower bounds for Drude weights and diffusion constants. In Secs. III.B and III.C, we describe methods to obtain closed-form analytical predictions for these quantities. In particular, Sec. III.B.3 reports on the predictions for spin and energy Drude weights obtained using the TBA formalism, whereas Sec. III.C gives an introduction to GHD and describes its predictions for the Drude weights and diffusion constants of all conserved charges. Most of the ideas are exemplified in the paradigmatic case of the spin-1/2 XXZ chain.

Sections III.B.1 and III.B.2 give a detailed introduction to the Bethe ansatz and TBA and establish a coherent formalism to express both the TBA results for transport coefficients and GHD.

A. Role of local and quasilocal conserved charges

Quantum integrability is based on the existence of two key objects (Korepin, Bogoliubov, and Izergin, 2005; Faddeev, 2016). The first one is the R matrix, which can be understood as an abstract unitary scattering operator $\check{R}_{j,l}(\lambda)$ acting over a pair of local finite-dimensional physical Hilbert spaces $\mathcal{H}_j \simeq \mathcal{H}_l \simeq \mathbb{C}^d$. The R matrix depends on a free complex spectral parameter λ and satisfies the Yang-Baxter equation. The second key object is the Lax operator $L_{j,a}(\lambda)$, which acts on a pair of Hilbert spaces that are in principle different: the local Hilbert space $\mathcal{H}_j$ and the so-called auxiliary space V_a of dimension N_a, which can be finite or infinite. These two spaces carry the physical and auxiliary representation of the quantum symmetry of the problem, respectively. This symmetry is concisely expressed by the so-called RLL relation[14]

[14]RLL stands for R-matrix—Lax matrix—Lax matrix.

$$\check{R}_{j,l}(\mu)L_{j,a}\left(\lambda+\frac{\mu}{2}\right)L_{l,a}\left(\lambda-\frac{\mu}{2}\right) = L_{j,a}\left(\lambda-\frac{\mu}{2}\right)L_{l,a}\left(\lambda+\frac{\mu}{2}\right)\check{R}_{j,l}(\mu). \tag{64}$$

The RLL equation is another form of the Yang-Baxter relation. For a given $\check{R}_{j,l}(\mu)$, one can construct the two-site local Hermitian operator

$$h_{j,j+1} = \frac{d}{d\lambda}\check{R}_{j,j+1}(\lambda)|_{\lambda=0}, \tag{65}$$

which gives the Hamiltonian density ($H=\sum_{j=1}^{L} h_{j,j+1}$) of the corresponding integrable model, where periodic boundary conditions can be assumed for simplicity.

A critical consequence of integrability is the existence of an extensive number of local conserved quantities, which are generated via logarithmic derivatives

$$Q_n = \frac{d^n}{d\lambda^n}\log\tau(\lambda)|_{\lambda=\lambda_0} \tag{66}$$

of the fundamental transfer matrix, an operator over $\bigotimes_j \mathcal{H}_j \simeq (\mathbb{C}^d)^{\otimes L}$ defined as follows:

$$\tau(\lambda) = \mathrm{tr}_0 L_{1,0}(\lambda)L_{2,0}(\lambda)\cdots L_{L,0}(\lambda). \tag{67}$$

Here $L_{j,0}(\lambda)$ is the Lax operator in the fundamental representation, where the auxiliary space is isomorphic to the local physical space. At the special point $\lambda=\lambda_0$, the Lax operator $L_{j,0}(\lambda)$ degenerates to a permutation operator $L_{j,0}(\lambda_0)=P_{j,0}$ acting as $P|\psi\rangle\otimes|\phi\rangle=|\phi\rangle\otimes|\psi\rangle$. This property is instrumental for showing that $Q_n=\sum_{l=1}^{L} q_l^{(n)}$ are in fact extensive sums of local densities $q_l^{(n)}$. The conservation law property $[H,\tau(\lambda)]\equiv[H,Q_k]\equiv 0$ is then a simple consequence of the RLL relation (64), and, similarly, the involution property $[\tau(\lambda),\tau(\mu)]\equiv[Q_j,Q_k]\equiv 0$ follows from another form of Yang-Baxter equation. In fact, one can fix normalization such that $H=Q_1$.

This construction applies to the paradigmatic example of the spin-1/2 XXZ chain. In this case, the local Hilbert space is $\mathcal{H}_j=\mathbb{C}^2$ and $\check{R}_{j,l}(\lambda)$ is the standard six-vertex R matrix (Baxter, 1982). Using the parametrization

$$\Delta = \cos(\eta), \tag{68}$$

the general Lax operator can be written as

$$L_{j,a}(\lambda,s) = \frac{2\sin\eta}{\sin\lambda}(S_a^+ s_j^- + S_a^- s_j^+) + \cos(\eta S_a^z)\mathbb{1} + 2(\cot\lambda)\sin(\eta S_a^z)s_j^z, \tag{69}$$

where the local spin operators $s_j^\alpha=(1/2)\sigma_j^\alpha$, $\alpha\in\{+,-,z\}$, act over the local physical space, while $S_a^{+,-,z}$ span an irreducible highest-weight representation of the q-deformed angular momentum algebra ($q=e^{i\eta}$) $\mathrm{SU}_q(2)$. This representation depends on a free complex parameter $s\in\mathbb{C}$ and is generically infinite dimensional

$$S_a^z = \sum_{n=0}^{\infty}(s-n)|n\rangle\langle n|,$$
$$S_a^+ = \sum_{n=1}^{\infty}\frac{\sin n\eta}{\sin\eta}|n-1\rangle\langle n|,$$
$$S_a^- = \sum_{n=1}^{\infty}\frac{\sin(2s-n+1)\eta}{\sin\eta}|n\rangle\langle n-1|. \tag{70}$$

However, either (i) for half-integer spin $s\in(1/2)\mathbb{Z}$ or (ii) for any $s\in\mathbb{C}$ but root-of-unity anisotropies $\eta=\pi\ell/m$ (ℓ,m coprime integers) this irreducible representation truncates to a finite dimension $N_a=2s+1$ or $N_a=m$, respectively. In this case, the sums in Eqs. (70) run up to $n=N_a-1$. One can thus define a general family of commuting transfer matrices

$$\tau(\lambda,s) = \mathrm{tr}_a L_{1,a}(\lambda,s)L_{2,a}(\lambda,s)\cdots L_{L,a}(\lambda,s), \tag{71}$$

satisfying $[H,\tau(\lambda,s)]=0$ for all λ, s, again as a consequence of Eq. (64), while $\tau(\lambda,1/2)\equiv\tau(\lambda)$.

For every fixed s, the transfer matrix $\tau(\lambda,s)$ generates the following sequence of additional conserved charges:

$$Q_{n,s} = \frac{d^n}{d\lambda^n}\log\tau(\lambda,s)|_{\lambda=\eta/2}. \tag{72}$$

Therefore, one can argue that the sequence of local charges Q_n stemming from the fundamental transfer-matrix equation (67) is not complete and is not sufficient to describe the statistical mechanics of integrable models. Indeed, Ilievski, Medenjak, and Prosen (2015) showed that for $s>1/2$ the charges in Eq. (72) are linearly independent from the family of local charges $Q_{n,s}\equiv Q_{n,1/2}$ and are essentially local. More formally, for any size L, a generic charge $Q=Q_{n,s}$ in Eq. (72) can be written as an extensive series $Q=\sum_r\sum_{l=1}^{L} q_{l,r}$ of r-site local densities $q_{l,r}$ with an exponentially decaying vector norm (i.e., $\langle[q_{l,r}]^2\rangle<Ce^{-r/\xi}$ for some fixed $C,\xi>0$). This property, called quasilocality, implies extensivity in the sense that $0<\lim_{L\to\infty}\langle Q^2\rangle/L<\infty$. One may argue that those in Eq. (72), together with the total magnetization S^z, form a complete set of charges for $|\Delta|\geq 1$. Note that for any Δ one can establish a one-to-one correspondence between the known (quasi)local charges and the string excitations using the so-called string-charge duality (Ilievski, Quinn *et al.*, 2016).

All the charges $Q_{n,s}$ generated by unitary representations of $\mathrm{SU}_q(2)$ are even under a generic $\mathbb{Z}_2$ particle-hole symmetry of the model, as in the case of the spin-1/2 XXZ chain, under the spin-reversal (spin-flip) transformation $F=\prod_{l=1}^{L}\sigma_l^x$, $FQ_{n,s}=Q_{n,s}F$. However, the spin current $\mathcal{J}^{(\mathrm{S})}$ is odd, $\mathcal{J}^{(\mathrm{S})}F=-F\mathcal{J}^{(\mathrm{S})}$, and hence $\langle\mathcal{J}^{(\mathrm{S})}Q_{n,s}\rangle=0$. In other words, irrespective of the temperature, these charges cannot contribute to the Mazur bound [Eq. (28)] at vanishing magnetization.

Nevertheless, one can explore nonunitary representations of the symmetry algebra $\mathrm{SU}_q(2)$ to search for charges that are not invariant under spin-reversal using the general relation $F\tau(\lambda,s)F^{-1}=\tau(\pi-\lambda,s)^{\mathrm{T}}$. For root-of-unity anisotropies $\eta=\pi\ell/m$ (ℓ,m coprime integers), this procedure leads to an additional family of quasilocal conserved charges that are non-Hermitian and odd under spin reversal (Prosen, 2014c). They can be expressed as

$$Z(\lambda) = \frac{\sin(\lambda)^2}{2\eta \sin(\eta)} \partial_s \tau(\lambda, s)\Big|_{s=0} - \frac{\sin(\lambda)\cos(\lambda)}{\sin(\eta)} S^z, \tag{73}$$

where λ lies inside the analyticity strip $\mathcal{S} = \{\lambda \in \mathbb{C}; |\mathrm{Re}\lambda - \pi/2| < \pi/2m\}$ and $S^z = \sum_{r=1}^{L} s_r^z$ denotes the total magnetization in the z direction.

1. Lower bound on spin Drude weight at high temperature

Since the quasilocal charges generated from nonunitary representations are not spin-reversal invariant, they have a nonvanishing overlap with the spin current and may contribute to the Mazur bound. For example, in the high-temperature regime ($\beta \to 0$), the overlap is also extensive [$\langle Z(\lambda)\mathcal{J}^{(\mathrm{S})}\rangle = iL/4$], yielding a finite contribution to Eq. (28). However, the $Z(\lambda)$ are not mutually orthogonal and their overlaps are given by the following analytic kernel:

$$\begin{aligned} K(\lambda,\mu) &= \lim_{L\to\infty} \frac{\langle Z(\bar{\lambda})^\dagger Z(\mu)\rangle}{L} \\ &= -\frac{\sin(\lambda)\sin(\mu)\sin[(m-1)(\lambda+\mu)]}{2\sin^2(\eta)\sin[m(\lambda+\mu)]}, \end{aligned}$$

while $\langle Z(\lambda)Z(\mu)\rangle \equiv 0$. The Mazur bound for the spin Drude weight generally follows (Ilievski and Prosen, 2013) from finding an extremum of the non-negative action

$$\mathcal{S}[f] \coloneqq \lim_{t\to\infty}\lim_{L\to\infty} \frac{1}{L}\langle (B_{L,t}[f])^\dagger B_{L,t}[f]\rangle \geq 0 \tag{74}$$

with respect to an unknown function $f(\lambda)$. Here we introduce

$$B_{L,t}[f(\lambda)] \coloneqq \frac{1}{t}\int_0^t ds \mathcal{J}^{(S)}(s) - \int_{\mathcal{S}} d^2\lambda f(\lambda) Z(\lambda). \tag{75}$$

The variation $\delta S/\delta f(\lambda) = 0$ results in the following Fredholm equation of the first kind on the two-dimensional complex domain $\mathcal{S}$:

$$\int_{\mathcal{S}} d^2\mu K(\lambda,\mu) f(\mu) = \langle Z(\lambda) j^{(\mathrm{S})}\rangle, \tag{76}$$

which for the spin-1/2 XXZ chain with $\Delta = \cos(\pi\ell/m)$ yields

$$f(\lambda) = \frac{m\sin^2(\pi/m)}{i\pi|\sin\lambda|^4}. \tag{77}$$

This in turn results in the following rigorous lower bound for the leading coefficient in the high-temperature expansion of the Drude weight $\tilde{\mathcal{D}}_{\mathrm{w}}^{(S)}$ in β, defined as

$$\begin{aligned} \tilde{\mathcal{D}}_{\mathrm{w}}^{(\mathrm{S})} &= \lim_{\beta\to 0}\frac{\mathcal{D}_{\mathrm{w}}^{(\mathrm{S})}}{\beta} \geq \frac{1}{2}\int_{\mathcal{S}} d\lambda^2 f(\lambda)\langle Z(\lambda) j_0^{(\mathrm{S})}\rangle \\ &= \frac{1}{16}\frac{\sin^2(\pi\ell/m)}{\sin^2(\pi/m)}\left[1 - \frac{m}{2\pi}\sin\left(\frac{2\pi}{m}\right)\right]. \end{aligned} \tag{78}$$

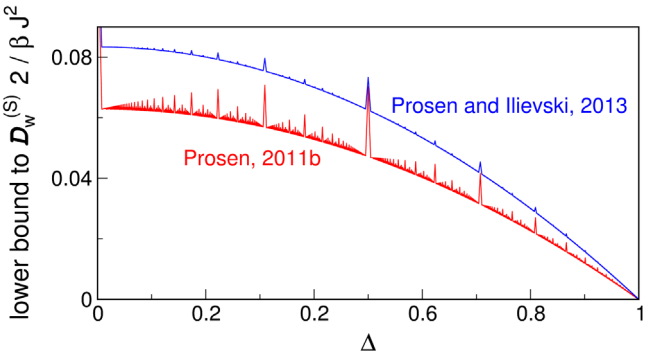

FIG. 4. Lower bound for the spin Drude weight $\mathcal{D}_{\mathrm{w}}^{(\mathrm{S})}$ of the spin-1/2 XXZ chain according to Eq. (78), as obtained by Prosen and Ilievski (2013), and another lower bound for $\mathcal{D}_{\mathrm{w}}^{(\mathrm{S})}$, as previously obtained by Prosen (2011b). Both bounds exhibit a pronounced fractal-like (i.e., nowhere continuous) dependence on the anisotropy parameter Δ.

Note that the rhs of Eq. (78) is a nowhere continuous function of Δ whose graph is a fractal set. The dependence on Δ is illustrated in Fig. 4.

See Sec. VI for a detailed discussion of the saturation of this bound and Matsui (2020) for an explanation of why the natural non-quasilocal extension of the quasilocal charges given in Eq. (72) cannot improve the bound. A more comprehensive review on quasilocal charges was given by Ilievski, Medenjak *et al.* (2016), while the extension of Drude weights and quasilocal charges to integrable periodically driven Floquet systems was given by Ljubotina, Zadnik, and Prosen (2019).

2. Lower bounds on spin-diffusion constant at high temperature

In typical integrable models such as the spin-1/2 XXZ chain for $|\Delta| \geq 1$ and the 1D Fermi-Hubbard model, the spin or charge Drude weight vanishes at zero magnetization $m_z = 2\langle S^z\rangle/L = 0$ and in the half-filled sector $\rho = N/L = 1/2$, respectively. However, moving slightly away from half filling, one typically obtains a finite Drude weight. More precisely, calling δ the small deviation from either zero magnetization or half filling, one observes a Drude-weight scaling as $\mathcal{D}_{\mathrm{w}}^{(Q)} \propto \delta^2$. At first sight, this seems to exclude the onset of spin diffusion: a finite Drude weight implies a diverging diffusion constant. Nevertheless, for large L, the Hilbert-space sector at $\delta = 0$ dominates over all sectors with $\delta \neq 0$. Therefore, one may argue that, after performing a careful (grand) canonical average, the two effects compensate, giving rise to a finite spin- or charge-diffusion constant in the thermodynamic limit.

In fact, this argument can be justified rigorously by studying the Mazur bound for the dynamical susceptibility in a double-scaling limit $L \to \infty$ and $t \to \infty$, with $L/t > v_{\mathrm{LR}}$, giving rise to a universal lower bound on the diffusion constant $D^{(Q)}$ in terms of the curvature of the Drude weight $\mathcal{D}_{\mathrm{w}}^{(Q)}(\beta,\delta)$ around $\delta = 0$ (Medenjak, Karrasch, and Prosen, 2017); see also Spohn (2018). For spin transport, one obtains

$$D^{(\mathrm{S})}(\beta) \geq \frac{1}{8\beta v_{\mathrm{LR}} \chi(\beta) f_1(\beta)} \frac{\partial^2}{\partial \delta^2} \mathcal{D}_{\mathrm{w}}^{(\mathrm{S})}(\beta, \delta)\Big|_{\delta=0}, \quad (79)$$

where v_{LR} is the Lieb-Robinson velocity (Lieb and Robinson, 1972) and

$$f_1(\beta) = \lim_{L\to\infty} \frac{1}{2L} \frac{\partial^2}{\partial \delta^2} F_L(\beta, \delta)\Big|_{\delta=0} \quad (80)$$

is a second derivative of the free-energy density at zero magnetization, while $\chi(\beta)$ is the static susceptibility $\chi(\beta)/\beta = \lim_{L\to\infty} \langle (S^z)^2 \rangle - (\langle S^z \rangle)^2/L$. The inequality holds in general, even for a nonintegrable system, if there are conserved quantities that would make Drude weights nonvanishing away from the symmetric Hilbert-space sector $\delta = 0$. However, for integrable systems with a well-understood quasiparticle content, such as the spin-1/2 XXZ chain, the inequality can be further refined by decomposing the contribution to the diffusion constant in terms of the curvatures of the Drude-weight contributions associated with independent Bethe-ansatz quasiparticle species; see Sec. III.C.1. In this case, the velocity v_{LR} can be replaced by the corresponding dressed quasiparticle velocity (Ilievski *et al.*, 2018).

One can approach lower bounds on diffusion constants from another angle. In the same way as with the Mazur bound, Eq. (28) suggests that a nonvanishing high-temperature Drude weight is connected to the existence of linearly extensive (i.e., proportional to the volume) (quasi)local charges, one might argue that a nonvanishing high-temperature diffusion constant suggests the existence of conserved charges that are quadratically extensive. Indeed, for any locally interacting lattice system, the existence of an almost conserved quadratically extensive operator Q that has an overlap with any current operator $j_r^{(Q')}$ associated with some charge Q' leads to a rigorous bound on high-temperature diffusion constants (Prosen, 2014b) associated with that current. In other words,

$$D^{(Q')}(\beta \to 0) \geq \frac{|Q^j|^2}{8 v_{\mathrm{LR}} q}, \quad (81)$$

where the commutator $[H, Q]$ contains only boundary terms ($0 < q := \lim_{L\to\infty} \langle Q^2 \rangle / L^2 < \infty$) and $Q^j := \lim_{L\to\infty} \langle j_r^{(Q')} Q \rangle$ is finite.

This gives nontrivial lower bounds for spin-diffusion constants in the spin-1/2 Heisenberg chain as well as for spin- and charge-diffusion constants for the 1D Fermi-Hubbard model. The bound has recently been generalized and formalized using the method of hydrodynamic projections by Doyon (2019a) (see Sec. III.C.1), who used similar ideas to provide bounds on anomalous (e.g., superdiffusive) transport, i.e., to estimate the dynamical exponents.

B. Bethe-Ansatz techniques

Here we consider an important subclass of integrable models: those treatable by the collection of techniques grouped under the name of Bethe ansatz. The key property of these models is that their energy eigenstates can be expressed as scattering states of stable quasiparticles (Essler *et al.*, 2005; Korepin, Bogoliubov, and Izergin, 2005; Faddeev, 2016). This gives direct access to their energy spectrum and, more generally, to their thermodynamic properties. Although the stable quasiparticles of integrable models generically undergo nontrivial scattering processes, integrability ensures that every scattering process can always be decomposed into a sequence of two-particle scatterings.

Focusing on the paradigmatic example of the spin-1/2 XXZ chain, we introduce the central equations of the Bethe ansatz (the Bethe equations), which give access to all possible eigenstates of the systems. Then we explain how to take their thermodynamic limit, arriving at the so-called TBA description (Takahashi, 1999), where one characterizes the eigenstates in terms of "densities" of quasiparticles. Finally, we recall some results for the energy and spin Drude weight obtained using the TBA.

1. Bethe equations

There are two known routes to diagonalize the Hamiltonian using Bethe-ansatz techniques. The first one consists in writing an ansatz many-body wave function in real coordinate space. This is the original method introduced by Bethe (1931) and is now known as the coordinate Bethe-ansatz approach. The second, more recent route consists of constructing a basis of eigenstates of the fundamental transfer matrix (67) for all values of the spectral parameter λ; cf. Sec. III.A. This is always possible since transfer matrices with different spectral parameters commute. Since the Hamiltonian is proportional to the logarithmic derivative of the transfer matrix [cf. the discussion after Eq. (67)], these states are also eigenstates of H. The latter route, called the algebraic Bethe ansatz, is more powerful: it gives direct insights into the conservation laws of the system and correlation functions (Essler *et al.*, 2005; Korepin, Bogoliubov, and Izergin, 2005; Faddeev, 2016). For brevity, we do not describe such approaches in detail but report only the final results; see the aforementioned references for the derivations.

The Bethe-ansatz procedure yields the eigenstates of the system parametrized by a set of generically complex numbers $\{\lambda_j\}$ called rapidities and obtained by solving a set of nonlinear algebraic equations. For example, in the case of the spin-1/2 XXZ chain, the eigenstates with magnetization $L/2 - N$ are parametrized by the solutions $\{\lambda_j\}_{j=1}^N$ of

$$\left[\frac{\sinh(\lambda_j + i\eta/2)}{\sinh(\lambda_j - i\eta/2)}\right]^L = -\prod_{k=1}^{N} \left[\frac{\sinh(\lambda_j - \lambda_k + i\eta)}{\sinh(\lambda_j - \lambda_k - i\eta)}\right] \quad (82)$$

for $j = 1, \ldots, N$. These are the Bethe equations, first given by Bethe (1931) for $\Delta = 1$ and then by Orbach (1958) for generic Δ.

All Bethe-ansatz integrable models produce sets of nonlinear, coupled algebraic equations of this form. In some cases, however, one needs to repeat the procedure multiple times before finding the eigenstates of the Hamiltonian. This produces multiple sets of equations similar to Eq. (82) involving different sets of rapidities that are coupled together. This procedure is known as the nested Bethe ansatz and is

necessary for the Fermi-Hubbard model. For simplicity, we restrict the discussion to the non-nested case in our presentation.

The eigenvalues of the quasimomentum[15] and the Hamiltonian in the eigenstate parametrized by $\{\lambda_j\}_{j=1}^N$ are given by

$$P=\left[\sum_{k=1}^{N} p\left(\lambda_k,\frac{1}{2}\right)\right] \bmod 2\pi, \qquad E=\sum_{k=1}^{N} e(\lambda_k)+e_0 L, \tag{83}$$

where we set $p(\lambda,s)=i\log[\sinh(\lambda-i\eta s)/\sinh(\lambda+i\eta s)]$, $e(\lambda)=-\sin\eta/2\partial_\lambda p(\lambda,1/2)$, and $e_0=\Delta/4$. An expression similar to the one for the energy holds for higher local and quasilocal conservation laws [Eq. (72)]. In particular, in the eigenvalue of $Q_{n,s}$ the function $e(\lambda)$ is replaced by $q_n(\lambda,s)=(-\sin\eta/2)^n\partial_\lambda^n p(\lambda,s)$, while the constant shift e_0 is replaced by 0.

The Bethe equations might be viewed as convoluted quantization conditions for the momenta (or, better, some function of the momenta) of a gas of quasiparticles confined in a finite volume L. However, one should be careful with such an interpretation as the solutions to these equations are generically complex: this is a common feature of many Bethe-ansatz integrable models.

To understand the distribution of the roots in the complex plane, it is useful to look at the solutions for $L\to\infty$ and fixed N (Takahashi, 1999; Essler *et al.*, 2005). In this case, any $\mathrm{Im}[\lambda_j]\neq 0$ causes the lhs to go to either infinity or 0. Requiring the rhs to do the same forces the solutions to follow ordered patterns in the complex plane known as "strings." Strings can be interpreted as stable bound states formed by the elementary particles (Essler *et al.*, 2005) and appear in all Bethe-ansatz integrable models with complex rapidities, but their specific form depends on the model and on the values of its parameters. Specifically, in the spin-1/2 XXZ chain, the string structure depends on whether η is real ($|\Delta|<1$) or imaginary ($|\Delta|>1$). For instance, for $\eta\in\mathbb{R}$, we have strings of the form (Takahashi, 1999)

$$\lambda_{\alpha,a}^k=\lambda_\alpha^k+i\frac{\eta}{2}(n_k+1-2a)+i\frac{\pi}{4}(1-\upsilon_k)+\delta_{\alpha,a}^k, \tag{84}$$

where $\lambda_\alpha^k\in\mathbb{R}$ is called the string center, $k=1,\ldots,N_s$ is called the string type, $\alpha=1,\ldots,M_k$ labels different strings of the same type, and $a=1,\ldots,n_k$ labels rapidities in the same string. Finally, the string deviations $\delta_{\alpha,a}^k$ are exponentially small in L.

The number N_s of type of strings, the length n_k of the kth string, and its parity υ_k depend on η in a discontinuous way: they change drastically depending on whether or not η/π is rational. For example, for $\eta=\pi/m$, we have $N_s=m$, $n_k=(k-1)(1-\delta_{k,m})+1$, and $\upsilon_k=1$–$2\delta_{k,m}$. A similar parametrization of strings can also be performed for $i\eta\in\mathbb{R}$ and, more generally, for other Bethe-ansatz integrable models (Takahashi, 1999).

[15]On the chain, the quasimomentum operator is defined as $-i\log\Pi$ (Π acts as the one-site-shift operator).

2. Thermodynamic Bethe-ansatz formalism

For small numbers of rapidities N, the Bethe equations can be easily solved on a computer; see Hagemans (2007) and Shevchuk (2012). For a full classification of the solutions of Eq. (82), this is feasible for $N\leq L=10$. However, this procedure quickly becomes impractical when N and L increase. In particular, to study the thermodynamic limit ($N,L\to\infty$ with finite N/L) a brute force numerical solution of the equations is unfeasible and some analytical treatment becomes unavoidable. The standard approach (known as the TBA) is based on the assumption that the solutions to Eq. (82) continue to follow the string patterns even at finite density (Bethe, 1931; Takahashi, 1971), i.e., when N is not fixed but instead goes to infinity with L. Although this assumption (usually called the string hypothesis) does not strictly hold for all states in large but finite systems, it is believed to describe exactly the thermodynamic properties of all Bethe-ansatz integrable models. In particular, Tsvelick and Wiegmann (1983) proved the self-consistency of the string hypothesis for the spin-1/2 XXZ chain at finite temperature. A more rigorous alternative to the string hypothesis exists (Suzuki and Inoue, 1987; Klümper, 1992, 1993) and is often referred to as the quantum-transfer-matrix approach. Even though this approach is powerful, it is generically less versatile than the TBA (most of the results have been found for thermal states). The two approaches have been shown to give an equivalent description of the thermodynamic properties of the spin-1/2 XXZ chain at finite temperatures (Klümper, 1992; Kuniba, Sakai, and Suzuki, 1998).

Embracing the string hypothesis and multiplying together all Bethe equations referring to particles in the same string, one arrives at a set of equations (known as Bethe-Takahashi equations) for the real string centers; cf. Eq. (84). These equations can readily be viewed as quantization conditions for the momenta of the original particles and all their bound states and are most commonly expressed in logarithmic form (taking $-i\log[\cdot]$ of both sides). In particular, the Bethe-Takahashi equations for the spin-1/2 XXZ chain read as (Takahashi, 1999)

$$L\theta_j(\lambda_\alpha^j)-\sum_{k=1}^{N_s}\sum_{\gamma=1}^{M_k}\Theta_{jk}(\lambda_\alpha^j-\lambda_\gamma^k)=2\pi I_\alpha^{(j)}, \tag{85}$$

where the quantum numbers $I_\alpha^{(j)}$ are integer (half-odd integers) for odd (even) $L-M_j$ (also their allowed ranges depend on $\{M_j\}$) and the string centers λ_α^j lie in the symmetric interval $[-\Lambda,\Lambda]\subset\mathbb{R}$, while the smooth functions $\theta_j(x)$ and $\Theta_{ij}(x)$ can be expressed as

$$\theta_j(x)=f(x;n_j,\upsilon_j), \tag{86}$$

$$\Theta_{ij}(x)=f(x;|n_i-n_j|,\upsilon_i\upsilon_j)+f(x;n_i+n_j,\upsilon_i\upsilon_j)+2\sum_{k=1}^{\min(n_i,n_j)-1}f(x;|n_i-n_j|+2k,\upsilon_i\upsilon_j). \tag{87}$$

Both Λ and the form of the auxiliary function $f(x;n;\upsilon)$ depend on whether $|\Delta|<1$ or ≥ 1; their form is reported in Table II.

TABLE II. Auxiliary function $f(x;n;\upsilon)$ for the spin-1/2 XXZ chain for $\Delta=\cos\eta$. We define $\gamma\equiv|\eta|$.

	$\lvert\Delta\rvert<1$		$\lvert\Delta\rvert\geq 1$
Λ	∞		$\pi/2$
$\frac{f(x;n;\upsilon)}{2}$	$\begin{cases}\upsilon\mathrm{atan}[\frac{\tanh x}{[\tan(n\gamma/2)]^{\upsilon}}], & n\gamma\notin\mathbb{Z},\\ 0, & n\gamma\in\mathbb{Z}\end{cases}$		$\mathrm{atan}[\frac{\tan x}{\tanh(n\gamma/2)}]+\pi\lfloor\frac{x}{\pi}+\frac{1}{2}\rfloor$

Furthermore, by substituting the string hypothesis into the expectation value of the energy density [see Eq. (83)], we have

$$E=\sum_{k=1}^{N_s}\sum_{\gamma=1}^{M_k}e_k(\lambda_\gamma^k)+e_0L, \tag{88}$$

where $e_k(\lambda)\equiv-\mathrm{sgn}(\Delta+1)[\sqrt{|\Delta^2-1|}/2]\partial_\lambda\theta_k(\lambda)$ are known as "bare energies." We see that the energy of an eigenstate is obtained by summing up the bare energies of all quasiparticles characterizing it. A similar expression holds for higher conservation laws.

The set $\{I_\alpha^{(j)}\}$ is in one-to-one correspondence with the set of string centers (or particle rapidities) $\{\lambda_\alpha^{(j)}\}$ and can be used to specify the state of the system, much like momentum occupation numbers in free systems. We note that the correspondence between $\{I_\alpha^{(j)}\}$ and the solutions of the Bethe equations has been used to prove the combinatorial completeness of the Bethe ansatz for the XXZ chain (Kirillov, 1984; Kirillov and Liskova, 1997) and the Fermi-Hubbard model (Essler, Korepin, and Schoutens, 1991). The correspondence is explicitly established by introducing the counting functions

$$z_j(x|\{\lambda_\alpha^{(j)}\})\equiv\theta_j(x)-\frac{1}{L}\sum_{k=1}^{N_s}\sum_{\gamma=1}^{M_k}\Theta_{jk}(x-\lambda_\gamma^k). \tag{89}$$

These functions are monotonic in x and by definition satisfy $z_j(\lambda_\gamma^{(k)}|\{\lambda_\alpha^{(j)}\})=2\pi I_\gamma^{(k)}/L$ [this is simply a rewriting of Eq. (85)]. There are, however, some holes $\{\bar\lambda_\gamma^j\}\not\subset\{\lambda_\alpha^{(j)}\}$ such that $z_j(\bar\lambda_\gamma^j|\{\lambda_\alpha^{(j)}\})=2\pi J_\gamma^{(j)}/L$, with $\{J_\alpha^{(j)}\}$ integers (or half-odd integers) in the allowed range to be quantum numbers but not appearing in $\{I_\alpha^{(j)}\}$ (they can be thought of as empty slots).

In the thermodynamic limit, both particle and hole rapidities become dense in $[-\Lambda,\Lambda]$ (differences of neighboring rapidities scale like L^{-1}) and it is convenient to switch to a coarse grained description of the system in terms of their densities $\{\rho_j(\lambda)\}$ and $\{\rho_j^h(\lambda)\}$ (h stands for hole). It is easy to verify that $2\pi\sigma_j[\rho_j(\lambda)+\rho_j^h(\lambda)]=\lim_{L\to\infty}\partial_\lambda z_j(\lambda|\{\lambda_\alpha^{(j)}\})$, where the sign $\sigma_j=\{\pm1\}$ accounts for strings where $z_j(x|\{\lambda_\alpha^{(j)}\})$ is monotonically decreasing (they occur for $|\Delta|<1$) (Takahashi, 1999). Computing the derivative explicitly, we find the so-called thermodynamic Bethe-Takahashi equations

$$\rho_j^t(\lambda)\equiv\rho_j(\lambda)+\rho_j^h(\lambda)=\sigma_j a_j(\lambda)-\sum_{k=1}^{N_s}\sigma_j T_{jk}*\rho_k(\lambda). \tag{90}$$

Here we have introduced the driving $a_j(\lambda)=(1/2\pi)\partial_\lambda\theta_j(\lambda)$ and the kernel $T_{jk}(\lambda)=(1/2\pi)\partial_\lambda\Theta_{jk}(\lambda)$ (encoding all information about the interactions), while the asterisk denotes the convolution $f*g(x)=\int_{-\Lambda}^{\Lambda}dy f(x-y)g(y)$.

Equation (90) fixes the densities of holes in terms of the densities of particles. In other words, for each state it provides the densities $\rho_j^t(\lambda)$ of rapidity slots (called "vacancies") that can be occupied by a particle. Because of the interactions, the density of slots depends on the state; cf. the second term on the rhs of Eq. (90). Integral equations of this form are common in the TBA. In the following, we find many instances of these equations with the same kernel but different driving functions.

Even though each eigenstate of the Hamiltonian corresponds to a set of densities $\{\rho_j(\lambda)\}$, the correspondence is generically not one to one: in a large finite volume L, there are approximately $\exp[Ls[\rho]]$ eigenstates of the Hamiltonian corresponding to the same set of densities $\{\rho_j(\lambda)\}$, where the functional $s[\rho]=\sum_k\int d\lambda(\rho_k^t\log\rho_k^t-\rho_k\log\rho_k-\rho_k^h\log\rho_k^h)$ is known as the Yang-Yang entropy density. This fact is often referred to by saying that the densities of rapidities specify a "macrostate" of the system, as opposed to a single eigenstate of the Hamiltonian, which is called a "microstate."

The densities of rapidities in principle allow one to compute the expectation values of all local operators in the thermodynamic limit. In practice, however, explicit expressions are known for only a few classes of observables; see also Sec. III.C. A relevant example is that of local and quasilocal conserved-charge densities. Specifically, considering the density of the generic charge Q, we have

$$q[\rho]=\sum_{k=1}^{N_s}\int d\lambda q_k(\lambda)\rho_k(\lambda), \tag{91}$$

where the set of functions $q_k(\lambda)$ specifies the charge and is often called the bare charge. The energy density is obtained by replacing $q_k(\lambda)$ with $e_k(\lambda)$ and adding the constant shift e_0. Moreover, setting $q_k(\lambda)=q_{n,k}(s,\lambda)$ for an appropriate $q_{n,k}(s,\lambda)$, one reproduces the density of higher conservation laws (72). In particular, for the densities $q_n[\rho]$ of the higher local conserved charges (66), we have $q_k(\lambda)=q_{n,k}(\lambda)=\{-\mathrm{sgn}(\Delta+1)[\sqrt{|\Delta^2-1|}/2]\partial_\lambda\}^{n+1}\theta_k(\lambda)$.

The TBA can also be used to analyze excitations over macrostates. We now take a large finite volume L and consider the system in one of the microstates corresponding to the densities $\{\rho_j(\lambda)\}$. Injecting an extra string of type j and rapidity λ induces a change in the expectation values of the conserved charges

$$Lq[\rho]\mapsto Lq[\rho]+q_j^d(\lambda). \tag{92}$$

Owing to the presence of interactions, $\{q_j^d(\lambda)\}$ differ from the bare charges of Eq. (91) and are commonly referred to as dressed charges. Specifically, given a set of bare charges $\{q_j(\lambda)\}$ one can find the corresponding dressed charges through the following integral equation:

$$\partial_\lambda q_j^d(\lambda)=\partial_\lambda q_j(\lambda)-\sum_{k=1}^{N_s}\sigma_k[T_{jk}*\vartheta_k\partial_\lambda q_k^d](\lambda), \tag{93}$$

where we have introduced the filling function

$$\vartheta_j(\lambda) \equiv \frac{\rho_j(\lambda)}{\rho_j^t(\lambda)}. \tag{94}$$

Even though the momentum is conserved only modulo 2π, a dressed momentum is well defined as long as $p_j^d(\lambda) < 2\pi$. In particular, since the bare charge related to the momentum is $\theta_j(\lambda)$ [cf. Eq. (83)], the dressed momentum fulfills $\partial_\lambda p_j^d(\lambda) = 2\pi\sigma_j\rho_j^t(\lambda)$. This can be established by comparing the equation for the dressed momentum with Eq. (90) and allows us to express the group velocity of the excitation (λ, j) as

$$v_j^d(\lambda) = \frac{\partial_\lambda e_j^d(\lambda)}{\partial_\lambda p_j^d(\lambda)} = \frac{\partial_\lambda e_j^d(\lambda)}{2\pi\sigma_j\rho_j^t(\lambda)}. \tag{95}$$

In other words, $2\pi\sigma_j\rho_j^t(\lambda)v_j^d(\lambda)$ fulfills Eq. (93) with $\partial_\lambda e_j(\lambda)$ as a driving. In addition to the dressed charge, we can associate another "dressed" quantity, sometimes called the effective charge, to each quasilocal conservation law (and also to the momentum). For a given bare charge $q_j(\lambda)$, we define the associated effective charge $q_j^{\mathrm{eff}}(\lambda)$ as the solution of the following equation, which has $q_j(\lambda)$ as its driving term,

$$q_j^{\mathrm{eff}}(\lambda) = q_j(\lambda) - \sum_{k=1}^{N_s} \sigma_k [T_{jk} * \vartheta_k q_k^{\mathrm{eff}}](\lambda). \tag{96}$$

Note that in this case, one directly dresses the charge and not its derivative, and hence dressed and effective charges do not coincide. We have, however, $\partial_\lambda(q_j^d(\lambda)) = (\partial_\lambda q_j(\lambda))^{\mathrm{eff}}$ such that we can equivalently express Eq. (95) as $v_j^d(\lambda) = (\partial_\lambda e_j(\lambda))^{\mathrm{eff}}/(\partial_\lambda p_j(\lambda))^{\mathrm{eff}}$. This formulation is used in a large portion of the GHD literature.

In closing, we remark that, even though here we assume the system to be in an eigenstate of the Hamiltonian, the TBA description can also be used for some stationary mixed states. This is true every time a generalized microcanonical representation applies (Essler and Fagotti, 2016; Vidmar and Rigol, 2016). In essence, this means that the expectation values of all local observables in the mixed state can be reproduced in the thermodynamic limit by expectation values in a single, appropriately chosen eigenstate of the Hamiltonian. For example, the densities corresponding to a generalized Gibbs ensemble (GGE) $\rho_{\mathrm{GGE}} \propto \exp[-\sum_n \beta_n Q_n]$ can be found minimizing the generalized free energy $f[\rho] = \sum_n \beta_n q_n[\rho] - s[\rho]$, which yields the following integral equation (Yang and Yang, 1969):

$$\log\eta_j(\lambda) = \sum_n \beta_n q_{n,j}(\lambda) + \sum_{k=1}^{N_s} \sigma_k T_{kj} * \log[1+\eta_k^{-1}](\lambda), \tag{97}$$

where we have introduced the function

$$\eta_j(\lambda) \equiv \frac{\rho_j^h(\lambda)}{\rho_j(\lambda)} = \frac{1}{\vartheta_j(\lambda)} - 1. \tag{98}$$

These equations, together with Eq. (90), completely fix the densities of the generalized Gibbs state. Note that if $\{\rho_j(\lambda)\}$ and $\{\rho_j^h(\lambda)\}$ solve Eqs. (90) and (97), the generalized free energy can be written compactly as

$$f = \frac{e_0}{T} - \sum_{k=1}^{N_s} \sigma_k \int_{-\Lambda}^{\Lambda} d\lambda\, a_k(\lambda) \log\left[1 + \frac{\rho_k(\lambda)}{\rho_k^h(\lambda)}\right]. \tag{99}$$

We also remark that the derivatives of $\log\eta_k(\lambda)$ with respect to the chemical potentials β_n are related to the dressed quantities. Indeed, comparing Eqs. (93) and (97) we find $\partial_{\beta_n}\log\eta_k(\lambda) = -\mathrm{sgn}(\Delta+1)[\sqrt{|\Delta^2-1|}/2]\partial_\lambda q_{n-1,k}^d(s,\lambda)$. To find the explicit form of $q_{n,k}(\lambda)$, we use the explicit form of $q_{n,k}(\lambda)$ reported after Eq. (91).

3. Drude weights from the TBA

As an application of the TBA formalism, here we present the calculation of certain Drude weights. We remark that the calculation of generic Drude weights remained unfeasible for a long time even in Bethe-ansatz integrable models. Indeed, Drude weights are expressed in terms of dynamical correlations and the calculation of the latter falls outside the compass of standard Bethe-ansatz techniques. In some cases, however, it has been possible to relate Drude weights to simple spectral or thermodynamic properties that can be efficiently determined using the TBA. In particular, here we review Zotos's calculations of the energy (Zotos, 2017) and spin (Zotos, 1999) Drude weights for the spin-1/2 XXZ chain with $\Delta = \cos(\pi/m)$ at finite temperature T. The results for the energy Drude weight are directly generalized to any Δ while those for the spin Drude have been extended to $\Delta = \cos(\pi\ell/m)$ with coprime integers ℓ and m (Urichuk *et al.*, 2019); see Sec. III.C.1 for a discussion.

We begin by considering the case of the energy Drude weight, which is considerably simpler. The crucial observation (Zotos, Naef, and Prelovšek, 1997) is that in the spin-1/2 XXZ chain the total energy current $\mathcal{J}^{(\mathrm{E})} = \sum_r j_r^{(\mathrm{E})}$ [see Eq. (5)] is itself a conserved quantity. In particular, in our notation $\mathcal{J}^{(\mathrm{E})}$ coincides with Q_2; see Eq. (66). This means that one can define a generalized Gibbs ensemble including such a current as a charge, i.e., $\rho_{\mathrm{GGE}} \propto e^{-\beta H - \xi\mathcal{J}^{(\mathrm{E})}}$, and compute its root densities following the method at the end of Sec. III.B.2. In particular, the free-energy density f_ξ of this state takes the form of Eq. (99), where the densities of rapidities fulfill Eqs. (90) and (97) with $\beta_1 = \beta$, $\beta_2 = \xi$, and $\beta_{n\geq 3} = 0$. The Drude weight is then straightforwardly evaluated as [see Eq. (21)]

$$\mathcal{D}_{\mathrm{w}}^{(\mathrm{E})} = \frac{\beta^2}{2L}\langle(\mathcal{J}^{(\mathrm{E})})^2\rangle = -\frac{\beta^3}{2}\partial_\xi^2 f_\xi|_{\xi=0}. \tag{100}$$

Note that this identity was first used by Klümper and Sakai (2002) to compute the energy Drude weight within the quantum-transfer-matrix approach. The results are shown in Fig. 5. Subsequently, Zotos found the explicit result from the TBA by combining Eqs. (90) and (97). Using some straightforward identities among the TBA functions [see Urichuk *et al.* (2019)], the final expression can be written as

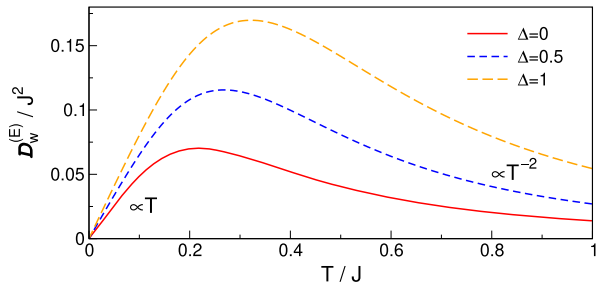

FIG. 5. Exact results for the energy Drude weight of the spin-1/2 *XXZ* chain given in Eq. (1) at zero magnetization. The data were taken from Klümper and Sakai (2002).

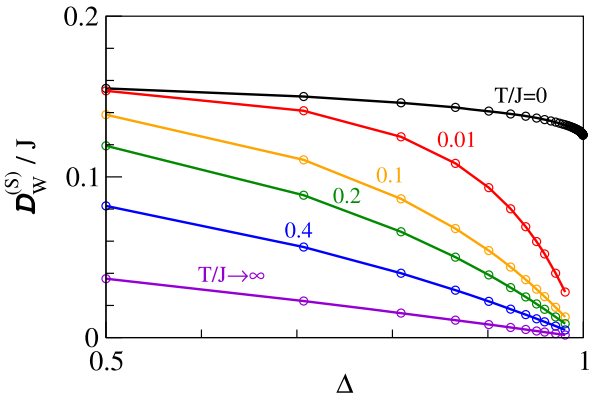

FIG. 6. TBA results for the spin Drude weight $\mathcal{D}_{\mathrm{w}}^{(\mathrm{S})}$ of the spin-1/2 *XXZ* chain vs Δ for different temperatures T (measured in units of J). From Zotos, 1999.

$$\mathcal{D}_{\mathrm{w}}^{(\mathrm{E})}=\frac{\beta^2}{2}\sum_{k=1}^{N_s}\int_{-\Lambda}^{\Lambda}d\lambda\frac{\rho_k^t(\lambda)[e_k^{\mathrm{eff}}(\lambda)]^2[v_k^d(\lambda)]^2}{[1+\eta_k(\lambda)][1+\eta_k^{-1}(\lambda)]},\tag{101}$$

where $e_k^{\mathrm{eff}}(\lambda)=-2\pi\mathrm{sgn}(\Delta+1)[\sqrt{|\Delta^2-1|}/2]\sigma_k\rho_k^t(\lambda)$ is the effective energy and $v_k^d(\lambda)$ is the group velocity of the dressed excitations; cf. Eq. (95). The same method can be used to find higher cumulants of $\mathcal{J}^{(E)}$ (Urichuk *et al.*, 2019; Zotos, 2017).

The complication arising when considering the spin Drude weight is that the total spin current, as opposed to the total energy current, is not conserved. The calculation, however, can still be performed by avoiding the explicit evaluation of correlation functions. The idea is to consider the system in a large finite volume L, introduce a finite magnetic flux ϕ through the chain, and compute the Drude weight using the finite-T Kohn formula (26), i.e., in terms of the second derivative of the energy density with respect to the magnetic flux. The insertion of a magnetic flux can be easily treated in the Bethe ansatz and results in a phase ("twist") $e^{i\phi}$ multiplying the rhs of Eq. (82). For ϕ finite in the thermodynamic limit (i.e., when ϕ does not scale with the volume), the twist modifies the position of the rapidities of the strings only at subleading orders. This leads to

$$\lambda_{\alpha,L}^j(\phi)=\lambda_{\alpha,\infty}^j+\frac{g_{1,j}(\lambda_{\alpha,\infty}^j,\phi)}{L}+\frac{g_{2,j}(\lambda_{\alpha,\infty}^j,\phi)}{L^2},\tag{102}$$

where we have neglected $O(L^{-3})$ and introduced the subscripts L and ∞ to label rapidities in finite and infinite volumes, respectively. The ϕ-dependent functions $g_{1,j}(x,\phi)$ and $g_{2,j}(x,\phi)$ fulfill some integral equations determined through a $1/L$ expansion of the Bethe-Takahashi equations (85). Plugging Eq. (102) into Eq. (88), one can determine the second derivative of the energy density with respect to the twist in the thermodynamic limit and hence the Drude weight. This method was introduced by Fujimoto and Kawakami (1998) for the calculation of the charge Drude weight in the Fermi-Hubbard model and was applied by Zotos (1999) to the spin-1/2 *XXZ* chain. In the case of the *XXZ* chain, the result can be cast into the following form:

$$\mathcal{D}_{\mathrm{w}}^{(\mathrm{S})}=\frac{\beta}{2}\sum_{k=1}^{N_s}\int_{-\Lambda}^{\Lambda}d\lambda\frac{\rho_k^t(\lambda)[n_k^{\mathrm{eff}}(\lambda)]^2[v_k^d(\lambda)]^2}{[1+\eta_k(\lambda)][1+\eta_k^{-1}(\lambda)]},\tag{103}$$

where $n_k^{\mathrm{eff}}(\lambda)=2\pi\sigma_k\rho_k^t(\lambda)\partial_\phi g_{1,k}(\lambda)$ fulfills the dressing equation (96) by replacing $n_k^{\mathrm{eff}}(\lambda)\to q_k^{\mathrm{eff}}(\lambda)$ with driving n_k, thus replacing $q_k(\lambda)$ with n_k in Eq. (96); cf. Eq. (84) for the definition of n_k. The temperature dependence of $\mathcal{D}_{\mathrm{w}}^{(\mathrm{S})}$ is illustrated in Fig. 6.

As we see in Sec. III.C, GHD provides a general framework for computing Drude weights in the TBA formalism. In particular, Eqs. (101) and (103) are both special cases of the generic GHD result given in Eq. (116), which describes the Drude weights of all conserved charges.

C. Generalized hydrodynamics

The theory of generalized hydrodynamics concerns the evolution of integrable systems initially prepared in a state ρ_0 that is spatially inhomogeneous and then left to evolve unitarily with a homogeneous Hamiltonian. The main idea is that at large times the expectation values of local observables become slowly varying functions of x and t. This is much like the situation observed in the case of homogeneous quantum quenches [see Eisert, Friesdorf, and Gogolin (2015), Essler and Fagotti (2016), and Gogolin and Eisert (2016)]: initially the expectation values of local observables display fast oscillations, but the latter dephase away for large times and expectation values become stationary even in the presence of a coherent unitary evolution. In the slow, late-time regime, it is reasonable to expect that the expectation values can be described by a quasistationary state, namely,

$$\mathrm{tr}[\mathcal{O}_x e^{-iHt}\rho_0 e^{iHt}]\overset{t\gg\tau_0}{\sim}\mathrm{tr}[\mathcal{O}_x\rho_{\mathrm{st}}(x,t)],\tag{104}$$

where H is the Hamiltonian of the system, $\mathcal{O}_x$ is a generic observable localized around the point x, $\rho_{\mathrm{st}}(x,t)$ is the density-matrix describing the quasistationary state (retaining a slow space-time dependence), and τ_0 is the timescale for local relaxation. In general, the x dependence in Eq. (104) is nontrivial for large but finite times, while it is typically washed away at infinite times. Think of the free expansion of a gas released from a trap: the density of the gas vanishes for all x at infinite times, corresponding to an x-independent $\lim_{t\to\infty}\rho_{\mathrm{st}}(x,t)$. There are some cases, however, where

nontrivial effects of the problem's inhomogeneity persist even at infinite times. In that case, one can explicitly take the infinite-time limit of Eq. (104), thereby turning it into an exact statement. An example is the so-called bipartitioning protocol, where one suddenly joins together two systems that are initially in different stationary states; see Sec. IX.B.

The state $\rho_{\rm st}(x,t)$ in Eq. (104) has been termed the locally quasistationary state by Bertini and Fagotti (2016). Specifically, it was argued that, at the leading order in time, $\rho_{\rm st}(x,t)$ is a generalized Gibbs state constructed with the charges of the Hamiltonian that controls the unitary time evolution and (x,t)-dependent chemical potentials. Note that the timescale at which the simplification (104) arises (often referred to as Euler timescale) is much larger than the local relaxation timescale τ_0. This means that, at fixed (x,t), $\rho_{\rm st}(x,t)$ is homogeneous and stationary and admits a "microcanonical" representation in terms of a TBA representative eigenstate or, equivalently, of a set of densities of rapidities $\{\rho_k(\lambda,x,t)\}$. Determining such space-time–dependent functions is the central objective of the theory.

A macroscopic number of constraints on these functions are obtained by considering the expectation values of the continuity equations of all local and quasilocal conserved charges from Eq. (72), namely,

$$\partial_t q_x^{(n)}(t) + j_x^{(n)}(t) - j_{x-1}^{(n)}(t) = 0, \quad x = 1,\dots,L, \tag{105}$$

where $q_x^{(n)}$ is the density of charge Q_n and $j_x^{(n)}$ is its current.[16] Here and in the following we suppress the additional index s, keeping only the generic index n for conserved charges. Assuming the validity of Eq. (104), one obtains that, to leading order in time, the expectation value of Eq. (105) reads as

$$\partial_t {\rm tr}[q_0^{(n)}\rho_{\rm st}(x,t)] + \partial_x {\rm tr}[j_0^{(n)}\rho_{\rm st}(x,t)] = 0. \tag{106}$$

We remark that this equation is already in the thermodynamic limit and, moreover, on its rhs, there are subleading corrections of $\mathcal{O}(t^{-b})$ with $b>0$. As shown by Bertini *et al.* (2016) and Castro-Alvaredo, Doyon, and Yoshimura (2016), the constraint (106) is sufficient to fix the densities of rapidities to leading order in time. Specifically, Eq. (106) is equivalent to the following continuity equation for the densities of rapidities:

$$\partial_t \rho_k(\lambda,x,t) + \partial_x(v_k^d(\lambda,x,t)\rho_k(\lambda,x,t)) = 0. \tag{107}$$

Here $v_k^d(\lambda,x,t)$ is the group velocity of dressed excitations on the state $\rho_{\rm st}(x,t)$. The physical interpretation of this equation is straightforward: to leading order in time, the dynamics of $\{\rho_k(\lambda,x,t)\}$ can be described as if they were quasimomentum distributions for N_s species of free classical particles moving in a density-dependent background. Indeed, the only effect of the interaction is a dressing of the group velocity. These classical particles can be thought of as an asymptotic version of the stable modes characterizing Bethe-ansatz integrable models. Indeed, for long times and large distances, the modes lose all phase information and behave like classical particles.

The crucial step in passing from Eq. (106) to Eq. (107) makes use of the following expression for the expectation value of generic currents on the macrostate $\{\rho_n(\lambda)\}$:

$$j^{Q}[\rho] = \sum_{k=1}^{N_s} \int d\lambda q_k(\lambda) v_k^d(\lambda)\rho_k(\lambda), \tag{108}$$

where $q_k(\lambda)$ is the bare charge of the associated density; cf. Eq. (91). This form was originally proposed for relativistic integrable quantum-field theories with diagonal scattering (Castro-Alvaredo, Doyon, and Yoshimura, 2016) through a crossing-symmetry argument, and for the spin-1/2 XXZ chain (Bertini *et al.*, 2016) through a semiclassical argument. Initially, however, its validity could be established only numerically (Bertini *et al.*, 2016; Ilievski and De Nardis, 2017a) or for some special currents (Bertini *et al.*, 2016; Urichuk *et al.*, 2019). The numerical accuracy of Eq. (108) and its model-independent form triggered a fervent activity aimed at proving it rigorously (Fagotti, 2017a; Vu and Yoshimura, 2019; Borsi, Pozsgay, and Pristyák, 2020; Yoshimura and Spohn, 2020) for all Bethe-ansatz integrable models. This endeavor was concluded by Pozsgay (2020), who reported a complete proof of Eq. (108) in the framework of the quantum-inverse scattering method. This proof encompasses all Yang-Baxter integrable lattice systems. In particular, this includes all Bethe-ansatz integrable lattice models (nested or not), such as the spin-1/2 XXZ chain and the one-dimensional Fermi-Hubbard model. Finally, we remark that the form of Eq. (108) for the expectation values of currents has also been shown to hold for certain integrable classical field theories (Bastianello *et al.*, 2018; Bulchandani, Cao, and Moore, 2019; Cao, Bulchandani, and Spohn, 2019; Doyon, 2019b; Spohn, 2020b).

The simplification introduced by Eq. (107) is noteworthy: to determine the late-time properties of an integrable quantum many-body system, one needs to solve a system of differential equations for a function of three variables, rather than the Schrödinger equation for a number of particles of the order of the Avogadro number. After discretizing the rapidity, one can treat these equations using standard methods for initial-value partial differential equations (Møller and Schmiedmayer, 2020), characteristics (Bulchandani, 2017; Doyon, Spohn, and Yoshimura, 2018), or molecular dynamics (Doyon, Yoshimura, and Caux, 2018), i.e., by simulating the dynamics of the classical gas whose rapidity distributions obey Eq. (107). There is, however, a remaining nontrivial step to make before a solution can be obtained: one has to find the right initial conditions for $\{\rho_k(\lambda,x,t)\}$. This problem has not yet been solved for all initial states ρ_0, but rather only for a number of particular choices (Bulchandani *et al.*, 2017, 2018; Doyon *et al.*, 2017; Caux *et al.*, 2019). Some of these choices give a good characterization of experimentally accessible initial configurations. This was explicitly demonstrated in two recent cold-atom experiments (Schemmer *et al.*, 2019; Malvania *et al.*, 2020) that showed that GHD describes the dynamics of nearly integrable 1D Bose gases accurately in all accessible interaction regimes.

[16] We simplify here the notation introduced in Sec. II by writing $j_x^{(n)}$ instead of $j_x^{(Q_n)}$.

We now focus on the most popular initial configuration accessible with GHD: the bipartitioning protocol, i.e., the time evolution of an initial state composed of the tensor product of two different homogeneous states $\rho_0 \sim \rho_L \otimes \rho_R$; see Sec. IX.B. As mentioned earlier, since in this case we can explicitly take the infinite-time limit, Eq. (107) becomes exact. The solution is a function of the scaling variable $\zeta = x/t$, usually termed the "ray," and can be implicitly written as (Bertini *et al.*, 2016; Castro-Alvaredo, Doyon, and Yoshimura, 2016)

$$\vartheta_k(\lambda,\zeta) = [\vartheta_k^{\mathrm{L}}(\lambda) - \vartheta_k^{\mathrm{R}}(\lambda)]\Theta[v_k^d(\lambda,\zeta) - \zeta] + \vartheta_k^{\mathrm{R}}(\lambda), \tag{109}$$

where $\Theta(x)$ is the step function and $\vartheta_k^{\mathrm{L/R}}(\lambda)$ characterize the homogeneous GGE emerging at infinite distance from the junction on the left and right, respectively.[17] This solution is implicit because $v_k^d(\lambda,\zeta)$ itself depends on $\vartheta_k(\lambda,\zeta)$. The explicit result is obtained by formulating an initial guess for $v_k^d(\lambda,\zeta)$ and iterating Eqs. (109), (90), and (96) until convergence is reached (typically in fewer than ten steps). This protocol has been used for studying nonlinear transport in integrable quantum many-body systems on the lattice (Bertini *et al.*, 2016; De Luca, Collura, and De Nardis, 2017; Bertini and Piroli, 2018; Bertini, Piroli, and Calabrese, 2018; Collura, De Luca, and Viti, 2018; Mazza *et al.*, 2018; Gruber and Eisler, 2019) as well as on the continuum (Castro-Alvaredo, Doyon, and Yoshimura, 2016; Bertini, Piroli, and Kormos, 2019; Mestyán *et al.*, 2019). Moreover, it has also been used for analyzing the dynamics of entanglement in inhomogeneous situations (Alba, 2018; Bertini *et al.*, 2018; Alba, Bertini, and Fagotti, 2019; Mestyán and Alba, 2020). In Sec. III.C.1, we discuss how this protocol can be used for computing Drude weights.

In concluding this review of GHD, we mention that Eq. (107) does not represent an end point: there are currently many ongoing efforts to extend its range of applicability. To begin, the equation furnishes only a leading-order-in-time characterization or, more precisely, describes the system for long times t and length scales $x \sim t$. In analogy with ordinary hydrodynamics, however, one would expect GHD to also describe the asymptotic behavior of the system on other length scales, such as the diffusive one where $x \sim \sqrt{t}$. This can be achieved by finding the subleading corrections in t to Eq. (107). In particular, in Sec. III.C.2, we discuss a correction, recently identified by De Nardis, Bernard, and Doyon (2018), which can describe diffusive behaviors. Currently, however, a systematic method to find all subleading corrections to Eq. (107) has been devised only in the non-interacting case (Fagotti, 2017b; Fagotti, 2020). Another active research strand is to extend Eq. (107) to the case in which the time evolution is determined by a spatially inhomogeneous or time-dependent Hamiltonian, where space and time variations are slow. In particular, Doyon and Yoshimura (2017) presented an extension that is valid in the case of a system confined to a slowly varying trapping potential, Bastianello, Alba, and Caux (2019) considered the case of position-dependent Hamiltonian parameters, and Bastianello and De Luca (2019) studied the effects of time-dependent magnetic fields. Finally, there are ongoing efforts to describe the evolution of the initial-state correlations under Eq. (107) (Ruggiero *et al.*, 2020).

1. GHD results for Drude weights

Drude weights can be computed within GHD following two different approaches that give coinciding results. Both approaches give access to the most general Drude weight

$$\begin{aligned}\mathcal{D}_{\mathrm{w}}^{(n,m)} &= \frac{\beta}{2}\lim_{t\to\infty}\frac{1}{t}\sum_r \int_{-t/2}^{t/2} ds \langle j_r^{(n)}(s) j_0^{(m)}(0)\rangle^{\mathrm{c}} \\ &= \frac{\beta}{2}\lim_{t\to\infty}\sum_r \mathrm{Re}[\langle j_r^{(n)}(t) j_0^{(m)}(0)\rangle^{\mathrm{c}}],\end{aligned} \tag{110}$$

where $\langle\cdot\rangle^{\mathrm{c}}$ denotes the connected expectation value in a grand-canonical Gibbs ensemble $\rho_{\mathrm{GE}} \propto \exp[-\beta H + \sum_i \lambda_i N_i]$ [the sum in the exponent of ρ_{GE} runs over all conserved U(1) charges N_i of the system, such as the total particle number and the magnetization]. In Eq. (110), n and m can label two different conserved charges. In the case where $n = m$, one recovers the usual diagonal Drude weight of the charge Q_n. All results, however, can be directly extended to the case of expectation values in more general GGEs. Note that (i) in order to treat all charges on the same footing, we divided the energy Drude weight by β, and (ii) the correlation function in Eq. (110) is not the Kubo correlation used in Eq. (9). In the limit $t \to \infty$, the two expressions can be shown to coincide under mild assumptions (Ilievski and Prosen, 2013).[18]

The first approach, proposed by Bulchandani *et al.* (2017) and Ilievski and De Nardis (2017b), evaluates the Drude weight using the following formulation. One considers a bipartitioning protocol that connects two halves of the system [left (L) and right (R)] initially prepared for the following GGEs:

$$\rho_{\mathrm{GGE,L/R}} \propto \exp\left[-\beta H + \sum_i \mu_i N_i \pm (\beta_m/2) Q_m\right], \tag{111}$$

where Q_m is the mth conserved charge of the system. In this setting, one can compute $\mathcal{D}_{\mathrm{w}}^{(n,m)}$ as follows (Vasseur, Karrasch, and Moore, 2015):

$$\mathcal{D}_{\mathrm{w}}^{(n,m)} = \lim_{\beta_m\to 0}\lim_{t\to\infty}\frac{\beta}{2t\beta_m}\mathrm{tr}[j_0^{(n)} e^{-iHt}\rho_0 e^{iHt}], \tag{112}$$

where $\rho_0 \sim \rho_{\mathrm{GGE,L}} \otimes \rho_{\mathrm{GGE,R}}$. Then, using Eq. (108) one can express this relation in terms of TBA quantities as

[17] We assume that $\rho_{\mathrm{L/R}}$ have cluster decomposition properties; namely, that they satisfy $\lim_{|x-y|\to\infty}\langle O_1(x)O_2(y)\rangle_{\mathrm{L/R}} = \langle O_1(x)\rangle_{\mathrm{L/R}}\langle O_2(y)\rangle_{\mathrm{L/R}}$, where the operators $O_i(x)$ are local (i.e, they act trivially far from the site x_i) and $\langle O(x)\rangle_{\mathrm{L/R}} \equiv \mathrm{tr}[O(x)\rho_{\mathrm{L/R}}]$.

[18] For integrable models, $\lim_{t\to\infty}\sum_r \langle j_r^{(n)}(t) j_0^{(n)}(0)\rangle^{\mathrm{c}}$ turns out to be real. This implies that the Drude weight can also be defined using an asymmetric integration, namely, $\mathcal{D}_{\mathrm{w}}^{(n,m)} = (\beta/2)\lim_{t\to\infty}(1/t)\sum_r \int_0^t ds \langle j_r^{(n)}(s) j_0^{(m)}(0)\rangle^{\mathrm{c}}$.

$$\mathcal{D}_{\mathrm{w}}^{(n,m)} = \frac{\beta}{2}\sum_{k=1}^{N_s}\int d\zeta \int_{-\Lambda}^{\Lambda} d\lambda q_{n,k}(\lambda)\frac{\partial[v_k^d(\lambda,\zeta)\rho_k(\lambda,\zeta)]}{\partial\beta_m}\Big|_{\beta_m=0}, \tag{113}$$

where $q_{n,k}(\lambda)$ are the bare charges corresponding to Q_n.

The second approach, introduced by Doyon and Spohn (2017), computes the Drude weight using hydrodynamic projections. The idea is to write the Drude weight in the form of Eq. (110) and expand it in the basis of appropriately orthogonalized conserved charges. More precisely, one views

$$\sum_r \langle j_r^{(n)}(t) j_0^{(n)}(0)\rangle^{\mathrm{c}} \equiv (j^{(n)}|j^{(m)}) \tag{114}$$

as a scalar product in the space of local operators and assumes that the only contributions surviving at infinite times are coming from the overlap with conserved-charge densities

$$\lim_{t\to\infty}(j^{(n)}|j^{(m)}) = \sum_{k,k'}(j^{(n)}|q^{(k)})[\mathfrak{C}^{-1}]_{kk'}(q^{(k')}|j^{(m)}), \tag{115}$$

where we define $\mathfrak{C}_{nm} = (q^{(n)}|q^{(m)})$. This reasoning is similar in spirit to that leading to the Mazur bound, but it is carried out directly in the thermodynamic limit. In general, this approach can be used to compute the asymptotic behavior (large t, large x) of dynamical correlation functions in generic inhomogeneous situations (Doyon, 2018).

The quantities appearing in Eq. (115) are all directly computed within GHD and lead to the following final result:

$$\mathcal{D}_{\mathrm{w}}^{(n,m)} = \frac{\beta}{2}\sum_{k=1}^{N_s}\int_{-\Lambda}^{\Lambda} d\lambda \frac{\rho_k^t(\lambda)[v_k^d(\lambda)]^2 q_{n,k}^{\mathrm{eff}}(\lambda) q_{m,k}^{\mathrm{eff}}(\lambda)}{[1+\eta_k(\lambda)][1+\eta_k^{-1}(\lambda)]}, \tag{116}$$

where $v_k^d(\lambda)$ and $q_{m,k}^{\mathrm{eff}}(\lambda)$ are the group velocity of excitations and the effective charge in the Gibbs state, respectively [i.e., with densities of rapidities obtained from solving Eqs. (90) and (97) with all Lagrange multipliers vanishing except β and μ]. As shown by Doyon and Spohn (2017), this expression agrees with that obtained from Eq. (113) if one plugs in the implicit solution [Eq. (109)] of the GHD equation for the bipartitioning protocol and takes the derivative explicitly.

Three generic features of Eq. (116) are (i) it is symmetric under the exchange of n and m, which is in accord with Onsager reciprocal relations; (ii) the Drude weight is obtained by summing up elementary Drude weights [the integrand of Eq. (116)] for each quasiparticle in the system; and (iii) the Drude weight of a certain quantity vanishes when the associated effective charges vanish. This happens in the case of the spin transport in the spin-1/2 XXZ chain with $|\Delta| \geq 1$ at zero magnetization and for the charge transport in the Fermi-Hubbard model at half filling.

Equation (116) holds for all TBA solvable models. Its generalization to the nested case was first reported by Ilievski and De Nardis (2017a) and, again, corresponds to a sum of elementary Drude weights for each type of quasiparticle in the system. In particular, we see that Eq. (116) agrees with the special cases of Eqs. (101) and (103) discussed in Sec. III.B.3 once one restores the trivial β factor in the energy Drude weight. Moreover, the nested generalization of Eq. (116) reproduces the result given by Fujimoto and Kawakami (1998) for the charge Drude weight in the Fermi-Hubbard model. This follows from a direct comparison between Eqs. (5) and (7) of Ilievski and De Nardis (2017a) and the expression derived by Fujimoto and Kawakami (1998) [see Eq. (35) in their work]; nonetheless, to the best of our knowledge it has not been noticed in the literature. The main point is to note that $\xi_c(k), \xi_{sk}(\lambda), \xi_{bk}(\lambda)$ given by Fujimoto and Kawakami (1998) are exactly the effective electron charges for the Fermi-Hubbard chain; cf. Eqs. (A46) in the Supplemental Material of Ilievski and De Nardis (2017a). In other words, they fulfill the nested generalization of the dressing equations (96) with driving terms, respectively, given by $\xi_c^0(k) = 1$, $\xi_{sk}^0(\lambda) = 0$, $\xi_{bk}^0(\lambda) = 2k$; cf. Eqs. (15)–(17) and (29)–(31) of Fujimoto and Kawakami (1998).

2. GHD results for diffusion constants

To access the diffusive regime, one needs to identify the leading corrections to Eq. (106), which go beyond the Euler scale. A scheme to achieve this goal (based on two main assumptions) was proposed by De Nardis, Bernard, and Doyon (2018); see also Gopalakrishnan *et al.* (2018), De Nardis, Bernard, and Doyon (2019), and Gopalakrishnan and Vasseur (2019). The first assumption is that for large t the system can also be characterized using hydrodynamics on length scales $x \sim \sqrt{t}$. Namely, one assumes that local observables are still described by a slowly varying quasistationary state $\rho_{\mathrm{st}}(x,t)$. This state, however, cannot be interpreted as a space-time–dependent GGE anymore, but it has contributions proportional to the spatial derivatives of the Lagrange multipliers. Under this assumption, Eq. (106) also continues to hold to the first subleading order. The expectation values of the currents are no longer given by Eq. (108) and include corrections written in terms of spatial derivatives of the densities of rapidities. Specifically, they can be written as (De Nardis, Bernard, and Doyon, 2019)

$$\mathrm{tr}[j_{n,0}\rho_{\mathrm{st}}(x,t)] = \sum_{k=1}^{N_s}\int d\lambda q_{n,k}(\lambda) v_k^d(\lambda)\rho_k(\lambda,x,t) - \frac{1}{2}\int d\lambda d\mu \sum_{k,k'=1}^{N_s} q_{n,k}(\lambda)\mathfrak{D}_{k,k'}(\lambda,\mu)\partial_x\rho_{k'}(\mu,x,t), \tag{117}$$

where the kernel $\mathfrak{D}_{k,k'}(\lambda,\mu)$ depends on $\{\rho_k(\mu,x,t)\}$. This kernel is related to the diffusion (Onsager) matrix defined as[19]

$$D_{n,m} = \sum_r \int_{-\infty}^{\infty} dt \left(\langle j_r^{(n)}(t) j_0^{(m)}(0)\rangle^c - \frac{2}{\beta}\mathcal{D}_{\mathrm{w}}^{(n,m)} \right) \tag{118}$$

as follows (De Nardis, Bernard, and Doyon, 2018):

[19]Note that Eq. (118) does not coincide with the Onsager matrix given in Eq. (15), as in the latter we use Kubo correlation functions. Once again, however, the two matrices can be shown to coincide under mild assumptions (Ilievski and Prosen, 2013).

$$D_{n,m} = \sum_p \int d\lambda d\mu \sum_{k,k'=1}^{N_s} q_{n,k}(\lambda)\mathfrak{D}_{k,k'}(\lambda,\mu)q_{p,k'}(\lambda)\mathfrak{C}_{pm}, \tag{119}$$

where the first sum is over all conserved charges of the system and the matrix $\mathfrak{C}_{pm}$ was introduced after Eq. (115). Note that it is always possible to add a derivative term $\propto o_x - o_{x-1}$ to a charge density (where o_x is a local operator) without modifying the total charge. This introduces an ambiguity in the definition of charge densities beyond the leading order; see Fagotti (2020) for more details. In particular, the kernel $\mathfrak{D}_{k,k'}(\lambda,\mu)$ depends on the specific choice of the densities of charges, while the Onsager matrix is invariant (De Nardis, Bernard, and Doyon, 2019). The simple relation (119) is obtained by taking charges and currents to be scalar under $\mathcal{PT}$ symmetry (De Nardis, Bernard, and Doyon, 2019). Finally, we remark that corrections similar to Eq. (117), i.e., depending on the spatial derivatives of the densities of rapidities, appear in the expectation values of all local observables with kernels that are generically unknown.

The explicit TBA expression for Eq. (118) in models with a single species of quasiparticles was determined by De Nardis, Bernard, and Doyon (2018) through an expansion in finite-temperature form factors.[20] In particular, it has been shown that Eq. (118) is fully determined by form factors involving two particle-hole excitations. The expression for an arbitrary number of quasiparticles species was later presented by De Nardis, Bernard, and Doyon (2019) and reads as

$$D_{n,m} = \int \frac{d\mu_1 d\mu_2}{2} \sum_{k,k'=1}^{N_s} \left\{ \frac{\rho_k^h(\mu_1)}{1+\eta_k(\mu_1)} \frac{\rho_{k'}^h(\mu_2)}{1+\eta_{k'}(\mu_2)} \left(\frac{T^{\mathrm{eff}}_{k',k}(\mu_2,\mu_1) q^{\mathrm{eff}}_{n,k'}(\mu_2)}{\sigma_{k'}\rho^t_{k'}(\mu_2)} - \frac{T^{\mathrm{eff}}_{k,k'}(\mu_1,\mu_2) q^{\mathrm{eff}}_{n,k}(\mu_1)}{\sigma_k \rho^t_k(\mu_1)} \right) \right.$$
$$\left. \times \left(\frac{T^{\mathrm{eff}}_{k',k}(\mu_2,\mu_1) q^{\mathrm{eff}}_{m,k'}(\mu_2)}{\sigma_{k'}\rho^t_{k'}(\mu_2)} - \frac{T^{\mathrm{eff}}_{k,k'}(\mu_1,\mu_2) q^{\mathrm{eff}}_{m,k}(\mu_1)}{\sigma_k \rho^t_k(\mu_1)} \right) |v^d_k(\mu_1) - v^d_{k'}(\mu_2)| \right\}, \tag{120}$$

where both the effective charges $q^{\mathrm{eff}}_{n,k}(\lambda)$ and the effective scattering kernel $T^{\mathrm{eff}}_{k,k'}(\lambda,\mu)$ fulfill Eq. (96), with driving functions given by $q_{n,k}(\lambda)$ and $T_{k,k'}(\lambda-\mu)$ [$T^{\mathrm{eff}}_{k,k'}(\lambda,\mu)$ for fixed values of its second arguments k' and μ], respectively. We note that to obtain Eq. (120) De Nardis, Bernard, and Doyon conjectured a general form for the kinematical poles for finite-density form factors: this represents the second main assumption made by De Nardis, Bernard, and Doyon (2018).

Equation (120) can be interpreted by realizing that at the diffusive scale the conserved modes of interacting integrable models, i.e., the quasiparticles, do not follow exactly free classical trajectories. As a consequence of the scattering, they undergo a noisy motion around the classical trajectories with a variance that grows as $\sqrt{t}$. Such noisy motion is responsible for the diffusive behavior (Gopalakrishnan *et al.*, 2018; De Nardis, Bernard, and Doyon, 2019; Gopalakrishnan and Vasseur, 2019). This simple argument can be refined to obtain a quantitative prediction in agreement with Eq. (120) in the linear-response regime (Gopalakrishnan *et al.*, 2018). Moreover, in accordance with this interpretation, Eq. (120) vanishes for noninteracting models. Finally, we mention that a nontrivial check of Eq. (120) was recently presented by Doyon (2019a) and Medenjak, De Nardis, and Yoshimura (2020), who reobtained the equation using the hydrodynamic projection method.

Including the diffusive correction equation (117) in the expectation value of the currents, the continuity equation for the space-time–dependent densities of rapidities takes the following Navier-Stokes form (De Nardis, Bernard, and Doyon, 2018):

$$\partial_t \rho_k(\lambda,x,t) + \partial_x\left(v^d_k(\lambda,x,t)\rho_k(\lambda,x,t)\right) = \frac{1}{2}\partial_x\left[\int d\mu \sum_{k'=1}^{N_s} \mathfrak{D}_{k,k'}(\lambda,\mu)\partial_x \rho_{k'}(\mu,x,t)\right]. \tag{121}$$

Of particular interest for this review is the case of the spin-1/2 XXZ chain with $|\Delta| > 1$ for small perturbations around a zero-magnetization ($m_z = 0$) equilibrium state. In this case, Eq. (121) leads to the following heatlike equation for the profile $m(x,t)$ of the magnetization density (De Nardis, Bernard, and Doyon, 2019):

$$\partial_t m_z(x,t) = D^{(\mathrm{S})}\partial_x^2 m_z(x,t), \tag{122}$$

where the spin-diffusion constant is given by the sum over the elementary diffusion constants of different quasiparticles

$$D^{(\mathrm{S})} = \sum_{k=1}^{N_s} \int_{-\pi/2}^{\pi/2} d\mu \frac{\rho^h_k(\mu)}{1+\eta_k(\mu)} |v^d_k(\mu)| \mathcal{W}_k^2. \tag{123}$$

Here the rapidity-independent coefficient $\mathcal{W}_k$ reads as (De Nardis *et al.*, 2019)

$$\mathcal{W}_k = \lim_{k'\to\infty} \frac{T^{\mathrm{eff}}_{k',k}(\mu,\lambda)}{\rho^t_{k'}(\mu)} = \frac{1}{2T\chi(\beta)}\partial_\delta n^{\mathrm{eff}}_k, \tag{124}$$

where n^{eff}_k is the effective magnetization [cf. Eq. (84) for the definition of n_k and Eq. (96) for that of effective charges], T is the temperature, $\chi(\beta)$ is the static susceptibility, and δ is a small deviation from zero magnetization.

As shown by De Nardis *et al.* (2019), substituting Eq. (124) into Eq. (123) and performing a few manipulations, one obtains an expression for the diffusion constant that has the

[20] In this context, the term "form factor" indicates the matrix element of a local operator between two Hamiltonian eigenstates.

same form as the right-hand side of the bound in Eq. (79) but involves a modified spin Drude weight.

IV. THEORETICAL AND COMPUTATIONAL METHODS

While integrable systems as such in principle allow for analytically exact solutions, computing the current autocorrelation functions that enter into the Kubo formalism is a formidable task, and no complete and general solution from Bethe-ansatz techniques currently exists. Moreover, for nonintegrable models one needs to resort to mostly numerical methods or universal low-energy descriptions such as bosonization.

We concentrate here on the discussion on the specifics of the spin-1/2 XXZ chain for concreteness and point out aspects that are important for the theoretical treatment of other models when necessary.

A. Low-energy theory

1. Field theory

The low-energy excitations of a large class of 1D models are not fermionic quasiparticles but rather collective bosonic modes, forming the so-called Tomonaga-Luttinger liquid (TLL) (Giamarchi, 2004; Schönhammer, 2004). The low-energy theory can be solved using bosonization, and the corresponding bosonic field theory takes the form (for one fermionic species)

$$H = \frac{v}{2}\int dx\ [\Pi^2 + (\partial_x\phi)^2], \tag{125}$$

where Π is the conjugate momentum of the bosonic field ϕ with the commutation relation $[\phi(x), \Pi(y)] = i\delta(x-y)$. The TLL parameter K, which usually appears as a prefactor $1/K^2$ in front of the second term, has already been absorbed via a canonical transformation of the fields. For multiple species, such as the case of the Hubbard chain, the low-energy Hamiltonian is a sum of independent Luttinger liquids. For the Hubbard chain, these describe collective charge and spin excitations.

For integrable systems, both K and the spin velocity v can be computed from the Bethe ansatz. For example, for the spin-1/2 XXZ chain, one obtains [see Essler and Konik (2005)]

$$K = \frac{\pi}{2}\frac{1}{\pi - \arccos(\Delta)}, \qquad v = J\frac{\pi}{2}\frac{\sqrt{1-\Delta^2}}{\arccos\Delta}. \tag{126}$$

The current operators associated with the spin density $\sim\partial_x\phi$ and the energy density of the Tomonaga-Luttinger-liquid Hamiltonian take the form (Heidrich-Meisner *et al.*, 2002; Giamarchi, 2004)

$$\mathcal{J}^{(\mathrm{S})} = -v\sqrt{\frac{K}{\pi}}\int dx\,\Pi, \qquad \mathcal{J}^{(\mathrm{E})} = -v^2\int dx\,\Pi\partial_x\phi \tag{127}$$

and are both strictly conserved. The corresponding Drude weights read

$$\mathcal{D}_{\mathrm{w}}^{(\mathrm{S})} = \frac{Kv}{2\pi}, \qquad \mathcal{D}_{\mathrm{w}}^{(\mathrm{E})} = \frac{\pi}{6}vT. \tag{128}$$

If a certain microscopic model falls into the TLL universality class, the low-energy behavior of various correlation functions, such as the momentum distribution or the local density of states, is determined by Eq. (125). Transport properties, however, are nonuniversal: On the microscopic level of lattice Hamiltonians, they depend on integrability and the model parameters. In contrast, all gapless spin chains fall into the TLL universality class and at low T map to Eq. (125), which by virtue of Eq. (128) describes a ballistic conductor (Giamarchi, 1991, 1992). Information about the microscopic origin of the integrability and the conserved charges is thus lost by going to the continuum limit. The information on integrability is in principle contained in relations between the irrelevant operators that are discarded in the process. Accounting for these relations in the calculation of transport coefficients in a systematic manner is technically difficult and has not yet been accomplished.

To describe transport beyond the purely ballistic case, one needs to resort to a more generic low-energy Hamiltonian. The RG irrelevant corrections to Eq. (125) that are most important in this context are given by umklapp scattering and band curvature as

$$H_{\mathrm{u}} = \lambda_{\mathrm{u}}\int dx\,\cos(4\sqrt{\pi K}\phi),$$
$$H_{\mathrm{b}} = \int dx[\lambda_+(\partial_x\phi_L)^2(\partial_x\phi_R)^2 + \lambda_-(\partial_x\phi_L)^4 + \lambda_-(\partial_x\phi_R)^4], \tag{129}$$

where $\phi = \phi_L + \phi_R$, and the prefactors $\lambda_{\mathrm{u},+,-}$ are known for integrable systems (Lukyanov, 1998). In an extension of earlier works (Giamarchi and Schulz, 1988; Giamarchi, 1992), the influence of these terms was studied via a finite-T bosonic self-energy perturbation theory (Sirker, Pereira, and Affleck, 2009, 2011). This leads to a purely diffusive form of the optical spin conductivity

$$\sigma_q(\omega) = \frac{Kv}{\pi}\frac{i\omega}{[1+b(T)]\omega^2 - [1+c(T)]v^2q^2 + 2i\gamma(T)\omega}, \tag{130}$$

whose real part takes the following Lorentzian form in the long-wavelength limit $q \to 0$:

$$\sigma'(\omega) = \frac{Kv}{\pi}\frac{2\gamma(T)}{[1+b(T)]^2\omega^2 + 4\gamma(T)^2}. \tag{131}$$

The coefficients $b(T)$ and $c(T)$ as well as the decay rate $\gamma(T)$ are functions of $v, K, \lambda_{\mathrm{u},+,-}$, with $\gamma, b, c \to 0$ for $T \to 0$. In the zero-temperature limit, Eq. (131) recovers the expression for $\mathcal{D}_{\mathrm{w}}^{(\mathrm{S})}$ from Eq. (128). The Drude-weight contribution to the conductivity at finite T, however, is missed and can presently be accounted for only by hand (Sirker, Pereira, and Affleck, 2011) using a memory-matrix approach; see Rosch and Andrei (2000).

Other exceptions to Luttinger-liquid universality are real-time, real-space correlators, which for free lattice fermions are already governed by high-energy excitations. Further insights can be gained from nonlinear TLL theory (Imambekov, Schmidt, and Glazman, 2012).

The previously mentioned bosonic self-energy perturbation-theory approach (Sirker, Pereira, and Affleck, 2011) can also be used to compute the density correlation function. One finds that at long times the density autocorrelations are governed by a diffusive term $\sim\sqrt{\gamma/t}$, which is consistent with numerical time-dependent DMRG (tDMRG) data (Karrasch, Pereira, and Sirker, 2015) but disagrees with earlier field-theory predictions (Narozhny, 1996). The formalism was subsequently extended to incorporate the effects of nonlinear Luttinger liquids at finite temperature (Karrasch, Pereira, and Sirker, 2015). While the integrability of a system drastically affects the longtime behavior of the global current autocorrelation function (i.e., the Drude weight), one does not expect such a drastic influence on the density-density correlations of local density operators such as s^z_r. Thus, there is no need to incorporate conserved quantities by hand, and field-theoretical approaches can be used to determine the longtime behavior of these quantities at low energies (Sirker, Pereira, and Affleck, 2011; Karrasch, Pereira, and Sirker, 2015).

2. Semiclassical approach

Damle and Sachdev introduced a semiclassical picture of thermally excited particles to compute the low-temperature behavior of the integrable, gapped, quantum O(3) nonlinear sigma model (Sachdev and Damle, 1997; Damle and Sachdev, 1998), as well as that of the sine-Gordon field theory (Damle and Sachdev, 2005). The former describes the low-energy behavior of integer-S (i.e., gapped) quantum spin chains in the limit of large S, for which the work of Damle and Sachdev predicts a zero Drude weight (Sachdev and Damle, 2000) and diffusive dynamics with a conductivity that at low temperatures diverges as $\sigma_{\mathrm{dc}} \propto 1/\sqrt{T}$. The methodology was subsequently extended into various directions: for example, a hybrid semiclassical-DMRG framework was developed (Moca, Kormos, and Zaránd, 2017) and out-of-equilibrium setups were studied (Bertini, Piroli, and Kormos, 2019; Werner *et al.*, 2019).

The range of validity of the semiclassical approach was investigated both for the sine-Gordon model and for integer-S spin chains by comparing them with DMRG or GHD results (Moca, Kormos, and Zaránd, 2017; Bertini, Piroli, and Kormos, 2019; De Nardis *et al.*, 2019; Werner *et al.*, 2019). The current belief is that semiclassics give the correct qualitative prediction for the low-temperature limit.

B. Exact diagonalization

Exact diagonalization (ED) has been a major workhorse in the numerical analysis of finite-temperature transport properties (Zotos and Prelovšek, 1996; Narozhny, Millis, and Andrei, 1998; Heidrich-Meisner *et al.*, 2003; Rabson, Narozhny, and Millis, 2004; Herbrych, Prelovšek, and Zotos, 2011; Karrasch *et al.*, 2013). The entire spectrum and all eigenstates are computed, and therefore practically any observable or correlation function can be extracted. However, there is the limitation that only small system sizes can be accessed. For the spin-1/2 XXZ chain, routinely, the Hamiltonian can be diagonalized for $L \sim 20$ sites by exploiting translational invariance [see Sandvik (2010) for the implementation of U(1) and discrete symmetries in ED]. Accessing $L \sim 24$ is possible with some effort (Heidrich-Meisner, Honecker, and Vekua, 2006) for spin-1/2 chains. For the Hubbard chain, the larger local Hibert space of four states further restricts the accessible system sizes, which can be overcome by using dynamical typicality as described in Sec. IV.C. Technically, one needs to properly account for the fermionic statistics, which is important for correlation functions yet a standard and well-known aspect of the numerical treatment of fermionic systems.

1. Formal expressions evaluated in ED

We illustrate the main aspects for the example of the thermal and the spin conductivity in the spin-1/2 XXZ chain. The relevant expressions result from Eq. (12) by expanding the thermal expectation values in a basis of many-body eigenstates $|n\rangle$, which we understand to be taken from a subspace with fixed total magnetization S^z. Strictly speaking, by doing so we work with a finite system and hence take $t \to \infty$ first and $L \to \infty$ next. We first discuss the expressions and then comment on this conceptual aspect. Note that one can work in a canonical ensemble, i.e., at a fixed S^z. In this case, the sums in the following expressions run over all eigenstates from that subspace. Alternatively, one can carry out a grand-canonical average over all values of S^z. Then the sums have to be understood as

$$\sum_n \to \sum_{S^z} \sum_{n(S^z)}, \tag{132}$$

where the second sum runs over all eigenstates in the subspace with fixed S^z.

For the spin conductivity, we obtain the following generic situation in which both the Drude weight $\mathcal{D}_{\mathrm{w}}^{(\mathrm{S})}$ and the regular part $\sigma_{\mathrm{reg}}(\omega)$ can be nonzero in finite systems:

$$\mathcal{D}_{\mathrm{w}}^{(\mathrm{S})} = \frac{1}{2L}\left[\langle -T_{\mathrm{kin}}\rangle - 2\sum_{\substack{n,n'\\ E_n\neq E_{n'}}} p_n \frac{|\langle n|\mathcal{J}^{(\mathrm{S})}|n'\rangle|^2}{E_{n'}-E_n}\right], \tag{133}$$

$$\sigma_{\mathrm{reg}}(\omega) = \frac{\pi}{L}\frac{1-e^{-\beta\omega}}{\omega}\sum_{\substack{n,n'\\ E_n\neq E_{n'}}} p_n |\langle n|\mathcal{J}^{(\mathrm{S})}|n'\rangle|^2 \delta(\omega-(E_{n'}-E_n)), \tag{134}$$

where $p_n = e^{-\beta E_n}/Z$ in the canonical case and $e^{-\beta E_n-\beta b S^z}/Z$ in the grand-canonical case and Z is the partition function (b is the magnetic field). T_{kin} is the kinetic energy, which for the spin-1/2 XXZ chain from Eq. (1) contains all terms except those proportional to $s^z_r s^z_{r+1}$.

In a 1D system, the Drude weight can also be obtained from the diagonal matrix elements of the current operator plus contributions from degenerate subspaces:

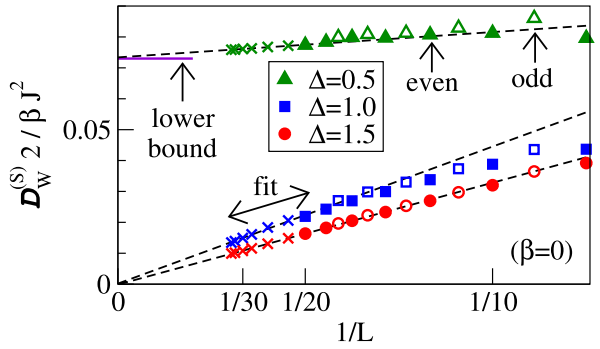

FIG. 7. Finite-size scaling of the spin Drude weight $\mathcal{D}_{\mathrm{w}}^{(\mathrm{S})}$ in the high-temperature limit $\beta = 0$, as presented by Steinigeweg, Gemmer, and Brenig (2014, 2015). Crosses indicate dynamical quantum typicality (DQT) data while other symbols indicate ED data. Similar ED data were given by Zotos and Prelovšek (1996), Heidrich-Meisner *et al.* (2003), Rabson, Narozhny, and Millis (2004), Herbrych, Prelovšek, and Zotos (2011), and Karrasch *et al.* (2013).

$$\mathcal{D}_{\mathrm{w}}^{(\mathrm{S})} = \frac{1}{2TL} \sum_{\substack{n,n' \\ E_n = E_{n'}}} p_n |\langle n|\mathcal{J}^{(\mathrm{S})}|n'\rangle|^2, \tag{135}$$

which results from the absence of any superfluid density in a 1D system at finite temperatures (Zotos, Naef, and Prelovšek, 1997). Equations (133) and (135) are identical at (i) $\beta = 0$ and (ii) $\beta > 0$ in the thermodynamic limit. Practically, they are already indistinguishable at sufficiently high temperatures for the accessible system sizes $L \lesssim 20$ (Heidrich-Meisner *et al.*, 2003; Mukerjee and Shastry, 2008).

An example for ED data for the spin Drude weight of the XXZ chain is shown in Fig. 7; the data were obtained in a grand-canonical ensemble using periodic boundary conditions. These results are discussed further in Sec. VI. Here we note that for $\beta = 0$ and the commensurate value $\Delta = \cos(\pi/3) = 1/2$, the convergence seems fast and indeed yields agreement with other methods such as the lower bound (Prosen and Ilievski, 2013), tDMRG (see the discussion in Sec. VI.C.4) or the TBA (Zotos, 1999; Urichuk *et al.*, 2019). A recent Bethe-ansatz-based calculation (Klümper and Sakai, 2019) of the spin Drude weight for commensurate values such as $m = 3, 4, 5, 6$ in $\Delta = \cos(\pi/m)$ observes increasingly large finite-size effects at lower temperatures. One should realize, though, that this calculation extracts the Drude weight from a set of rapidities, which is unlike the grand-canonical or canonical ensemble used in exact diagonalization. Therefore, no quantitative insight on the finite-size dependencies of other methods can be gained from Klümper and Sakai (2019).

For thermal transport (or any transport channel for which the current is exactly conserved), the expression for the associated Drude weight can be further simplified from the form of Eq. (135), resulting in

$$\mathcal{D}_{\mathrm{w}}^{(\mathrm{E})} = \frac{1}{2T^2 L} \sum_n p_n \langle n|(\mathcal{J}^{(\mathrm{E})})^2|n\rangle. \tag{136}$$

This quantity exhibits the same mild finite-size dependencies as the specific heat (Alvarez and Gros, 2002a). For instance, for $L = 20$ the ED data agree well with the exact solution for $\mathcal{D}_{\mathrm{w}}^{(\mathrm{E})}$ down to $T \gtrsim 0.25J$ (Heidrich-Meisner *et al.*, 2002).

As an alternative to the aforementioned expressions, one can also extract the spin Drude weight from the average curvature of many-body eigenstates in systems with twisted boundary conditions parametrized via ϕ (Kohn, 1964):

$$\mathcal{D}_{\mathrm{w}}^{(\mathrm{S})} = \frac{1}{2L} \sum_n p_n \left(\frac{\partial^2 E_n(\phi)}{\partial \phi^2} \right) \Big|_{\phi=0}. \tag{137}$$

This has the advantage that only eigenenergies need to be evaluated, but a numerical differentiation is required.

2. Role of boundary conditions, symmetries, and choice of ensemble

The choice of the boundary conditions, symmetries, and ensemble can all affect the finite-size data and their convergence to the $L \to \infty$ limit.

For systems with periodic boundary conditions, one observes weight in $\sigma_{\mathrm{reg}}(\omega)$ in a frequency window $\omega < 1/L$ for certain values of the anisotropy Δ (Naef and Zotos, 1998; Herbrych, Steinigeweg, and Prelovšek, 2012). Similarly, for systems with open boundary conditions, the Drude weight is exactly zero for finite L, but there are precursor peaks in $\sigma_{\mathrm{reg}}(\omega)$ at small frequencies that move toward $\omega = 0$ as L increases (Rigol and Shastry, 2008; Brenes *et al.*, 2018). These observations suggest subtleties in extracting $\mathcal{D}_{\mathrm{w}}^{(\mathrm{S})}$ from finite-size data at exactly zero frequency. A useful strategy is to work with twisted boundary conditions [also inspired by Kohn's expression (137)] and a finite nonzero twist angle. This reduces the symmetries of the problem (see the later discussion) and the convergence with respect to L can be accelerated (Sánchez and Varma, 2017).

The choice of the ensemble for the computation of the Drude weight can matter as well. Specifically, states appearing in the sum over n in Eq. (135) can be chosen from either a single subspace with a fixed S^z (canonical approach) or an average over all S^z (grand-canonical version). For concreteness, we focus on the case of a vanishing external magnetic field corresponding to a vanishing average $\langle S^z \rangle = 0$. For large systems, one expects these different ensembles to yield the same result, which is confirmed in numerical simulations (Karrasch *et al.*, 2013; Sánchez and Varma, 2017), yet in finite systems the differences can be significant. For instance, at $\Delta = 0$ the grand-canonical version converges faster to the $L = \infty$ result, while close to $\Delta = 1$ the convergence of canonical data seems to be faster (Herbrych, Prelovšek, and Zotos, 2011; Karrasch *et al.*, 2013).

Symmetry constraints on the matrix elements of $\langle n|\mathcal{J}^{(\mathrm{S})}|m\rangle$ play another important role and are at the root of some of the aforementioned finite-size dependencies. For instance, in the $S^z = 0$ subspace (L even) that is symmetric under spin inversion $F^\dagger s_r^z F = -s_r^z$, all diagonal matrix elements vanish identically, i.e., $\langle n|\mathcal{J}^{(\mathrm{S})}|n\rangle = 0$, since the spin current is antisymmetric under F. One can extend this to show that there is no contribution from the $S^z = 0$ subspace on finite systems with L even and incommensurate values of $\Delta \neq \cos(\pi \ell/m)$ (for $m > \ell$ and ℓ, m coprimes, $L > 2m$) at all

(Sánchez and Varma, 2017). Therefore, in a canonical evaluation of $\mathcal{D}_{\mathrm{w}}^{(\mathrm{S})}$, the leading contribution for small S^z comes from odd L and $S^z = 1/2$ (Herbrych, Prelovšek, and Zotos, 2011). For commensurate $\Delta = \cos(\pi\ell/m)$, degeneracies appear for $L \geq L_{\mathrm{min}} = 2m$ (Sánchez and Varma, 2017), implying that for certain values of Δ and small L essential contributions to $\mathcal{D}_{\mathrm{w}}^{(\mathrm{S})}$ are missed. Because of the sum rule, these contributions must sit at small frequencies on smaller system sizes, and therefore a rather intricate, size-dependent transfer of weight from low to zero frequency occurs; see Naef and Zotos (1998) for an early discussion. A comprehensive discussion of symmetry constraints on the matrix elements of the spin current and an analysis of contributions of degenerate and nondegenerate subspaces were given by Narozhny, Millis, and Andrei (1998), Mukerjee and Shastry (2008), and, in particular, Sánchez and Varma (2017).

A theory for the finite-size dependencies of the Drude weight would be highly desirable. An interpretation was put forward by Steinigeweg, Herbrych, and Prelovšek (2013) [see also Prosen (1999)]: the Drude weight [see Eq. (135)] up to degeneracies measures the spread of diagonal matrix elements of current operators in eigenstates and is thus a measure of how closely this observable already obeys the eigenstate thermalization hypothesis (ETH) (D'Alessio *et al.*, 2016) on finite systems. On general grounds, one therefore expects an exponential decrease with system size for nonintegrable models [which is consistent with many ED studies; see Zotos and Prelovšek (1996), Prosen (1999), and Heidrich-Meisner *et al.* (2004b)], which obey ETH, and a power-law dependence for integrable models. These qualitative expectations for the L dependence of the Drude weight are supported in most cases for system sizes larger than a crossover length scale (Steinigeweg, Herbrych, and Prelovšek, 2013).

The calculation of the regular part requires a strategy to deal with the δ functions such as broadening or binning procedures when working directly in frequency space. The finite system size sets a lower bound on the accessible frequency range below which finite-size effects dominate. At low temperatures, a conservative estimate is $\omega \gtrsim 1/L$, while at high temperatures much lower frequencies can be accessed due to the dominant contributions from dense portions of the many-body spectrum.

3. Pitfalls

We now discuss the subtle point of the order of limits that was taken, i.e., $L \to \infty$ after $t \to \infty$, which is the opposite of what is formally required. This is born out of the desire to operate with a closed expression for Drude weights rather than having to compute time-dependent quantities first and then carry out the limits. In fact, there is no known way of expressing the Drude weight other than introducing a discrete set of eigenstates and hence going to infinite t at finite L first.

In ED, this approach is unavoidable, since system sizes are finite by definition. What could go wrong? One might be worried about mistaking a nonintegrable system for a ballistic conductor, since every finite system with discrete lattice translation invariance can have nonzero finite-T Drude weights in the spin, charge, or energy channel. Thus, a careful finite-size analysis is required to deal with this. In those cases

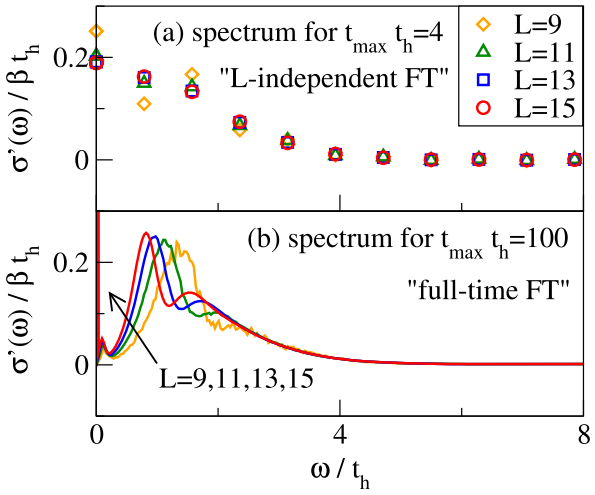

FIG. 8. Frequency dependence of the charge conductivity in the Fermi-Hubbard chain at $U/t_{\mathrm{h}} = 16$ and $\beta = 0$ and at half filling, as obtained from Fourier transforming real-time data that uses (a) short times that are L independent, $t_{\mathrm{max}} t_{\mathrm{h}} = 4$, and (b) long times of $t_{\mathrm{max}} t_{\mathrm{h}} = 100$ (Jin *et al.*, 2015). See Sec. VII and Eq. (178) for the definition of the Hamiltonian.

for which exact or accepted results for the Drude weight are known (such as free systems or the energy Drude weight of the spin-1/2 XXZ chain), increasing the system size in ED data leads to systematic convergence to the correct result. This observation lends confidence to the reliability of the analysis of finite-size trends. Care must be taken in the vicinity of integrable points, including limiting cases of free particles such as the spin-1/2 XX chain, where the generic expectation is that microscopic physics will unveil itself only once large systems are reached. Thus, the ED analysis of nonintegrable points better commences from points deep in the nonintegrable regime (Heidrich-Meisner *et al.*, 2004b).

Another pitfall can arise in the analysis of finite-frequency contributions, either from real-time data or directly in frequency space. A conservative approach is to consider only data that are L independent, thus discarding the long times and low-frequency regime. An example is illustrated in the upper panel of Fig. 8; if the Fourier transformation is cut off at a short timescale, convergence in L can be achieved. The Fourier transformation of longtime data (lower panel) shows significant finite-size effects at small frequencies (Prelovšek *et al.*, 2004; Jin *et al.*, 2015).

C. Dynamical quantum typicality

The concept of quantum typicality essentially states that a single pure state $|\psi\rangle$ can have the same properties as the ensemble density matrix ρ (Gemmer and Mahler, 2003; Goldstein *et al.*, 2006; Popescu, Short, and Winter, 2006). To be specific, here we look at the expectation value of an observable A, i.e.,

$$\mathrm{tr}[\rho(t)A] = \langle\psi(t)|A|\psi(t)\rangle + \varepsilon \tag{138}$$

(Reimann, 2007; Bartsch and Gemmer, 2009), where ε is a negligibly small correction (as discussed later in more

detail). If $|\psi\rangle = |n\rangle$ is a single eigenstate with energy E_n and $\rho = \rho_{\mathrm{mc}}$ is the microcanonical ensemble in an energy shell $E \approx E_n$, then Eq. (138) becomes the diagonal part of the well-known ETH

$$\mathrm{tr}[\rho_{\mathrm{mc}} A] = \langle n|A|n\rangle + \varepsilon \tag{139}$$

(Deutsch, 1991; Srednicki, 1994; Rigol, Dunjko, and Olshanii, 2008). Even though the ETH is an assumption, there is solid evidence that it holds for local few-body observables in nonintegrable many-body systems (Nandkishore and Huse, 2015; D'Alessio *et al.*, 2016). However, in contrast to ETH, Eq. (138) is a mathematically rigorous statement if $|\psi\rangle$ is essentially drawn at random from a sufficiently large Hilbert space (Reimann, 2007; Bartsch and Gemmer, 2009). In fact, the idea of using random states $|\psi\rangle$ has a long history (Alben *et al.*, 1975; De Raedt and De Vries, 1989; Jaklič and Prelovšek, 1994) and is at the basis of various numerical approaches to the density of states (Hams and De Raedt, 2000), thermodynamic quantities (De Vries and De Raedt, 1993; Sugiura and Shimizu, 2012, 2013; Wietek *et al.*, 2019), equilibrium correlation functions (Iitaka and Ebisuzaki, 2003; Elsayed and Fine, 2013; Steinigeweg, Gemmer, and Brenig, 2014; Steinigeweg, Herbrych, Zotos, and Brenig, 2016; Rousochatzakis *et al.*, 2019), nonequilibrium processes (Monnai and Sugita, 2014; Endo, Hotta, and Shimizu, 2018; Richter, Lamann *et al.*, 2019), and ETH (Steinigeweg, Khodja *et al.*, 2014). In this review, we focus on the case of equilibrium correlation functions.

Using the idea of quantum typicality and considering the canonical ensemble $\rho \propto e^{-\beta H}$, the equilibrium autocorrelation function of an operator A can be written as (Iitaka and Ebisuzaki, 2003; Elsayed and Fine, 2013; Steinigeweg, Gemmer, and Brenig, 2014; Steinigeweg, Herbrych, Zotos, and Brenig, 2016)

$$\mathrm{Re}\langle A(t)A\rangle = \mathrm{Re}\langle\psi|A(t)A|\psi\rangle + \varepsilon, \tag{140}$$

with the pure state

$$|\psi\rangle = \frac{\sqrt{\rho}|\Phi\rangle}{\sqrt{\langle\Phi|\rho|\Phi\rangle}}, \qquad \rho \propto e^{-\beta H}, \tag{141}$$

where the reference pure state $|\Phi\rangle$ reads

$$|\Phi\rangle = \sum_k c_k |k\rangle. \tag{142}$$

Here $|k\rangle$ can be any orthonormal basis; for example, it can be the common eigenbasis of symmetries. In the basis considered, the complex coefficients c_k must be chosen according to the unitary invariant Haar measure (Bartsch and Gemmer, 2009); i.e., $\mathrm{Re}c_k$ and $\mathrm{Im}c_k$ have to be drawn at random from a Gaussian distribution with zero mean.[21] Assuming A to be a local operator in real space (or a sum of L such operators), the statistical error ε in Eq. (140) is bounded from above by

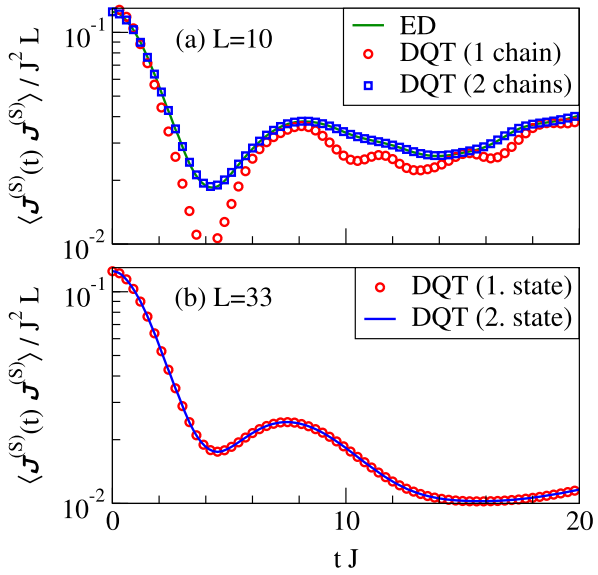

FIG. 9. Accuracy of the DQT approximation, illustrated for the spin-current autocorrelation function in the spin-1/2 XXZ chain at the isotropic point $\Delta = 1$ and infinite temperatures $\beta = 0$ (Steinigeweg, Gemmer, and Brenig, 2015). (a) ED vs DQT for a chain (with a total Hilbert-space dimension of $\dim = 2^L$) and an uncoupled ladder ($\dim = 4^L \gg 2^L$) with $L = 10$. (b) DQT for $L = 33$ and two randomly drawn pure states. For the behavior of spin-spin correlations see Balz *et al.* (2018).

$\varepsilon < \mathcal{O}(1/\sqrt{\dim_{\mathrm{eff}}})$, where $\dim_{\mathrm{eff}} = \mathrm{tr}[e^{-\beta(H-E_0)}]$ is the partition function with the ground-state energy E_0. At $\beta = 0$, $\dim_{\mathrm{eff}} = \dim$. Thus, ε decreases exponentially fast as L is increased and eventually vanishes for $L \to \infty$. At $\beta \neq 0$, ε can still be expected to decrease exponentially, but less quickly. The accuracy of the approximation (140) for finite L is illustrated in Fig. 9 and can be checked in practice by comparing it to the exact correlation function or by comparing the results for two or more randomly drawn pure states. For a discussion of the full probability distribution of pure-state expectation values, see Reimann and Gemmer (2019).

The central advantage of the rhs of Eq. (140) is that its evaluation can be done without knowing eigenstates and eigenenergies. To this end, it is convenient to introduce the two auxiliary pure states

$$|\Phi_\beta(t)\rangle = e^{-iHt}\sqrt{\rho}|\phi\rangle, \qquad |\varphi_\beta(t)\rangle = e^{-iHt}A\sqrt{\rho}|\phi\rangle \tag{143}$$

and rewrite Eq. (140) as

$$\mathrm{Re}\langle A(t)A\rangle = \frac{\mathrm{Re}\langle\Phi_\beta(t)|A|\varphi_\beta(t)\rangle}{\langle\Phi_\beta(0)|\Phi_\beta(0)\rangle} + \varepsilon \tag{144}$$

(Iitaka and Ebisuzaki, 2003; Elsayed and Fine, 2013; Steinigeweg, Gemmer, and Brenig, 2014; Steinigeweg, Herbrych, Zotos, and Brenig, 2016). Then the dependence on t and β occurs as a property of pure states only and can be obtained by solving the Schrödinger equation in real and imaginary time, respectively. For this purpose, any forward-iteration scheme can be used, including standard fourth-order Runge-Kutta (Elsayed and Fine, 2013) or more sophisticated

[21] Note that other types of randomness have also been suggested (Alben *et al.*, 1975; Iitaka and Ebisuzaki, 2004).

Suzuki-Trotter decompositions (De Vries and De Raedt, 1993) and Chebyshev polynomials (Tal-Ezer and Kosloff, 1984; Dobrovitski and De Raedt, 2003; Weiße *et al.*, 2006). Since in these schemes the required matrix-vector multiplications can be performed without storing full matrices in computer memory, they can access longtime dynamics in large Hilbert spaces. For instance, the spin Drude weight of the spin-1/2 XXZ chain with $L = 33$ ($\dim = 2^{33}$) (Steinigeweg, Gemmer, and Brenig, 2014) (see Fig. 7) and the charge Drude weight of the Fermi-Hubbard chain with $L = 16$ ($\dim = 2^{32}$) (Jin *et al.*, 2015) have been calculated. As with tDMRG (see Sec. IV.E), real-time data can be Fourier transformed to obtain information in frequency space (Iitaka and Ebisuzaki, 2003) such as the optical conductivity (Steinigeweg, Herbrych, Zotos, and Brenig, 2016).

Note that recently dynamical quantum typicality has been combined with numerical linked-cluster expansions (Tang, Khatami, and Rigol, 2013) to obtain current autocorrelations in the thermodynamic limit (Richter and Steinigeweg, 2019).

D. Microcanonical Lanczos method

The microcanonical Lanczos method (MCLM) (Long *et al.*, 2003) also works with single pure states drawn at random. Yet, in contrast to Sec. IV.C, these states are constructed so as to give an accurate approximation to equilibrium expectation values in the microcanonical ensemble; i.e., Eq. (141) becomes

$$|\psi\rangle = \frac{\sqrt{\rho}|\Phi\rangle}{\sqrt{\langle\Phi|\rho|\Phi\rangle}}, \qquad \rho = \rho_{\mathrm{mc}} \propto \sum_{n=1}^{N} |n\rangle\langle n|, \tag{145}$$

where ρ_{mc} is a projector onto an energy shell that (i) is narrow but at the same time (ii) contains sufficiently many energy eigenstates $N \gg 1$. Therefore, because of (ii), ETH is not required and typicality arguments can still be applied (Steinigeweg, Khodja *et al.*, 2014). Moreover, the MCLM has been designed to work directly in frequency space (instead of the time domain discussed before). See Long *et al.* (2003) for an extensive discussion of the method.

In the algorithm presented by Long *et al.* (2003), a pure state $|\psi\rangle$ is prepared around a desired energy E by performing a Lanczos procedure on $K = (H - E)^2$. Then the conductivity is obtained from

$$\sigma'(\omega) = -\lim_{\eta\to 0} \frac{\mathrm{Im}\langle\psi|\mathcal{J}^{(\mathrm{S})}[1/(z - H + E)]\mathcal{J}^{(\mathrm{S})}|\psi\rangle}{\pi\langle\psi|(\mathcal{J}^{(\mathrm{S})})^2|\psi\rangle}, \tag{146}$$

where $z = \omega + i\eta$ by using a continued fraction expansion. The quality of the corresponding results was demonstrated for $\sigma'(\omega)$ of spin-1/2 XXZ chains (Long *et al.*, 2003). For the extraction of the Drude weight, which cannot be directly resolved in this approach but appears to be a contribution at small frequencies $\omega < 1/L$, an *ad hoc* integration over a low-frequency regime needs to be employed.

Since the MCLM is a pure-state, Lanczos-based approach, it can access system sizes comparable to those accessible by the schemes based on dynamical quantum typicality. For example, for spin-1/2 chains the method can access systems of $L = 32$ sites. The approach has been applied to various physical situations, including spin-1/2 chains (Long *et al.*, 2003; Mierzejewski, Bonča, and Prelovšek, 2011; Herbrych, Steinigeweg, and Prelovšek, 2012; Okamoto *et al.*, 2018), ladders (Zotos, 2004; Steinigeweg, Herbrych, Zotos, and Brenig, 2016), spin-1 chains (Karadamoglou and Zotos, 2004), spinful fermions (Prelovšek *et al.*, 2004), and disordered spin systems (Karahalios *et al.*, 2009; Barišić *et al.*, 2016). Although the MCLM was originally formulated in the frequency domain, carrying out microcanonical calculations in the time domain is also possible (Steinigeweg, Khodja *et al.*, 2014). Moreover, energy filters other than $K = (H-E)^2$ can be chosen (Yamaji, Suzuki, and Kawamura, 2018). For reviews on the MCLM and other methods in the context of Lanczos diagonalization, see Dagotto (1994), Jaklič and Prelovšek (2000), and Prelovšek and Bonča (2013).

E. Finite-temperature matrix-product-state methods

The DMRG method was originally devised as a tool to accurately determine static ground-state properties of one-dimensional systems (White, 1992). The method was later extended in various directions, such as accessing spectral functions, real-time evolutions, or thermodynamics (Schollwöck, 2005). From a modern perspective, all DMRG algorithms can be formulated elegantly if one introduces the concept of matrix-product states (MPSs) (Schollwöck, 2011)

$$|\psi\rangle = \sum_{\{\sigma_r\}} \mathrm{tr}[M^{\sigma_1} \cdot M^{\sigma_2} \cdots M^{\sigma_L}]|\sigma_1\sigma_2 \ldots \sigma_L\rangle, \tag{147}$$

where σ_r denote single-site quantum numbers at the rth site. The so-called bond dimension χ of the matrices M^{σ_l} grows exponentially with the amount of entanglement in the state $|\psi\rangle$. The idea of a ground-state DMRG calculation is to determine M^{σ_l} variationally for a fixed, small χ, which is a tactic well suited to 1D systems obeying the area law (Eisert, Cramer, and Plenio, 2010).

This language allows one to deal with pure states and is thus not directly applicable at finite temperatures. To access $T > 0$, one can introduce the notion of matrix-product operators or, equivalently, one can purify the thermal density matrix $\rho = e^{-\beta H}/Z$ by expressing it as a partial trace over a pure state living in an enlarged Hilbert space

$$\rho = \mathrm{tr}_{\mathcal{Q}}|\Psi_\beta\rangle\langle\Psi_\beta|, \tag{148}$$

where auxiliary degrees of freedom $\mathcal{Q}$ encode the thermal bath (Verstraete, García-Ripoll, and Cirac, 2004; Feiguin and White, 2005; Barthel, Schollwöck, and White, 2009; Barthel, 2013). This purification step is not unique, and a simple choice is for the bath to be a copy of the system's degrees of freedom, yet without any unitary dynamics of its own.

The key point is that a purification of the infinite-temperature state $\rho = 1/Z$ can be written down analytically. Again the representation of this state is not unique and a common choice is to put each physical degree of freedom into a maximally entangled state with its copy in the bath by putting both into a singlet state. A subsequent imaginary time evolution where H acts only on the physical degrees of freedom that is carried out using standard DMRG

time-evolution methods can then in principle provide a purified version of the thermal state ρ at any finite temperature. The final thermal expectation values are obtained by taking the trace over the auxiliary degrees of freedom. Note that imaginary, real-time evolution and the trace operation are linear, and therefore we exploit the fact that they can be applied in arbitrary order.

For instance, correlation functions can be obtained [similar to Eq. (140)] using

$$\langle A(t)B\rangle = \langle\Psi_0|e^{-\beta H/2}U(t)^\dagger AU(t)Be^{-\beta H/2}|\Psi_0\rangle, \qquad (149)$$

where the matrix-product state $|\Psi_0\rangle$ purifies $\rho = 1/Z$ at $\beta = 0$. If the Hamiltonian at hand contains only short-range interactions, both the real and imaginary time evolutions appearing in Eq. (149) can be computed straightforwardly (Daley *et al.*, 2004; Vidal, 2004; White and Feiguin, 2004) by splitting them into small steps $U(t) = \exp(-iHt) = \exp(-iH\delta t)\exp(-iH\delta t)\cdots$. One can then Trotter decompose the exponentials $\exp(-iH\delta t)$ into mutually commuting local terms, which can be applied straightforwardly to a MPS (Vidal, 2004; Schollwöck, 2011; Paeckel *et al.*, 2019). Other ways to incorporate finite temperatures within the DMRG include a Lindbladian superoperator approach (Zwolak and Vidal, 2004), a transfer-matrix formulation (Sirker and Klümper, 2005), and a probabilistic sampling over pure states (White, 2009; Stoudenmire and White, 2010).

The crucial step when applying $e^{-iH\delta t}$ to a given MPS is to truncate the bond dimension by neglecting singular values below a certain threshold. This is the best approximation in the 2-norm of the wave function. The discarded weight is the key numerical control parameter; fixing it means fixing the error of the calculation. One usually runs calculations for several different values until physical observables have converged up to a desired accuracy [an example for this is shown in Fig. 10(c)].

If entanglement builds up linearly with time, the bond dimension χ grows exponentially, and so does the computational effort. This severely limits the accessible timescales (Barthel, Schollwöck, and White, 2009). For the tDMRG data in Fig. 10 and the calculation of expressions such as current correlations in general, one can choose system sizes such that on the accessible timescales, the results are for the thermodynamic limit [due to a finite effective speed of information propagation (Lieb and Robinson (1972)]. Moreover, tDMRG is not limited to integrable models or translationally invariant cases.

At finite temperatures, one can exploit the fact that some of the entanglement growth is "unphysically" taking place in $\mathcal{Q}$ and thus can be removed (Karrasch, Bardarson, and Moore, 2012, 2013). Mathematically, the state $|\Psi_\beta\rangle$ appearing in Eq. (148) is not unique but only determined up to an arbitrary unitary rotation, which can be chosen such that the entanglement is minimized. If this unitary is taken as a backward time evolution in $\mathcal{Q}$ with an operator $H_\mathcal{Q}$ that has the same form as H (but acts in $\mathcal{Q}$), which amounts to replacing $U(t)$ with $\tilde{U}(t) = \exp\{-i(H - H_\mathcal{Q})t\}$ in Eq. (149), then the entanglement growth is slowed significantly and larger timescales become accessible. This is illustrated in Fig. 10(a) and by Karrasch, Bardarson, and Moore (2012, 2013). It was later shown that the backward time evolution in $\mathcal{Q}$ appears naturally in an operator-space language (Barthel, 2013; Tiegel *et al.*, 2014). Its form can also be motivated from the fact that $|\Psi_\beta\rangle$ is an eigenstate of $H - H_\mathcal{Q}$ but not of H (Kennes and Karrasch, 2016). Further optimization schemes were discussed by Barthel (2013) and Karrasch, Bardarson, and Moore (2013). A method that in practice allows one to find the minimally entangled representation by iteratively minimizing the second Renyi entropy was presented by Hauschild *et al.* (2018).

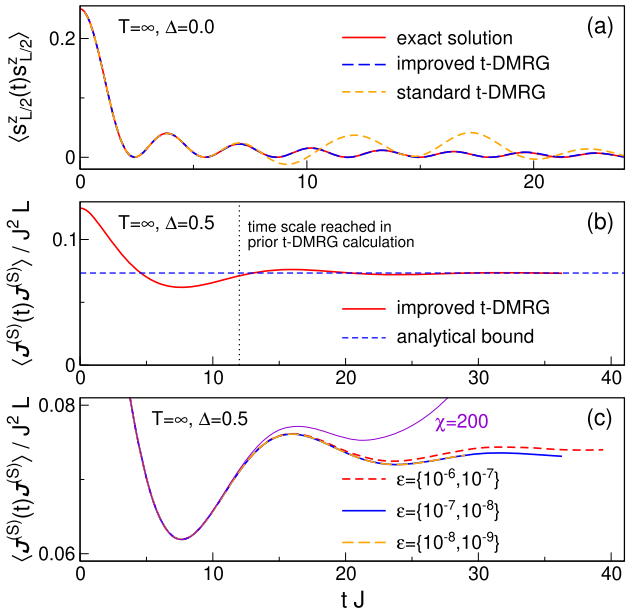

FIG. 10. Benchmark of the improved finite-T tDMRG algorithm for the spin-1/2 XXZ chain [Eq. (1)]. (a) Spin autocorrelation function for $\Delta = 0$ computed using both the standard algorithm [Eq. (149)] and the improved version (U replaced by $\tilde{U}$) with a fixed bond dimension of $\chi = 60$. The exact solution is shown as a reference. The data were taken from Karrasch, Bardarson, and Moore (2012). (b) Spin-current autocorrelation function at $\Delta = 0.5$ calculated using Eq. (150) with a fixed discarded weight. The data were taken from Karrasch, Kennes, and Heidrich-Meisner (2015). Both the analytical result given by Prosen and Ilievski (2013) (horizontal dashed line) and the timescale reached in the tDMRG calculation given by Sirker, Pereira, and Affleck (2009) (vertical dotted line) are shown for comparison. (c) Same as (b) but for discarded weights that each differ by 1 order of magnitude [the two values denote the discarded weight during the two different time evolutions in Eq. (150); see Kennes and Karrasch (2016)]. Data obtained using a fixed bond dimension of $\chi = 200$ are shown for comparison.

Moreover, it was suggested (Barthel, 2013) to rewrite $\langle A(2t)B\rangle = \langle A(t)B(-t)\rangle$ as

$$\langle A(2t)B\rangle = \underbrace{\langle\Psi_0|e^{-\beta H/2}A\tilde{U}(t)}_{\langle\phi_1|}\underbrace{\tilde{U}(t)Be^{-\beta H/2}|\Psi_0\rangle}_{|\phi_2\rangle}, \qquad (150)$$

and to determine the states $|\phi_{1,2}\rangle$ via separate time evolutions. This again gives access to larger timescales by about a factor of 2 or less; see Fig. 10(b).

The improved finite-T tDMRG algorithm can be used to determine Drude weights and diffusion constants by looking at the longtime limit of the current correlation function (Karrasch, Bardarson, and Moore, 2012; Karrasch *et al.*, 2013; Karrasch, Kennes, and Moore, 2014; Karrasch, Moore, and Heidrich-Meisner, 2014; Karrasch, Kennes, and Heidrich-Meisner, 2015) or from local quenches (Karrasch, Moore, and Heidrich-Meisner, 2014; Karrasch, Prosen, and Heidrich-Meisner, 2017), as well as in the bipartitioning protocol (Vasseur, Karrasch, and Moore, 2015; Karrasch, 2017a). The strength of such quenches can be tuned in order to reduce the buildup of entanglement and thus extend the simulation time, and we observe that certain bipartitioning protocols (see also Sec. IX.B) are best suited to determine Drude weights (Karrasch, 2017a). Frequency-resolved quantities can be determined from Fourier transformations (Karrasch, Kennes, and Moore, 2014; Karrasch, Kennes, and Heidrich-Meisner, 2015, 2016), which can be improved by using so-called linear prediction methods (Barthel, Schollwöck, and White, 2009).

Another possibility to obtain transport properties on longer timescales is to employ the time-dependent variational principle approach (Haegeman *et al.*, 2011), but the approach has its own advantages (Leviatan *et al.*, 2017) and shortcomings (Kloss, Lev, and Reichman, 2018). Descendants of Lanczos DMRG methods, which directly yield frequency-dependent quantities (Holzner *et al.*, 2011; Tiegel *et al.*, 2014), are another promising avenue, but one that has not yet been pursued in transport setups. A promising direction was recently pursued by Rakovszky, von Keyserlingk, and Pollmann (2020). Operators with a local support are evolved in the presence of a bath with a coupling strength Γ that controls dissipation. The diffusion constant is recovered in the limit of $\Gamma \to 0$ and agreement with previous studies has been observed (Steinigeweg, Heidrich-Meisner *et al.*, 2014).

F. Quantum Monte Carlo methods

For all spin systems on nonfrustrated lattices, quantum Monte Carlo methods, such as the stochastic series expansion (Syljuåsen and Sandvik, 2002; Sandvik, 2010) and the cluster methods using loop updates (Evertz, Lana, and Marcu, 1993), provide essentially exact results for the thermodynamics and static correlations on large systems. Computing frequency-resolved quantities, though, is difficult due to the ill-defined problem of the analytic continuation from imaginary time to real time. One can avoid the problem by directly computing the response on the imaginary axis and comparing it to theoretical predictions expressed in imaginary rather than real time. This method works best at low temperatures, where the set of available Matsubara frequencies $\omega_n = 2\pi n/\beta$ ($n \in \mathbb{Z}$) is more dense. Therefore, quantum Monte Carlo (QMC) studies of transport in 1D spin systems (Alvarez and Gros, 2002b, 2002c; Louis and Gros, 2003; Heidarian and Sorella, 2007; Grossjohann and Brenig, 2010) and Fermi-Hubbard models (Kirchner, Evertz, and Hanke, 1999) are complementary to finite-temperature DMRG, ED, and dynamical typicality. The conclusions of some of these QMC studies conflict with the bulk of the literature. For instance, both Kirchner, Evertz, and Hanke (1999) and Heidarian and Sorella (2007) claimed evidence of ballistic transport in gapless nonintegrable models. While there has not been any systematic comparison between QMC data and other numerical methods (which is hampered by the different temperature regimes that these methods work in), a generic issue related to the analytical continuation from the imaginary axis to the real-frequency axis arises at low temperatures. Since Matsubara frequencies $\omega_n \propto T$, there is a poor resolution whenever the width of a peak in the spectral feature is smaller than $k_B T$.

The statistical errors in QMC calculations are typically larger for higher-order correlation functions, and it is therefore preferable (Alvarez and Gros, 2002b, 2002c; Grossjohann and Brenig, 2010) to work with two-site correlation functions instead of directly evaluating current-current correlations (Heidarian and Sorella, 2007). At finite momentum q and frequency ω_n, one can relate the dynamical conductivity $\sigma_q(\omega_n)$ given by (Alvarez and Gros, 2002c)

$$\sigma_q(\omega_n) = \frac{\langle -T_{\mathrm{kin}} \rangle - J_q^{(\mathrm{S})}(\omega_n)}{\omega_n} \tag{151}$$

to the dynamical spin susceptibility $S_q(\omega_n)$ via

$$\langle -T_{\mathrm{kin}} \rangle - J_q^{(\mathrm{S})}(\omega_n) = \frac{\omega_n^2}{\tilde{q}^2} S_q(\omega_n). \tag{152}$$

Note that unlike in Eq. (61) there is a minus sign, due to imaginary time. The expressions entering here are

$$J_q^{(\mathrm{S})}(\omega_n) = \frac{1}{L}\int_0^\beta e^{i\omega_n \tau} \langle j_q^{(\mathrm{S})}(\tau) j_{-q}^{(\mathrm{S})}(0) \rangle d\tau, \tag{153}$$

$$S_q(\omega_n) = \frac{1}{L}\int_0^\beta e^{i\omega_n \tau} \langle s_q^z(\tau) s_{-q}^z(0) \rangle d\tau, \tag{154}$$

where τ is imaginary time.

The strategy pursued by Alvarez and Gros (2002b, 2002c) was to fit the numerical data to a phenomenological ansatz; see Alvarez and Gros (2002c) for details. One notable result given by Alvarez and Gros (2002b, 2002c) was a Drude weight $\mathcal{D}_{\mathrm{w}}^{(\mathrm{S})}(T) = \mathrm{const}$ at low temperatures for commensurate points $\Delta = \cos(\pi/m)$ ($m = 1, 2, \ldots$) in the gapless phase of the spin-1/2 XXZ chain, in contradiction to the TBA results for the temperature dependence (Zotos, 1999). It thus remains an open question as to whether or not the specific ansatz given by Alvarez and Gros (2002c) is justified and whether or not finite temperatures were actually resolved in these QMC studies, which reproduce the zero-temperature Drude weight away from $\Delta = 1$ with excellent accuracy.

Another QMC work (Grossjohann and Brenig, 2010) focused on the spin-1/2 XXX chain and aimed at verifying the field-theoretical prediction given by Sirker, Pereira, and Affleck (2009, 2011) for the dynamical spin susceptibility $S_q(\omega_n)$. Qualitatively, a diffusive form at small wavelength is expected based on the perturbative bosonization analysis given by Sirker, Pereira, and Affleck (2009); cf. Sec. IV.A. This is consistent with QMC data, but quantitative deviations for the decay rate γ were reported.

V. OPEN QUANTUM SYSTEMS

In this section, we describe methods that use an explicit external driving, such that a system evolves to a NESS (Schmittmann and Zia, 1995; Marro and Dickman, 1999). The NESS describes a time-averaged system's density operator, from which one can then evaluate expectation values of observables. A particular emphasis is put on the boundary-driven Lindblad setting being the most frequently used framework to obtain the NESS.

We note that open quantum systems are sometimes also studied numerically with a unitary time evolution; i.e., the leads are treated on the Hamiltonian level and as a finite system. We do not further discuss this approach here but mention studies that looked at spin chains (Branschädel, Schneider, and Schmitteckert, 2010; Lange, Ejima, and Fehske, 2018, 2019) or electronic systems (Heidrich-Meisner *et al.*, 2010; Kirino and Ueda, 2010; Knap, von der Linden, and Arrigoni, 2011; Einhellinger, Cojuhovschi, and Jeckelmann, 2012) sandwiched between leads. An alternative formulation used in studies of mesoscopic systems, particularly in the absence of interactions, is to describe the system's properties using a scattering matrix and the leads by occupation numbers, leading to Landauer-Büttiker type formulas (Nazarov and Blanter, 2009). Finally, we mention that there are some settings that are able to produce a NESS within the unitary dynamics. One is the bipartitioning protocol where one prepares two semi-infinite chains in different initial states and then evolves unitarily in time; see Sec. IX.B. Another is to use a Lagrange multiplier to add a current operator to the Hamiltonian; see Antal, Rácz, and Sasvári (1997).

A. Nonequilibrium steady-state driving

A canonical way of studying nonequilibrium properties is to induce a NESS using some kind of reservoirs and to measure its properties. In studies of classical systems (Lepri, Livi, and Politi, 2003; Dhar, 2008), where many different types of reservoirs are available, this is in fact a method of choice to study transport (Schmittmann and Zia, 1995; Marro and Dickman, 1999; Derrida, 2007). Compared to linear-response calculations, no extra care is needed when treating anomalous transport often observed in classical nonintegrable 1D systems, such as that in the Fermi-Pasta-Ulam-Tsingou model (Fermi, Pasta, and Ulam, 1955; Dauxois, 2008). Quantum NESS studies are fewer, with one reason being that it is not easy to construct quantum reservoirs that one can efficiently simulate. As we see in this section, the situation has been changing in recent years, with increased research into quantum master equations.

In a one-dimensional system it suffices to use one reservoir at each chain end and, provided that they are different, the system will evolve into a NESS ρ_∞ after a long time. Once one gets the NESS, the main quantity used to assess the transport is the NESS current $j^{(\mathrm{S})}$, which is simply the expectation value of the current operator. The current is always defined such that the continuity equation holds. Therefore, at sites r on which the reservoirs act it must account also for the bath action. In the bulk, though, where the evolution is unitary, the current operator is the standard $j_r^{(\mathrm{S})}$ obtained from the commutator between h_r and the local density s_r^z [see Eq. (4)], and therefore the NESS current is $j^{(\mathrm{S})} = \mathrm{tr}(\rho_\infty j_r^{(\mathrm{S})})$. Because of the continuity equation, $j^{(\mathrm{S})}$ is independent of the lattice site r. Provided that one has diffusion, the current will scale as $j^{(\mathrm{S})} = -D^{(\mathrm{S})}\Delta\mu/L$ (i.e., Fourier's, Fick's, or Ohm's law), where $\Delta\mu$ is the difference in driving potentials[22] and $D^{(\mathrm{S})}$ is a diffusion constant. If the system is not diffusive, one will instead have a more general scaling; namely, keeping $\Delta\mu$ fixed the current will scale with system length L as

$$j^{(\mathrm{S})} \sim \frac{1}{L^\gamma}. \tag{155}$$

Depending on γ one has (i) diffusive transport for $\gamma = 1$, (ii) ballistic transport for $\gamma = 0$, (iii) superdiffusive transport for $0 < \gamma < 1$, or (iv) subdiffusive transport for $\gamma > 1$. Localization corresponds to $\gamma \to \infty$. See Dhar, Kundu, and Kundu (2019) for a review of anomalous transport in classical systems. The type of transport can also be recognized from the NESS profile of a conserved density. As in classical systems, one expects some finite boundary "jumps" close to the location of driving, i.e., an impedance mismatch. Disregarding those, in the bulk one will have a linear profile for a diffusive system, a flat profile for a ballistic system, and a domain-wall-like profile for an insulator. In short, in order to keep $j^{(\mathrm{S})}$ constant, local areas with higher resistivity will support higher density gradients and vice versa. Heuristic profile shapes can also be associated with anomalous γ (Žnidarič, 2011b; Žnidarič, Scardicchio, and Varma, 2016), though it is not clear how universal they are. Assuming a single-exponent scaling (Li and Wang, 2003), these γ are connected to the corresponding dynamical exponents in the context of linear-response functions [see Eq. (41)]

$$\alpha' = \frac{2}{\gamma + 1}. \tag{156}$$

A crucial question is how to efficiently implement reservoirs. One possibility is to describe the system and the infinite reservoirs as one large Hamiltonian system. Then one can derive the evolution equation of the system alone by tracing out the reservoir degrees of freedom. A problem with this approach is that the obtained equations are in general complicated. For instance, the resulting master equation is nonlocal in time with a complicated memory kernel and in general is no easier to solve than the original problem (Breuer and Petruccione, 2002). Depending on further approximations one gets a so-called Redfield master equation (Redfield, 1965), which we do not discuss here, or a simpler Lindblad master equation. An exception involves quadratic systems (i.e., noninteracting), where the physics is simple since quadratic translationally invariant systems display ballistic transport.

[22]For spin transport $\Delta\mu$ will be equal to a magnetization difference between chain ends and should not be confused with the chemical potential.

A more pragmatic approach is to simply seek an evolution equation for the system's density matrix that is able to describe the NESS situation and that is as simple as possible, meaning that it still obeys all the rules of quantum mechanics. After all, in the thermodynamic limit, the bulk conductivity or transport type should not depend on the details of the driving provided that the dynamics is sufficiently ergodic. While this is seemingly natural, this assumption has to be checked in each individual system, especially in integrable systems. Next we elaborate on such a setting.

B. Lindblad master equation

We now argue for the simplest master equation governing the evolution of the system's density operator. Quantum mechanics is linear, and therefore we require the evolution of $\rho(t)$ to also be linear, and furthermore that it maps density operators to density operators. Namely, if $\rho(0) \geq 0$, $\rho(t) \geq 0$ should also hold. Requiring also that a map that is trivially extended to a larger space (i.e., one that acts as an identity on added degrees of freedom) also maps any positive semidefinite operator on that larger space to a positive semidefinite operator means that such a map should be completely positive and not just positive. Such maps are known as completely positive trace-preserving (CPTP) maps (Alicki and Lendi, 2007). The class of CPTP maps is still too broad of a set, and therefore one requires an additional property, namely, that the action of reservoirs is as random as possible. In other words, the maps have no memory; i.e., they correspond to a Markovian evolution. Formally, this means that the evolution generated by the linear (super)operator $\mathcal{L}$ should form a dynamical semigroup: the evolution can be split into smaller steps $\rho(t_1 + t_2) = e^{\mathcal{L}\cdot(t_1+t_2)}\rho(0) = e^{\mathcal{L}\cdot t_1}e^{\mathcal{L}\cdot t_2}\rho(0)$. It has been shown that any such evolution in a finite Hilbert space (Gorini, Kossakowski, and Sudarshan, 1976) as well as in an infinite one (Lindblad, 1976) can be written in the form of the Lindblad master equation (also Lindblad, Gorini, Kossakowski, and Sudarshan, which is known as LGKS)

$$\frac{d}{dt}\rho(t) = \mathcal{L}(\rho(t)) = i[\rho(t), H] + \mathcal{L}^{\text{diss}}(\rho(t)),$$
$$\mathcal{L}^{\text{diss}}(\rho) = \sum_j [L_j\rho, L_j^\dagger] + [L_j, \rho L_j^\dagger], \qquad (157)$$

where L_j are Lindblad operators that describe the action of reservoirs. Note that the L_j can be any operators, including non-Hermitian ones. Conversely, a Lindblad master equation with given L_j and H generates a CPTP map. For a historical account and earlier uses and occurrences of such an equation, see Chruściński and Pascazio (2017). In a finite-dimensional Hilbert space, Brouwer's fixed point theorem (Milnor, 1965) guarantees the existence of at least one fixed point. Namely, a continuous map, $e^{\mathcal{L}t}$ in our case, of a compact convex set (a set of density matrices) on itself has a fixed point $\mathcal{L}\rho_\infty = 0$. Typically and under certain algebraic conditions on L_j and H (Evans, 1977; Frigerio, 1977; Spohn, 1977), there is exactly one steady state, and therefore any initial state converges after a long time to that unique NESS $\lim_{t\to\infty} e^{\mathcal{L}\cdot t}\rho(0) = \rho_\infty$. Systems described by the Lindblad equation are often called open systems (Breuer and Petruccione, 2002; Alicki and Lendi, 2007), as opposed to closed systems, where the evolution is unitary.

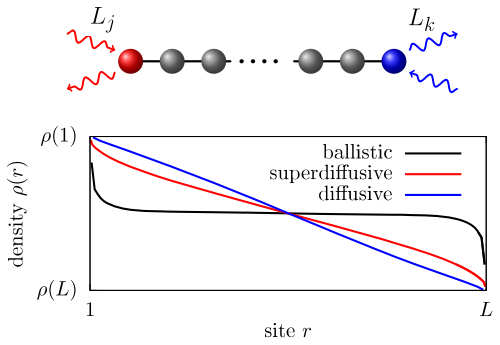

FIG. 11. Top panel: NESS boundary Lindblad driving. Bottom panel: typical NESS density profiles for diffusive (blue line), superdiffusive (red line), and ballistic transport (black line).

Depending on the driving type, one can distinguish the cases of global L_j (Saito, Takesue, and Miyashita, 2000); Saito and Miyashita, 2002; Saito, 2003a) and local L_j cases (Michel *et al.*, 2003; Mejia-Monasterio and Wichterich, 2007; Steinigeweg, Ogiewa, and Gemmer, 2009). A somewhat related scheme is that of a stochastic heat bath in which one measures and stochastically resets the boundary spin (Mejia-Monasterio, Prosen, and Casati, 2005; Mejia-Monasterio and Wichterich, 2007). Another hybrid way to model a bath is by describing it as a lead with a certain number of lattice sites that is also coupled to a Lindbladian dissipation. For noninteracting leads, one can construct dissipators that thermalize such free systems (Dzhioev and Kosov, 2011; Ajisaka *et al.*, 2012; Guimarães, Landi, and de Oliveira, 2016) or model nontrivial spectral properties of the bath (Arrigoni, Knap, and von der Linden, 2013; Schwarz *et al.*, 2016; Brenes, Mendoza-Arenas *et al.*, 2020). For a discussion of thermalization properties of such baths, see Reichental *et al.* (2018).

One of the simplest choices involves local L_j that act only on the edges of the chain such that the bulk dynamics is still fully coherent and determined by H; see Fig. 11. This is similar to the way in which classical nonequilibrium lattice models are driven (Schmittmann and Zia, 1995; Marro and Dickman, 1999; Derrida, 2007), where the bath acts only on the boundary. The resulting locally driven Lindblad equation is a mathematically sound NESS setting, without shortcomings such as the violation of positivity at short times encountered in the Redfield equation. Moreover, this setting often allows for the simulation of large systems (hundreds of spins) and sometimes even permits exact solutions. Justifying local L_j on microscopic grounds is not easy; the standard weak-coupling microscopic derivation (Breuer and Petruccione, 2002) typically results in nonlocal L_j. In particular, requiring an exact thermal steady state for equilibrium driving demands nonlocal L_j [so-called Davies generators (Davies, 1974)] that have to be constructed by diagonalizing each H. This is neither practical nor an effective bath description that is system independent. From a practical point of view, demanding exact thermal states is too strong as it suffices that one is sufficiently close. For a system possessing

good thermalization properties, it should not matter how one drives such a system in the thermodynamic limit. The reason for this is that far from the boundaries a generic system self-thermalizes anyway, and therefore boundary effects protruding a finite distance into the system are expected to cause only subleading corrections. This behavior, however, is not guaranteed in an integrable system (Žnidarič *et al.*, 2010; Mendoza-Arenas, Clark, and Jaksch, 2015).

Note that things are different if one studies small systems: there one should pay close attention to thermodynamic details of local Lindblad driving (Barra, 2015), as well as to the fact that quantities such as the temperature might not have a well-defined thermodynamic meaning (Hartmann, Mahler, and Hess, 2004; Kliesch *et al.*, 2014). One can nevertheless also provide a kind of microscopic picture of local L_j. Hermitian L_j, such as the dephasing $L_j \sim s_j^z$, can be obtained via Gaussian noise (Gardiner and Zoller, 1991), while general L_j can be somewhat more artificially obtained by a continuous nonideal measurement (Breuer and Petruccione, 2002) or by an instantaneous repeated interaction with a bath (Attal and Pautrat, 2006; Karevski and Platini, 2009).

1. Infinite-temperature magnetization driving

We now take a closer look at one of the simplest cases of Lindblad driving, where the Lindblad operators act on a single site and induce infinite-temperature spin transport. A one-site driving is given by two Lindblad operators that flip a spin up or down with different probabilities, thereby trying to induce a net magnetization at that site. They are given by

$$L_1 = \sqrt{\Gamma(1+\mu)}s_r^+, \qquad L_2 = \sqrt{\Gamma(1-\mu)}s_r^-, \tag{158}$$

where Γ is the coupling strength, μ is the driving strength, and $s_r^\pm = s_r^x \pm i s_r^y$. In the absence of any Hamiltonian, that is, driving a single-site system, they have a unique one-site steady state $\rho \sim \mathbb{1} + \mu 2 s_r^z$, and therefore they model a bath that tries to induce a magnetization $+\mu$ at site r, i.e., $2\mathrm{tr}(s_r^z \rho) = \mu$.

To induce a NESS in a long chain, one uses one such pair of L's at each chain end. For instance, using $+\mu$ driving at the left end and $-\mu$ at the right end results in a NESS with a position-dependent magnetization along the chain and a nonzero spin current; see Fig. 11. Similar Lindblad driving was already in use in early studies (Michel *et al.*, 2003; Michel, Gemmer, and Mahler, 2004; Wichterich *et al.*, 2007) and in numerous subsequent ones (Prosen and Žnidarič, 2009; Mendoza-Arenas, Al-Assam *et al.*, 2013; Popkov, Karevski, and Schütz, 2013; Landi *et al.*, 2014; Balachandran *et al.*, 2018). For $\mu = 0$, one has a trivial steady state $\rho \sim \mathbb{1}$, i.e., an infinite-temperature state, and one can interpret Eq. (158) as spin driving at infinite temperature. For nonzero μ, the NESS current $j^{(\mathrm{S})}$ is nonzero and is the main observable.

As described in Sec. V.A, the transport type can then be extracted by evaluating the expectation value of the current $j_r^{(\mathrm{S})}$ and the magnetization $s_{r=1,L}^z$. Owing to a "boundary resistance" associated with a particular driving, one typically has boundary jumps in magnetization: the expectation value of $s_{r=1,L}^z$ is not exactly $\pm\mu$. However, the size of such a jump is proportional to $j^{(\mathrm{S})}$ and therefore goes to zero in the thermodynamic limit provided that the current goes to zero, which is true for sub-ballistic transport. In the thermodynamic limit, the difference in driving potential is therefore simply $\Delta s^z = \mu$, and furthermore the current expectation value in the NESS can be evaluated at any site r. From its dependence on L, which is given in Eq. (155), one can therefore extract the transport type and, in the case of diffusion, also the diffusion constant from $j^{(\mathrm{S})} = -D^{(\mathrm{S})}\mu/L$.

We note that the Lindblad driving parameters are in general not simply related or equal to thermodynamic parameters. For instance, for a one-site spin driving (158) and $H = 0$ one gets a one-site steady-state density operator $\rho \sim \mathbb{1} + \mu\sigma^z$ for which the ratio of the probabilities of finding the spin in up and down states is $(1+\mu)/(1-\mu)$. Arguing that this ratio can be equated to $e^{-\Delta E/T}$ given by the equilibrium distribution, where ΔE is the energy difference between the up and down states, would incorrectly associate a particular finite T with a given μ. At the boundary where the L act, there is a nontrivial interplay between driving and a nonzero H (boundary effects), causing the state there in general not to be thermal. However, far from the boundaries one does expect thermalization (at least in nonintegrable systems), and therefore thermodynamic parameters describing local equilibrium can be determined from local observables (Žnidarič *et al.*, 2010; Mendoza-Arenas, Clark, and Jaksch, 2015); see also Shirai and Mori (2020) for an alternative.

An important question is whether the linear-response Green-Kubo type calculation and the NESS one in the limit of small μ give the same transport coefficient. This is in general a difficult question, with no rigorous mathematical connection between the two transport coefficients known in general for either quantum or classical systems (Bonetto, Lebowitz, and Rey-Bellet, 2000). We now outline one specific result for the spin driving given in Eq. (158).

In the limit of weak driving $\mu \ll 1$, one can use perturbation theory to get the NESS linear-response correction to the infinite-temperature equilibrium state $\sim\mathbb{1}$. As in classical systems (Kundu, Dhar, and Narayan, 2009), one can derive a NESS Kubo-like expression (Kamiya and Takesue, 2013; Žnidarič, 2019) for the diffusion constant $D^{(\mathrm{S})}$ at infinite temperature

$$D^{(\mathrm{S})} = \lim_{L\to\infty} 4L \int_0^\infty \frac{\mathrm{tr}[j_r^{(\mathrm{S})} j_{r'}^{(\mathrm{S})}(t)]}{2^L}\, dt, \tag{159}$$

for any r and r', where $j_r^{(\mathrm{S})}(t) \coloneqq e^{\mathcal{L}_0 t} j_r^{(\mathrm{S})}$, with $\mathcal{L}_0$ the equilibrium Liouvillian propagator (i.e., $\mathcal{L}$ with $\mu = 0$). Although looking similar to the equilibrium Kubo formula equation (12), the content is quite different. For instance, the time integral is always well defined due to the dissipative nature of $\mathcal{L}_0$, even for finite L. Alternatively, the expression can be rewritten as (Žnidarič, 2019)

$$D^{(\mathrm{S})} = L(8\Gamma)^2 \int_0^\infty \frac{\mathrm{tr}[s_L^z s_1^z(t)]}{2^L}\, dt, \tag{160}$$

where $s_1^z(t) \coloneqq e^{\mathcal{L}_0 t} s_1^z$. The NESS diffusion constant $D^{(\mathrm{S})}$ is equal to the transfer probability across the chain under evolution by $\mathcal{L}_0$ that is unitary in the bulk and dissipative

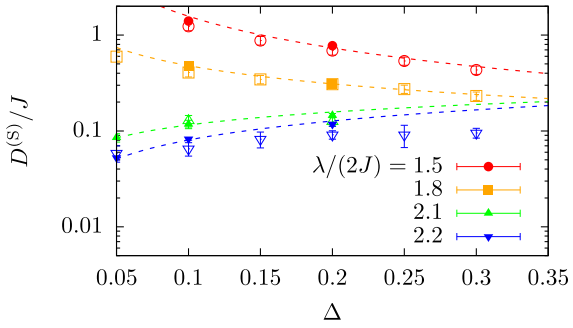

FIG. 12. Comparison of results for the spin-diffusion constant $D^{(S)}$ obtained from NESS simulations (empty symbols) and unitary domain-wall spreading (solid symbols) in the spin-1/2 XXZ chain with a quasiperiodic magnetic field of amplitude λ. Details were given by Žnidarič and Ljubotina (2018). Unitary domain-wall spreading is a particular case of a bipartitioning protocol; see Sec. IX.B for details.

at the edges. Even though it looks as if $D^{(S)}$ depends on Γ, this is not the case. One can show that in the thermodynamic limit, provided that the unitary dynamics is perfectly diffusive and all parameters are held fixed (including Γ), this dependence is exactly compensated for by a dissipative decay of $s_1^z(t)$, resulting in exactly the same diffusion constant as in the unitary Green-Kubo approach (Žnidarič, 2019). Quantitative agreement between the Lindblad and unitary linear-response Green-Kubo calculations of the diffusion constant has been verified in chaotic models such as the spin-1/2 XX ladder (Žnidarič, 2013a; Steinigeweg, Heidrich-Meisner *et al.*, 2014). Similarly, one can compare the Lindblad approach with the unitary dynamics in an out-of-equilibrium setting. Once again, to have a meaningful comparison one should focus on quantities accessible by both methods, such as the diffusion constant. An extensive comparison has yet not been performed; however, an example is shown in Fig. 12 for a spin-1/2 XXZ model in the presence of a quasiperiodic potential. Specifically, the figure shows a comparison between the diffusion constant obtained in the Lindblad evolution using a driving as specified in Eq. (158) and that extracted from the domain-wall spreading in a bipartitioning protocol; see Sec. IX.B.

For nondiffusive systems (i.e., superdiffusive or subdiffusive ones) the relationship between unitary and NESS approaches is less clear, although the same scaling exponent is usually observed [both for superdiffusive systems such as the spin-1/2 Heisenberg chain (Ljubotina, Žnidarič, and Prosen, 2017) and for subdiffusive dynamics in a quasiperiodic potential (Varma and Žnidarič, 2019)]. It has been also demonstrated (Jin, Filippone, and Giamarchi, 2020) that for ballistic systems the Lindblad driving (158) gives the same result as the Landauer-Büttiker formula at infinite temperature. One case that is believed to be special, where NESS and unitary dynamics do not agree, is a noninteracting critical model displaying multifractality (Varma, de Mulatier, and Žnidarič, 2017; Purkayastha *et al.*, 2018). One should also be aware that in the non-linear-response regime, i.e., at large μ, one can get a different behavior. An explicit example is the spin-1/2 XXZ chain at maximal driving $\mu = 1$ (Prosen, 2011a) or close-to-maximal driving (Benenti, Casati, Prosen, and Rossini, 2009; Benenti, Casati, Prosen, Rossini, and Žnidarič, 2009). It remains to be explored whether and how a boundary-driven Lindblad setting can be used to extract the Drude weight or a frequency-dependent conductivity. Using simply a time-periodic driving μ in a Markovian Lindblad equation (Floquet Lindblad) [see Žnidarič, Žunkovič, and Prosen (2011)] likely does not give the same information as $\sigma'(\omega)$.

Note that the coupling strength Γ introduces an energy scale into the system, and therefore the limits of $\Gamma \to 0$ (or $\Gamma \to \infty$) will typically not commute with either the thermodynamic limit or the limit of $\Delta \to \infty$ in the Heisenberg model. The limit of weak boundary coupling $\Gamma \to 0$ causes a decoupling of the bulk from the boundary, resulting in a different scaling of current and density with Γ (Prosen, 2011b). This means that weak boundary coupling $\Gamma \ll 1$ cannot be used to probe bulk transport. Similar caution is also required in the limit of $\Gamma \to \infty$, especially if there is any other diverging energy scale with which a scale introduced by Γ can compete. As an example, if one takes the limit of $\Delta \to \infty$ in the spin-1/2 XXZ spin chain, then a different behavior of the diffusion constant might be obtained depending on how one scales Γ (Žnidarič, 2011a). This is a likely cause of the discrepancy between the value of the diffusion constant at large Δ between closed-system Kubo formula calculations (Steinigeweg and Gemmer, 2009; Karrasch, Moore, and Heidrich-Meisner, 2014) and the NESS result (Žnidarič, 2011a) obtained for a particular coupling-strength scaling $\Gamma \sim \Delta$. Namely, in the studies by Steinigeweg and Gemmer (2009) and Karrasch, Moore, and Heidrich-Meisner (2014) the infinite-temperature limit is taken first. Therefore, even at large Δ one has a coupling between all states. The Lindblad setting, by contrast, with its finite but large Γ, is closer to the case in which one takes the limit $\Delta \to \infty$ first; i.e., at finite T in the limit $\Delta \to \infty$ one decouples states with differing numbers of domain walls.

2. Solving the Lindblad equation

How does one solve a many-body Lindblad equation? Provided that the entire Liouvillian is quadratic in fermionic operators, one can use the so-called third quantization method (Prosen, 2008), simplifying diagonalization of the full $4^L \times 4^L$ Liouvillian to a diagonalization (Prosen, 2010) of a $2L \times 2L$ matrix describing decay modes. In some exceptional quadratic (Žnidarič, 2010b) as well as nonquadratic systems [see Prosen (2011a), Karevski, Popkov, and Schütz (2013), Popkov and Livi (2013), Prosen (2014a), Prosen (2015), Ilievski (2017), and Vanicat, Zadnik, and Prosen (2018)], one can even get a closed matrix-product-operator (MPO) NESS solution.

Numerically, one can use full diagonalization (allowing $L \approx 10$ for spin-1/2 operators), or an explicit integration of an exponential set of differential equations; see Weimer, Kshetrimayum, and Orus (2021) for an overview. An alternative approach often used in atomic, molecular, and optical systems is the quantum-trajectory method (Breuer and Petruccione, 2002), which evolves $|\psi(t)\rangle$ and averages over stochastic jumps to get ρ. Writing $|\psi(t)\rangle$ in full one is again limited to small systems $L \approx 16$ (Johansson, Nation, and Nori,

2012); however, using the MPS ansatz one can extend the available system sizes (Daley, 2014). For the large systems needed in transport studies, the method of choice is a version of tDMRG (Daley *et al.*, 2004; Verstraete, García-Ripoll, and Cirac, 2004; White and Feiguin, 2004; Zwolak and Vidal, 2004), also called the time-evolved block-decimation method, used to evolve in time $\rho(t)$ until the NESS is reached. One could also try to avoid time evolution by directly targeting the NESS (i.e., the ground state of a non-Hermitian $\mathcal{L}$) using Lanczos type methods (Arnoldi, $L \approx 15$) or again employ the DMRG (Cui, Cirac, and Bañuls, 2015; Casagrande, Poletti, and Landi, 2020). Invariably, though, as in time evolution, the bottleneck will be a small spectral gap of $\mathcal{L}$ (Žnidarič, 2015).

The tDMRG for Lindblad equations works by writing the state ρ in terms of a matrix-product-operator ansatz, the same as for pure states (147), with the only difference being that the local Hilbert-space dimension in the operator space is the square of the pure-state dimension. For instance, for spin-1/2 operators, it is 4, spanned by Pauli matrices and the identity, which are orthogonal with respect to the Hilbert-Schmidt inner product. By discretizing the time evolution into small time steps δt and by using a Trotter-Suzuki decomposition of the time-evolution operator resulting in $e^{\mathcal{L}\delta t}$, one propagates an initial density operator, such as $\rho(0) \sim \mathbb{1}$, in time until it converges to the NESS. The basic ingredient is a two-site nearest-neighbor transformation similar to the time evolution of matrix-product states (Schollwöck, 2011). Because non-unitary evolution eventually spoils the optimal truncation via Schmidt decomposition, it is worthwhile to occasionally reorthogonalize the state; see Žnidarič (2010a). For further implementations by various groups, including open-source codes, see Al-Assam, Clark, and Jaksch (2016), Bernier *et al.* (2018), Brenes *et al.* (2018), Schulz *et al.* (2018), Volokitin *et al.* (2019), and Fishman, White, and Stoudenmire (2020).

In unitary tDMRG simulations of MPSs or MPOs (see Sec. IV.E), where one needs to account for the unavoidable entanglement growth, one fixes the discarded weight to a set number. As a consequence, the bond dimension necessary to maintain the same truncation per time step grows as a function of time generically in an exponential way (Schollwöck, 2011). As a consequence, the accessible time-scales are of the order of several $10/J$. The tDMRG simulations for solving Lindblad master equations, on the other hand, are often carried out with a fixed bond dimension. This methodological choice (fixed bond dimension) is motivated by two arguments: First, dissipative dynamics is expected to exhibit a much milder entanglement growth than pure-state simulations, albeit a still present growth; see the discussion given by Prosen and Žnidarič (2009). Second, one is not interested in the time evolution of currents as such, but instead only in their NESS values. Since the NESS is unique in the cases of interest, different initial states should lead to the same NESS. Thus, numerical errors in accounting for the real-time evolution due to working at a fixed bond dimension should, to a certain degree, not prevent the system from converging to the correct NESS. A detailed analysis regarding the role of the discarded weight in tDMRG simulations of

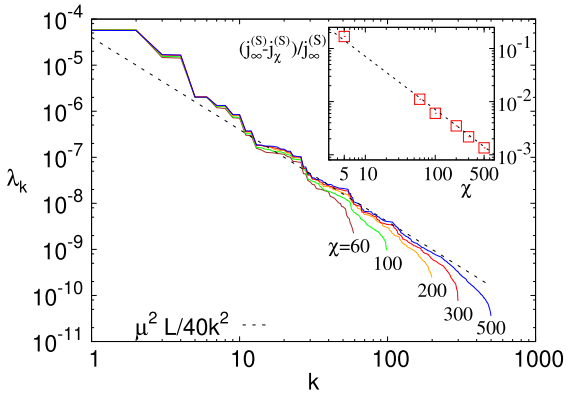

FIG. 13. Schmidt spectrum for the NESS of a boundary-driven spin-1/2 Heisenberg chain ($\Delta = 1$) with $L = 64$ sites, $\mu = 0.005$, and MPO bond dimensions $\chi = 60$–500. The dashed line is the best-fitting asymptotic decay. Inset: convergence of the NESS current j_χ obtained from a fixed-χ calculation, with the dashed line the predicted error from the main plot $(j_\infty - j_\chi)/j_\infty \approx L/90\chi$ (no fitting parameters).

Lindblad equations has not been reported in the literature. For instance, it is unclear whether significant truncation errors during the time evolution can possibly spoil the approach to the correct NESS. In the practical analysis of tDMRG simulations of Lindblad systems, one checks the convergence of the NESS currrent with the bond dimension, as we illustrate next.

There are two main quantities that determine the efficiency and accuracy of the tDMRG simulations for Lindblad equations. One is the truncation error caused by representing the NESS with a finite-bond MPO, and the other is the required convergence time to the NESS that is given by the inverse gap of the Lindbladian superoperator $\mathcal{L}$ from Eq. (157). Note that the Trotter time step should be chosen small enough that it does not dominate over the truncation error. The size of the truncation error is connected to the operator "entanglement" (Prosen and Pižorn, 2007) of the resulting NESS $\rho_\infty = \sum_k \sqrt{\lambda_k} A_k \otimes B_k$ given by the Shannon entropy of the non-negative λ_k ($\sum_k \lambda_k = 1$) obtained via the operator Schmidt decomposition, for instance, for a symmetric bipartition. If one starts from an identity initial state, which has zero operator entanglement, the operator entanglement will typically monotonically grow with time until it reaches its maximum value once the NESS is reached. Provided that the operator entanglement of the NESS is low, the method is efficient, as a small bond dimension suffices. For a small magnetization driving μ [Eq. (158)], one typically observes the asymptotic scaling

$$\lambda_k \sim \mu^2 L^r / k^p \tag{161}$$

for large k, with the model-dependent power-law exponents r and p. The powers r and p determine the size of the truncation error, and therefore the required bond dimension χ.

An example of the truncation-error analysis for the isotropic spin-1/2 Heisenberg model is shown in Fig. 13. Note that in this case the NESS spin current (4) scales superdiffusively

with $j^{(S)} \approx \mu(0.39/\sqrt{L})$ (Žnidarič, 2011a). We evolve with a fixed bond dimension χ until the NESS is reached. The spectrum λ_k in the NESS is plotted in Fig. 13. Analyzing its dependence on L and k one gets that the two exponents characterizing the NESS are $r \approx 1$ and $p \approx 2$. At fixed bond dimension χ, the discarded probability weight is given by all dropped eigenvalues $\sum_{k=\chi}^{\infty} \lambda_k$ and therefore scales as $\approx \mu^2(L/40\chi)$, where $1/40$ is an empirically fitted parameter obtained in the main plot of Fig. 13. Since one has $\rho_\infty \sim \mathbb{1} + \mathcal{O}(\mu)$ for small μ, the largest eigenvalue is trivially $\lambda_0 \approx 1$. For relative precision, what matters is the ratio of the discarded weight and the first nontrivial eigenvalue λ_1, which is $\lambda_1 \approx 2.3\mu^2$ for the data shown. The relative error of the NESS calculated using a finite χ can therefore be estimated as $\approx L/90\chi$ [$1/90 \approx 1/(2.3 \times 40)$]. Even though the error of a particular observable, such as the current, could involve some extra factors due to overlaps of Schmidt eigenvectors with the observable, we see in the inset of Fig. 13 that the agreement of the error estimate based only on the Schmidt spectrum with the actual error of the NESS current without any additional fitting parameters is good.[23] For the boundary-driven Heisenberg chain, one therefore has to increase the bond dimension as $\chi \propto L^{r/(p-1)} \sim L$ if one wants to keep the error constant. For instance, $\chi \sim 100$ results in a relative error of about 1% at $L = 100$. If a slightly larger error of a few percent suffices and one uses larger χ, even systems with close to $L = 10^3$ sites can be simulated. Such simulations, though, take weeks of CPU time.

The other important parameter is the relaxation time required to converge to the NESS. For the spin-1/2 Heisenberg model, it scales as $\sim L^3$ (Žnidarič, 2015), and therefore the complexity of finding the NESS with a fixed precision ($\chi \sim L$) scales as $L^3 L\chi^3 \sim L^7$. However, in the spin-1/2 Heisenberg chain, it turns out that the spin current actually relaxes on a shorter timescale $\sim L^{1.5}$ (Žnidarič, 2011b), and therefore a fixed-precision NESS current can be obtained in $\mathcal{O}(L^{5.5})$ steps.

We note that if the Schmidt spectrum λ_k decays slower than $1/k^2$ (which often happens), the required bond-dimension scaling will be worse; see Prosen and Žnidarič (2009) for some examples. Nevertheless, at infinite or sufficiently high temperature, when the NESS is close to $\mathbb{1}$ (which is a product operator), the method typically works well since high temperatures are expected to decrease entanglement, especially compared to unitary evolution, for which the complexity of $\rho(t)$ typically grows exponentially with time, regardless of whether dynamics is chaotic or integrable (Prosen and Žnidarič, 2007). For slow transport (such as strongly subdiffusive dynamics), a long convergence time to the steady state can become a problem, rendering a boundary-driven Lindblad setting less suitable.

The previously described single-site driving can be generalized to many sites. That is, one can choose Lindblad operators such that in the absence of H the steady state on those sites is a thermal state (or any other ρ) (Prosen and Žnidarič, 2009; Žnidarič *et al.*, 2010). Such many-site driving is required to have an efficient coupling to the energy density (being at least a two-site operator) and therefore is used to study energy transport (Prosen and Žnidarič, 2009; Žnidarič, 2011b; Mendoza-Arenas, Clark, and Jaksch, 2015; Palmero *et al.*, 2019). An exception involves weakly coupled systems (Michel *et al.*, 2003, 2008; Steinigeweg, Ogiewa, and Gemmer, 2009), for which energy transport is essentially the same as spin transport.

Comparisons of Lindblad and other master equations, such as the Redfield one, were given by Wichterich *et al.* (2007), Prosen and Zunkovic (2010), Purkayastha, Dhar, and Kulkarni (2016), and Xu *et al.* (2019), and a comparison to the Landauer-Büttiker formalism was given by Jin, Filippone, and Giamarchi (2020).

VI. TRANSPORT IN THE SPIN-1/2 *XXZ* CHAIN

Recently significant progress has been made in the computation of finite-temperature linear-response transport properties of one of the seemingly simplest interacting one-dimensional lattice models, the spin-1/2 *XXZ* chain.

In this section, we give an overview of the current understanding rather than an account of its historical development. We are presenting the results in the following order and discuss the relation between them: (i) exact statements, (ii) analytical results involving assumptions, and (iii) results from numerical methods. We first discuss results for $\kappa(\omega)$ and $\sigma(\omega)$ in the linear-response regime in Secs. VI.B–VI.D and then cover insights from numerical open-quantum-system simulations in Sec. VI.E.

In the evolution of the field, Zotos, Naef, and Prelovšek (1997) played a seminal role, as they established the first exact lower bounds to the energy and spin Drude weight of the spin-1/2 *XXZ* chain. Numerous early exact-diagonalization studies laid out the foundations for much of the future research; see Zotos and Prelovšek (1996), Fabricius and McCoy (1998), Naef and Zotos (1998), and Narozhny, Millis, and Andrei (1998). The next milestone involved Klümper and Sakai (Klümper and Sakai, 2002; Sakai and Klümper, 2003), who computed the full temperature dependence of the energy Drude weight in the entire parameter range of the model from the quantum-transfer-matrix method at zero magnetization. Finite-temperature Bethe-ansatz calculations of the spin Drude weight were carried out by Zotos (1999) and Benz *et al.* (2005) using different assumptions; see the discussion in Sec. III.B.3. The significance of the work by Prosen (2011b) and Prosen and Ilievski (2013) in proving the existence of nonzero finite-temperature Drude weights at vanishing magnetization was highlighted in Sec. III.A. GHD has recently emerged as a complete theoretical framework for the description of transport in integrable lattice models (Bertini *et al.*, 2016; Castro-Alvaredo, Doyon, and Yoshimura, 2016) and is thus frequently referred to later in the review. From the field-theory side, Sirker, Pereira, and Affleck (2009, 2011) played a particularly important role as they established the generic expectation for a gapless model after accounting for umklapp scattering. This can be considered the currently most advanced effective theory for the low-temperature transport of nonintegrable models (Sirker, 2020). For the integrable spin-1/2

[23]The current $j_\infty^{(S)} = j_{\chi\to\infty}^{(S)}$ was estimated using linear extrapolation in $1/\chi$.

XXZ chain, the theory predicts a diffusive form of spin autocorrelations at low T (Karrasch, Pereira, and Sirker, 2015). For a recent review on transport in this model from the field-theory and Bethe-ansatz perspectives, see Sirker (2020).

Many results from numerical methods, such as ED, tDMRG, and dynamical typicality, were covered in Sec. IV and are mentioned in the context of the spin-1/2 XXZ chain in this section.

In the context of transport in the spin-1/2 XXZ chain and related models, open quantum systems had already been studied by Saito, Takesue, and Miyashita (1996), Michel *et al.* (2003, 2008), and Saito (2003a), yet acquired a much larger weight and higher reception after the first studies using tDMRG as the solver of the underlying Lindblad equations (Prosen and Žnidarič, 2009; Žnidarič, 2011a). Numerical tDMRG solutions of Lindblad equations for transport through spin-1/2 XXZ chains were first in making predictions for superdiffusion in the spin-1/2 Heisenberg chain and provided strong support for diffusive dynamics in the regime of $\Delta > 1$ (Žnidarič, 2011a).

A. The model

The Hamiltonian governing the spin-1/2 XXZ chain is given in Eq. (1). For our choice of units ($J > 0$), $\Delta > 0$ and < 0 correspond to the antiferromagnetic and ferromagnetic regimes, respectively. By using a Jordan-Wigner transformation (Giamarchi, 2004)

$$s_r^+ = c_r^\dagger e^{i\pi \sum_{k=1}^{r-1} n_k}, \qquad s_r^z = n_r - \tfrac{1}{2}, \tag{162}$$

the spin-1/2 XXZ chain can be mapped to the following system of spinless lattice fermions $c_r^{(\dagger)}$:

$$h_{r,r+1} = \frac{J}{2} c_r^\dagger c_{r+1} + \text{H.c.} + J\Delta \left(n_r - \frac{1}{2}\right)\left(n_{r+1} - \frac{1}{2}\right). \tag{163}$$

The limit $\Delta = 0$ corresponds to free fermions and can thus be solved analytically by a simple Fourier transform from real to (quasi)momentum space.[24]

In this section, we focus mainly on $m_z = 2\langle s_r^z \rangle = 0$, which corresponds to zero magnetization (half filling) in the spin (fermion) language. The system is then gapless for $|\Delta| \leq 1$ and at low energies falls within the Tomonaga-Luttinger-liquid universality class (Giamarchi, 2004). A gap opens for $|\Delta| > 1$. There the ground state is twofold degenerate and exhibits staggered spin order in the antiferromagnetic regime $\Delta > 1$, while in the ferromagnetic case $\Delta < -1$ the system exhibits phase separation. For finite $0 < |m_z| < 1$, the system is a gapless Tomonaga-Luttinger liquid at any Δ.

B. Thermal transport

The energy-current operator, which is given in Eq. (5), is exactly conserved for periodic boundary conditions $[H, \mathcal{J}^{(\mathrm{E})}] = 0$ (Huber and Semura, 1969; Niemeijer and van Vianen, 1971; Zotos, Naef, and Prelovšek, 1997). Thus, the zero-frequency thermal conductivity is divergent at all temperatures and, as a consequence, the Drude weight is nonzero

$$\mathcal{D}_{\mathrm{w}}^{(\mathrm{E})}(T > 0) > 0, \qquad \kappa_{\mathrm{reg}} = 0. \tag{164}$$

At $\Delta = 0$, the XXZ chain maps to free fermions via Eq. (163) and $\mathcal{D}_{\mathrm{w}}^{(\mathrm{E})}$ can be obtained analytically for any $T \geq 0$:

$$\mathcal{D}_{\mathrm{w}}^{(\mathrm{E})} = \frac{1}{4\pi T^2} \int_{-\pi}^{\pi} [\epsilon_k v_k f(\epsilon_k)]^2 e^{\epsilon_k/T} dk, \tag{165}$$

where $\epsilon_k = J\cos(k)$ denotes the single-particle dispersion, $v_k = \partial_k \epsilon_k$, and $f(\epsilon) = 1/(1 + e^{\epsilon/T})$.

The energy Drude weight of the XXZ chain has been calculated analytically for $\Delta \neq 0$ and arbitrary temperatures by exploiting the integrability of the system (Klümper and Sakai, 2002; Sakai and Klümper, 2003). Since $\mathcal{J}^{(\mathrm{E})}$ is a conserved quantity, $\mathcal{D}_{\mathrm{w}}^{(\mathrm{E})} \sim \langle (\mathcal{J}^{(\mathrm{E})})^2 \rangle$. This time-independent expectation value can be computed from a modified partition function $\rho \propto \mathrm{tr}[e^{-\beta H + \lambda \mathcal{J}^{(\mathrm{E})}}]$, which serves as a generating functional and which can be determined within a quantum-transfer-matrix formalism. One ultimately obtains an expression for $\mathcal{D}_{\mathrm{w}}^{(\mathrm{E})}$ in terms of a set of nonlinear integral equations. For high and low temperatures, these equations were solved analytically, and the result in the gapless phase $|\Delta| \leq 1$ reads

$$\mathcal{D}_{\mathrm{w}}^{(\mathrm{E})} = \begin{cases} \dfrac{\pi}{6} v T, & T \to 0 \\ \dfrac{1}{128\pi}\left[3 + \dfrac{\sin(3\eta)}{\sin(\eta)}\right]\dfrac{J^4}{T^2}, & T \to \infty, \end{cases} \tag{166}$$

with v as defined in Eq. (126) and $\Delta = \cos(\eta)$. The low-T limit agrees with Eq. (128), which was obtained using bosonization (Heidrich-Meisner *et al.*, 2002). In the gapped regime, one finds $\mathcal{D}_{\mathrm{w}}^{(\mathrm{E})} \sim 1/T^2$ at high T as well as $\mathcal{D}_{\mathrm{w}}^{(\mathrm{E})} \sim e^{-\delta/T}/\sqrt{T}$ at low T, where δ is the one-spinon gap in the antiferromagnetic regime $\Delta > 1$ and the one-magnon gap in the ferromagnetic regime $\Delta < -1$. For arbitrary T, the set of nonlinear integral equations can be solved numerically. Results for $0 \leq \Delta \leq 1$ and $|\Delta| > 1$ were presented by Klümper and Sakai (2002) and Sakai and Klümper (2003), respectively. The temperature dependence of $\mathcal{D}_{\mathrm{w}}^{(\mathrm{E})}$ is shown in Fig. 5 for three values of Δ.

It was subsequently shown that for $|\Delta| < 1$ the energy Drude weight can also be computed using the thermodynamic Bethe ansatz (Zotos, 2017). On the numerical side, $\mathcal{D}_{\mathrm{w}}^{(\mathrm{E})}$ was calculated via an exact diagonalization of small systems (Alvarez and Gros, 2002a; Heidrich-Meisner *et al.*, 2002). At sufficiently high temperatures, the ED results are in agreement with the exact ones (obtained in the thermodynamic limit).

The energy Drude weight away from zero magnetization was obtained exactly using the quantum-transfer-matrix approach (Sakai and Klümper, 2005) and the TBA (Zotos, 2017) as well as via exact diagonalization (Louis and Gros,

[24] We assume translational invariance.

2003; Heidrich-Meisner, Honecker, and Brenig, 2005) and quantum Monte Carlo simulations (Louis and Gros, 2003). Magnetothermal corrections to the energy Drude weight due to the coupling of the energy to the spin current were addressed by Louis and Gros (2003), Heidrich-Meisner, Honecker, and Brenig (2005), Sakai and Klümper (2005), Psaroudaki and Zotos (2016), and Zotos (2017).

For a discussion of the energy Drude weight in other integrable spin chains, see Ribeiro, Crampé, and Klümper (2010).

C. Spin transport: Drude weight

For the spin Drude weight, the following picture has been established at zero magnetization. $\mathcal{D}_{\mathrm{w}}^{(\mathrm{S})}$ is known exactly in the limit $T=0$ via the Bethe ansatz (Shastry and Sutherland, 1990), as well as in the limit $\Delta=0$ at any T via a mapping to free fermions. At $T=0$, $\mathcal{D}_{\mathrm{w}}^{(\mathrm{S})}>0$ for $|\Delta|\leq 1$ and $\mathcal{D}_{\mathrm{w}}^{(\mathrm{S})}=0$ otherwise. Using the Mazur inequality, one can prove for a dense set of commensurate anisotropies covering the range $|\Delta|<1$ that $\mathcal{D}_{\mathrm{w}}^{(\mathrm{S})}$ is nonzero for any temperature $T>0$ (Prosen, 2011b; Prosen and Ilievski, 2013). These are the only exact statements available at $m_z=0$; they are complemented by various analytical and numerical results. The spin Drude weight can be computed using GHD at $T>0$ for any Δ (Ilievski and De Nardis, 2017b; Bulchandani *et al.*, 2018). For $|\Delta|<1$, the GHD prediction coincides with the lower Mazur bound at infinite temperature (Prosen and Ilievski, 2013), as well as with the result obtained using the thermodynamic Bethe ansatz (Zotos, 1999) at any $T>0$ (Urichuk *et al.*, 2019). At $|\Delta|>1$, GHD predicts that the Drude weight will vanish. In addition to these analytical statements, numerical data for the Drude weight are provided by ED, tDMRG, and dynamical typicality; see Secs. IV.B–IV.E.

Away from zero magnetization ($m_z\neq 0$), the Drude weight is finite for any value of T and Δ. This follows from the exact Bethe-ansatz calculation at $T=0$ (Shastry and Sutherland, 1990) and the exact lower Mazur bound (Zotos, Naef, and Prelovšek, 1997), respectively. The Drude weight was also computed numerically (Heidrich-Meisner, Honecker, and Brenig, 2005).

We now discuss the previous results in more detail; see Fig. 14 for a summary.

1. Free fermions and Bethe ansatz at $T=0$

At $\Delta=0$, the spin Drude weight $\mathcal{D}_{\mathrm{w}}^{(\mathrm{S})}$ can be obtained analytically for any $T\geq 0$ by using the mapping to free fermions. The result is given by (Giamarchi, 2004)

$$\mathcal{D}_{\mathrm{w}}^{(\mathrm{S})}=\frac{1}{4\pi T}\int_{-\pi}^{\pi}[v_k f(\epsilon_k)]^2 e^{\epsilon_k/T}dk. \tag{167}$$

In the zero-temperature limit, the spin Drude weight can be computed exactly for any Δ by evaluating Kohn's formula [Eq. (26)] (Kohn, 1964) via the Bethe ansatz (Shastry and Sutherland, 1990). The result for $|\Delta|\leq 1$ reads

$$\mathcal{D}_{\mathrm{w}}^{(\mathrm{S})}=\frac{Kv}{2\pi}, \tag{168}$$

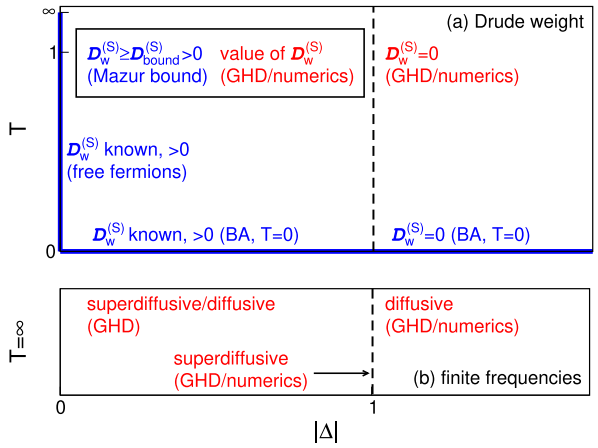

FIG. 14. (a) Overview of all known exact results [free fermions, Bethe ansatz (BA) at $T=0$, and Mazur bounds] as well as predictions obtained using GHD and numerics for the spin Drude weight of the spin-1/2 XXZ chain at zero magnetization. (b) Overview of the high-temperature results for the leading contribution at low but finite frequencies. In the regime $|\Delta|<1$, this low-frequency contribution is either superdiffusive or diffusive.

with K and v given in Eq. (126) for $m_z=0$. This agrees with Eq. (128), which was obtained using bosonization. For $|\Delta|>1$, the Drude weight vanishes. Note that Eq. (168) does not approach zero for $\Delta\nearrow 1$, and $\mathcal{D}_{\mathrm{w}}^{(\mathrm{S})}$ thus shows a discontinuity at $\Delta=1$ for $T=0$.

2. Mazur bounds

Away from zero magnetization (i.e., for $m_z\neq 0$), the spin Drude weight is finite for any value of T and Δ. This can be shown by evaluating the Mazur inequality [Eq. (28)] with the energy-current operator as a single conserved local charge $Q_2=\mathcal{J}^{(\mathrm{E})}$ that has a nonzero overlap with $\mathcal{J}^{(\mathrm{S})}$ in the thermodynamic limit. At high T, the bound can be evaluated analytically (Zotos, Naef, and Prelovšek, 1997)

$$\mathcal{D}_{\mathrm{w}}^{(\mathrm{S})}\geq\frac{J^2}{T}\frac{\Delta^2 m_z^2}{4}\frac{(1-m_z^2)}{1+\Delta^2(2+2m_z^2)}>0, \tag{169}$$

which is valid for any value of Δ. In the gapless phase at low T and close to $m_z=0$, one can add a Zeeman term $b\sum_r s_r^z$ to the Hamiltonian (b is the magnetic field) and then use bosonization to obtain (Sirker, Pereira, and Affleck, 2011)

$$\mathcal{D}_{\mathrm{w}}^{(\mathrm{S})}\geq\frac{Kv}{2\pi}\frac{1}{1+(\pi^2/3K)(T/b)^2}>0. \tag{170}$$

Directly at zero magnetization, the energy-current operator has a vanishing overlap with the spin-current operator and thus does not yield a nonzero contribution to the Mazur inequality [Eq. (28)]. This follows from symmetry arguments and can also be seen by setting $m_z=0$ in Eq. (169): Q_2 is even under the transformation $s_r^z\to -s_r^z$, $s_r^{\pm}\to s_r^{\mp}$ while $\mathcal{J}^{(\mathrm{S})}$ is odd, and hence $\langle Q_2\mathcal{J}^{(\mathrm{S})}\rangle=0$. The same holds true for all other strictly local conserved quantities associated with the integrability of the system. Note that the vanishing of $\langle Q_2\mathcal{J}^{(\mathrm{S})}\rangle$ also implies

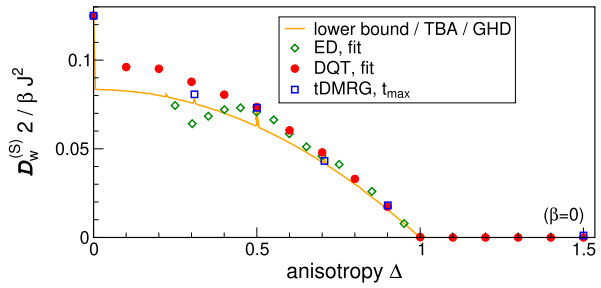

FIG. 15. Comparison of different results for the spin Drude weight $\mathcal{D}_{\mathrm{w}}^{(\mathrm{S})}$ in the high-temperature limit $\beta = 0$ at zero magnetization: the solid line shows the lower bound (Prosen and Ilievski, 2013), which is given by Eq. (78) and which at infinite temperature coincides with the TBA result (Zotos, 1999; Urichuk *et al.*, 2019; Pavlis and Zotos, 2020) and the GHD prediction (Ilievski and De Nardis, 2017b; Bulchandani *et al.*, 2018). Moreover, we show ED (Herbrych, Prelovšek, and Zotos, 2011), DQT (Steinigeweg, Gemmer, and Brenig, 2014, 2015), and tDMRG data taken from Karrasch, Kennes, and Moore (2014) and Karrasch, Kennes, and Heidrich-Meisner (2015); see also Karrasch, Bardarson, and Moore (2012), Karrasch *et al.* (2013), and Karrasch (2017a). For the tDMRG data, the Drude weight is taken as the value of $\langle \mathcal{J}^{(\mathrm{S})}(t)\mathcal{J}^{(\mathrm{S})}\rangle/L$ at the largest accessible time without any further extrapolation. Note that while the lower bound was computed only for commensurate $\Delta = \cos(\ell\pi/m)$, numerical data are also shown away from these points.

the absence of a magnetothermal correction in the zero-magnetization sector (Louis and Gros, 2003), while this term generally contributes at finite magnetizations.

As discussed in detail in Sec. III.A, an exact lower bound can be derived for zero magnetization as well by using quasilocal conserved charges that do have a nonzero overlap with the spin-current operator (Prosen, 2011b; Prosen and Ilievski, 2013). This bound is given in Eq. (78) and is visualized in Fig. 4 (see also Fig. 15); it generally features a fractal dependence on Δ. An important question concerns the completeness of this set of charges: a numerical study of finite systems suggests that there are no additional charges beyond the known ones (Mierzejewski, Prelovšek, and Prosen, 2015).

3. Bethe ansatz at $T > 0$ and GHD

An exact Bethe-ansatz calculation at finite T using Kohn's formula is hindered by the fact that excited states can be treated only approximately. Zotos (1999) carried out the calculation by means of the thermodynamic Bethe ansatz, which as discussed in Sec. III.B.2 involves the string hypothesis for bound states of magnons. An alternative calculation based on a spinon-antispinon basis was presented by Benz *et al.* (2005). The thermodynamic Bethe-ansatz approach predicts that $\mathcal{D}_{\mathrm{w}}^{(\mathrm{S})}(T)$ is finite in the gapless phase and decreases monotonically with T except at the isotropic point $\Delta = 1$ where $\mathcal{D}_{\mathrm{w}}^{(\mathrm{S})}(T > 0) = 0$. At low T, one obtains a nontrivial power-law dependence for commensurate values of $\Delta = \cos(\pi/m)$, $m = 1, 2, \ldots$:

$$\mathcal{D}_{\mathrm{w}}^{(\mathrm{S})}(T) = \mathcal{D}_{\mathrm{w}}^{(\mathrm{S})}(T=0) - \mathrm{const} \times T^{\alpha}, \quad \alpha = \frac{2}{m-1}. \tag{171}$$

For $\Delta = 1$, a second Bethe-ansatz-based calculation (Carmelo, Prosen, and Campbell, 2015) concludes in favor of $\mathcal{D}_{\mathrm{w}}^{(\mathrm{S})} = 0$, which is in agreement with GHD (Ilievski *et al.*, 2018).

One can show that for commensurate values of $\Delta = \cos(\ell\pi/m)$ (ℓ, m coprime) the TBA result given by Zotos (1999) coincides with the GHD prediction (Ilievski and De Nardis, 2017b; Bulchandani *et al.*, 2018) at any temperature (Urichuk *et al.*, 2019). Moreover, it also coincides with the exact lower bound given by Prosen and Ilievski (2013) at infinite temperature, which is given in Eq. (78) and shown in Fig. 4. In a nutshell,

$$\frac{\mathcal{D}_{\mathrm{w}}^{(\mathrm{S})}|_{\mathrm{TBA}}}{\beta} = \frac{\mathcal{D}_{\mathrm{w}}^{(\mathrm{S})}|_{\mathrm{GHD}}}{\beta} \overset{T\to\infty}{=} \tilde{\mathcal{D}}_{\mathrm{w}}^{(\mathrm{S})}|_{\mathrm{bound}}. \tag{172}$$

For $\Delta > 1$, both GHD (Ilievski and De Nardis, 2017b) and a TBA-based analytical calculation (Peres *et al.*, 1999) suggest that the Drude weight vanishes in this regime.

4. Numerical approaches

A variety of numerical methods have been used to compute the spin Drude weight $\mathcal{D}_{\mathrm{w}}^{(\mathrm{S})}$ in the thermodynamic limit, including (i) exact diagonalization, which is limited to small systems $L \leq 20$ (Zotos and Prelovšek, 1996; Narozhny, Millis, and Andrei, 1998; Heidrich-Meisner *et al.*, 2003; Rabson, Narozhny, and Millis, 2004; Herbrych, Prelovšek, and Zotos, 2011; Karrasch *et al.*, 2013; Sánchez and Varma, 2017); (ii) the microcanonical Lanczos method, which is also limited to small $L \leq 28$ (Long *et al.*, 2003); (iii) quantum Monte Carlo methods, which requires an analytical continuation to extract $\mathcal{D}_{\mathrm{w}}^{(\mathrm{S})}$ (Alvarez and Gros, 2002c; Heidarian and Sorella, 2007); (iv) the time-dependent DMRG, where the accessible timescales are bounded by the entanglement growth (Karrasch, Bardarson, and Moore, 2012; Karrasch *et al.*, 2013; Karrasch, Kennes, and Moore, 2014; Karrasch, Kennes, and Heidrich-Meisner, 2015; Karrasch, 2017a); and (v) dynamical typicality (Steinigeweg, Gemmer, and Brenig, 2014, 2015), which is also limited in terms of the system size $L \leq 36$.

Figure 15 shows a comparison of tDMRG (Karrasch, Bardarson, and Moore, 2012; Karrasch *et al.*, 2013; Karrasch, Kennes, and Moore, 2014; Karrasch, Kennes, and Heidrich-Meisner, 2015; Karrasch, 2017a), exact diagonalization (Herbrych, Prelovšek, and Zotos, 2011; Karrasch *et al.*, 2013), and dynamical typicality data (Steinigeweg, Gemmer, and Brenig, 2014, 2015) with the lower bound (Prosen and Ilievski, 2013) at infinite temperature. Note that the numerical results are also shown away from commensurate Δ. At certain commensurate points such as $\Delta = 1/2$, the numerical results and the bound agree well. For generic values at $\Delta > 1/2$, all methods result in larger values than the bound. For $0 < \Delta < 1/2$ and, in particular, close to $\Delta = 0$, the disagreement is evident and has not yet been resolved; see Secs. IV.B, IV.C, and IV.E for a discussion of the strengths and limitations of the numerical approaches, and Sec. VI.E for a discussion of open questions concerning the spin-1/2 XXZ chain.

For $\Delta > 1$, there are no exact results available for $T > 0$ at zero magnetization. Both GHD and a TBA-based analytical calculation (Peres *et al.*, 1999) suggest that the Drude weight vanishes in the regime. Numerical studies also point in this direction (Zotos and Prelovšek, 1996; Heidrich-Meisner *et al.*, 2003; Karrasch, Bardarson, and Moore, 2012; Steinigeweg, Gemmer, and Brenig, 2014). In particular, one observes a clean scaling of the Drude weight as $\mathcal{D}_{\mathrm{w}}^{(\mathrm{S})} \propto 1/L$ in systems of finite size. As an example, Fig. 7 shows the scaling found by Steinigeweg, Gemmer, and Brenig (2014, 2015).

At $\Delta = 1$, exact-diagonalization results indicate a vanishing (Herbrych, Prelovšek, and Zotos, 2011) or at best small Drude weight (Heidrich-Meisner *et al.*, 2003), with the actual numbers depending on details of the finite-size extrapolation (Karrasch *et al.*, 2013; Sánchez and Varma, 2017); see Sec. IV.B. Both dynamical typicality (Steinigeweg, Gemmer, and Brenig, 2014, 2015) and tDMRG (Sirker, Pereira, and Affleck, 2009; Karrasch, Bardarson, and Moore, 2012; Kennes and Karrasch, 2016) yield a current correlation function $\langle \mathcal{J}^{(\mathrm{S})}(t)\mathcal{J}^{(\mathrm{S})}\rangle$ that decays slowly. The DQT data were interpreted in terms of a zero (finite) Drude weight at infinite (finite) temperature; the tDMRG results were interpreted in terms of a finite Drude weight.

The previous discussion focused on infinite temperature, but the temperature dependence of the Drude weight is also of interest (Zotos, 1999; Alvarez and Gros, 2002c; Fujimoto and Kawakami, 2003; Heidrich-Meisner *et al.*, 2003; Benz *et al.*, 2005; Karrasch *et al.*, 2013). The verification of the TBA result for the low-T behavior [Eq. (171)] in a numerical calculation has not yet been accomplished (Alvarez and Gros, 2002c; Karrasch *et al.*, 2013).

D. Spin transport: Finite frequencies

We recall that it is now established exactly that at zero magnetization the Drude weight $\mathcal{D}_{\mathrm{w}}^{(\mathrm{S})}$ is finite for $\Delta < 1$ at any temperature $T \geq 0$. For the regime $\Delta > 1$, the current understanding is that $\mathcal{D}_{\mathrm{w}}^{(\mathrm{S})}$ vanishes. In recent years, there has been substantial progress in understanding the spin transport in the XXZ chain beyond the mere existence of the spin Drude weight. In this section, we summarize results for the regular part of the spin conductivity in the three different regimes $\Delta > 1$, < 1, and $= 1$. We focus exclusively on zero magnetization. See Gopalakrishnan, Vasseur, and Ware (2019) for a recent GHD study of spin transport and dynamics in the $m_z \neq 0$ regime.

As outlined in Sec. II.B, one can envision three different scenarios for the low-frequency behavior: The spin conductivity is (a) diffusive $\sigma_{\mathrm{reg}}(\omega \to 0) = \sigma_{\mathrm{dc}} > 0$, (b) superdiffusive $\sigma_{\mathrm{reg}}(\omega) \sim \omega^{\alpha}$, with $\alpha < 0$, or (c) subdiffusive $\sigma_{\mathrm{reg}}(\omega) \sim \omega^{\alpha}$, with $\alpha > 0$. This is illustrated in Fig. 1.

1. $\Delta > 1$

A lower bound for the diffusion constant, which is related to the dc conductivity via Eq. (24), was established by Medenjak, Karrasch, and Prosen (2017) and Ilievski *et al.* (2018); see Sec. III.A.2. The diffusion constant is expressed in terms of the magnetization dependence (i.e., curvature) of the Drude weight, which can be bounded from below using conserved charges. It was shown that the bound is finite for $\Delta > 1$, which rules out a subdiffusive form of $\sigma_{\mathrm{reg}}(\omega)$ in this regime (Medenjak, Karrasch, and Prosen, 2017; Ilievski *et al.*, 2018). This is an exact result.

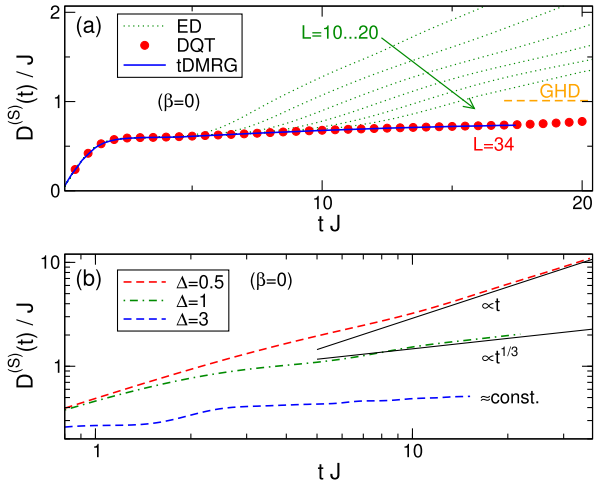

FIG. 16. (a) Comparison of different results for the time-dependent diffusion constant $D^{(\mathrm{S})}(t)$ of the spin-1/2 XXZ chain at $\Delta = 1.5$ in the infinite-temperature limit $\beta = 0$: ED (Steinigeweg and Gemmer, 2009), DQT (Steinigeweg, Gemmer, and Brenig, 2015), and tDMRG (Karrasch, Moore, and Heidrich-Meisner, 2014). (b) tDMRG data for $D^{(\mathrm{S})}(t)$ at various Δ [obtained from integrating the current autocorrelation function given by Karrasch, Kennes, and Moore (2014) and Karrasch, Kennes, and Heidrich-Meisner (2015)].

One can define a time-dependent diffusion constant $D^{(\mathrm{S})}(t)$, $D^{(\mathrm{S})}(t \to \infty) = D^{(\mathrm{S})}$ using the generalized Einstein relation (37) via a time integral of the current autocorrelation function (Bohm and Leschke, 1992; Steinigeweg and Gemmer, 2009; Yan, Jiang, and Zhao, 2015). This quantity was evaluated using GHD at infinite temperature and arbitrary Δ (De Nardis, Bernard, and Doyon, 2019; Gopalakrishnan and Vasseur, 2019). In the limit of large Δ, the result takes the form

$$\lim_{\Delta\to\infty}\lim_{t\to\infty} D^{(\mathrm{S})}(t) = \lim_{\Delta\to\infty} D^{(\mathrm{S})} \approx 0.42J, \tag{173}$$

which is consistent with the nonvanishing lower bound for the diffusion constant given by Ilievski *et al.* (2018) and, moreover, predicts that transport is diffusive and not superdiffusive. Within GHD, the finite-time corrections have the form $D^{(\mathrm{S})}(t) = a + b/\sqrt{t}$.

The time-dependent diffusion constant has also been calculated numerically via ED and DQT (Steinigeweg and Gemmer, 2009; Steinigeweg, Gemmer, and Brenig, 2015) as well as by using tDMRG (Karrasch, Moore, and Heidrich-Meisner, 2014). We show $D^{(\mathrm{S})}(t)$ at infinite temperature for $\Delta = 1.5$ and 3 in Figs. 16(a) and 16(b), respectively (the curves with $\Delta = 0.5$, 1 are discussed later). The system size can be chosen large enough, within both DQT and tDMRG, such that the results are effectively in the thermodynamic limit at the largest time depicted in the figure, which is illustrated explicitly in the case of DQT. These data were interpreted in terms of a finite diffusion constant $D^{(\mathrm{S})} = D^{(\mathrm{S})}(t \to \infty)$ and

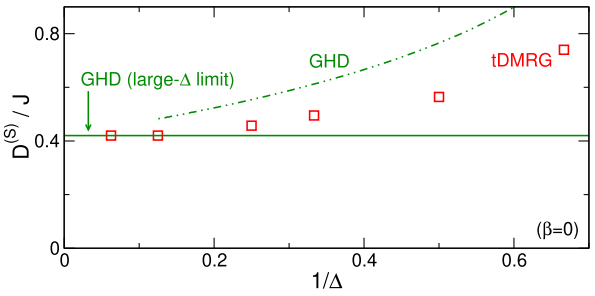

FIG. 17. Diffusion constant of the spin-1/2 XXZ chain at infinite temperature as a function of $1/\Delta$ for $\Delta > 1$. tDMRG results (Karrasch, Moore, and Heidrich-Meisner, 2014) are compared to the GHD prediction for $\Delta \to \infty$ [cf. Eq. (173)] and $\Delta < \infty$ (De Nardis, Bernard, and Doyon, 2019). The tDMRG results close to $\Delta = 1$ give only a lower bound to the true diffusion constant.

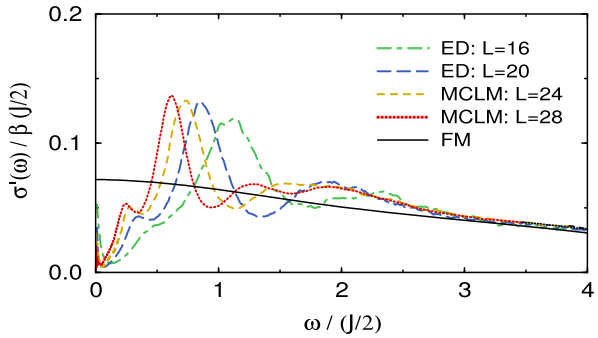

FIG. 18. Real part of the optical conductivity $\sigma(\omega)$ of the spin-1/2 XXZ chain, as obtained by Prelovšek *et al.* (2004) from ED and the MCLM for $\Delta = 2$ and infinite temperature $\beta = 0$. The anomalous scaling with system size is still consistent with a well-behaved low-frequency part and a finite dc conductivity in the thermodynamic limit. The solid line results from computing frequency moments (FM).

thus regular diffusive transport. In Fig. 17, we show a comparison between the GHD prediction for large Δ and the value of $D^{(\mathrm{S})}$ extracted from the tDMRG data (Karrasch, Moore, and Heidrich-Meisner, 2014); the results agree in the limit $\Delta \to \infty$. The tDMRG results close to $\Delta = 1$ give a lower bound only to the true diffusion constant.

The time-dependent diffusion constant was also studied via perturbation theory in powers of Δ under the assumption that the current autocorrelation function decays monotonically in time to zero (Steinigeweg and Schnalle, 2010; Steinigeweg, 2011). A good agreement with numerics was found at short and intermediate timescales, where this assumption is well satisfied.

The full frequency-dependent conductivity $\sigma_{\mathrm{reg}}(\omega)$ was investigated for $\Delta > 1$ using ED and the MCLM (Prelovšek *et al.*, 2004). As illustrated in Fig. 18, for system sizes accessible to those methods, $\sigma_{\mathrm{reg}}(\omega)$ typically has an anomalous form, with strongly reduced spectral weight at small ω in the vicinity of the finite-size spin Drude weight $\mathcal{D}_{\mathrm{w}}^{(\mathrm{S})}$ and a pronounced shoulder at larger ω. As argued by Prelovšek *et al.* (2004), however, the position of this shoulder moves with increasing system size to smaller ω as $1/L$ and might eventually take on a simple form with a well-behaved low-frequency part and a finite dc conductivity in the thermodynamic limit. Whether this anomalous form is indeed a spurious effect of small systems or whether it persists for large systems is still an open problem; see the discussion in Sec. IV.B. Yet it is clear that the degree of anomalous behavior substantially depends on the frequency scale or, equivalently, the timescale considered (Jin *et al.*, 2015; Steinigeweg, Herbrych, Pollmann, and Brenig, 2016).

The full frequency-dependent conductivity $\sigma_{\mathrm{reg}}(\omega)$ was also calculated for $\Delta > 1$ via a Fourier transform of finite-time tDMRG data (Karrasch, Kennes, and Moore, 2014). It shows a regular diffusive peak at small frequencies as well as contributions for frequencies above the spectral gap.

In addition to the numerous works on current-current correlations, a significant body of works has studied density-density correlations as well, in either momentum or real space (Huber and Semura, 1969; Fabricius, Löw, and Stolze, 1997; Fabricius and McCoy, 1998). This allows one to also study the momentum dependence of the diffusion coefficient. In the context of diffusion, a result from exact and Lanczos diagonalization (Steinigeweg and Brenig, 2011; Steinigeweg *et al.*, 2012) is that the time-dependent susceptibility $\chi_q(t)$ defined in Eq. (57) decays at small β according to

$$\frac{d\chi_q(t)}{dt} = -\tilde{q}^2 D_q^{(\mathrm{S})}(t)\chi_q(t). \tag{174}$$

Here the decay rate $D_q^{(\mathrm{S})}(t)$ becomes independent of q for small momenta $q > 0$ in a finite lattice and coincides with the time-dependent diffusion coefficient $D^{(\mathrm{S})}(t)$ in the Einstein relation (37). The number of diffusive momenta was shown to decrease with decreasing temperature, while the diffusion constant increases as long as the temperature is sufficiently larger than the gap.

2. $\Delta < 1$

The Drude weight has been shown to be finite for any commensurate value of $\Delta < 1$ with $\Delta = \cos(\ell\pi/m)$ and is thus conjectured to be finite everywhere. An exact lower bound for the diffusion constant was also obtained in this regime (Ilievski *et al.*, 2018). It was shown analytically that the bound is finite for commensurate $\Delta = \cos(\pi/m)$, which rules out a subdiffusive form of $\sigma_{\mathrm{reg}}(\omega)$ for these parameters. For incommensurate values of Δ (i.e., almost everywhere), the lower bound diverges, and transport cannot be diffusive but must be faster than diffusive. Combined with the expectation that the frequency-integrated conductivity should be continuous everywhere due to sum rules, this hints at the possibility of superdiffusive corrections away from the commensurate points. This conjecture was put onto firmer ground by Agrawal *et al.* (2020). We now consider a value $\Delta = \cos(\pi\eta_\infty)$, where η_∞ is a generic irrational number. The reasoning uses the fact that η_∞ can be approximated by a series of rational values $\eta_m = \ell/m$ with growing denominators m. Using fairly general arguments, one can show that the dc conductivity at infinite temperature can be approximated as

$$\sigma_{\mathrm{dc}}(\eta_m) \sim m^{2\alpha/(1-\alpha)}. \tag{175}$$

Equation (175) leads to a subleading correction to $\sigma'(\omega)$ at η_∞ that diverges, giving rise to subdiffusion (Agrawal *et al.* 2020).

GHD allows one to obtain the exponents associated with the superdiffusive correction (Agrawal *et al.*, 2020): The low-frequency conductivity behaves as $\sigma_{\mathrm{reg}}(\omega) \propto \omega^{-\alpha}$, with $\alpha = 1/2$ for generic values of Δ. This divergence is cut off at the rational points, leading to a diffusive correction. Furthermore, a qualitative picture emerges from GHD: the subleading correction arises from scattering of charged quasiparticles off neutral quasiparticles, and an interpretation in terms of a Lévy flight has been put forward (Agrawal *et al.*, 2020).

At low temperatures, a field-theory calculation that incorporates the leading irrelevant umklapp term and accounts for conserved charges via the memory-matrix formalism suggests a diffusive form of the subleading $\sigma_{\mathrm{reg}}(\omega)$ (Sirker, Pereira, and Affleck, 2011); see Sirker (2006) for earlier work. This is consistent with earlier results for the generic behavior of a Tomonaga-Luttinger liquid in the presence of umklapp scattering (Giamarchi, 1991), but it is an open question as to whether field theory away from commensurate values of Δ is consistent with the GHD result that subleading correction cannot be diffusive there. The field theory was used to compute the density-density correlation function and a diffusive behavior was found, in agreement with tDMRG data (Karrasch, Pereira, and Sirker, 2015).

The spin conductivity has been computed numerically via various approaches. Using Lanczos diagonalization, it was concluded that $\sigma_{\mathrm{reg}}(\omega) \sim \omega^2$ at low frequencies (Herbrych, Steinigeweg, and Prelovšek, 2012), which is at odds with the lower bound established by Ilievski *et al.* (2018). The Fourier transform of finite-time tDMRG data is consistent with a finite $\sigma_{\mathrm{reg}}(\omega \to 0) = \sigma_{\mathrm{dc}} > 0$, and for certain values of Δ it suggests an additional peak structure at larger frequencies (Karrasch, Kennes, and Heidrich-Meisner, 2015). For completeness, Fig. 16(b) depicts tDMRG results for $D^{(\mathrm{S})}(t)$ at $\Delta = 0.5$. One finds that $D^{(\mathrm{S})}(t) \sim t$ for $tJ \gtrsim 10$ due to the finite Drude weight. A convincing numerical confirmation of the GHD prediction for the power-law decay of $C(t)$ at generic values of Δ toward the Drude weight is still missing.

3. $\Delta = 1$

While no exact results are available, the current belief is that the Drude weight vanishes at the isotropic point $\Delta = 1$ in the thermodynamic limit. There is in principle the possibility of diffusive transport occurring (Sirker, Pereira, and Affleck, 2009, 2011). However, this scenario has been controversially discussed in the literature and, in contrast to the regime $\Delta > 1$, there is mounting evidence that diffusion is not realized.

The exact lower bound on the diffusion constant diverges in the limit $\Delta \to 1$ at infinite temperature (Ilievski *et al.*, 2018), which is indicative of superdiffusion at this point. A divergence was also obtained within the GHD approach, and for $\Delta \to 1^+$ it was found that (De Nardis, Bernard, and Doyon, 2019)

$$D^{(\mathrm{S})} = \lim_{t\to\infty} D^{(\mathrm{S})}(t) \propto \frac{1}{\sqrt{\Delta - 1}}. \tag{176}$$

The same result has been derived via a GHD-based kinetic picture (Gopalakrishnan and Vasseur, 2019), and the time-dependent diffusion constant was predicted to scale as $D^{(\mathrm{S})}(t) \propto t^{1/3}$. This was confirmed in another GHD study (Agrawal *et al.*, 2020).

This superdiffusive behavior is consistent with finite-time tDMRG data for $D^{(\mathrm{S})}(t)$ at $\Delta = 1$ [see Fig. 16(b)] as well as with numerical linked-cluster expansions (Richter and Steinigeweg, 2019; Richter *et al.*, 2020). Signatures of superdiffusion at $\Delta = 1$ were found in the unitary evolution of inhomogeneous initial states (Ljubotina, Žnidarič, and Prosen, 2017). In particular, for initial states with a magnetization profile of the domain-wall type, the profiles at later times collapse after a rescaling of space with the power law $t^{3/2}$, which corresponds to $D^{(\mathrm{S})}(t) \sim t^{1/3}$ (Ljubotina, Žnidarič, and Prosen, 2017).

The field-theory calculation given by Sirker, Pereira, and Affleck (2009, 2011) was also carried out directly at $\Delta = 1$. It predicts diffusive dynamics of density-density correlations in the hydrodynamic regime of small momenta $q \to 0$ and low frequencies $\omega \to 0$, where the diffusion constant scales with temperature as

$$D^{(\mathrm{S})} \propto \frac{\ln T}{T}. \tag{177}$$

The possibility of diffusion in the hydrodynamic regime was also scrutinized in quantum Monte Carlo simulations (Grossjohann and Brenig, 2010), where the bosonization prediction was transformed to imaginary time to avoid transformations of Monte Carlo data to real times. A fit of these QMC data to the bosonization result supports a finite diffusion constant $D^{(\mathrm{S})}$. It is presently not fully understood how this can be reconciled with the fact that the lower bound and GHD predict superdiffusion at $\Delta = 1$.

E. Open quantum systems

Complementary to works on Kubo response functions in closed systems, one can study open quantum systems, particularly using the Lindblad equation with a driving at the two boundaries of the XXZ chain; cf. Sec. V.B. For $\Delta > 1$ and in the case of weak driving, i.e., in the linear-response regime, a linear magnetization profile as well as a spin-current scaling as $\mathcal{J}^{(\mathrm{S})} \propto 1/L$ was observed, which corresponds to diffusion (Michel *et al.*, 2008; Prosen and Žnidarič, 2009; Žnidarič, 2011a). In the limit of large Δ, the Lindblad approach yields a scaling of the diffusion constant as $D^{(\mathrm{S})} \propto 1/\Delta$ (Žnidarič, 2011a), which is different from the $D^{(\mathrm{S})} =$ const result coming from tDMRG calculations (Karrasch, Moore, and Heidrich-Meisner, 2014) and generalized hydrodynamics (De Nardis, Bernard, and Doyon, 2019; Gopalakrishnan and Vasseur, 2019); see Fig. 17. However, an equivalence of the linear-response and open-system results

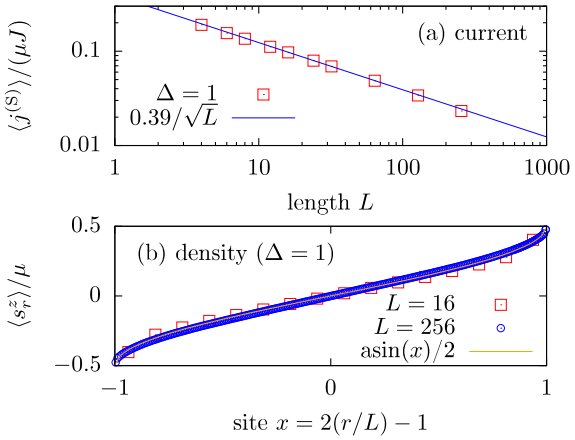

FIG. 19. Results from the Lindblad quantum master equation for simulating spin transport in the spin-1/2 XXZ chain, as obtained by Žnidarič (2011a) for $\Delta = 1$. (a) Superdiffusive scaling of the spin current as $j^{(S)} \propto 1/\sqrt{L}$. (b) L-independent magnetization profile.

is not expected for the choice of the system-bath coupling made by Žnidarič (2011a), where $\Gamma \sim \Delta$.

At $\Delta = 1$ and high T, the open-system spin current no longer scales as $\mathcal{J}^{(S)} \propto 1/L$ but is instead found to scale slower according to the power law $\mathcal{J}^{(S)} \propto 1/\sqrt{L}$; see Fig. 19. Since the magnetization profile does not show a significant dependence on L, this scaling of the spin current shows the emergence of superdiffusion in the Lindblad approach (Žnidarič, 2011a, 2011b), which was the first observation of this behavior in the spin-1/2 Heisenberg chain. This is in agreement with numerics for unitary time evolution (Ljubotina, Žnidarič, and Prosen, 2017) and with the fact that the lower bound to the diffusion constant diverges for $\Delta \to 1$ (Ilievski *et al.*, 2018).

F. Open questions

As discussed earlier, our theoretical understanding of transport in the spin-1/2 XXZ chain at nonzero temperatures has seen substantial progress over the past decade due to a combination of various analytical and numerical techniques. Yet there are many open questions. A few of these questions are summarized in the following.

One important question is whether or not the exact lower bound for the spin Drude weight $\mathcal{D}_w^{(S)}$ in Eq. (78) is exhaustive for all commensurate values of $|\Delta| < 1$. It is now established that at infinite temperature this lower bound coincides with the TBA (Zotos, 1999) and GHD (Ilievski and De Nardis, 2017b; Bulchandani *et al.*, 2018) results, which are also identical at any T for $|\Delta| < 1$ (Urichuk *et al.*, 2019). However, a central assumption invoked within the TBA and therefore GHD, which is formulated in the TBA language, is the string hypothesis. It is an interesting open question as to whether or not GHD can be formulated without resorting to the string hypothesis. Similarly, the question remains whether the spin Drude weight can be computed in a Bethe-ansatz approach without resorting to the string hypothesis. A recent study by Klümper and Sakai (2019) carried out such an alternative calculation without using the string hypothesis. Results for $\mathcal{D}_w^{(S)}(T)$ were obtained by using a numerical solution of the resulting nonlinear equations for $\Delta = \cos(\pi/m)$. These exhibit finite-size effects that become more significant as temperature is lowered. Eventually, the data converge to the TBA results given by Zotos (1999) in the thermodynamic limit.

Moreover, while the possibility of a fractal-like dependence of $\mathcal{D}_w^{(S)}$ on Δ is intriguing, no numerical method will likely be capable to confirm the fractal structure. The sudden drop of $\mathcal{D}_w^{(S)}$ when going from $\Delta = 0$ to $\Delta > 0$ has not yet been numerically verified. Particularly useful would be a lower bound with finite-size corrections, which would allow for more reliable extrapolations to the limit of large system sizes as well.

Another important and closely related issue concerns subleading corrections to the spin Drude weight $\mathcal{D}_w^{(S)}$ in the regime $|\Delta| < 1$. It is now established from exact lower bounds and GHD that the diffusion constant is finite for commensurate values of Δ but diverges away from these points (Ilievski *et al.*, 2018; Agrawal *et al.*, 2020). This rapid change is explained by a significant weight transfer in the low-frequency window as one goes from commensurate values of Δ to incommensurate ones; concrete exponents for the divergence of $\sigma_{\rm reg}(\omega)$ at generic values of $\Delta < 1$ and $= 1$ were obtained from GHD (Agrawal *et al.*, 2020). This results in a more appealing picture as it satisfies the physical expectation of a smooth parameter dependence of at least the integral over the low-frequency part of $\sigma_{\rm reg}(\omega)$. Nevertheless, at least within GHD, the distinction between rational and irrational values again relates to properties of the quasiparticles, and thus the existence of both diffusive and superdiffusive corrections may also rely on Takahashi's string hypothesis. This leads to the same question again: can the string hypothesis be replaced in GHD and what would the results be? A convincing numerical confirmation of the exponents for the subleading correction for generic values of $\Delta < 1$ is also missing.

Several open questions remain in the regime $\Delta > 1$ as well. While an analytical calculation based on certain assumptions (Carmelo, Prosen, and Campbell, 2015) concludes in favor of $\mathcal{D}_w^{(S)} = 0$ at $T > 0$, a strict proof is still missing. An exact lower bound to the diffusion constant was obtained and shown to be finite, ruling out subdiffusion (Ilievski *et al.*, 2018). While substantial evidence has been provided that spin dynamics is diffusive, it still needs to be qualitatively explained why diffusion can occur in integrable systems, where concepts such as chaos, ergodicity, etc., do not apply. It would be interesting to obtain a better numerical estimate for the diffusion constant in the longtime limit, since the deviation from the GHD data in Fig. 17 is most likely related to the finite times reached in the simulations.

Another puzzling issue concerns the notion of a mean free path. While the quantitative values for the diffusion constant suggest a mean free path on the order of one lattice site, strong finite-size effects and anomalous scaling to the thermodynamic limit appear nonetheless (Prelovšek *et al.*, 2004), which suggests

that the mean free path is not the only length scale involved for a finite system (Steinigeweg *et al.*, 2012). It would be interesting to investigate the behavior of higher-order current correlation functions (Steinigeweg and Prosen, 2013).

At the isotropic point $\Delta = 1$, transport at infinite temperature is faster than diffusive since the exact lower bound to the diffusion constant diverges for $\Delta \to 1$ (Ilievski *et al.*, 2018); such a divergence is also observed in GHD calculations (De Nardis, Bernard, and Doyon, 2019; Agrawal *et al.*, 2020). Numerical simulations (Žnidarič, 2011a; Prosen and Žunkovič, 2013) point to the emergence of superdiffusion. However, the origin and nature of this nondiffusive process is not yet fully understood. First attempts have been undertaken, and there is mounting support for the dynamical exponent of $z = 3/2$ (Ljubotina, Žnidarič, and Prosen, 2017), which is consistent with Kardar-Parisi-Zhang (KPZ) scaling (Ljubotina, Žnidarič, and Prosen, 2019) and was further corroborated and discussed by Gopalakrishnan and Vasseur (2019), Bulchandani (2020), De Nardis, Gopalakrishnan *et al.* (2020), Spohn (2020a), and Weiner *et al.* (2020). Whether the KPZ-like scaling persists in other isotropic spin models with or without integrability is currently the object of intense scrutiny; see De Nardis *et al.* (2019) and Dupont and Moore (2020). Recent studies concluded that superdiffusion with an exponent of $z = 3/2$ is generally realized in all integrable, Heisenberg-like magnets that are invariant under global non-Abelian continuous symmetry (Ilievski *et al.*, 2020; Krajnik, Ilievski, and Prosen, 2020). A first-principle derivation of KPZ scaling for these integrable models (besides predicting the exponent) is still lacking and the possibility of other types of superdiffusion in integrable spin chains cannot be fully ruled out either (Žnidarič, 2013b).

From a methodological point of view, it is unclear how the field-theory prediction of diffusion (Sirker, Pereira, and Affleck, 2009) and the associated low-T QMC data (Grossjohann and Brenig, 2010) for $\Delta = 1$ can be reconciled with the exact statement that the diffusion constant diverges at high T. Note that GHD also predicts superdiffusion at the isotropic point (Ilievski *et al.*, 2018; Agrawal *et al.*, 2020) and includes more types of excitations such as bound states than what is captured by field theory.

Numerical methods such as ED, DQT, and tDMRG become less useful at low T since the relevant time scales and finite-size effects are known to increase substantially as temperature is reduced from infinity; see the discussion in Secs. IV.B and IV.E.

To date there has been no example of the spin-1/2 XXZ chain for which open-system simulations and the linear response agree for the actual values of the diffusion constants. It would be interesting to further investigate whether or not agreement between the open-system and linear-response calculations can be achieved. This is also of fundamental interest, and respective studies may shed light on the differences between the dynamics in isolated and open systems in a much broader context.

A phenomenological picture of transport in the spin-1/2 XXZ chain was developed by Huber (2012) and Sánchez, Varma, and Oganesyan (2018). The rich phenomenology of transport in the XXZ chain [ballistic with (super)diffusive corrections for $0 \leq \Delta \leq 1$, superdiffusive at $\Delta = 1$, and diffusive for $\Delta > 1$] partially carries over to other integrable spin models; see Piroli and Vernier (2016) and Dupont and Moore (2020). For instance, the $S = 1$ Zamolodchikov-Fateev model (Zamolodchikov and Fateev, 1980) exhibits a similar transport behavior (Dupont and Moore, 2020), with the exception of extra superdiffusion at $\Delta = 0$. The exact general necessary and sufficient criteria for superdiffusion to occur, such as the role of SU(N) symmetry, are not fully understood.

Our discussion focused entirely on the longitudinal current component. However, in the presence of time-dependent transverse magnetization components $\langle s_r^x(t)\rangle$ and $\langle s_r^y(t)\rangle$, transverse current components arise as well [see Steinigeweg *et al.* (2011) for theoretical work and the experiment by Hild *et al* (2014)].

Generally, it is an important question as to if and for how long the rich dynamical behavior of the spin-1/2 XXZ chain is stable against weak integrability-breaking perturbations (Zotos, 2004; Jung, Helmes, and Rosch, 2006; Jung and Rosch, 2007; Huang, Karrasch, and Moore, 2013; Steinigeweg, Herbrych, Zotos, and Brenig, 2016); see Sec. VIII. From a theoretical point of view, this question is challenging because conventional perturbation theory starts from a noninteracting problem. From an experimental point of view, this question is vital, because the coupling to environments or other degrees of freedom can never be suppressed completely; see also Sec. X.

VII. TRANSPORT IN THE HUBBARD CHAIN

The 1D fermionic Hubbard model $H = \sum_r h_r$ with

$$h_r = -t_h \sum_\sigma (c_{r\sigma}^\dagger c_{r+1\sigma} + \text{H.c.}) + U(n_{r\uparrow} - \tfrac{1}{2})(n_{r\downarrow} - \tfrac{1}{2}) \qquad (178)$$

is a more general integrable model than the spin-1/2 XXZ chain, as it also includes charge fluctuations. Much less attention has been devoted to computing its finite-temperature transport properties for charge, spin, or thermal transport. The main thermodynamic parameters characterizing transport properties in the Hubbard chain are, besides temperature T, the chemical potential and the magnetic field. These control the filling $\rho = (N_\uparrow + N_\downarrow)/(2L)$ and the magnetization density $m_z = (N_\uparrow - N_\downarrow)/L$. Here we mostly assume a canonical situation where ρ and m_z are fixed.

The fermionic Hubbard model possesses a pair of global SU(2) symmetries (Essler *et al.*, 2005) where one of them, the spin symmetry, is related to transport of magnetization, while the other, the so-called η-spin symmetry, is related to charge conservation and transport of charge. While the integrability of the Hubbard model was already shown by the coordinate Bethe ansatz by Lieb and Wu (1968), it was only in 1986 when Shastry (1986) proposed the Lax operator and the toolbox of algebraic integrability, which allowed him to explicitly construct an infinite sequence of local conservation laws. These conservation laws allow one to obtain some rigorous results for transport properties.

GHD has also been applied to investigate Drude weights (Ilievski and De Nardis, 2017a; Ilievski *et al.*, 2018; Fava *et al.*, 2020) and the emergence of diffusion and superdiffusion, as well as KPZ behavior (Fava *et al.*, 2020) in

the Hubbard chain. A comprehensive overview was given by Fava *et al.* (2020).

A. Thermal conductivity

The energy-current operator $\mathcal{J}^{(\mathrm{E})}$ is given by (Zotos, Naef, and Prelovšek, 1997)

$$\mathcal{J}^{(\mathrm{E})} = \sum_{r,\sigma} t_{\mathrm{h}}^2 \Big[(i c^{\dagger}_{r+1\sigma} c_{r-1\sigma} + \mathrm{H.c.}) - \frac{U}{2} (j^{(\mathrm{C})}_{r-1\sigma} + j^{(\mathrm{C})}_{r\sigma}) \Big(n_{r\bar{\sigma}} - \frac{1}{2} \Big) \Big], \tag{179}$$

where $j^{(\mathrm{C})}_{r,\sigma}$ is the charge current and $\bar{\sigma} = \uparrow\ (\downarrow)$ for $\sigma = \downarrow\ (\uparrow)$. Here we restrict the discussion to the case of a vanishing chemical potential and magnetic field, and therefore half filling and zero magnetization. Under these conditions, the energy current does not couple to the charge or spin current and off-diagonal matrix elements in the Onsager matrix of transport coefficients can be ignored (Mahan, 1990). This is equivalent to saying that the Seebeck coefficient, which is proportional to $\langle \mathcal{J}^{(\mathrm{E})}(t) \mathcal{J}^{(\mathrm{C})} \rangle$, vanishes identically at half filling at all temperatures (Beni and Coll, 1975), where $\mathcal{J}^{(\mathrm{C})}$ is the particle current.

Similar to the spin-1/2 XXZ chain, the Hubbard model is a ballistic thermal conductor (Zotos, Naef, and Prelovšek, 1997). This is a rigorous statement: While $\mathcal{J}^{(\mathrm{E})}$ is not conserved, it still has a nonzero overlap with a local conserved quantity Q_2. This Q_2 is the first nontrivial conserved charge in the Hubbard chain beyond energy E, particle number N, and the z component S^z of the total spin, and it happens to be similar to $\mathcal{J}^{(\mathrm{E})}$ in structure: Q_2 results from $\mathcal{J}^{(\mathrm{E})}$ by $U/2 \to U$. Consequently, the Mazur inequality (28) provides a nonzero lower bound.

The lower bound to the energy Drude weight was evaluated analytically by Zotos, Naef, and Prelovšek (1997) for $T = \infty$ and reads as

$$\mathcal{D}^{(\mathrm{E})}_{\mathrm{w}} \geq \frac{\beta^2}{2L} \sum_{\sigma} 2\rho_\sigma (1-\rho_\sigma) + \frac{U^4}{4} \frac{[\sum_\sigma 2\rho_\sigma(1-\rho_\sigma)(2\rho^2_{-\sigma} - 2\rho_{-\sigma} + 1)]^2}{\sum_\sigma 2\rho_\sigma(1-\rho_\sigma)[1 + U^2(2\rho^2_{-\sigma} - 2\rho_{-\sigma} + 1)]}, \tag{180}$$

where ρ_σ is the density of electrons with spin $\sigma = \uparrow, \downarrow$. A tDMRG study showed that contributions from other conserved charges $Q_{n>2}$ with a nonzero overlap with $\mathcal{J}^{(\mathrm{E})}$ are fairly small for all U/t_{h} (Karrasch, Kennes, and Heidrich-Meisner, 2016) at infinite temperature and half filling.

The full temperature dependence of the energy Drude weight was computed only recently from both finite-T tDMRG (Karrasch, Kennes, and Heidrich-Meisner, 2016; Karrasch, 2017a) and GHD (Ilievski and De Nardis, 2017a), which are in quantitative agreement. This Drude weight has, for $U \gg t_{\mathrm{h}}$, two maxima: the low-temperature regime $T \lesssim \Delta_{\mathrm{Mott}}$ is dominated by spin excitations, where Δ_{Mott} is the charge gap. This part of $\mathcal{D}^{(\mathrm{E})}_{\mathrm{w}}(T)$ agrees well with the results for the spin-1/2 Heisenberg chain given by Klümper and Sakai (2002). At high temperatures, charge contributions are activated and dominate the thermal transport.

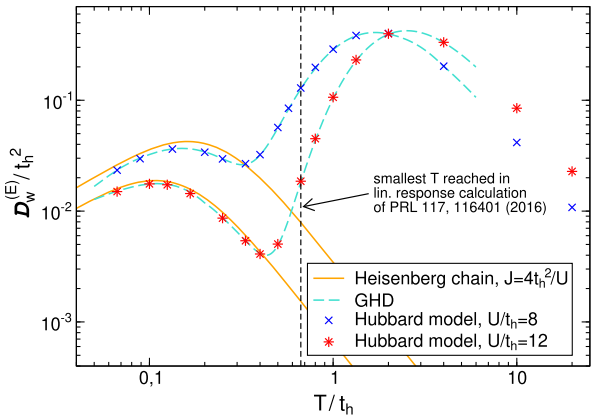

FIG. 20. Energy Drude weight of the Fermi-Hubbard chain as a function of temperature computed from the finite-T tDMRG (Karrasch, Kennes, and Heidrich-Meisner, 2016; Karrasch, 2017a) and GHD (Ilievski and De Nardis, 2017a).

This behavior is illustrated in Fig. 20. A more complete picture of the various temperature regimes and the relevant contributing excitations was described by Fava *et al.* (2020).

Since the energy current is not exactly conserved, there are finite-frequency contributions that were studied by Karrasch, Kennes, and Heidrich-Meisner (2016), but a conclusion about the nature of the subleading correction at low frequencies could not be drawn. Other related directions include the thermolelectric response of the model (Zemljič and Prelovšek, 2005; Peterson *et al.*, 2007).

B. Charge conductivity

The local conserved charges have a nonzero overlap with the charge current away from half filling $\rho \neq 1/2$. Using the Mazur inequality (28), one can thus show that charge transport is ballistic, i.e., the charge Drude weight is nonzero $\mathcal{D}^{(\mathrm{C})}_{\mathrm{w}} > 0$ (Zotos, Naef, and Prelovšek, 1997; Garst and Rosch, 2001). This is a rigorous statement. At half filling, which corresponds to the most symmetric and thermodynamically dominant sector, the Mazur bound based on the known local charges vanishes. However, this does not imply that the Drude weight necessarily has to be zero.

Nevertheless, some rigorous results have been obtained at half filling. It was shown by Carmelo, Nemati, and Prosen (2018) that for any $U > 0$ and any positive temperature $T > 0$ and within the canonical ensemble where $N = N_\uparrow + N_\downarrow - L$ is held fixed (while $L \to \infty$) one has a strict upper bound on the charge Drude weight

$$\mathcal{D}^{(\mathrm{C})}_{\mathrm{w}}|_{\mathrm{canonical}} \leq \frac{c'(U) t_{\mathrm{h}}^2}{T} L (2\rho - 1)^2, \tag{181}$$

which scales as $1/L$ at half filling $\rho = 1/2$ since, by including leading finite-size corrections, $2\rho - 1 = 0 + \mathcal{O}(1/L)$. Therefore, the rhs of Eq. (181) vanishes in the thermodynamic limit.

One can argue that within the grand-canonical ensemble where the number of electrons fluctuates according to the law of large numbers,

$$\langle [2(N/L) - 1]^2 \rangle_{\mathrm{grand\text{-}can}} \propto 1/L, \tag{182}$$

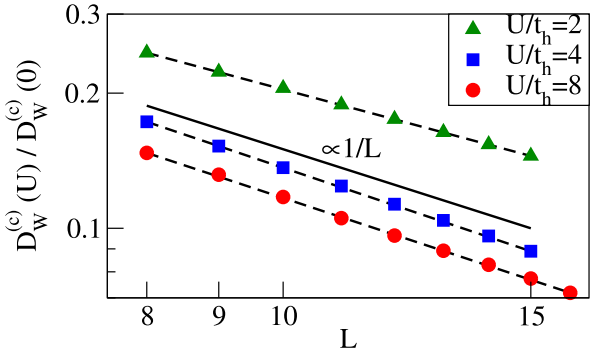

FIG. 21. Charge Drude weight of the Fermi-Hubbard chain at half filling and infinite temperature versus system size obtained from dynamical typicality (Jin *et al.*, 2015), plotted using a logarithmic scale on both axes.

this bound is no longer useful. There one can instead derive an improved bound that holds only within leading order in $1/T$ but for any value and sign of U

$$\mathcal{D}_{\mathrm{w}}^{(\mathrm{C})}|_{\text{grand-can}} \leq \frac{c(U)t_{\mathrm{h}}^2}{T}(2\rho-1)^2. \tag{183}$$

This bound indicates that $\mathcal{D}_{\mathrm{w}}^{(\mathrm{C})}=0$ if $\rho=1/2$, which is consistent with the GHD result (Ilievski *et al.*, 2018). The full temperature dependence of the charge Drude weight $\mathcal{D}_{\mathrm{w}}^{(\mathrm{C})}$ at $0<\rho<1/2$ was computed in a recent GHD study (Ilievski and De Nardis, 2017a). Ballistic charge transport away from half filling was observed numerically in a tDMRG study (Karrasch, 2017a).

The question of whether or not the charge Drude weight in the half-filled Fermi-Hubbard chain is zero has historically been a controversial topic. Several early studies reported evidence for a finite Drude weight (Fujimoto and Kawakami, 1998; Kirchner, Evertz, and Hanke, 1999). This result was later challenged by Bethe-ansatz studies that emphasized symmetry constraints on the diagonal matrix elements of the charge-current operator (Carmelo, Gu, and Sacramento, 2013; Carmelo, Nemati, and Prosen, 2018). Numerically, charge transport was studied using exact diagonalization and the MCLM (Prelovšek *et al.*, 2004), finite-T tDMRG (Karrasch, Kennes, and Moore, 2014; Karrasch, Kennes, and Heidrich-Meisner, 2016), dynamical typicality (Jin *et al.*, 2015), and tDMRG simulations of open quantum systems (Prosen and Žnidarič, 2012). All these studies agree insofar as they find no evidence for a ballistic contribution. As an example, we show the infinite-temperature Drude weight computed from dynamical typicality in Fig. 21 as a function of system size for several values of U/t_{h}. The Drude weight decays with a power law in $1/L$, which is consistent with the observation for other integrable models; see the large Δ phase of the spin-1/2 XXZ chain (Heidrich-Meisner *et al.*, 2003; Steinigeweg, Gemmer, and Brenig, 2014).

A rigorous lower bound using the method given by Medenjak, Karrasch, and Prosen (2017) for the charge-diffusion constant was recently obtained (Ilievski *et al.*, 2018). This bound diverges at half filling, which shows that transport cannot be diffusive. Therefore, the charge transport is similar to the spin transport in the spin-1/2 Heisenberg chain, with presumably no Drude weight in both cases and superdiffusion. Still, the spreading of density perturbations at finite times and in finite systems is indicative of diffusion (Steinigeweg, Jin, De Raedt *et al.*, 2017) (see also Sec. IX.A), which leaves the reconciliation of these two observations as an open problem.

Using finite-T tDMRG (Karrasch, Kennes, and Moore, 2014), an attempt was made to extract the temperature dependence of the dc conductivity at low temperatures in order to verify field-theoretical predictions given by Sachdev and Damle (1997) and Damle and Sachdev (1998). The presence of anomalous finite-size effects in $\sigma'(\omega)$ was pointed out in the MCLM study given by Prelovšek *et al.* (2004). Both of these numerical works and Jin *et al.* (2015) argued for a diffusive form of the conductivity, which is at odds with the rigorous results given by Ilievski *et al.* (2018).

Prosen and Žnidarič (2012) used the steady-state master equation with boundary Lindblad reservoirs to investigate transport in the Hubbard model. It was argued that transport is diffusive in the thermodynamic limit (results were reported for $L\sim 100$). Indications for superdiffusion were presented for short systems and large U/t_{h}, leading to the speculation that the two limits $U/t_{\mathrm{h}}\to\infty$ and $L\to\infty$ may not commute (Prosen and Žnidarič, 2012).

C. Spin conductivity

For a nonzero magnetization $m_z\neq 0$, the Mazur inequality (28) shows that the spin Drude weight is finite (Zotos, Naef, and Prelovšek, 1997).

One can make rigorous statements similar to Eqs. (181) and (183) about spin transport in the Hubbard model $U<0$. Specifically, under a partial particle-hole transformation where $(c_{r\uparrow},c_{r\uparrow}^\dagger,c_{r\downarrow},c_{r\downarrow}^\dagger)\to(c_{r\uparrow},c_{r\uparrow}^\dagger,c_{r\downarrow}^\dagger,c_{r\downarrow})$, the sign of U changes ($U\to -U$), while the spin current (spin Drude weight) maps to charge current (charge Drude weight) and vice versa. At asymptotically high temperatures, the sign of U becomes irrelevant, and we then have a full symmetry between spin and charge transport. For example, at zero magnetization, the leading term in a high-T expansion of the spin Drude weight vanishes. It is believed that $\mathcal{D}_{\mathrm{w}}^{(\mathrm{S})}=0$ at $m_z=0$.

The full temperature dependence of the spin Drude weight $\mathcal{D}_{\mathrm{w}}^{(\mathrm{S})}$ at $0<m_z<1$ was computed in a recent GHD study (Ilievski and De Nardis, 2017a). At zero magnetization, GHD predicts $\mathcal{D}_{\mathrm{w}}^{(\mathrm{S})}=0$ (Ilievski *et al.*, 2018), and in the same regime the spin-diffusion constant was shown to diverge (Ilievski *et al.*, 2018). Ballistic spin transport away from $m_z=0$ was observed numerically in a tDMRG study of the spreading of density wave packets (Karrasch, Prosen, and Heidrich-Meisner, 2017).

Clarifying the nature of the deviations from diffusion and investigating exactly how the Heisenberg regime is recovered out of the transport properties of the Hubbard chain in the low-temperature regime are open problems. For instance, the most recent developments of finite-T tDMRG methods have not yet been exploited to address these questions again (Karrasch, 2017a).

In a recent GHD study, several aspects of spin transport were explored, including the crossover from the spin-coherent

to the spin-incoherent regime and the emergence of superdiffusion at points with non-Abelian symmetry (vanishing chemical potential and/or magnetic field) (Fava *et al.*, 2020).

VIII. BEYOND INTEGRABLE SYSTEMS

While integrability is particularly appealing because it allows for exact solutions, most systems of relevance in condensed matter physics (experimental or theoretical) do not share this property. In particular, even though the spin-$1/2$ XXZ chain describes many features of real materials (such as thermodynamics and spectral functions), it cannot describe generic transport. Indeed, the latter is governed by relaxation mechanisms and external scattering off impurities or phonons is unavoidable.

In this section, we assume that the only relevant conserved quantities are energy, particle number, and magnetization. Hence, we exclude Floquet systems, where energy is not conserved, and unusual or specifically engineered nonintegrable systems that possess a finite number of nontrivial conserved quantities.

Theoretically, there is much interest in the stability of properties of integrable models against adding integrability-breaking perturbations. In classical systems of few particles, the Kolmogorov-Arnold-Moser theorem (Gutzwiller, 1990) makes a precise statement on this stability, whereas there is no such result for quantum systems. Within the wider field of nonequilibrium dynamics in closed quantum systems, the accepted view is that in most cases any arbitrarily small strength of an integrability-breaking term leads to thermalization (D'Alessio *et al.*, 2016) and diffusive transport. This, however, may not be easy to see in actual numerical simulations. For finite timescales, the perturbed system may well still remember the existence of now only approximately conserved quantities and exhibit prethermalization behavior (Moeckel and Kehrein, 2008; Kollar, Wolf, and Eckstein, 2011; Essler *et al.*, 2014; Bertini *et al.*, 2015; Mallayya, Rigol, and De Roeck, 2019). For transport, there have been only a few studies that have explicitly made a connection between prethermalization and the respective behavior in a transport coefficient [see the discussion given by Nessi and Iucci (2015)], while a number of studies have touched upon the topic; see Jung, Helmes, and Rosch (2006) and Jung and Rosch (2007). The observation of slow dynamics in finite-size simulations is ascribed to weak violations of conservation laws or quasilocalization physics in translational invariant systems; see Schiulaz and Müller (2014), Yao *et al.* (2016), and Michailidis *et al.* (2018).

We concentrate the discussion on nonintegrable models that result from perturbing the spin-$1/2$ XXZ chain. The choice of the integrability-breaking term is motivated by a particular relevance for experiments (such as spin-$1/2$ Heisenberg ladders), by the possibility of obtaining analytical or exact results (e.g., for the spin-$1/2$ XXZ chain with a staggered magnetic field), or by the desire to obtain the simplest possible cases (such as spin-$1/2$ XX ladders or simple types of short-range interactions). See Fig. 22 for an illustration of ladders and frustrated chains.

In this section, we present the statements that describe the majority of those models and cover selected examples for which there are particularly convincing either numerical or analytical results. Relevant and important results have certainly been obtained for many other models that are not covered in detail here. These include spin-S XXZ chains with $S > 1/2$ (Karadamoglou and Zotos, 2004; Richter, Casper *et al.*, 2019; Dupont and Moore, 2020), Kitaev-Heisenberg chains and ladders (Steinigeweg and Brenig, 2016; Metavitsiadis and Brenig, 2017; Metavitsiadis, Psaroudaki, and Brenig, 2019; Pidatella, Metavitsiadis, and Brenig, 2019), and Hubbard models with integrability-breaking terms (Žnidarič, 2013a, 2013b; Karrasch, Kennes, and Moore (2014); Karrasch, Kennes, and Heidrich-Meisner, 2016; Karrasch, 2017a, 2017b). We focus here on results obtained via the Kubo formula for closed quantum systems; studies of open quantum systems were given by Žnidarič, 2013a, 2013b; Mendoza-Arenas, Clark, and Jaksch, 2015.

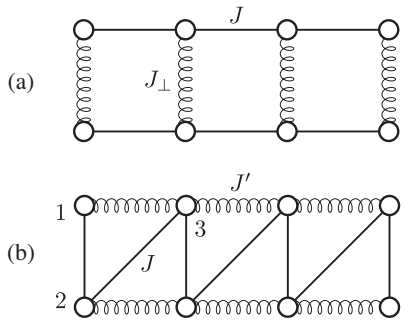

FIG. 22. (a) Spin-$1/2$ ladder with a coupling strength J and $J_\perp$ along the legs and rungs, respectively, and (b) a frustrated chain with a next-nearest-neighbor coupling of strength J'.

A. Universal description of the low-energy behavior

We first turn to the predictions from field theory for the low-temperature behavior. In a generic gapless system, the field theory developed by Sirker, Pereira, and Affleck (2011) provides the generic behavior: a Tomonaga-Luttinger liquid becomes a diffusive conductor after including sufficiently many umklapp terms (Rosch and Andrei, 2000). As an example for spin transport in a gapless system, we consider a spin-$1/2$ XXZ chain with a staggered magnetic field of strength h that breaks the integrability. For small values of h, the system is in the Tomonaga-Luttinger-liquid phase, and by applying the field theory given by Sirker, Pereira, and Affleck (2011) one obtains (Huang, Karrasch, and Moore, 2013)

$$\sigma_{\mathrm{dc}} \propto h^{-2} T^{3-2K}, \tag{184}$$

where K is the TLL parameter. Further related studies were conducted by Szasz, Ilan, and Moore (2017) and Bulchandani, Karrasch, and Moore (2020).

Another generic insight can be drawn from the fact that, at low-energy scales, regular momentum emerges as an additonal approximate conserved quantity due to the mapping to a continuum model. This does not give rise to a finite Drude weight at small but finite temperatures but causes the dc conductivities of those currents with a finite overlap with momentum to be exponentially large as a function of decreasing temperature (Rosch and Andrei, 2000; Rosch,

2006). These predictions are based on a memory-matrix formalism.

For gapped systems, the semiclassical theory given by Damle and Sachdev (1998) leads to (see Sec. IV.A)

$$\sigma_{\rm dc} \propto \frac{1}{\sqrt{T}}. \tag{185}$$

This divergence (as $T \to 0$) can be understood from the fact that, on the one hand, the density of carriers is exponentially suppressed but, on the other hand, this dilution leads to an exponential suppression of scattering as well. The available tDMRG results (Karrasch, Kennes, and Moore, 2014) for the Hubbard chain with a nearest-neighbor repulsion and the gapped phase of the integrable spin-1/2 XXZ chain seem to be more consistent with a $1/T$ dependence. An outstanding question is to compute $\sigma_{\rm dc}(T)$ for a spin-1 chain or a spin-1/2 ladder, for which the predictions given by Damle and Sachdev (2005) were developed.

B. Absence of Drude weights

Within our previously given working definition of nonintegrable models, there is no nonzero Mazur bound for Drude weights. Hence, the expectation is that Drude weights vanish at any finite temperature. Note that at zero temperature any metallic phase has a nonzero Drude weight as long as the system preserves translational invariance (Scalapino, White, and Zhang, 1993; Mastropietro, 2013). This nonzero spin and charge Drude weight results from the fact that the low-energy theory is a gapless Tomonaga-Luttinger liquid with one or more modes and is thus a consequence of the conservation of momentum in the continuum limit. Yet these zero-temperature Drude weights are not related to the integrability of the microscopic models. A concrete example is the frustrated spin-1/2 Heisenberg chain, which in its gapless phase has a nonzero spin Drude weight at $T = 0$ (Bonča *et al.*, 1994).

Most numerical studies confirm the expectation that spin, charge, and energy Drude weights vanish in nonintegrable models at any $T > 0$, including spin-1/2 Heisenberg ladders (Heidrich-Meisner *et al.*, 2003; Zotos, 2004; Rezania *et al.*, 2014), frustrated spin-1/2 Heisenberg chains (Heidrich-Meisner *et al.*, 2003, 2004a, 2004b, 2005), dimerized spin-1/2 Heisenberg chains (Heidrich-Meisner *et al.*, 2003, 2004a), spin-1/2 XXZ chains with additional nearest-neighbor interactions $S^z_r S^z_{r+2}$ (equivalent to spinless fermions with density-density interactions) (Zotos and Prelovšek, 1996), and spin-1/2 XXZ chains with staggered magnetic fields (Huang, Karrasch, and Moore, 2013; Steinigeweg, Gemmer, and Brenig, 2015).

In the vicinity of integrable models and on finite systems, the Drude weight may still account for most of the weight in the conductivity $\sigma'(\omega)$ with only a slow transfer of weight to finite frequencies. An interesting example is the spin-1/2 frustrated Heisenberg chain where the relevant parameter is the ratio $\alpha = J'/J$ and J (J') are the nearest (next-to-nearest) neighbor exchange couplings; see Fig. 22(b). The Hamiltonian reads

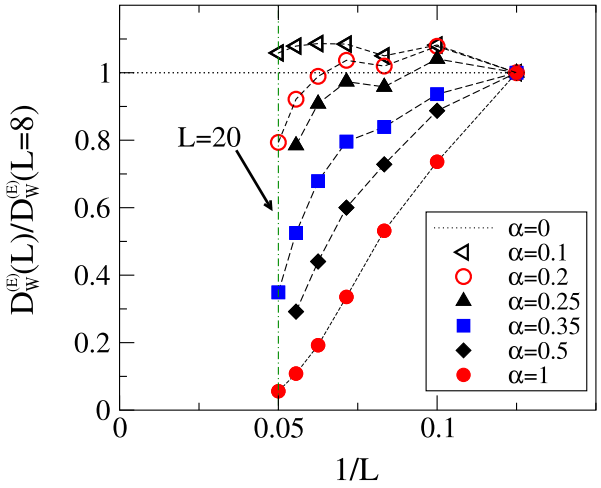

FIG. 23. Infinite-temperature energy Drude weight of frustrated spin-1/2 Heisenberg chains computed with exact diagonalization (Heidrich-Meisner *et al.*, 2003, 2004b).

$$H = J \sum_{r=1}^{L} h_{r,r+1} + J' \sum_{r=1}^{L} h_{r,r+2}, \tag{186}$$

where we assume periodic boundary conditions. As an example, we show exact-diagonalization data for the energy Drude weight in Fig. 23; specifically, for its leading coefficient $\tilde{\mathcal{D}}_{\rm w}^{\rm (E)}$ in a $1/T$ expansion

$$\mathcal{D}_{\rm w}^{\rm (E)} = \frac{\tilde{\mathcal{D}}_{\rm w}^{\rm (E)}}{T^2} + \cdots. \tag{187}$$

At small values of $\alpha \lesssim 0.3$ and for the accessible system sizes, $\tilde{\mathcal{D}}_{\rm w}^{\rm (E)}$ decays only mildly relative to the integrable case and seems to saturate (Alvarez and Gros, 2002a; Heidrich-Meisner *et al.*, 2004b). Upon increasing α, though, the decrease of $\tilde{\mathcal{D}}_{\rm w}^{\rm (E)}$ with L becomes faster and is consistent with an exponential decay, or at least one that is faster than any power law. The latter is expected from ETH arguments (Steinigeweg, Herbrych, and Prelovšek, 2013) and has been numerically observed in nonintegrable models far from integrable limits (Zotos and Prelovšek, 1996; Prosen, 1999; Heidrich-Meisner *et al.*, 2004b; Rabson, Narozhny, and Millis, 2004; Jin *et al.*, 2015).

For the frustrated spin-1/2 chain, there is a theoretical argument that explains why on small system sizes and for small values of $\alpha \lesssim 0.3$ the thermal Drude weight still amounts to a substantial fraction of the total spectral weight. It turns out that the energy-current conservation is violated only at next-to-leading order in α (Jung, Helmes, and Rosch, 2006). Within the memory-matrix formalism, one can then show that current lifetimes are enhanced in the small-α regime.

Other cases in which the proximity to integrable limits can lead to a slow decay of Drude weights on finite systems (or to a slow temporal decay of current autocorrelations computed with tDMRG) are certain spin-1/2 dimerized XXZ chains (Karrasch, Ilan, and Moore, 2013) and gapped quantum models in large magnetic fields (Langer *et al.*, 2010; Psaroudaki *et al.*, 2014; Stolpp *et al.*, 2019). In the former

case, the existence of several integrable limits (vanishing dimerization, zero exchange anisotropy $\Delta = 0$, decoupled dimers) has been speculated to give rise to a slow decay of current correlation functions. In the latter case, the application of a longitudinal magnetic field induces a transition into a gapless phase. For spin-1 chains (Psaroudaki *et al.*, 2014), the field-induced phase can be approximately described by an effective spin-1/2 XXZ chain Hamiltonian, which explains the numerically observed large finite-size Drude weights. In none of these examples is there any theoretical evidence to believe that the finite-size Drude weights remain nonzero for $L \to \infty$. Other claims of nonzero Drude weights in generic spin ladders, frustrated spin chains, or dimerized spin chains were either based on a mapping to noninteracting effective theories (Orignac, Chitra, and Citro, 2003; Saito, 2003b) or due to the difficulties involved with interpreting finite-size exact diagonalization (Alvarez and Gros, 2002a) or QMC data (Kirchner, Evertz, and Hanke, 1999).

C. Frequency dependence of the conductivity

The simplest picture for the frequency dependence was already given in Sec. II and is based on the Drude model: a Lorentzian whose width is controlled by a single relaxation time. One may wonder whether such a simple structure is possible at all in strongly correlated models in one dimension where there is no Landau quasiparticle picture in the first place.

For infinite temperature, there are many numerical results available. A particularly clear picture emerges for spin-1/2 XX ladders. In that case, the integrable limits are two chains that have only a Drude weight, i.e., $\sigma'(\omega) = 2\pi \mathcal{D}_{\mathrm{w}}^{(\mathrm{S})} \delta(\omega)$. The Hamiltonian reads (with $\Delta = 0$ in the $h_r^{\parallel,\perp}$ terms)

$$H = H^{\parallel} + H^{\perp} = J \sum_{\ell=1,2} \sum_{r=1}^{L} h^{\parallel}_{\ell;r,r+1} + J_{\perp} \sum_{r=1}^{L} h^{\perp}_{r}. \quad (188)$$

$\ell = 1, 2$ labels the two legs of the ladder. Upon coupling the chains with a nonzero $J_{\perp}$, the Drude peak is broadened into a Lorentzian. This is illustrated in Fig. 24, obtained from tDMRG (Karrasch, Kennes, and Heidrich-Meisner, 2015), which agrees with dynamical typicality and perturbation theory (Steinigeweg, Heidrich-Meisner *et al.*, 2014; Richter, Jin *et al.*, 2019; Richter *et al.*, 2020). For more complicated models, the situation is less clear based on the numerical data. For instance, in spin-1/2 Heisenberg ladders, there is presumably superdiffusion for $J_{\perp} = 0$ (see Sec. VI.D.3) and it is not obvious (Richter *et al.*, 2020; Dabelow and Reimann, 2021) that there is a single Lorentzian at low frequencies. Numerical results for $\sigma'(\omega)$ of nonintegrable models are available for spin-1/2 XXZ ladders (Karrasch, Kennes, and Heidrich-Meisner, 2015), spin-1/2 XXZ chains with a staggered magnetic field (Huang, Karrasch, and Moore, 2013), dimerized spin-1/2 Heisenberg chains (Langer *et al.*, 2010), interacting spinless fermions with next-to-nearest-neighbor and nearest-neighbor hopping (Mukerjee, Oganesyan, and Huse, 2006), and the Fermi-Hubbard model with next-nearest-neighbor interactions (Karrasch, Kennes, and Moore, 2014). The thermal conductivity $\kappa(\omega)$ was computed numerically for spin-1/2 XXZ chains with a staggered magnetic field (Huang, Karrasch, and Moore, 2013; Steinigeweg, Gemmer, and Brenig, 2015).

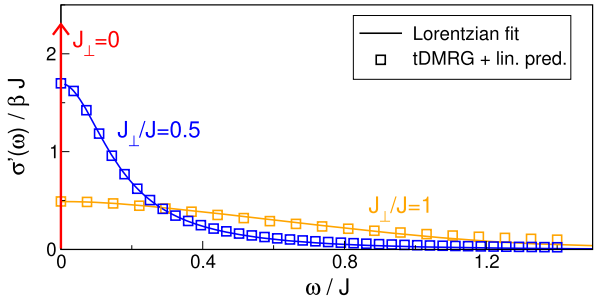

FIG. 24. Spin conductivity of a spin-1/2 XX ladder for various rung couplings $J_{\perp}$ (Karrasch, Kennes, and Heidrich-Meisner, 2015).

While a finite dc limit is enough to classify the system as a normal conductor, there remains the possibility of potential anomalous low-frequency behaviors; see Garst and Rosch (2001) for a discussion of the mass-imbalanced Hubbard model. Evidence for such a situation was reported for a nonintegrable model of spinless fermions (Mukerjee, Oganesyan, and Huse, 2006), where $\sigma'(\omega) = a - b\sqrt{|\omega|} + \cdots$ was observed in numerical data and explained as a hydrodynamic tail. The corresponding $\sigma'(\omega)$ is shown in Fig. 25. A systematic study of such tails in nonintegrable models for larger systems and a broader class of models remains to be done [see also Zotos (2004)], in particular, by making more quantitative contact with the predictions of hydrodynamics.

D. dc conductivity and diffusion constant

We next turn to the available results for the temperature dependence of dc conductivities and diffusion constants and

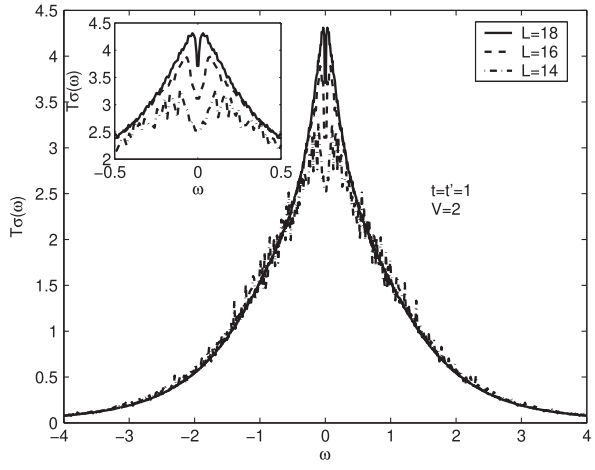

FIG. 25. Real part of the conductivity of a nonintegrable model vs ω (in units of t), namely, spinless fermions with a nearest-neighbor repulsion of strength $V = 2t$ and an additional next-to-nearest-neighbor hopping $t' = t$, where t is the nearest-neighbor hopping matrix element. The exact-diagonalization data indicate that the low-frequency behavior is incompatible with a simple Lorentzian; see Mukerjee, Oganesyan, and Huse (2006) for a discussion. Other examples of a similar shape were reported by Zotos (2004) and Heidrich-Meisner *et al.* (2005). From Mukerjee, Oganesyan, and Huse, 2006.

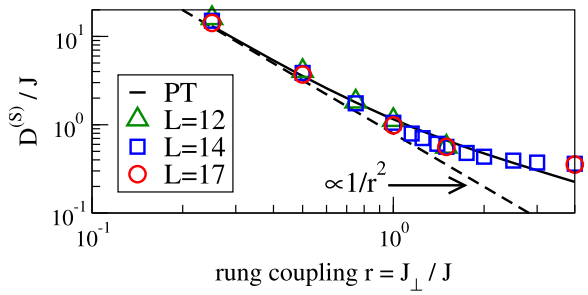

FIG. 26. Spin-diffusion constant of the spin-1/2 *XX* ladder as a function of $r = J_\perp/J$ at infinite temperature, as obtained from dynamical typicality for $L = 12, 14, 17$ rungs (i.e., $2L$ sites in the ladder) (Steinigeweg, Heidrich-Meisner *et al.*, 2014) and perturbation theory (PT) (Richter *et al.*, 2020), with $D^{(S)}/J = 1/(2\gamma r^2)$ and $\gamma \approx 0.63$ in the limit of small r with no free parameter.

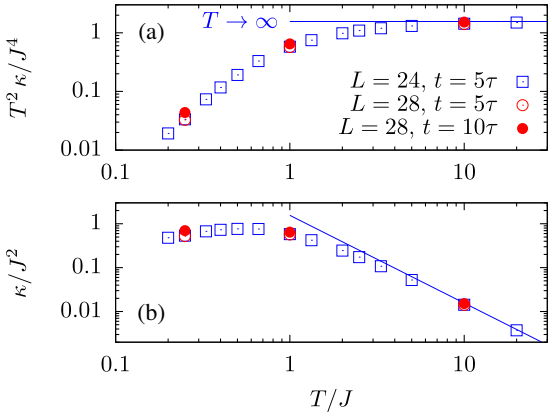

FIG. 27. Temperature dependence of the thermal conductivity κ in a Heisenberg chain with a staggered field, as given by Steinigeweg, Gemmer, and Brenig (2015); see also Huang, Karrasch, and Moore (2013). τ is the relaxation time, defined as the time at which the current correlation has decayed to a fraction of $1/e$ (Steinigeweg, Gemmer, and Brenig, 2015).

their dependence on model parameters. The latter dependency is relevant to understand the effect of integrability-breaking terms (parametrized by a coupling constant J_{pert}). The crossover from GHD describing integrable models to regular hydrodynamics in nonintegrable models was discussed by Friedman, Gopalakrishnan, and Vasseur (2020). Based on Fermi's golden rule, one generically expects $D^{(Q)} \propto 1/J_{\text{pert}}^2$ and thus a similar scaling for the conductivity (Zotos, 2004; Jung and Rosch, 2007; Steinigeweg, Herbrych, Zotos, and Brenig, 2016).

We first discuss the infinite-temperature limit and then move on to cover predictions and results for finite temperatures. Numerical results for the diffusion constant and (via Einstein relations) the dc conductivity are available for spin transport in spin-1/2 *XX* and *XXZ* ladders (Žnidarič, 2013a; Steinigeweg, Heidrich-Meisner *et al.*, 2014; Karrasch, Kennes, and Heidrich-Meisner, 2015) and thermal transport in spin-1/2 *XXZ* ladders (Heidrich-Meisner *et al.*, 2003; Zotos, 2004; Steinigeweg, Herbrych, Zotos, and Brenig, 2016) and spin-1/2 chains with staggered magnetic fields (Huang, Karrasch, and Moore, 2013; Steinigeweg, Gemmer, and Brenig, 2015), as well as for charge transport in the mass-imbalanced Fermi-Hubbard chain (Jin *et al.*, 2015; Heitmann *et al.*, 2020); see also Garst and Rosch (2001).

Figure 26 shows the dependence of the spin-diffusion constant $D^{(S)}$ on $J_\perp$ for spin-1/2 *XX* ladders: at small $J_\perp$, $D^{(S)} \propto 1/J_\perp^2$, which is in agreement with perturbation theory (Steinigeweg, Heidrich-Meisner *et al.*, 2014; Richter *et al.*, 2020) with a crossover to $D^{(S)} = \text{const}$ at large $J_\perp \gg J$. The latter behavior is typical for systems with a band structure (here controlled by $J_\perp$ in the strong dimer limit) at $T = \infty$. A perturbative dependence of diffusion constants on an integrability-breaking parameter was reported for thermal transport in spin ladders as well (Zotos, 2004; Steinigeweg, Herbrych, Zotos, and Brenig, 2016).

Numerical methods now also give access to a wider temperature range. As an example, we show the thermal conductivity of spin-1/2 *XXZ* chains with a staggered magnetic field in Fig. 27 (Huang, Karrasch, and Moore, 2013; Steinigeweg, Gemmer, and Brenig, 2015); see also (Prosen and Žnidarič (2009). The maximum at a temperature $T \sim \mathcal{O}(J)$ is resolved, while the data indicate a power-law dependence at low T.

E. Special cases and outlook

We conclude in this section by giving an account of special cases and ongoing directions.

Local perturbations that act on only one or a few sites can behave completely differently from global perturbations that have been covered thus far. Having in mind that integrable systems possess infinitely long-lived excitations, this is not surprising: looking at the transmission from one end to the other, an excitation scatters only once, regardless of the system's length, and therefore one has zero bulk resistance and ballistic transport.

We now take a concrete model, the spin-1/2 *XXZ* Heisenberg chain [Eq. (1)] and a single impurity at the middle of the chain described by $(h/2)s^z_{L/2}$, where h is a local magnetic field. Analyzing the distribution of energy spacings between nearest-eigenenergy levels (Santos, 2004, 2008; Barišić *et al.*, 2009; Torres-Herrera and Santos, 2014; Fagotti, 2017a; Brenes *et al.*, 2018), one observes level repulsion and agreement with random-matrix theory for a wide range of h (in the thermodynamic limit likely for any nonzero h), which is typical of quantum-chaotic systems. Studies of spin transport with a boundary-driven Lindblad setting as well as with a linear-response calculation of $\sigma'(\omega)$ suggest ballistic transport (Brenes *et al.*, 2018; Brenes, LeBlond *et al.*, 2020); see Fig. 28 and Brenes, Goold, and Rigol (2020). We note that in order to identify a nonzero Drude weight, one has to carry out a careful finite-size scaling analysis of $\sigma'(\omega)$ because under open boundary conditions $\mathcal{D}_{\text{w}}^{(S)}$ gets transferred to finite frequencies (Rigol and Shastry, 2008), getting a Lorentzian (Cauchy) representation of a Dirac delta function whose width decreases to $\sim 1/L$, while its height increases as $\sim L$. For the case of a spin-S impurity with

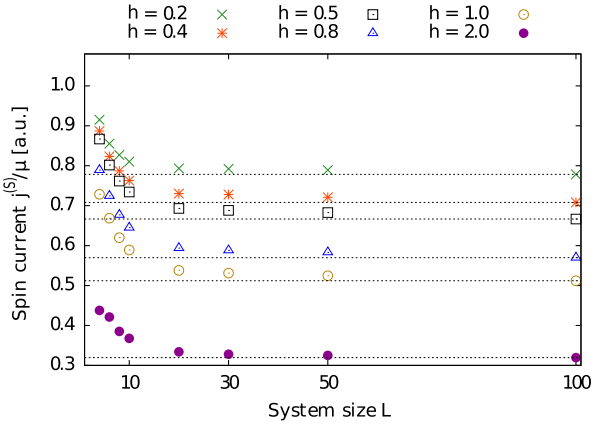

FIG. 28. Dependence of the NESS spin current on system size L for a spin-1/2 XXZ chain ($\Delta = 0.5$) with a single impurity of strength h. Adapted from Brenes *et al.*, 2018.

$S > 1/2$, this was interpreted by Metavitsiadis *et al.* (2010) and Metavitsiadis (2011) as an "anomalous incoherent" energy and spin transport. One therefore has a quantum-chaotic system according to the level-spacing statistics but ballistic transport, which is typically associated with integrability and conserved quantities.

How can one reconcile these two seemingly contradicting findings? In a many-body system, the level spacing is exponentially small in L in the thermodynamic limit. Therefore, starting with eigenstates of the integrable spin-1/2 XXZ chain, even a small local perturbation can cause mixing of close eigenenergies, leading to level repulsion. However, level spacing measures properties on an exponentially small energy scale that can potentially be irrelevant for local physics. For transport, timescales that are polynomial in L are what matters.

A currently investigated question concerns the precise timescale and conditions for hydrodynamics to set in; see Khemani, Vishwanath, and Huse (2018), Glorioso *et al.* (2021), and Lopez-Piqueres *et al.* (2021). This question is not new, yet numerical methods are now in a position to simulate this while novel theoretical concepts from quantum information theory such as entanglement spreading or out-of-time-ordered correlators provide for a complementary view of this problem. In that regime, the system should behave classically and be subject to the laws of hydrodynamics (Lux *et al.*, 2014; Bohrdt *et al.*, 2017; Leviatan *et al.*, 2017; Rakovszky, Pollmann, and von Keyserlingk, 2018; Ye *et al.*, 2020). Recently a generalized relaxation-time approximation framework was proposed to study the crossover from generalized hydrodynamics, applicable to integrable systems, to hydrodynamics in a generic model (Lopez-Piqueres *et al.*, 2021). Related efforts address the emergence of hydrodynamics in random unitary circuits; see Nahum, Ruhman, and Huse (2018) and Rakovszky, Pollmann, and von Keyserlingk (2018).

Earlier work studied the emergence of diffusion in Hamiltonian systems with random couplings (Steinigeweg, Gemmer, and Michel, 2006; Steinigeweg, Breuer, and Gemmer, 2007). In addition to a hydrodynamical description as a generic framework and numerical approaches, a semiclassical method based on the truncated Wigner approximations has recently been developed to study diffusion in spin systems (Wurtz and Polkovnikov, 2020). Finally, the possibility of anomalous transport in nonintegrable models is still of interest, and an example of subdiffusion has been reported in systems that conserve dipole and/or higher moments (Feldmeier *et al.*, 2020).

IX. FAR-FROM-EQUILIBRIUM TRANSPORT

There is growing interest in the nonequilibrium dynamics induced by initial states with inhomogeneous densities across various branches of theoretical physics, including condensed matter theory (Liu and Andrei, 2014), quantum-field theory (Bernard and Doyon, 2016), AdS/CFT correspondence (Bhaseen *et al.*, 2015), statistical physics (Antal, Rácz, and Sasvári, 1997), and ultracold quantum gases (Schneider *et al.*, 2012; Ronzheimer *et al.*, 2013; Vidmar *et al.*, 2015; Vidmar, Iyer, and Rigol, 2017).

A. Spreading of density perturbations

A prototypical nonequilibrium setup is to prepare a local energy-, charge-, or spin-density perturbation in an otherwise equilibrated background. Such a wave packet can be realized via an initial density matrix of the form $\rho_L(T) \otimes \rho_C \otimes \rho_R(T)$, where the density matrices $\rho_{L,R}$ associated with the left and right regions have the standard equilibrium form. The center region can be chosen as a thermal density matrix with a different temperature $T + \Delta T$ in order to model an energy-density perturbation.

In Sec. II.C.1, it was discussed that if this initial local perturbation is small ($\Delta T \to 0$ and the size of the center region C small in the previously mentioned example), the time evolution of its variance $\Sigma(t)$ is related to the time-dependent diffusion constant via Eq. (37) (Bohm and Leschke, 1992; Steinigeweg, Wichterich, and Gemmer, 2009; Yan, Jiang, and Zhao, 2015). This implies that at long times $\Sigma \sim t$ for ballistic transport and $\Sigma \sim \sqrt{t}$ for diffusive transport, with the prefactors given by the Drude weight and the diffusion constant, respectively. In the context of this review, the validity of the time-dependent Einstein relation was confirmed numerically for spin, charge, and energy transport within the spin-1/2 XXZ chain and the Fermi-Hubbard model by tDMRG (Karrasch, Prosen, and Heidrich-Meisner, 2017) and dynamical typicality calculations (Steinigeweg, Jin, De Raedt *et al.*, 2017; Steinigeweg, Jin, Schmidtke *et al.*, 2017).

One still expects that the longtime behavior of the variance is of the previously mentioned form ($\Sigma \sim t$ and $\Sigma \sim \sqrt{t}$, respectively), even if one considers the spreading of local perturbations that are not necessarily small. This was first shown for the integrable spin-1/2 XXZ chain as well as nonintegrable systems at zero temperature using tDMRG (Langer *et al.*, 2009, 2011; Jesenko and Žnidarič, 2011). For instance, it was illustrated that spin propagates ballistically for $\Delta < 1$ and diffusively for $\Delta > 1$, in agreement with the zero-temperature behavior of the Drude weight, which is finite in the former case but vanishes in the latter (Langer

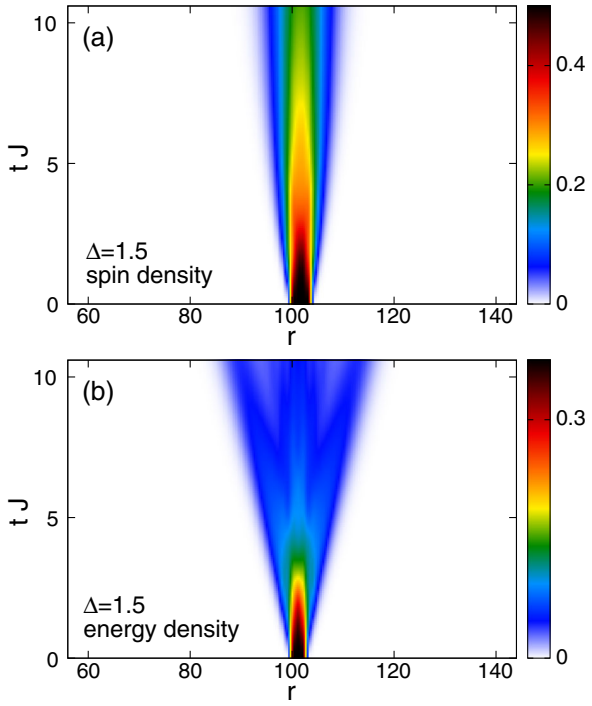

FIG. 29. Densities as a function of time t and position r for a local quench inducing (a) spin dynamics and (b) energy dynamics in the spin-$1/2$ XXZ chain at $\Delta = 1.5$ at $T = \infty$. The dynamics is induced by introducing a local perturbation in the initial state. Adapted from Karrasch, Moore, and Heidrich-Meisner, 2014.

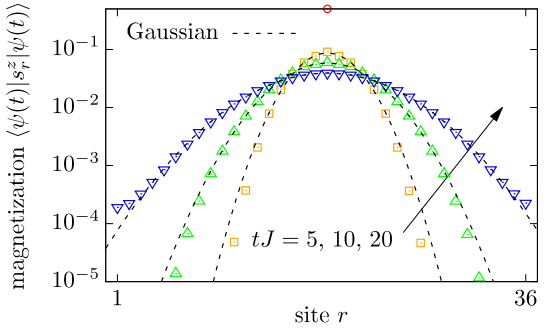

FIG. 30. Spatial dependence of magnetization profiles at different times as obtained by Steinigeweg, Jin, Schmidtke *et al.* (2017) for a spin-$1/2$ XXZ chain at $\Delta = 1.5$, the full Hilbert space of $L = 36$ sites, and a randomly chosen initial pure state with a δ peak on top of a many-particle background at high temperatures. These profiles are well described by Gaussian fits over several orders of magnitude. Similar Gaussian profiles were found by Ljubotina, Žnidarič, and Prosen (2017).

et al., 2009), while energy always propagates ballistically at any Δ (Langer *et al.*, 2011).

These studies were extended to finite temperatures and to pure-state dynamics, and the spreading of spin and energy wave packets were studied for the spin-$1/2$ XXZ chain, spin ladders, and the Fermi-Hubbard model (Foster, Yuzbashyan, and Altshuler, 2010; Foster *et al.*, 2011; Karrasch, Moore, and Heidrich-Meisner, 2014; Karrasch, Prosen, and Heidrich-Meisner, 2017; Steinigeweg, Jin, Schmidtke *et al.*, 2017; Richter *et al.*, 2018; Richter, Jin *et al.*, 2019), including the mass-imbalanced case (Heitmann *et al.*, 2020). For instance, one can prepare a spin-polarized central region in a $T = \infty$ background within the XXZ chain, which leads to a simultaneous propagation of spin and energy densities. In this setup, spin propagates diffusively and energy propagates ballistically for $\Delta > 1$, and both quantities propagate ballistically for $\Delta < 1$. The typical behavior of the spin and energy densities after local quenches of this type is illustrated in Fig. 29 for $\Delta = 1.5$. On the timescales accessed in these tDMRG simulations, the variance behaves as $\Sigma^2 \propto t^{1.2}$ for the spin density and $\Sigma^2 \propto t^2$ for the energy density (Karrasch, Moore, and Heidrich-Meisner, 2014). Similar initial states can be prepared within the Fermi-Hubbard model and could in principle be realized in a cold-atom experiment (Karrasch, Prosen, and Heidrich-Meisner, 2017).

The generic behavior of a diffusive spreading of a local perturbation in nonintegrable models was investigated by Langer *et al.* (2009), Kim and Huse (2013), Karrasch, Kennes, and Heidrich-Meisner (2016), and Leviatan *et al.* (2017).

We mention that solving the problem of the real-time evolution from a state with a few spins flipped compared to a background of full polarization is also of interest in the integrability community, as some aspects of the finite-time dynamics can be understood exactly in this case; see Ganahl *et al.* (2012) and Liu and Andrei (2014).

Recently the analysis of the time- and space-dependent densities was extended beyond just the spatial variance; see Ljubotina, Žnidarič, and Prosen (2017) and Steinigeweg, Jin, Schmidtke *et al.* (2017). For $\Delta > 1$, as illustrated in Fig. 30, clean Gaussian profiles can be observed and provide additional strong evidence of diffusion.

B. Bipartitioning protocols

Bipartitioning protocols have emerged in the last two decades as a paradigmatic setting to study far-from-equilibrium transport in the context of isolated quantum many-body systems.[25] These protocols are simple: one prepares the two halves of the system in different homogeneous states, then joins them and lets the entire system evolve under the dynamics of a spatially homogeneous Hamiltonian. In formulas, the state of the system at time t is represented as

$$\rho(t) = e^{-iHt}(\rho_{\mathrm{L}} \otimes \rho_{\mathrm{R}})e^{iHt}, \tag{189}$$

where H is the homogeneous Hamiltonian of the entire system and $\rho_{\mathrm{R/L}}$ are the two initial homogeneous states of the two halves. See Fig. 31 for a pictorial illustration of the setting. Relevant examples, extensively studied in the literature, include the sudden junction of two half chains prepared at different temperatures [see Ogata (2002), Aschbacher and Pillet (2003), Aschbacher and Barbaroux (2006), De Luca *et al.* (2013, 2014), Karrasch, Ilan, and Moore (2013),

[25]For a recent and more extended discussion, see the reviews by Bernard and Doyon (2016) and Vasseur and Moore (2016), which are dedicated to the subject.

FIG. 31. Pictorial representation of a generic bipartitioning protocol. The two halves of the chain are prepared in two different homogeneous states at time $t = 0$. A nonequilibrium region emerges from the junction at the middle and expands at the maximal allowed speed.

Castro-Alvaredo *et al.* (2014), Collura and Karevski (2014), Collura and Martelloni (2014), Eisler and Zimborás (2014), Bhaseen *et al.* (2015), De Luca, Martelloni, and Viti (2015), Doyon (2015), Doyon *et al.* (2015), Bertini *et al.* (2016), Biella *et al.* (2016), Castro-Alvaredo, Doyon, and Yoshimura (2016), Karrasch (2017b), Kormos (2017), Zotos (2017), Bertini and Piroli (2018), Mazza *et al.* (2018), Bertini, Piroli, and Kormos (2019), Karevski and Schütz (2019), Mestyán *et al.* (2019), and Nozawa and Tsunetsugu (2020)] or at different averaged magnetizations or filling [see Antal *et al.* (1998, 1999), Gobert *et al.* (2005), Antal, Krapivsky, and Rákos (2008), Calabrese, Hagendorf, and Le Doussal (2008), Santos (2008, 2009), Lancaster, Gull, and Mitra (2010), Lancaster and Mitra (2010), Santos and Mitra (2011), Eisler and Rácz (2013), Sabetta and Misguich (2013), Alba and Heidrich-Meisner (2014), Hauschild, Pollmann, and Heidrich-Meisner (2015), Vidmar *et al.* (2015), Bertini *et al.* (2016), Eisler, Maislinger, and Evertz (2016), Viti *et al.* (2016), De Luca, Collura, and De Nardis (2017), Ljubotina, Žnidarič, and Prosen (2017), Misguich, Mallick, and Krapivsky (2017), Piroli *et al.* (2017), Vidmar, Iyer, and Rigol (2017), Collura, De Luca, and Viti (2018), and Collura *et al.* (2020)]. We note that the latter kind of bipartitioning protocols, also referred to as geometric quenches in the literature (Mossel, Palacios, and Caux, 2010), can be realized in experiments on the sudden expansion of quantum gases in optical lattices; cf. Sec. X.B.

In the two previous examples, the two halves are prepared in homogeneous stationary states. This means that a nontrivial time evolution is observed only in a region, the "light cone," expanding from the junction at the maximal allowed speed. In locally interacting lattice models with a finite-dimensional Hilbert space, this velocity is finite (Lieb and Robinson, 1972). The light-cone region contains information about the inhomogeneous nature of the system; see Fig. 31. In general, one can also prepare the two halves in homogeneous, nonstationary states also generating nontrivial dynamics away from the junction. However, the information about the inhomogeneous nature of the system is still contained in a light-cone region expanding from the junction at the maximal speed.

Bipartitioning protocols are appealing because they give a minimal setting in which a genuine NESS, i.e., steady states supporting nontrivial currents, can be observed at infinite times. This was first analytically observed in noninteracting systems (Antal *et al.*, 1999), then in conformal field theories (Bernard and Doyon, 2012, 2015), and finally (with the introduction of GHD) in interacting integrable models (Bertini *et al.*, 2016; Castro-Alvaredo, Doyon, and Yoshimura, 2016). On the contrary, for generic systems (at least for those with Hamiltonians invariant either under space inversion P or time reversal $\mathcal{T}$) currents are seen to vanish in numerical studies (Karrasch, Ilan, and Moore, 2013; Biella *et al.*, 2016, 2019; Karrasch, 2017b).

This fact can be explained using the hydrodynamic picture discussed in Sec. III.C. Assuming that at large times the expectation values of local observables can be computed in a locally quasistationary state, we generically have

$$\lim_{t\to\infty} \mathrm{tr}[j_x^{(Q)} e^{-iHt}\rho_0 e^{iHt}] = \mathrm{tr}[j_0^{(Q)}\rho_{\mathrm{st}}(x,\infty)] \qquad (190)$$

for any current $j_x^{(Q)}$. For generic systems, we can assume that at the leading order in time $\rho_{\mathrm{st}}(x,t)$ is a Gibbs ensemble with a space-time–dependent inverse temperature [and chemical potential if the system has some U(1) symmetry]. Generic lattice systems with a P-invariant Hamiltonian have no P-odd charge since momentum is not conserved (P is parity). This means that if the Hamiltonian is P symmetric, so is the Gibbs state. Noting that $j_x^{(Q)}$ is P odd, we then conclude that Eq. (190) vanishes. The same reasoning applies for $\mathcal{T}$-symmetric systems ($\mathcal{T}$ is time reversal). On the contrary, for integrable models, the state $\rho_{\mathrm{st}}(x,t)$ is a GGE at each fixed (x,t), and it generically includes parity-odd and time-reversal-odd charges. In this case, the expectation values of the currents are generically nonzero. Note that this reasoning applies only in the infinite-time limit. At finite times, the quasistationary state of a nonintegrable system is not exactly a space-time–dependent Gibbs ensemble: it includes corrections (proportional to gradients of temperature and chemical potentials) that produce nonzero expectation values of the currents. These corrections, however, vanish at infinite times.

For integrable systems, this argument can be checked by comparing the GHD solution; cf. Eq. (109) with tDMRG. In particular, note that for bipartitioning protocols GHD predicts that $\rho_{\mathrm{st}}(x,t)$ will become a function of the scaling variable $\zeta = x/t$ for large times, which is in agreement with previous observations in the context of noninteracting systems (Antal *et al.*, 1999). This can be understood intuitively by noting that an observer moving away from the junction at velocity ζ measures quasiparticles coming from the left (right) state if their velocity is larger (smaller) than ζ. Since quasiparticles from the left and right states have different densities, it is natural to expect the result of the measurement to depend on ζ. Therefore, when studying bipartitioning protocols, it is customary to view expectation values of physical quantities for large times as functions of ζ. As a representative example, in Fig. 32 we report the comparison between GHD and tDMRG for profiles of energy and spin currents as a function of ζ for the spin-1/2 XXZ chain for different values of $\Delta \in [0,1]$ taken from Bertini *et al.* (2016). The upper panel of Fig. 32 displays the profile of the energy current at infinite times after joining together two chains prepared at different temperatures, while the lower panel describes the profile of the spin current at infinite times after connecting two chains

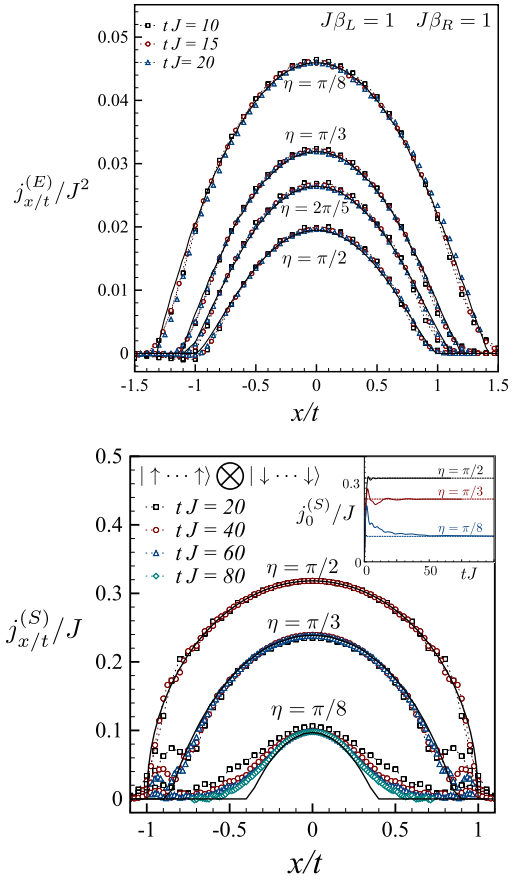

FIG. 32. Profiles of the local currents in the spin-1/2 XXZ chain for different values of $\Delta = \cos(\eta)$ as a function of rescaled position x/t. Symbols denote time-evolving block-decimation data for a chain of length $L = 60$ (top panel), $L = 120$ (bottom panel), and different times; full black lines are the GHD predictions. Top panel: energy current after the two halves of the system were initially prepared at inverse temperatures $\beta_L = 1$ and $\beta_R = 2$. Bottom panel: spin current after the two halves were prepared in two ferromagnetic states with opposite magnetization. Inset: time-dependent approach of $j_x^{(S)}$ (solid colored lines) to the prediction (dashed lines). Adapted from Bertini *et al.*, 2016.

prepared in two ferromagnetic states with opposite magnetization. This state is also known as the "domain-wall" state. From Fig. 32, we see that the current is finite within a light cone propagating from the junction, with a velocity that generically depends on the interaction strength.

The emergence of a nonzero current at infinite times in integrable models signals ballistic transport of the related charge by the stable quasiparticles and corresponds to a finite Drude weight in the linear-response regime. In accordance with the linear-response physics, also when studying bipartitioning protocols, there can be cases where certain currents vanish at infinite times, signaling sub-ballistic transport. Such an inhibition of the transport of specific charges is typically caused by discrete symmetries. For instance, this happens for the transport of spin in the spin-1/2 XXZ chain with $|\Delta| \geq 1$, where all local conserved charges are invariant under a $\mathbb{Z}_2$ spin-reversal symmetry except for the total magnetization (Piroli *et al.*, 2017). In this case, considering a bipartitioning protocol that connects a chain in a certain state with one in its spin-reversed copy (for example, two thermal states at the same temperature but with opposite magnetization), one finds a vanishing spin current in the infinite-time limit. In particular, the transport of spin has been observed to be diffusive for $|\Delta| > 1$ and superdiffusive for $\Delta = 1$ (Ljubotina, Žnidarič, and Prosen, 2017, 2019). The former case is described by GHD with diffusive corrections (De Nardis, Bernard, and Doyon, 2019) (see Sec. III.C.2), while a complete theoretical description of the latter is still missing and the problem is currently the subject of active research (De Nardis *et al.*, 2019; Gopalakrishnan and Vasseur, 2019; Agrawal *et al.*, 2020; Bulchandani, 2020; De Nardis, Medenjak *et al.*, 2020; Medenjak and De Nardis, 2020; Weiner *et al.*, 2020).

Finally, we note that, even though in generic spin chains no nontrivial NESS is believed to emerge at infinite times, NESS-like physics can emerge in some intermediate-time window. This is the case for gapless systems subject to low-temperature bipartitioning protocols. Namely, these are bipartitioning protocols connecting two thermal states at different temperatures that are both small (Bernard and Doyon, 2016). In this regime, for large intermediate times the behavior of energy density and current is well described by the Tomonaga-Luttinger-liquid theory. The energy current is nonzero in the light-cone region and takes a conformal form (Bernard and Doyon, 2012, 2015). On the other hand, for describing the profiles of generic observables, such as the spin current in the gapless phase of the spin-1/2 XXZ chain, it is necessary to keep track of the nonlinearities in the dispersion of low-energy modes. One can make progress in this direction by using the framework of nonlinear Tomonaga-Luttinger liquids (Bertini, Piroli, and Calabrese, 2018). For gapless integrable models at low temperatures, this approach reproduces the low-T expansion of the GHD solution (Bertini and Piroli, 2018; Mestyán *et al.*, 2019).

X. OVERVIEW OVER EXPERIMENTS

In this final section, we give an account of some of the experimental efforts devoted to investigating transport in either quantum magnets or with ultracold quantum gases. We stress that the survey of the literature cannot be complete and refer the interested reader to recent reviews where they are available (Chien, Peotta, and Di Ventra, 2015; Krinner, Esslinger, and Brantut, 2017; Tarruell and Sanchez-Palencia, 2018; Hess, 2019).

A. Quantum magnets

While this review focuses on theoretical developments and results, the field has also been strongly driven by experimental results. Most notably, many cuprate-based low-dimensional magnets exhibit a contribution from magnetic excitations to the thermal conductivity; see Hess (2007, 2019) and Sologubenko, Lorenz *et al.* (2007) for reviews. The values of the thermal conductivity κ can be extremely large given that these materials are electrical insulators and that they typically have complicated structures. Originally the largest thermal conductivities were reported for spin-ladder materials (Sologubenko, Gianno *et al.*, 2000; Hess *et al.*, 2001), but

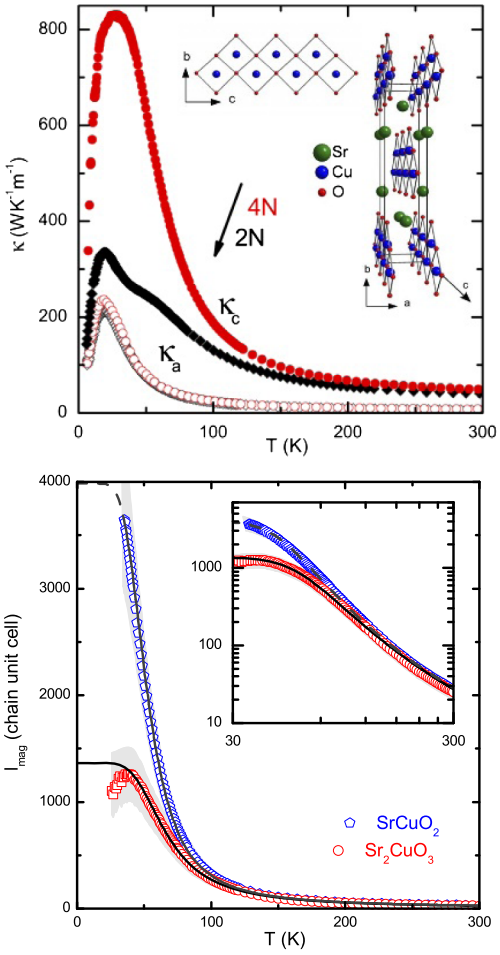

FIG. 33. Top panel: experimental data for the thermal conductivity of $SrCuO_2$ for two sample purities [2N (black curves) and 4N (red curves)]. The high-quality samples (4N) show a high thermal conductivity κ_c in the crystal direction that is parallel to the spin chains, which is attributed to spin excitations. In the transverse directions, presumably only phonons contribute. From Hlubek *et al.*, 2010. Bottom panel: extracted magnetic mean free paths of spinons. From Hlubek *et al.*, 2012.

later on much purer samples of the spin-chain materials $SrCuO_2$ (Hlubek *et al.*, 2010) and Sr_2CuO_3 (Hlubek *et al.*, 2012; Kawamata *et al.*, 2008) became available that show higher thermal conductivities; see Sologubenko, Felder *et al.* (2000) and Sologubenko *et al.* (2001) for earlier experimental results. Those compounds are good realizations of the isotropic Heisenberg spin-chain model formed by Cu–O–Cu bonds, with the exchange coupling $J/k_B \sim$ 2000–3000 K and the coupling between the chains $|J_\perp/J| \sim 10^{-1}$. The results for $\kappa(T)$, probing energy transport at low temperatures ($k_BT \ll J$), are shown in Fig. 33. Considering the complicated structure of these materials, the conductivities are large. Other examples of one-dimensional materials that show a similar phenomenology are copper pyrazine dinitrate (Sologubenko, Berggold *et al.*, 2007), $CaCu_2O_3$ (Hess *et al.*, 2007), and Haldane chains (Sologubenko *et al.*, 2008).

While it is tempting to relate these large conductivities to the integrability of the underlying spin-chain Hamiltonians, a rigorous experimental or theoretical verification of such a connection is difficult: measuring thermal transport necessarily requires a coupling of phonons to spins, and thus a complete theory of thermal transport in such material requires the incorporation of phonons; see Narozhny (1996), Shimshoni, Andrei, and Rosch (2003), Chernyshev and Rozhkov (2005, 2016), Louis and Zotos (2005), Rozhkov and Chernyshev (2005), Louis, Prelovšek, and Zotos (2006), Boulat *et al.* (2007), Gangadharaiah, Chernyshev, and Brenig (2010), Bartsch and Brenig (2013), and Chernyshev and Brenig (2015).

Assuming simple additivity of different contributions to conductivity, one can subtract the phononic contribution by measuring κ in the direction orthogonal to the orientation of spin chains [where only phonons contribute and whose contribution can be well described (Kawamata *et al.*, 2008) by the Debye model]. The resulting magnetic $\kappa_{\rm mag}$ contribution is then finite despite the ballistic energy transport in the Heisenberg model. This is caused by residual scattering on a few magnetic impurities (due to residual impurity of solvents used in the crystal growth) or a nonzero interchain coupling and/or due to spinon-phonon scattering. One can even deliberately introduce impurity doping (Kawamata *et al.*, 2008) and study how such disorder reduces transport (Hlubek *et al.*, 2011; Mohan *et al.*, 2014). Precisely accounting for different scattering effects is not easy (Hlubek *et al.*, 2012); however, a picture that seems to account for most experimentally measured features seems to be compatible with a dominant impurity scattering at low temperatures ($T < 50$ K), while spinon-phonon scattering is the leading term at higher T. One can in fact infer (Sologubenko, Felder *et al.*, 2000) the mean free path $l_{\rm mag}$ of magnetic excitations (spinons) by using a simple kinetic expression for the conductivity of spinons $\kappa_{\rm mag} = Cvl_{\rm mag}$, where C and v are the heat capacity and the velocity of spinons, respectively. The heat capacity of the spin-1/2 Heisenberg model at low T is proportional to T (Takahashi, 1973), leading to $l_{\rm mag} \propto \kappa_{\rm mag}/k_BT$; see Fig. 33, bottom panel.

The quasi-2D parent compounds of the high-temperature superconductors (HT_C's) also exhibit a magnon contribution to the thermal conductivity in La_2CuO_4 (Hess *et al.*, 2003), $Sr_2CuO_2Cl_2$ (Hofmann *et al.*, 2003), $Ba_2Cu_3O_4Cl_2$ (Ohno *et al.*, 2019), or Nd_2CuO_4 (Jin *et al.*, 2003). The values are smaller than in their quasi-one-dimensional relatives (where $l_{\rm mag} \sim 1$ μm; see Fig. 33), yet this can be partially ascribed to the dependence of the specific heat on dimensionality.

Thermal transport in quantum magnets can be measured not only in the steady state but also by using time-resolved methods or at specific finite frequencies. In the context of spin ladders, both the time-domain thermoreflectance method (Hohensee *et al.*, 2014) and the fluorescent microthermal imaging technique (Otter *et al.*, 2009, 2012) were used. Moreover, one can induce a heat pulse on one end of a macroscopically large sample and then measure the time-resolved evolution of temperature at its other end (Montagnese *et al.*, 2013). Such techniques can be used to extract the electron-phonon coupling strength.

Measuring spin transport is much more difficult: until recently, the only experiments were indirect ones using NMR (Thurber *et al.*, 2001; Kühne *et al.*, 2009) or muon-spin resonance (μSR) techniques to obtain a relaxation rate of

a nuclear spin in NMR or a muon in μSR, which is given by the spin autocorrelation function. The frequency dependence of the latter can be probed by the magnetic-field dependence of the relaxation rate, allowing one to distinguish diffusive from ballistic behavior from the tail of the spin autocorrelation function. NMR studies on $SrCuO_2$ found diffusive relaxation (Thurber *et al.*, 2001), while μSR experiments on high-purity samples found ballistic relaxation (Maeter *et al.*, 2013) (both studies probe $k_BT \ll J$). μSR measurements on an organic salt (Pratt *et al.*, 2006) or $Cu(C_4H_4N_2)(NO_3)_2$ (Xiao *et al.*, 2015) were interpreted in terms of diffusion, while a more recent μSR experiment (Huddart *et al.*, 2021) on $[\text{pym-Cu}(NO_3)_2(H_2O)_2]$ and $[Cu(pym)(H_2O)_4]SiF_6 \cdot H_2O$ reported ballistic and diffusive dynamics, respectively.[26] Recently the spin-Seebeck effect was exploited to directly induce and measure spin currents in a quasi-1D cuprate material (Hirobe *et al.*, 2017).

We mention that within solid-state NMR, experimental schemes were developed to study spin transport in quasi-1D spin-chain systems after initializing the system in a state with an inhomogeneous magnetization. An example is an apatite crystal in which flourine atoms form chains that can be under an appropriate pulse sequence described by a nearest-neighbor dipolar Hamiltonian (related to the XX Hamiltonian by a unitary transformation), and with an interchain coupling as small as $|J_\perp/J| \sim 0.02$. A mixed initial state with a boundary imbalance of magnetization can be prepared (exploiting different energy scales of bulk and boundary spins) whose time evolution can then be studied (Ramanathan *et al.*, 2011; Kaur and Cappellaro, 2012).

Besides experiments with bulk materials, there are novel synthetic one-dimensional structures that may be used in the future to study transport in correlated one-dimensional systems. These include arrays of atoms arranged on various surfaces (metallic, insulating, or superconducting), whose properties are in some realizations believed to be related to the physics of spin systems (Khajetoorians *et al.*, 2013; Toskovic *et al.*, 2016).

The prediction of superdiffusive dynamics of the Kardar-Parisi-Zhang type for the spin-1/2 Heisenberg chain has stimulated a recent neutron-scattering study using the well-known quasi-one-dimensional material $KCuF_3$ (Scheie *et al.*, 2021). By studying the regime of high temperatures $\hbar\omega \ll k_BT$, Scheie *et al.* reported evidence that the data are more consistent with KPZ behavior than diffusive or ballistic dynamics.

As a future challenge for theory, the development of efficient numerical methods for the description of transport in electron-phonon systems is desirable. An open question is the applicability of wave-function-based methods to the study of transport in spin-phonon systems. Recent advances with DMRG methods using optimized local phonon bases (Zhang, Jeckelmann, and White, 1998) have already given us access to real-time dynamics in electron-phonon systems (Guo *et al.*, 2012; Brockt *et al.*, 2015; Dorfner *et al.*, 2015; Kloss, Reichman, and Tempelaar, 2019; Stolpp *et al.*, 2020), which calls for extensions to finite temperatures (Jansen, Bonča, and Heidrich-Meisner, 2020) and spin-phonon systems [see also Köhler, Stolpp, and Paeckel (2021)].

B. Ultracold quantum gases in optical lattices

Ultracold quantum gases provide another promising route to experimentally study the transport properties of low-dimensional many-body systems. In optical lattices, both Fermi-Hubbard and Bose-Hubbard models can be rather routinely realized (Bloch, Dalibard, and Zwerger, 2008; Gross and Bloch, 2017). A direct emulation of Heisenberg models or, even more generally, spin-1/2 XXZ systems is more difficult: starting from single bands and contact interactions, these models arise only in the strong-coupling regime of Hubbard models, and the degree to which they can be realized with high fidelity depends on the quality of the loading processes and the state preparation. The fact that here we are interested in finite-temperature properties implies that no particular cooling schemes are needed, unlike in the ongoing efforts to reach the regime of long-range antiferromagnetic correlations in the Fermi-Hubbard model (Jördens *et al.*, 2008; Schneider *et al.*, 2008; Cheuk *et al.*, 2015, 2016a, 2016b; Edge *et al.*, 2015; Haller *et al.*, 2015; Hart *et al.*, 2015; Omran *et al.*, 2015; Parsons *et al.*, 2015; Boll *et al.*, 2016; Cocchi *et al.*, 2016; Greif *et al.*, 2016; Parsons *et al.*, 2016; Hilker *et al.*, 2017; Mazurenko *et al.*, 2017; Salomon *et al.*, 2019).

In addition to working with the Fermi-Hubbard model, one can also emulate the Heisenberg model in two-component Bose-Hubbard models. Using this route, the decay of a spin-spiral initial state was studied in 1D and 2D Heisenberg systems with a ferromagnetic exchange coupling (Hild *et al.*, 2014). For a 1D system with an isotropic exchange interaction, a diffusive decay of the spin spiral was found. A recent study succeeded in extending this to the entire range of exchange anisotropies by working with a different atomic species (namely, the bosonic isotope ^{7}Li) and by exploiting a specific Feshbach resonance (Jepsen *et al.*, 2020). As a main result, the transition from a ballistic decay at $\Delta = 0$ to a variety of transport behaviors is reported: superdiffusion for a range of $0 < \Delta < 1$, diffusion at $\Delta = 1$, and subdiffusive dynamics for $\Delta > 1$. These observations are quite different from the linear-response predictions discussed in Sec. VI.C, but the initial spiral state may lead to genuinely nonequilibrium dynamics.

Studying the role of integrability directly with Fermi-Hubbard models may be a promising route. Given the rapid emergence of many fermionic quantum-gas microscopes (Cheuk *et al.*, 2015, 2016b; Edge *et al.*, 2015; Haller *et al.*, 2015; Omran *et al.*, 2015; Parsons *et al.*, 2015, 2016; Boll *et al.*, 2016; Cocchi *et al.*, 2016; Greif *et al.*, 2016; Hilker *et al.*, 2017; Mazurenko *et al.*, 2017; Brown *et al.*, 2019; Nichols *et al.*, 2019; Salomon *et al.*, 2019; Guardado-Sanchez *et al.*, 2020), which all work with the two-dimensional Fermi-Hubbard model and which allow one to chop such 2D systems into individual 1D systems (Boll *et al.*, 2016; Salomon *et al.*, 2019; Vijayan *et al.*, 2020), the finite-temperature transport properties of the 1D Fermi-Hubbard model might be the

[26]Both materials are perfect realizations of the antiferromagnetic isotropic Heisenberg model with $J/k_B \sim 10$–50 K and $|J_\perp/J| \lesssim 10^{-3}$.

easiest accessible integrable lattice model. Ultracold quantum gases have some drawbacks: particle numbers and system sizes cannot be made arbitrarily large, the systems have a finite lifetime, and they realize closed quantum systems; i.e., it is not straightforward to couple such a gas to leads; see Brantut *et al.* (2012, 2013), Stadler *et al.* (2012), and Krinner, Esslinger, and Brantut (2017). Nevertheless, one could exploit the single-site manipulation and resolution capabilities of quantum-gas microscopes to investigate the spreading of perturbations in the particle or spin density, as suggested by Karrasch, Prosen, and Heidrich-Meisner (2017). Numerical simulations show that it is possible to resolve the difference between presumably diffusive and ballistic dynamics at high temperatures $T \gg J$ on timescales of less than $4/t_{\mathrm{h}}$, where t_{h} is the hopping-matrix element and thus within the time window of coherent many-body dynamics in such systems (Trotzky *et al.*, 2012). Such an experiment could directly probe the linear-response regime. A recent experiment addressing spin-charge separation in the 1D Hubbard model utilizes a similar protocol to induce spin and charge dynamics (Vijayan *et al.*, 2020).

Nonequilibrium mass transport can be investigated in a much more straightforward fashion using optical lattices. In the so-called sudden expansion, an originally trapped quantum gas is released from its confining potential and allowed to expand in a homogeneous and flat optical lattice. This method was used to study the nonequilibrium transport of the 2D Fermi-Hubbard model (Schneider *et al.*, 2012) and the Fermi-Hubbard chain (Scherg *et al.*, 2018), as well as of bosons in 1D and 2D lattices (Ronzheimer *et al.*, 2013). In Ronzheimer *et al.*'s experiment with bosons, an impressive difference between the dynamics of strongly interacting bosons in 1D versus 2D lattices was observed: in 1D, the sudden expansion is as fast as for noninteracting bosons (assuming the same initial conditions), while in 2D the cloud expands much slower, which is more consistent with the notion that interactions should induce scattering and degrade currents; see Fig. 34. The reason for the behavior of such strongly interacting 1D gases lies in their exact mapping onto spinless noninteracting fermions via a Jordan-Wigner transformation (Cazalilla *et al.*, 2011). Therefore, strongly interacting bosons with densities not exceeding unity realize an integrable model in 1D equivalent to the spin-1/2 XX chain. Experimentally, integrability can be broken in three ways: (i) coupling 1D systems to a 2D system, (ii) inducing double occupancies in the initial state, and (iii) going to finite interaction strength $0 < U/t_{\mathrm{h}} < \infty$, where the Bose-Hubbard model is nonintegrable. All three cases show deviations from the fast and ballistic expansion of hard-core bosons. In cases (i) and (ii), this can be traced back to the breaking of integrability (Vidmar *et al.*, 2013; Steinigeweg, Heidrich-Meisner *et al.*, 2014). The dynamics in the 1D Bose-Hubbard model at $U/t_{\mathrm{h}} < \infty$ is more involved in this particular experiment as it also involves a quantum quench in the interaction and thus probes the dynamics at different energy densities, depending on U/t_{h} (Vidmar *et al.*, 2013). The experiment (Ronzheimer *et al.*, 2013) is therefore a realization of integrability-protected ballistic mass transport in the spirit of this review, albeit in the nonequilibrium regime; see Sec. IX.B. Extensions of this approach are possible using quantum-gas microscopes as well, where to date only the expansion dynamics of two bosons has been investigated (Preiss *et al.*, 2015; Tai *et al.*, 2017). More recent experiments studied transport in the two-dimensional Fermi-Hubbard model using the capabilities of quantum-gas microscopes (Brown *et al.*, 2019; Nichols *et al.*, 2019; Vijayan *et al.*, 2020). All of these studies investigated the interplay of spin and charge in transport, with Vijayan *et al.* (2020) focusing on spin-charge separation in one dimension, while Brown *et al.* (2019) and Nichols *et al.* (2019) observed diffusion in two-dimensional systems.

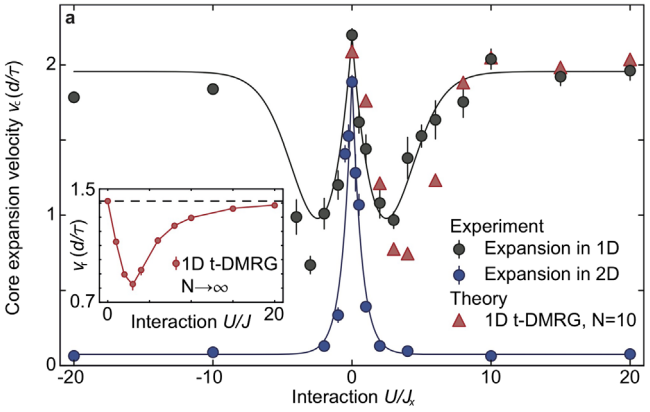

FIG. 34. Expansion velocity of a cloud of bosons that are released from a trap into an empty optical lattice. Main panel: experimental and DMRG data for the expansion velocity as a function of interaction strength U/J_x extracted from the half width at half maximum. J_x is the hopping-matrix element along the x direction of the two-dimensional lattice and $J_x = J$ for the one-dimensional case. U is the on-site interaction strength in the Bose-Hubbard model. Inset: DMRG data for the radial velocity as a function of U/J. Both noninteracting and strongly interacting bosons expand ballistically with the same expansion velocity (Ronzheimer *et al.*, 2013).

We note that experiments with ultracold bosons in optical lattices in the strongly interacting regime thus offer a unique and controlled way to study integrability breaking by perturbing around the limit of the spin-1/2 XX chain, resulting then in the 2D XX model or ladders (Vidmar *et al.*, 2013; Steinigeweg, Heidrich-Meisner *et al.*, 2014; Hauschild, Pollmann, and Heidrich-Meisner, 2015). In addition to measuring densities, one can further study one-body correlations in such sudden expansions, for which theory predicts a dynamical quasicondensation phenomenon (Micheli *et al.*, 2004; Rigol and Muramatsu, 2004) as a result of the emergent eigenstate solution for this nonequilibrium problem (Vidmar, Iyer, and Rigol, 2017). Even this effect, the dynamical quasicondensation, another consequence of integrability in nonequilibrium transport, has been observed experimentally (Vidmar *et al.*, 2015).

XI. SUMMARY AND OUTLOOK

This review has examined the state of the art of the understanding of transport in translationally invariant one-dimensional quantum lattice models at finite temperatures from the theoretical physics perspective. We have discussed, in particular, the important role of integrability and its

breaking, focusing primarily on the paradigmatic spin-1/2 *XXZ* and the Fermi-Hubbard chain as minimal models for spin, charge, and energy transport. The progress that has been achieved in recent years for these systems and their theoretical description in general is due to methodological breakthroughs, in fundamental concepts, such as establishing the existence of quasilocal conservation laws (Prosen, 2011b, 2014c; Prosen and Ilievski, 2013; Pereira *et al.*, 2014; Ilievski, Medenjak, and Prosen, 2015) and their connection to a complete hydrodynamic description [the so-called generalized hydrodynamics (Bertini *et al.*, 2016; Castro-Alvaredo, Doyon, and Yoshimura, 2016)], as well as in numerical methods such as matrix-product-based techniques (Karrasch, Bardarson, and Moore, 2012, 2013; Karrasch, 2017a) and dynamical typicality (Steinigeweg, Gemmer, and Brenig, 2014; Steinigeweg, Herbrych, Zotos, and Brenig, 2016) for utilizing time-evolution methods at finite temperatures for the calculation of transport properties. Establishing time-dependent DMRG as a solver of Lindblad master equations (Prosen and Žnidarič, 2009) opened up possibilities for complementary qualitative and quantitative insights from studying open quantum systems (Žnidarič, 2011a).

We can say that the understanding of ballistic transport at high temperatures or even in nonequilibrium states has by now matured. The thermal Drude weight in both the spin-1/2 *XXZ* chain and the 1D Fermi-Hubbard model were computed as a function of model parameters and temperature (Klümper and Sakai, 2002; Sakai and Klümper, 2003; Ilievski and De Nardis, 2017a; Karrasch, 2017a). The exact and complete calculation of magnetothermal corrections involving off-diagonal coefficients and the spin Drude weight at finite magnetizations remains an open task (Louis and Gros, 2003; Heidrich-Meisner, Honecker, and Brenig, 2005; Sakai and Klümper, 2005; Zotos, 2017), particularly for the Fermi-Hubbard model, where in principle three currents can couple. The calculation of all cross coefficients could be accomplished using the methodology of GHD.

For spin transport in the spin-1/2 *XXZ* chain, the existence of a finite-temperature Drude weight at nonzero magnetization and any Δ (Zotos, Naef, and Prelovšek, 1997) and for zero magnetization at $|\Delta| < 1$ is now well established and accepted (Zotos, 1999; Prosen, 2011b; Prosen and Ilievski, 2013; Pereira *et al.*, 2014; Urichuk *et al.*, 2019). Its full temperature dependence is accessible as well (Zotos, 1999; Ilievski and De Nardis, 2017b; Urichuk *et al.*, 2019) yet has not been convincingly computed with numerical methods. The agreement between the TBA, GHD, and the lower bound supports the notion of a fractal structure as a function of Δ, yet neither approach is rigorous, as the approach either involves Takahashi's string hypothesis or relies on the assumption of knowing all relevant charges. For the spin-1/2 Heisenberg chain, the overwhelming evidence suggests that the spin Drude weight vanishes at finite temperature. The same goes for the regime of $\Delta > 1$, while in both cases a rigorous proof is missing.

For those cases that prohibit ballistic transport channels or when studying subleading corrections, the situation is still much less clear, yet actively studied. Although normal diffusion is the most commonly observed type of nonballistic transport, in both integrable (De Nardis, Bernard, and Doyon, 2018) and nonintegrable quantum lattice systems (Sirker, Pereira, and Affleck, 2009; Sirker, Pereira, and Affleck, 2011), one also often encounters other types of transport, including, in particular, superdiffusive dynamics (Žnidarič, 2011a; Ljubotina, Žnidarič, and Prosen, 2017). Notably, the conjectured KPZ scaling (Ljubotina, Žnidarič, and Prosen, 2019) [see also Das *et al.* (2019), Bulchandani (2020), De Nardis, Gopalakrishnan *et al.* (2020), Dupont and Moore (2020), Fava *et al.* (2020), Ilievski *et al.* (2020), and Krajnik and Prosen (2020)] of spin-correlation functions and spin transport in the isotropic Heisenberg chain and other integrable models of magnetism with non-Abelian symmetries is a particularly pressing question on which much work is expected in the near future [for a recent review on superdiffusion, see Bulchandani, Gopalakrishnan, and Ilievski (2021)]. Another universal option suggested by recent studies is the one of marginally superdiffusive transport characterized by a diffusive exponent and a logarithmic correction (De Nardis, Medenjak *et al.*, 2020). The exact nature of subleading corrections in the ballistic regimes of the 1D Fermi-Hubbard model or the exact nature of spin and charge transport at zero magnetization and filling is much less well understood. In general, a complete qualitative understanding of the emergence of diffusion in integrable models is still lacking.

The now solidly established aspects of spin transport in the spin-1/2 *XXZ* chain and the open questions on superdiffusion and the connection between linear-response behavior and transport in specific far-from-equilibrium settings have stimulated additional recent experiments using both quasi-one-dimensional materials (Scheie *et al.*, 2021) and ultracold atoms (Hild *et al.*, 2014; Jepsen *et al.*, 2020). The neutron-scattering study conducted by Scheie *et al.* (2021) reported consistency of their data with the KPZ scenario.

For nonintegrable models, we presented examples where the notion of diffusion is supported by approximate analytical methods as well as numerically exact techniques. These include the dimerized spin-1/2 *XX* ladder (Steinigeweg, Heidrich-Meisner *et al.*, 2014), spin-1/2 chains with a staggered magnetic field (Huang, Karrasch, and Moore, 2013; Steinigeweg, Gemmer, and Brenig, 2015), and general spin ladders and frustrated chains (Zotos, 2004; Karrasch, Kennes, and Heidrich-Meisner, 2015; Steinigeweg, Herbrych, Zotos, and Brenig, 2016). In the final category, the longtime dynamics is usually more complex and diffusion is harder to establish. At low energies, field-theoretical studies are strongly suggestive of diffusive dynamics as well; see, in particular, Sirker, Pereira, and Affleck (2011).

Although the work presented here considers only quantum lattice systems, it is not clear whether the transport phenomena are in any fundamental way affected by the quantum nature of the microscopic equation of motions relative to the classical deterministic Hamiltonian dynamics governing classical lattice systems. Thus far we have seen no argument against the conclusion that all the emerging transport phenomena at finite temperatures have analogous counterparts in classical lattice models. An exception might be the putative many-body localization (Nandkishore and Huse, 2015; Abanin *et al.*, 2019), where temperature is ill defined. However, both a systematic semiclassical analysis and elucidating the quantum-classical correspondence for transport in many-body lattice systems will be desirable in the future.

The transition between diffusion to types of nondiffusive transport can be expected to be a manifestation of a form of ergodicity breaking. The latter is currently being intensely studied even in translationally invariant, disorder-free settings, with prominent examples being the so-called quantum scars in models with constrained dynamics; see Bernien *et al.* (2017), Lan *et al.* (2018), Moudgalya, Regnault, and Bernevig (2018), and Turner *et al.* (2018). However, a possible connection to finite-temperature transport in such models has not been investigated. Another interesting set of open questions in relation to ergodicity breaking concerns the connection between spectral statistics, described by random-matrix theory, and transport properties. Since spectral statistics contain information on different timescales, it may turn out (Brenes *et al.*, 2018) that models with a local integrability breaking are ergodic on the Heisenberg timescale, i.e., on timescales controlled by the inverse mean level spacing, while transport is ballistic on shorter timescales.

ACKNOWLEDGMENTS

We thank H. De Raedt, J. Gemmer, C. Hess, P. Maass, V. Meden, J. Moore, P. Prelovšek, U. Schneider, H. Spohn, and X. Zotos for discussions and for their comments on a previous version of the manuscript. We thank M. Fagotti for valuable discussions and his contributions to this project in its early stages. Furthermore, we acknowledge helpful comments from S. Gopalakrishnan, D. Huse, E. Ilievski, A. Klümper, and L. Santos on a previous version of the manuscript. This work was supported in part by Starting Grant No. 679722 and Advanced Grant OMNES No. 694544 of the European Research Council (ERC). F. H.-M. and M. Z. are grateful for the hospitality at KITP, where part of this work was performed. This research was supported in part by the National Science Foundation under Grant No. NSF PHY-1748958. C. K. acknowledges support from the Deutsche Forschungsgemeinschaft (DFG, German Science Foundation) through the Emmy Noether Program (Grant No. KA 3360/2-1) and through CRC-TR 183 (Project No. A01), as well as from "Niedersächsisches Vorab" through the "Quantum- and Nano-Metrology (QUANOMET)" initiative within Project No. P-1. R. S. acknowledges support from the DFG [Grant No. 397067869 (STE 2243/3-1)] within the DFG Research Unit FOR 2692 (Grant No. 355031190). F. H.-M. was supported by the DFG Grant No. 217133147 via CRC 1073 (Project No. B09). B. B., M. Z., and T. P. acknowledge support from Program No. P1-0402 of the Slovenian Research Agency (ARRS). M. Z. acknowledges support from Grants No. J1-7279 and No. J1-1698 of the ARRS.

REFERENCES

Abanin, D. A., E. Altman, I. Bloch, and M. Serbyn, 2019, Rev. Mod. Phys. **91**, 021001.

Abanin, D. A., J. H. Bardarson, G. D. Tomasi, S. Gopalakrishnan, V. Khemani, S. A. Parameswaran, F. Pollmann, A. C. Potter, M. Serbyn, and R. Vasseur, 2021, Ann. Phys. (Amsterdam) **427**, 168415.

Agarwal, K., S. Gopalakrishnan, M. Knap, M. Müller, and E. Demler, 2015, Phys. Rev. Lett. **114**, 160401.

Agrawal, U., S. Gopalakrishnan, R. Vasseur, and B. Ware, 2020, Phys. Rev. B **101**, 224415.

Ajisaka, S., F. Barra, C. Mejia-Monasterio, and T. Prosen, 2012, Phys. Rev. B **86**, 125111.

Al-Assam, S., S. R. Clark, and D. Jaksch, 2016, Tensor Network Theory library, beta version 1.0.13, http://www.tensornetworktheory.org.

Alba, V., 2018, Phys. Rev. B **97**, 245135.

Alba, V., B. Bertini, and M. Fagotti, 2019, SciPost Phys. **7**, 5.

Alba, V., and F. Heidrich-Meisner, 2014, Phys. Rev. B **90**, 075144.

Alben, R., M. Blume, H. Krakauer, and L. Schwartz, 1975, Phys. Rev. B **12**, 4090.

Alicki, R., and K. Lendi, 2007, *Quantum Dynamical Semigroups and Applications* (Springer-Verlag, Berlin).

Altman, E., and R. Vosk, 2015, Annu. Rev. Condens. Matter Phys. **6**, 383.

Alvarez, J. V., and C. Gros, 2002a, Phys. Rev. Lett. **89**, 156603.

Alvarez, J. V., and C. Gros, 2002b, Phys. Rev. B **66**, 094403.

Alvarez, J. V., and C. Gros, 2002c, Phys. Rev. Lett. **88**, 077203.

Antal, T., P. L. Krapivsky, and A. Rákos, 2008, Phys. Rev. E **78**, 061115.

Antal, T., Z. Rácz, A. Rákos, and G. M. Schütz, 1998, Phys. Rev. E **57**, 5184.

Antal, T., Z. Rácz, A. Rákos, and G. M. Schütz, 1999, Phys. Rev. E **59**, 4912.

Antal, T., Z. Rácz, and L. Sasvári, 1997, Phys. Rev. Lett. **78**, 167.

Arrigoni, E., M. Knap, and W. von der Linden, 2013, Phys. Rev. Lett. **110**, 086403.

Aschbacher, W. H., and J.-M. Barbaroux, 2006, Lett. Math. Phys. **77**, 11.

Aschbacher, W. H., and C.-A. Pillet, 2003, J. Stat. Phys. **112**, 1153.

Ashcroft, N. W., and N. D. Mermin, 1976, *Solid State Physics* (Saunders College Publishing, Philadelphia).

Attal, S., and Y. Pautrat, 2006, Ann. Henri Poincaré **7**, 59.

Balachandran, V., G. Benenti, E. Pereira, G. Casati, and D. Poletti, 2018, Phys. Rev. Lett. **120**, 200603.

Balz, B. N., J. Richter, J. Gemmer, R. Steinigeweg, and P. Reimann, 2018, in *Thermodynamics in the Quantum Regime: Fundamental Aspects and New Directions*, edited by F. Binder, L. A. Correa, C. Gogolin, J. Anders, and G. Adesso (Springer International Publishing, Cham, Switzerland), pp. 413–433.

Barišić, O. S., J. Kokalj, I. Balog, and P. Prelovšek, 2016, Phys. Rev. B **94**, 045126.

Barišić, O. S., P. Prelovšek, A. Metavitsiadis, and X. Zotos, 2009, Phys. Rev. B **80**, 125118.

Barra, F., 2015, Sci. Rep. **5**, 14873.

Barthel, T., 2013, New J. Phys. **15**, 073010.

Barthel, T., U. Schollwöck, and S. R. White, 2009, Phys. Rev. B **79**, 245101.

Bartsch, C., and W. Brenig, 2013, Phys. Rev. B **88**, 214412.

Bartsch, C., and J. Gemmer, 2009, Phys. Rev. Lett. **102**, 110403.

Bastianello, A., V. Alba, and J.-S. Caux, 2019, Phys. Rev. Lett. **123**, 130602.

Bastianello, A., and A. De Luca, 2019, Phys. Rev. Lett. **122**, 240606.

Bastianello, A., B. Doyon, G. Watts, and T. Yoshimura, 2018, SciPost Phys. **4**, 45.

Baxter, R. J., 1982, *Exactly Solved Models in Statistical Mechanics* (Academic Press, New York).

Benenti, G., G. Casati, T. Prosen, and D. Rossini, 2009, Europhys. Lett. **85**, 37001.

Benenti, G., G. Casati, T. Prosen, D. Rossini, and M. Žnidarič, 2009, Phys. Rev. B **80**, 035110.

Benenti, G., S. Lepri, and R. Livi, 2020, Front. Phys. **8**, 292.
Beni, G., and C. F. Coll, 1975, Phys. Rev. B **11**, 573.
Benz, J., T. Fukui, A. Klümper, and C. Scheeren, 2005, J. Phys. Soc. Jpn. Suppl. **74**, 181.
Bera, S., G. De Tomasi, F. Weiner, and F. Evers, 2017, Phys. Rev. Lett. **118**, 196801.
Bernard, D., and B. Doyon, 2012, J. Phys. A **45**, 362001.
Bernard, D., and B. Doyon, 2015, Ann. Henri Poincaré **16**, 113.
Bernard, D., and B. Doyon, 2016, J. Stat. Mech. 064005.
Bernien, H., *et al.*, 2017, Nature (London) **551**, 579.
Bernier, J.-S., R. Tan, L. Bonnes, C. Guo, D. Poletti, and C. Kollath, 2018, Phys. Rev. Lett. **120**, 020401.
Bertini, B., M. Collura, J. De Nardis, and M. Fagotti, 2016, Phys. Rev. Lett. **117**, 207201.
Bertini, B., F. H. L. Essler, S. Groha, and N. J. Robinson, 2015, Phys. Rev. Lett. **115**, 180601.
Bertini, B., and M. Fagotti, 2016, Phys. Rev. Lett. **117**, 130402.
Bertini, B., M. Fagotti, L. Piroli, and P. Calabrese, 2018, J. Phys. A **51**, 39LT01.
Bertini, B., and L. Piroli, 2018, J. Stat. Mech. 033104.
Bertini, B., L. Piroli, and P. Calabrese, 2018, Phys. Rev. Lett. **120**, 176801.
Bertini, B., L. Piroli, and M. Kormos, 2019, Phys. Rev. B **100**, 035108.
Bethe, H., 1931, Z. Phys. **71**, 205.
Bhaseen, M. J., B. Doyon, A. Lucas, and K. Schalm, 2015, Nat. Phys. **11**, 509.
Biella, A., M. Collura, D. Rossini, A. De Luca, and L. Mazza, 2019, Nat. Commun. **10**, 4820.
Biella, A., A. De Luca, J. Viti, D. Rossini, L. Mazza, and R. Fazio, 2016, Phys. Rev. B **93**, 205121.
Bloch, I., J. Dalibard, and W. Zwerger, 2008, Rev. Mod. Phys. **80**, 885.
Bohm, M., and H. Leschke, 1992, J. Phys. A **25**, 1043.
Bohrdt, A., C. B. Mendl, M. Endres, and M. Knap, 2017, New J. Phys. **19**, 063001.
Boll, M., T. A. Hilker, G. Salomon, A. Omran, J. Nespolo, L. Pollet, I. Bloch, and C. Gross, 2016, Science **353**, 1257.
Bonča, J., J. P. Rodriguez, J. Ferrer, and K. S. Bedell, 1994, Phys. Rev. B **50**, 3415.
Bonetto, F., J. L. Lebowitz, and L. Rey-Bellet, 2000, in *Mathematical Physics 2000*, edited by A. Fokas, A. Grigoryan, T. Kibble, and B. Zegarlinski (Imperial College Press, London).
Borsi, M., B. Pozsgay, and L. Pristyák, 2020, Phys. Rev. X **10**, 011054.
Boulat, E., P. Mehta, N. Andrei, E. Shimshoni, and A. Rosch, 2007, Phys. Rev. B **76**, 214411.
Branschädel, A., G. Schneider, and P. Schmitteckert, 2010, Ann. Phys. (Berlin) **522**, 657.
Brantut, J.-P., C. Grenier, J. Meineke, D. Stadler, S. Krinner, C. Kollath, T. Esslinger, and A. Georges, 2013, Science **342**, 713.
Brantut, J.-P., J. Meineke, D. Stadler, S. Krinner, and T. Esslinger, 2012, Science **337**, 1069.
Brenes, M., J. Goold, and M. Rigol, 2020, Phys. Rev. B **102**, 075127.
Brenes, M., T. LeBlond, J. Goold, and M. Rigol, 2020, Phys. Rev. Lett. **125**, 070605.
Brenes, M., E. Mascarenhas, M. Rigol, and J. Goold, 2018, Phys. Rev. B **98**, 235128.
Brenes, M., J. J. Mendoza-Arenas, A. Purkayastha, M. T. Mitchison, S. R. Clark, and J. Goold, 2020, Phys. Rev. X **10**, 031040.
Breuer, H.-P., and F. Petruccione, 2002, *The Theory of Open Quantum Systems* (Oxford University Press, New York).
Brockt, C., F. Dorfner, L. Vidmar, F. Heidrich-Meisner, and E. Jeckelmann, 2015, Phys. Rev. B **92**, 241106.
Brown, P. T., *et al.*, 2019, Science **363**, 379.
Buchanan, M., 2005, Nat. Phys. **1**, 71.
Bulchandani, V. B., 2017, J. Phys. A **50**, 435203.
Bulchandani, V. B., 2020, Phys. Rev. B **101**, 041411(R).
Bulchandani, V. B., X. Cao, and J. E. Moore, 2019, J. Phys. A **52**, 33LT01.
Bulchandani, V. B., S. Gopalakrishnan, and E. Ilievski, 2021, arXiv:2103.01976.
Bulchandani, V. B., C. Karrasch, and J. E. Moore, 2020, Proc. Natl. Acad. Sci. U.S.A. **117**, 12713.
Bulchandani, V. B., R. Vasseur, C. Karrasch, and J. E. Moore, 2017, Phys. Rev. Lett. **119**, 220604.
Bulchandani, V. B., R. Vasseur, C. Karrasch, and J. E. Moore, 2018, Phys. Rev. B **97**, 045407.
Calabrese, P., F. H. L. Essler, and G. Mussardo, 2016, J. Stat. Mech. 064001.
Calabrese, P., C. Hagendorf, and P. Le Doussal, 2008, J. Stat. Mech. P07013.
Callen, H. B., and T. A. Welton, 1951, Phys. Rev. **83**, 34.
Cao, X., V. B. Bulchandani, and H. Spohn, 2019, J. Phys. A **52**, 495003.
Carmelo, J., S.-J. Gu, and P. Sacramento, 2013, Ann. Phys. (Amsterdam) **339**, 484.
Carmelo, J., S. Nemati, and T. Prosen, 2018, Nucl. Phys. **B930**, 418.
Carmelo, J. M. P., T. Prosen, and D. K. Campbell, 2015, Phys. Rev. B **92**, 165133.
Casagrande, H. P., D. Poletti, and G. T. Landi, 2020, arXiv:2009.08200.
Casati, G., J. Ford, F. Vivaldi, and W. M. Visscher, 1984, Phys. Rev. Lett. **52**, 1861.
Castella, H., X. Zotos, and P. Prelovšek, 1995, Phys. Rev. Lett. **74**, 972.
Castro-Alvaredo, O., Y. Chen, B. Doyon, and M. Hoogeveen, 2014, J. Stat. Mech. P03011.
Castro-Alvaredo, O. A., B. Doyon, and T. Yoshimura, 2016, Phys. Rev. X **6**, 041065.
Caux, J., and J. Mossel, 2011, J. Stat. Mech. P02023.
Caux, J.-S., B. Doyon, J. Dubail, R. Konik, and T. Yoshimura, 2019, SciPost Phys. **6**, 70.
Caux, J.-S., and J. M. Maillet,2005, Phys. Rev. Lett. **95**, 077201.
Cazalilla, M. A., R. Citro, T. Giamarchi, E. Orignac, and M. Rigol, 2011, Rev. Mod. Phys. **83**, 1405.
Cheneau, M., P. Barmettler, D. Poletti, M. Endres, P. Schauß, T. Fukuhara, C. Gross, I. Bloch, C. Kollath, and S. Kuhr, 2012, Nature (London) **481**, 484.
Chernyshev, A. L., and W. Brenig, 2015, Phys. Rev. B **92**, 054409.
Chernyshev, A. L., and A. V. Rozhkov, 2005, Phys. Rev. B **72**, 104423.
Chernyshev, A. L., and A. V. Rozhkov, 2016, Phys. Rev. Lett. **116**, 017204.
Cheuk, L. W., M. A. Nichols, K. R. Lawrence, M. Okan, H. Zhang, E. Khatami, N. Trivedi, T. Paiva, M. Rigol, and M. W. Zwierlein, 2016a, Science **353**, 1260.
Cheuk, L. W., M. A. Nichols, K. R. Lawrence, M. Okan, H. Zhang, and M. W. Zwierlein, 2016b, Phys. Rev. Lett. **116**, 235301.
Cheuk, L. W., M. A. Nichols, M. Okan, T. Gersdorf, V. V. Ramasesh, W. S. Bakr, T. Lompe, and M. W. Zwierlein, 2015, Phys. Rev. Lett. **114**, 193001.
Chien, C.-C., S. Peotta, and M. Di Ventra, 2015, Nat. Phys. **11**, 998.
Chruściński, D., and S. Pascazio, 2017, Open Syst. Inf. Dyn. **24**, 1740001.
Cocchi, E., L. A. Miller, J. H. Drewes, M. Koschorreck, D. Pertot, F. Brennecke, and M. Köhl, 2016, Phys. Rev. Lett. **116**, 175301.

Collura, M., A. De Luca, and J. Viti, 2018, Phys. Rev. B **97**, 081111.
Collura, M., and D. Karevski, 2014, Phys. Rev. B **89**, 214308.
Collura, M., A. D. Luca, P. Calabrese, and J. Dubail, 2020, Phys. Rev. B **102**, 180409.
Collura, M., and G. Martelloni, 2014, J. Stat. Mech. P08006.
Cui, J., J. I. Cirac, and M. C. Bañuls, 2015, Phys. Rev. Lett. **114**, 220601.
Dabelow, L., and P. Reimann, 2021, J. Stat. Mech. 013106.
Dagotto, E., 1994, Rev. Mod. Phys. **66**, 763.
D'Alessio, L., Y. Kafri, A. Polkovnikov, and M. Rigol, 2016, Adv. Phys. **65**, 239.
Daley, A., C. Kollath, U. Schollwöck, and G. Vidal, 2004, J. Stat. Mech. P04005.
Daley, A. J., 2014, Adv. Phys. **63**, 77.
Damle, K., and S. Sachdev, 1998, Phys. Rev. B **57**, 8307.
Damle, K., and S. Sachdev, 2005, Phys. Rev. Lett. **95**, 187201.
Das, A., M. Kulkarni, H. Spohn, and A. Dhar, 2019, Phys. Rev. E **100**, 042116.
Dauxois, T., 2008, Phys. Today **61**, No. 1, 55.
Davies, E. B., 1974, Commun. Math. Phys. **39**, 91.
De Luca, A., M. Collura, and J. De Nardis, 2017, Phys. Rev. B **96**, 020403.
De Luca, A., G. Martelloni, and J. Viti, 2015, Phys. Rev. A **91**, 021603.
De Luca, A., J. Viti, D. Bernard, and B. Doyon, 2013, Phys. Rev. B **88**, 134301.
De Luca, A., J. Viti, L. Mazza, and D. Rossini, 2014, Phys. Rev. B **90**, 161101.
De Nardis, J., D. Bernard, and B. Doyon, 2018, Phys. Rev. Lett. **121**, 160603.
De Nardis, J., D. Bernard, and B. Doyon, 2019, SciPost Phys. **6**, 49.
De Nardis, J., S. Gopalakrishnan, E. Ilievski, and R. Vasseur, 2020, Phys. Rev. Lett. **125**, 070601.
De Nardis, J., M. Medenjak, C. Karrasch, and E. Ilievski, 2019, Phys. Rev. Lett. **123**, 186601.
De Nardis, J., M. Medenjak, C. Karrasch, and E. Ilievski, 2020, Phys. Rev. Lett. **124**, 210605.
De Raedt, H., and P. De Vries, 1989, Z. Phys. B **77**, 243.
Derrida, B., 2007, J. Stat. Mech. P07023.
Deutsch, J. M., 1991, Phys. Rev. A **43**, 2046.
De Vries, P., and H. De Raedt, 1993, Phys. Rev. B **47**, 7929.
Dhar, A., 2008, Adv. Phys. **57**, 457.
Dhar, A., A. Kundu, and A. Kundu, 2019, Front. Phys. **7**, 159.
Dobrovitski, V. V., and H. A. De Raedt, 2003, Phys. Rev. E **67**, 056702.
Dorfman, J. R., 1999, *An Introduction to Chaos in Nonequilibrium Statistical Mechanics* (Cambridge University Press, Cambridge, England).
Dorfner, F., L. Vidmar, C. Brockt, E. Jeckelmann, and F. Heidrich-Meisner, 2015, Phys. Rev. B **91**, 104302.
Doyon, B., 2015, Nucl. Phys. **B892**, 190.
Doyon, B., 2018, SciPost Phys. **5**, 54.
Doyon, B., 2019a, arXiv:1912.01551.
Doyon, B., 2019b, J. Math. Phys. (N.Y.) **60**, 073302.
Doyon, B., 2020, SciPost Phys. Lect. Notes **18**.
Doyon, B., J. Dubail, R. Konik, and T. Yoshimura, 2017, Phys. Rev. Lett. **119**, 195301.
Doyon, B., A. Lucas, K. Schalm, and M. J. Bhaseen, 2015, J. Phys. A **48**, 095002.
Doyon, B., and H. Spohn, 2017, SciPost Phys. **3**, 039.
Doyon, B., H. Spohn, and T. Yoshimura, 2018, Nucl. Phys. **B926**, 570.
Doyon, B., and T. Yoshimura, 2017, SciPost Phys. **2**, 014.
Doyon, B., T. Yoshimura, and J.-S. Caux, 2018, Phys. Rev. Lett. **120**, 045301.
Dubail, J., J.-M. Stéphan, J. Viti, and P. Calabrese, 2017, SciPost Phys. **2**, 002.
Dupont, M., and J. E. Moore, 2020, Phys. Rev. B **101**, 121106.
Dyre, J. C., P. Maass, B. Roling, and D. L. Sidebottom, 2009, Rep. Prog. Phys. **72**, 046501.
Dzhioev, A. A., and D. S. Kosov, 2011, J. Chem. Phys. **135**, 174111.
Edge, G. J. A., R. Anderson, D. Jervis, D. C. McKay, R. Day, S. Trotzky, and J. H. Thywissen, 2015, Phys. Rev. A **92**, 063406.
Einhellinger, M., A. Cojuhovschi, and E. Jeckelmann, 2012, Phys. Rev. B **85**, 235141.
Eisert, J., M. Cramer, and M. B. Plenio, 2010, Rev. Mod. Phys. **82**, 277.
Eisert, J., M. Friesdorf, and C. Gogolin, 2015, Nat. Phys. **11**, 124.
Eisler, V., F. Maislinger, and H. G. Evertz, 2016, SciPost Phys. **1**, 014.
Eisler, V., and Z. Rácz, 2013, Phys. Rev. Lett. **110**, 060602.
Eisler, V., and Z. Zimborás, 2014, New J. Phys. **16**, 123020.
Elsayed, T. A., and B. V. Fine, 2013, Phys. Rev. Lett. **110**, 070404.
Endo, H., C. Hotta, and A. Shimizu, 2018, Phys. Rev. Lett. **121**, 220601.
Essler, F., and M. Fagotti, 2016, J. Stat. Mech. 064002.
Essler, F., H. Frahm, F. Göhmann, A. Klümper, and V. E. Korepin, 2005, *The One-Dimensional Hubbard Model* (Cambridge University Press, Cambridge, England).
Essler, F. H. L., S. Kehrein, S. R. Manmana, and N. J. Robinson, 2014, Phys. Rev. B **89**, 165104.
Essler, F. H. L., and R. M. Konik, 2005, *From Fields to Strings: Circumnavigating Theoretical Physics* (World Scientific, Singapore).
Essler, F. H. L., V. E. Korepin, and K. Schoutens, 1991, Phys. Rev. Lett. **67**, 3848.
Evans, D. E., 1977, Commun. Math. Phys. **54**, 293.
Evertz, H. G., G. Lana, and M. Marcu, 1993, Phys. Rev. Lett. **70**, 875.
Fabricius, K., U. Löw, and J. Stolze, 1997, Phys. Rev. B **55**, 5833.
Fabricius, K., and B. M. McCoy, 1998, Phys. Rev. B **57**, 8340.
Faddeev, L., 2016, in *Fifty Years of Mathematical Physics: Selected Works of Ludwig Faddeev*, edited by M. Ge and A. Niemi, World Scientific Series in 21st Century Mathematics Vol. 2 (World Scientific, Singapore), pp. 370–439.
Fagotti, M., 2017a, J. Phys. A **50**, 034005.
Fagotti, M., 2017b, Phys. Rev. B **96**, 220302.
Fagotti, M., 2020, SciPost Phys. **8**, 48.
Fava, M., B. Ware, S. Gopalakrishnan, R. Vasseur, and S. A. Parameswaran, 2020, Phys. Rev. B **102**, 115121.
Feiguin, A. E., and S. R. White, 2005, Phys. Rev. B **72**, 220401.
Feldmeier, J., P. Sala, G. de Tomasi, F. Pollmann, and M. Knap, 2020, Phys. Rev. Lett. **125**, 245303.
Fermi, E., J. Pasta, and S. M. Ulam, 1955, Los Alamos Scientific Laboratory Technical Report No. LA-1940.
Fishman, M., S. R. White, and E. M. Stoudenmire, 2020, arXiv:2007.14822.
Forster, D., 1990, *Hydrodynamic Fluctuations, Broken Symmetry, and Correlation Functions* (Taylor & Francis, London).
Foster, M. S., T. C. Berkelbach, D. R. Reichman, and E. A. Yuzbashyan, 2011, Phys. Rev. B **84**, 085146.
Foster, M. S., E. A. Yuzbashyan, and B. L. Altshuler, 2010, Phys. Rev. Lett. **105**, 135701.
Fourier, J.-B. J., 1822, *Théorie Analytique de la Chaleur* (F. Didot, Paris).
Friedman, A. J., S. Gopalakrishnan, and R. Vasseur, 2020, Phys. Rev. B **101**, 180302.
Frigerio, A., 1977, Lett. Math. Phys. **2**, 79.
Fujimoto, S., and N. Kawakami, 1998, J. Phys. A **31**, 465.

Fujimoto, S., and N. Kawakami, 2003, Phys. Rev. Lett. **90**, 197202.
Fukuhara, T., P. Schauß, M. Endres, S. Hild, M. Cheneau, I. Bloch, and C. Gross, 2013, Nature (London) **502**, 76.
Fukuhara, T., *et al.*, 2013, Nat. Phys. **9**, 235.
Ganahl, M., E. Rabel, F. H. L. Essler, and H. G. Evertz, 2012, Phys. Rev. Lett. **108**, 077206.
Gangadharaiah, S., A. L. Chernyshev, and W. Brenig, 2010, Phys. Rev. B **82**, 134421.
Gardiner, C., and P. Zoller, 1991, *Quantum Noise* (Springer, Berlin).
Garst, M., and A. Rosch, 2001, Europhys. Lett. **55**, 66.
Gaudin, M., 1967, Phys. Lett. **24A**, 55.
Gaudin, M., 1971, Phys. Rev. Lett. **26**, 1301.
Gemmer, J., and G. Mahler, 2003, Eur. Phys. J. B **31**, 249.
Gemmer, J., R. Steinigeweg, and M. Michel, 2006, Phys. Rev. B **73**, 104302.
Giamarchi, T., 1991, Phys. Rev. B **44**, 2905.
Giamarchi, T., 1992, Phys. Rev. B **46**, 342.
Giamarchi, T., 2004, *Quantum Physics in One Dimension* (Clarendon Press, Oxford).
Giamarchi, T., and H. J. Schulz, 1988, Phys. Rev. B **37**, 325.
Glorioso, P., L. V. Delacretaz, X. Chen, R. M. Nandkishore, and A. Lucas, 2021, SciPost Phys. **10**, 015.
Gobert, D., C. Kollath, U. Schollwöck, and G. Schütz, 2005, Phys. Rev. E **71**, 036102.
Gogolin, C., and J. Eisert, 2016, Rep. Prog. Phys. **79**, 056001.
Goldstein, S., J. L. Lebowitz, R. Tumulka, and N. Zanghì, 2006, Phys. Rev. Lett. **96**, 050403.
Gopalakrishnan, S., D. A. Huse, V. Khemani, and R. Vasseur, 2018, Phys. Rev. B **98**, 220303.
Gopalakrishnan, S., and S. A. Parameswaran, 2020, Phys. Rep. **862**, 1.
Gopalakrishnan, S., and R. Vasseur, 2019, Phys. Rev. Lett. **122**, 127202.
Gopalakrishnan, S., R. Vasseur, and B. Ware, 2019, Proc. Natl. Acad. Sci. U.S.A. **116**, 16250.
Gorini, V., A. Kossakowski, and E. C. G. Sudarshan, 1976, J. Math. Phys. (N.Y.) **17**, 821.
Grabowski, M. P., and P. Mathieu, 1995, Ann. Phys. (N.Y.) **243**, 299.
Green, M. S., 1952, J. Chem. Phys. **20**, 1281.
Green, M. S., 1954, J. Chem. Phys. **22**, 398.
Greif, D., M. F. Parsons, A. Mazurenko, C. S. Chiu, S. Blatt, F. Huber, G. Ji, and M. Greiner, 2016, Science **351**, 953.
Gross, C., and I. Bloch, 2017, Science **357**, 995.
Grossjohann, S., and W. Brenig, 2010, Phys. Rev. B **81**, 012404.
Gruber, M., and V. Eisler, 2019, Phys. Rev. B **99**, 174403.
Guan, X.-W., M. T. Batchelor, and C. Lee, 2013, Rev. Mod. Phys. **85**, 1633.
Guardado-Sanchez, E., A. Morningstar, B. M. Spar, P. T. Brown, D. A. Huse, and W. S. Bakr, 2020, Phys. Rev. X **10**, 011042.
Guimarães, P. H., G. T. Landi, and M. J. de Oliveira, 2016, Phys. Rev. E **94**, 032139.
Guo, C., A. Weichselbaum, J. von Delft, and M. Vojta, 2012, Phys. Rev. Lett. **108**, 160401.
Gutzwiller, M. C., 1990, *Chaos in Classical and Quantum Mechanics* (Springer, New York).
Haegeman, J., J. I. Cirac, T. J. Osborne, I. Pižorn, H. Verschelde, and F. Verstraete, 2011, Phys. Rev. Lett. **107**, 070601.
Hagemans, R. L., 2007, Ph.D. thesis (University of Amsterdam).
Haller, E., J. Hudson, A. Kelly, D. Cotta, B. Peaudecerf, G. Bruce, and S. Kuhr, 2015, Nat. Phys. **11**, 738.
Hams, A., and H. De Raedt, 2000, Phys. Rev. E **62**, 4365.
Hart, R. A., P. M. Duarte, T.-L. Yang, X. Liu, T. Paiva, E. Khatami, R. T. Scalettar, N. Trivedi, D. A. Huse, and R. G. Hulet, 2015, Nature (London) **519**, 211.
Hartmann, M., G. Mahler, and O. Hess, 2004, Phys. Rev. Lett. **93**, 080402.
Hauschild, J., E. Leviatan, J. H. Bardarson, E. Altman, M. P. Zaletel, and F. Pollmann, 2018, Phys. Rev. B **98**, 235163.
Hauschild, J., F. Pollmann, and F. Heidrich-Meisner, 2015, Phys. Rev. A **92**, 053629.
Heidarian, D., and S. Sorella, 2007, Phys. Rev. B **75**, 241104(R).
Heidrich-Meisner, F., I. González, K. A. Al-Hassanieh, A. E. Feiguin, M. J. Rozenberg, and E. Dagotto, 2010, Phys. Rev. B **82**, 205110.
Heidrich-Meisner, F., A. Honecker, and W. Brenig, 2005, Phys. Rev. B **71**, 184415.
Heidrich-Meisner, F., A. Honecker, and W. Brenig, 2007, Eur. Phys. J. Special Topics **151**, 135.
Heidrich-Meisner, F., A. Honecker, D. C. Cabra, and W. Brenig, 2002, Phys. Rev. B **66**, 140406.
Heidrich-Meisner, F., A. Honecker, D. C. Cabra, and W. Brenig, 2003, Phys. Rev. B **68**, 134436.
Heidrich-Meisner, F., A. Honecker, D. C. Cabra, and W. Brenig, 2004a, J. Magn. Magn. Mater. **272–276**, 890.
Heidrich-Meisner, F., A. Honecker, D. C. Cabra, and W. Brenig, 2004b, Phys. Rev. Lett. **92**, 069703.
Heidrich-Meisner, F., A. Honecker, D. C. Cabra, and W. Brenig, 2005, Physica (Amsterdam) **359B–361B**, 1394.
Heidrich-Meisner, F., A. Honecker, and T. Vekua, 2006, Phys. Rev. B **74**, 020403.
Heitmann, T., J. Richter, T. Dahm, and R. Steinigeweg, 2020, Phys. Rev. B **102**, 045137.
Herbrych, J., P. Prelovšek, and X. Zotos, 2011, Phys. Rev. B **84**, 155125.
Herbrych, J., R. Steinigeweg, and P. Prelovšek, 2012, Phys. Rev. B **86**, 115106.
Hess, C., 2007, Eur. Phys. J. Special Topics **151**, 73.
Hess, C., 2019, Phys. Rep. **811**, 1.
Hess, C., C. Baumann, U. Ammerahl, B. Büchner, F. Heidrich-Meisner, W. Brenig, and A. Revcolevschi, 2001, Phys. Rev. B **64**, 184305.
Hess, C., B. Büchner, U. Ammerahl, L. Colonescu, F. Heidrich-Meisner, W. Brenig, and A. Revcolevschi, 2003, Phys. Rev. Lett. **90**, 197002.
Hess, C., H. ElHaes, A. Waske, B. Büchner, C. Sekar, G. Krabbes, F. Heidrich-Meisner, and W. Brenig, 2007, Phys. Rev. Lett. **98**, 027201.
Hild, S., T. Fukuhara, P. Schauß, J. Zeiher, M. Knap, E. Demler, I. Bloch, and C. Gross, 2014, Phys. Rev. Lett. **113**, 147205.
Hilker, T. A., G. Salomon, F. Grusdt, A. Omran, M. Boll, E. Demler, I. Bloch, and C. Gross, 2017, Science **357**, 484.
Hirobe, D., M. Sato, T. Kawamata, Y. Shiomi, K.-i. Uchida, R. Iguchi, Y. Koike, S. Maekawa, and E. Saitoh, 2017, Nat. Phys. **13**, 30.
Hlubek, N., P. Ribeiro, R. Saint-Martin, A. Revcolevschi, G. Roth, G. Behr, B. Büchner, and C. Hess, 2010, Phys. Rev. B **81**, 020405.
Hlubek, N., X. Zotos, S. Singh, R. Saint-Martin, A. Revcolevschi, B. Büchner, and C. Hess, 2012, J. Stat. Mech. P03006.
Hlubek, N., *et al.*, 2011, Phys. Rev. B **84**, 214419.
Hofferberth, S., I. Lesanovsky, B. Fisher, T. Schumm, and J. Schmiedmayer, 2007, Nature (London) **449**, 324.
Hofmann, M., T. Lorenz, K. Berggold, M. Grüninger, A. Freimuth, G. S. Uhrig, and E. Brück, 2003, Phys. Rev. B **67**, 184502.
Hohensee, G. T., R. B. Wilson, J. P. Feser, and D. G. Cahill, 2014, Phys. Rev. B **89**, 024422.
Holzner, A., A. Weichselbaum, I. P. McCulloch, U. Schollwöck, and J. von Delft, 2011, Phys. Rev. B **83**, 195115.

Huang, Y., C. Karrasch, and J. E. Moore, 2013, Phys. Rev. B **88**, 115126.
Huber, D., 2012, Physica (Amsterdam) **407B**, 4274.
Huber, D. L., and J. S. Semura, 1969, Phys. Rev. **182**, 602.
Huddart, B. M., M. Gomilsek, T. J. Hicken, F. L. Pratt, S. J. Blundell, P. A. Goddard, S. J. Kaech, J. L. Manson, and T. Lancaster, 2021, Phys. Rev. B **103**, L060405.
Iitaka, T., and T. Ebisuzaki, 2003, Phys. Rev. Lett. **90**, 047203.
Iitaka, T., and T. Ebisuzaki, 2004, Phys. Rev. E **69**, 057701.
Ilievski, E., 2017, SciPost Phys. **3**, 031.
Ilievski, E., and J. De Nardis, 2017a, Phys. Rev. B **96**, 081118.
Ilievski, E., and J. De Nardis, 2017b, Phys. Rev. Lett. **119**, 020602.
Ilievski, E., J. De Nardis, M. Medenjak, and T. Prosen, 2018, Phys. Rev. Lett. **121**, 230602.
Ilievski, E., M. Medenjak, and T. Prosen, 2015, Phys. Rev. Lett. **115**, 120601.
Ilievski, E., M. Medenjak, T. Prosen, and L. Zadnik, 2016, J. Stat. Mech. 064008.
Ilievski, E., J. D. Nardis, S. Gopalakrishnan, R. Vasseur, and B. Ware, 2020, arXiv:2009.08425.
Ilievski, E., and T. Prosen, 2013, Commun. Math. Phys. **318**, 809.
Ilievski, E., E. Quinn, J. De Nardis, and M. Brockmann, 2016, J. Stat. Mech. 063101.
Imambekov, A., T. L. Schmidt, and L. I. Glazman, 2012, Rev. Mod. Phys. **84**, 1253.
Jaklič, J., and P. Prelovšek, 1994, Phys. Rev. B **49**, 5065.
Jaklič, J., and P. Prelovšek, 2000, Adv. Phys. **49**, 1.
Jansen, D., J. Bonča, and F. Heidrich-Meisner, 2020, Phys. Rev. B **102**, 165155.
Jepsen, N., J. Amato-Grill, I. Dimitrova, W. W. Ho, E. Demler, and W. Ketterle, 2020, Nature (London) **588**, 403.
Jesenko, S., and M. Žnidarič, 2011, Phys. Rev. B **84**, 174438.
Jin, F., R. Steinigeweg, F. Heidrich-Meisner, K. Michielsen, and H. De Raedt, 2015, Phys. Rev. B **92**, 205103.
Jin, R., Y. Onose, Y. Tokura, D. Mandrus, P. Dai, and B. C. Sales, 2003, Phys. Rev. Lett. **91**, 146601.
Jin, T., M. Filippone, and T. Giamarchi, 2020, Phys. Rev. B **102**, 205131.
Johansson, J., P. Nation, and F. Nori, 2012, Comput. Phys. Commun. **183**, 1760.
Jördens, R., N. Strohmaier, K. Günter, H. Moritz, and T. Esslinger, 2008, Nature (London) **455**, 204.
Jung, P., R. W. Helmes, and A. Rosch, 2006, Phys. Rev. Lett. **96**, 067202.
Jung, P., and A. Rosch, 2007, Phys. Rev. B **76**, 245108.
Kadanoff, L. P., and P. C. Martin, 1963, Ann. Phys. (N.Y.) **24**, 419.
Kamiya, N., and S. Takesue, 2013, J. Phys. Soc. Jpn. **82**, 114002.
Karadamoglou, J., and X. Zotos, 2004, Phys. Rev. Lett. **93**, 177203.
Karahalios, A., A. Metavitsiadis, X. Zotos, A. Gorczyca, and P. Prelovšek, 2009, Phys. Rev. B **79**, 024425.
Kardar, M., G. Parisi, and Y.-C. Zhang, 1986, Phys. Rev. Lett. **56**, 889.
Karevski, D., and T. Platini, 2009, Phys. Rev. Lett. **102**, 207207.
Karevski, D., V. Popkov, and G. M. Schütz, 2013, Phys. Rev. Lett. **110**, 047201.
Karevski, D., and G. Schütz, 2019, SciPost Phys. **6**, 068.
Karrasch, C., 2017a, New J. Phys. **19**, 033027.
Karrasch, C., 2017b, Phys. Rev. B **95**, 115148.
Karrasch, C., J. Bardarson, and J. Moore, 2012, Phys. Rev. Lett. **108**, 227206.
Karrasch, C., J. H. Bardarson, and J. E. Moore, 2013, New J. Phys. **15**, 083031.
Karrasch, C., J. Hauschild, S. Langer, and F. Heidrich-Meisner, 2013, Phys. Rev. B **87**, 245128.
Karrasch, C., R. Ilan, and J. E. Moore, 2013, Phys. Rev. B **88**, 195129.
Karrasch, C., D. M. Kennes, and F. Heidrich-Meisner, 2015, Phys. Rev. B **91**, 115130.
Karrasch, C., D. M. Kennes, and F. Heidrich-Meisner, 2016, Phys. Rev. Lett. **117**, 116401.
Karrasch, C., D. M. Kennes, and J. E. Moore, 2014, Phys. Rev. B **90**, 155104.
Karrasch, C., J. E. Moore, and F. Heidrich-Meisner, 2014, Phys. Rev. B **89**, 075139.
Karrasch, C., R. G. Pereira, and J. Sirker, 2015, New J. Phys. **17**, 103003.
Karrasch, C., T. Prosen, and F. Heidrich-Meisner, 2017, Phys. Rev. B **95**, 060406.
Katzer, M., W. Knorr, R. Finsterhölzl, and A. Carmele, 2020, Phys. Rev. B **102**, 125101.
Kaufman, A. M., M. E. Tai, A. Lukin, M. Rispoli, R. Schittko, P. M. Preiss, and M. Greiner, 2016, Science **353**, 794.
Kaur, G., and P. Cappellaro, 2012, New J. Phys. **14**, 083005.
Kawamata, T., N. Takahashi, T. Adachi, T. Noji, K. Kudo, N. Kobayashi, and Y. Koike, 2008, J. Phys. Soc. Jpn. **77**, 034607.
Kennes, D., and C. Karrasch, 2016, Comput. Phys. Commun. **200**, 37.
Khajetoorians, A. A., *et al.*, 2013, Science **339**, 55.
Khemani, V., A. Vishwanath, and D. A. Huse, 2018, Phys. Rev. X **8**, 031057.
Kim, H., and D. A. Huse, 2013, Phys. Rev. Lett. **111**, 127205.
Kinoshita, T., T. Wenger, and D. S. Weiss, 2004, Science **305**, 1125.
Kinoshita, T., T. Wenger, and D. S. Weiss, 2006, Nature (London) **440**, 900.
Kirchner, S., H. G. Evertz, and W. Hanke, 1999, Phys. Rev. B **59**, 1825.
Kirillov, A. N., 1984, Zap. Nauchn. Semin. LOMI **131**, 88.
Kirillov, A. N., and N. A. Liskova, 1997, J. Phys. A **30**, 1209.
Kirino, S., and K. Ueda, 2010, J. Phys. Soc. Jpn. **79**, 093710.
Klauser, A., J. Mossel, J.-S. Caux, and J. van den Brink, 2011, Phys. Rev. Lett. **106**, 157205.
Kliesch, M., C. Gogolin, M. J. Kastoryano, A. Riera, and J. Eisert, 2014, Phys. Rev. X **4**, 031019.
Kloss, B., Y. B. Lev, and D. Reichman, 2018, Phys. Rev. B **97**, 024307.
Kloss, B., D. R. Reichman, and R. Tempelaar, 2019, Phys. Rev. Lett. **123**, 126601.
Klümper, A., 1992, Ann. Phys. (N.Y.) **504**, 540.
Klümper, A., 1993, Z. Phys. B **91**, 507.
Klümper, A., and D. C. Johnston, 2000, Phys. Rev. Lett. **84**, 4701.
Klümper, A., and K. Sakai, 2002, J. Phys. A **35**, 2173.
Klümper, A., and K. Sakai, 2019, arXiv:1904.11253.
Knap, M., W. von der Linden, and E. Arrigoni, 2011, Phys. Rev. B **84**, 115145.
Köhler, T., J. Stolpp, and S. Paeckel, 2021, SciPost Phys. **10**, 058.
Kohn, W., 1964, Phys. Rev. **133**, A171.
Kollar, M., F. A. Wolf, and M. Eckstein, 2011, Phys. Rev. B **84**, 054304.
Korepin, V. E., N. M. Bogoliubov, and A. G. Izergin, 2005, *Quantum Inverse Scattering Method and Correlation Functions* (Cambridge University Press, Cambridge, England).
Kormos, M., 2017, SciPost Phys. **3**, 020.
Krajnik, Z., E. Ilievski, and T. Prosen, 2020, SciPost Phys. **9**, 38.
Krajnik, Z., and T. Prosen, 2020, J. Stat. Phys. **179**, 110.
Krinner, S., T. Esslinger, and J.-P. Brantut, 2017, J. Phys. Condens. Matter **29**, 343003.
Kubo, R., 1957, J. Phys. Soc. Jpn. **12**, 570.
Kubo, R., M. Toda, and N. Hashitsume, 1991, *Statistical Physics II* (Springer, Berlin).

Kühne, H., H.-H. Klauss, S. Grossjohann, W. Brenig, F. J. Litterst, A. P. Reyes, P. L. Kuhns, M. M. Turnbull, and C. P. Landee, 2009, Phys. Rev. B **80**, 045110.
Kundu, A., A. Dhar, and O. Narayan, 2009, J. Stat. Mech. L03001.
Kuniba, A., K. Sakai, and J. Suzuki, 1998, Nucl. Phys. **B525**, 597.
Lan, Z., M. van Horssen, S. Powell, and J. P. Garrahan, 2018, Phys. Rev. Lett. **121**, 040603.
Lancaster, J., E. Gull, and A. Mitra, 2010, Phys. Rev. B **82**, 235124.
Lancaster, J., and A. Mitra, 2010, Phys. Rev. E **81**, 061134.
Landi, G. T., E. Novais, M. J. de Oliveira, and D. Karevski, 2014, Phys. Rev. E **90**, 042142.
Lange, F., S. Ejima, and H. Fehske, 2018, Phys. Rev. B **97**, 060403.
Lange, F., S. Ejima, and H. Fehske, 2019, Europhys. Lett. **125**, 17001.
Lange, F., Z. Lenarčič, and A. Rosch, 2018, Phys. Rev. B **97**, 165138.
Langen, T., S. Erne, R. Geiger, B. Rauer, T. Schweigler, M. Kuhnert, W. Rohringer, I. E. Mazets, T. Gasenzer, and J. Schmiedmayer, 2015, Science **348**, 207.
Langer, S., R. Darradi, F. Heidrich-Meisner, and W. Brenig, 2010, Phys. Rev. B **82**, 104424.
Langer, S., F. Heidrich-Meisner, J. Gemmer, I. McCulloch, and U. Schollwöck, 2009, Phys. Rev. B **79**, 214409.
Langer, S., M. Heyl, I. P. McCulloch, and F. Heidrich-Meisner, 2011, Phys. Rev. B **84**, 205115.
Lenarčič, Z., E. Altman, and A. Rosch, 2018, Phys. Rev. Lett. **121**, 267603.
Lenarčič, Z., F. Lange, and A. Rosch, 2018, Phys. Rev. B **97**, 024302.
Lepri, S., R. Livi, and A. Politi, 2003, Phys. Rep. **377**, 1.
Leviatan, E., F. Pollmann, J. H. Bardarson, and E. Altman, 2017, arXiv:1702.08894.
Li, B., and J. Wang, 2003, Phys. Rev. Lett. **91**, 044301.
Liao, Y.-A., A. S. C. Rittner, T. Paprotta, W. Li, G. B. Partridge, R. G. Hulet, S. K. Baur, and E. J. Mueller, 2010, Nature (London) **467**, 567.
Lieb, E. H., and W. Liniger, 1963, Phys. Rev. **130**, 1605.
Lieb, E. H., and D. Robinson, 1972, Commun. Math. Phys. **28**, 251.
Lieb, E. H., and F. Y. Wu, 1968, Phys. Rev. Lett. **20**, 1445.
Lindblad, G., 1976, Commun. Math. Phys. **48**, 119.
Liu, W., and N. Andrei, 2014, Phys. Rev. Lett. **112**, 257204.
Ljubotina, M., L. Zadnik, and T. Prosen, 2019, Phys. Rev. Lett. **122**, 150605.
Ljubotina, M., M. Žnidarič, and T. Prosen, 2017, Nat. Commun. **8**, 16117.
Ljubotina, M., M. Žnidarič, and T. Prosen, 2019, Phys. Rev. Lett. **122**, 210602.
Long, M. W., P. Prelovšek, S. ElShawish, J. Karadamoglou, and X. Zotos, 2003, Phys. Rev. B **68**, 235106.
Lopez-Piqueres, J., B. Ware, S. Gopalakrishnan, and R. Vasseur, 2021, Phys. Rev. B **103**, L060302.
Louis, K., and C. Gros, 2003, Phys. Rev. B **67**, 224410.
Louis, K., P. Prelovšek, and X. Zotos, 2006, Phys. Rev. B **74**, 235118.
Louis, K., and X. Zotos, 2005, Phys. Rev. B **72**, 214415.
Luitz, D. J., and Y. B. Lev, 2017, Ann. Phys. (Amsterdam) **529**, 1600350.
Lukyanov, S., 1998, Nucl. Phys. **B522**, 533.
Luttinger, J. M., 1964, Phys. Rev. **135**, A1505.
Lux, J., J. Müller, A. Mitra, and A. Rosch, 2014, Phys. Rev. A **89**, 053608.
Maass, P., J. Petersen, A. Bunde, W. Dieterich, and H. E. Roman, 1991, Phys. Rev. Lett. **66**, 52.
Maeter, H., A. A. Zvyagin, H. Luetkens, G. Pascua, Z. Shermadini, R. Saint-Martin, A. Revcolevschi, C. Hess, B. Büchner, and H.-H. Klauss, 2013, J. Phys. Condens. Matter **25**, 365601.
Mahan, G. D., 1990, *Many-Particle Physics* (Plenum Press, New York).
Mallayya, K., M. Rigol, and W. De Roeck, 2019, Phys. Rev. X **9**, 021027.
Malvania, N., Y. Zhang, Y. Le, J. Dubail, M. Rigol, and D. S. Weiss, 2020, arXiv:2009.06651.
Marro, J., and R. Dickman, 1999, *Nonequilibirum Phase Transitions in Lattice Models* (Cambridge University Press, Cambridge, England).
Mastropietro, V., 2013, Phys. Rev. E **87**, 042121.
Matsui, C., 2020, J. Phys. A **53**, 134001.
Mazur, P., 1969, Physica (Amsterdam) **43**, 533.
Mazurenko, A., C. S. Chiu, G. Ji, M. F. Parsons, M. Kanasz-Nagy, R. Schmidt, F. Grusdt, E. Demler, D. Greif, and M. Greiner, 2017, Nature (London) **545**, 462.
Mazza, L., J. Viti, M. Carrega, D. Rossini, and A. De Luca, 2018, Phys. Rev. B **98**, 075421.
Medenjak, M., and J. De Nardis, 2020, Phys. Rev. B **101**, 081411.
Medenjak, M., J. De Nardis, and T. Yoshimura, 2020, SciPost Phys. **9**, 075.
Medenjak, M., C. Karrasch, and T. Prosen, 2017, Phys. Rev. Lett. **119**, 080602.
Mejia-Monasterio, C., T. Prosen, and G. Casati, 2005, Europhys. Lett. **72**, 520.
Mejia-Monasterio, C., and H. Wichterich, 2007, Eur. Phys. J. Special Topics **151**, 113.
Mendoza-Arenas, J. J., S. Al-Assam, S. R. Clark, and D. Jaksch, 2013, J. Stat. Mech. P07007.
Mendoza-Arenas, J. J., S. R. Clark, and D. Jaksch, 2015, Phys. Rev. E **91**, 042129.
Mendoza-Arenas, J. J., T. Grujic, D. Jaksch, and S. R. Clark, 2013, Phys. Rev. B **87**, 235130.
Mestyán, M., and V. Alba, 2020, SciPost Phys. **8**, 55.
Mestyán, M., B. Bertini, L. Piroli, and P. Calabrese, 2019, Phys. Rev. B **99**, 014305.
Metavitsiadis, A., 2011, Phys. Rev. B **83**, 054409.
Metavitsiadis, A., and W. Brenig, 2017, Phys. Rev. B **96**, 041115.
Metavitsiadis, A., C. Psaroudaki, and W. Brenig, 2019, Phys. Rev. B **99**, 205129.
Metavitsiadis, A., X. Zotos, O. S. Barišić, and P. Prelovšek, 2010, Phys. Rev. B **81**, 205101.
Michailidis, A. A., M. Žnidarič, M. Medvedyeva, D. A. Abanin, T. Prosen, and Z. Papić, 2018, Phys. Rev. B **97**, 104307.
Michel, M., J. Gemmer, and G. Mahler, 2004, Eur. Phys. J. B **42**, 555.
Michel, M., M. Hartmann, J. Gemmer, and G. Mahler, 2003, Eur. Phys. J. B **34**, 325.
Michel, M., O. Hess, H. Wichterich, and J. Gemmer, 2008, Phys. Rev. B **77**, 104303.
Michel, M., G. Mahler, and J. Gemmer, 2005, Phys. Rev. Lett. **95**, 180602.
Micheli, A., A. J. Daley, D. Jaksch, and P. Zoller, 2004, Phys. Rev. Lett. **93**, 140408.
Mierzejewski, M., J. Bonča, and P. Prelovšek, 2011, Phys. Rev. Lett. **107**, 126601.
Mierzejewski, M., P. Prelovšek, and T. Prosen, 2014, Phys. Rev. Lett. **113**, 020602.
Mierzejewski, M., P. Prelovšek, and T. Prosen, 2015, Phys. Rev. Lett. **114**, 140601.
Milnor, J. W., 1965, *Topology from the Differentiable Viewpoint* (University Press of Virginia, Charlottesville).
Misguich, G., K. Mallick, and P. L. Krapivsky, 2017, Phys. Rev. B **96**, 195151.
Moca, C. P., M. Kormos, and G. Zaránd, 2017, Phys. Rev. Lett. **119**, 100603.

Moeckel, M., and S. Kehrein, 2008, Phys. Rev. Lett. **100**, 175702.
Mohan, A., N. S. Beesetty, N. Hlubek, R. Saint-Martin, A. Revcolevschi, B. Büchner, and C. Hess, 2014, Phys. Rev. B **89**, 104302.
Møller, F. S., and J. Schmiedmayer, 2020, SciPost Phys. **8**, 041.
Monnai, T., and A. Sugita, 2014, J. Phys. Soc. Jpn. **83**, 094001.
Montagnese, M., *et al.*, 2013, Phys. Rev. Lett. **110**, 147206.
Mori, H., 1965, Prog. Theor. Phys. **33**, 423.
Mossel, J., G. Palacios, and J.-S. Caux, 2010, J. Stat. Mech. L09001.
Moudgalya, S., N. Regnault, and B. A. Bernevig, 2018, Phys. Rev. B **98**, 235156.
Mukerjee, S., V. Oganesyan, and D. Huse, 2006, Phys. Rev. B **73**, 035113.
Mukerjee, S., and B. S. Shastry, 2008, Phys. Rev. B **77**, 245131.
Naef, F., and X. Zotos, 1998, J. Phys. C **10**, L183.
Nahum, A., J. Ruhman, and D. A. Huse, 2018, Phys. Rev. B **98**, 035118.
Nandkishore, R., and D. Huse, 2015, Annu. Rev. Condens. Matter Phys. **6**, 15.
Narasimhan, T., 1999, Rev. Geophys. **37**, 151.
Narozhny, B. N., 1996, Phys. Rev. B **54**, 3311.
Narozhny, B. N., A. J. Millis, and N. Andrei, 1998, Phys. Rev. B **58**, R2921.
Nazarov, Y. V., and Y. M. Blanter, 2009, *Quantum Transport: Introduction to Nanoscience* (Cambridge University Press, Cambridge, England).
Nessi, N., and A. Iucci, 2015, arXiv:1503.02507.
Nichols, M. A., L. W. Cheuk, M. Okan, T. R. Hartke, E. Mendez, T. Senthil, E. Khatami, H. Zhang, and M. W. Zwierlein, 2019, Science **363**, 383.
Niemeijer, T., and H. van Vianen, 1971, Phys. Lett. **34A**, 401.
Nozawa, Y., and H. Tsunetsugu, 2020, Phys. Rev. B **101**, 035121.
Ogata, Y., 2002, Phys. Rev. E **66**, 066123.
Ohno, M., T. Kawamata, M. Akoshima, and Y. Koike, 2019, J. Phys. Soc. Jpn. **88**, 064708.
Okamoto, S., G. Alvarez, E. Dagotto, and T. Tohyama, 2018, Phys. Rev. E **97**, 043308.
Omran, A., M. Boll, T. A. Hilker, K. Kleinlein, G. Salomon, I. Bloch, and C. Gross, 2015, Phys. Rev. Lett. **115**, 263001.
Orbach, R., 1958, Phys. Rev. **112**, 309.
Orignac, E., R. Chitra, and R. Citro, 2003, Phys. Rev. B **67**, 134426.
Otter, M., V. Krasnikov, D. Fishman, M. Pshenichnikov, R. Saint-Martin, A. Revcolevschi, and P. van Loodsrecht, 2009, J. Magn. Magn. Mater. **321**, 796.
Otter, M., *et al.*, 2012, Int. J. Heat Mass Transf. **55**, 2531.
Paeckel, S., T. Köhler, A. Swoboda, S. R. Manmana, U. Schollwöck, and C. Hubig, 2019, Ann. Phys. (N.Y.) **411**, 167998.
Palmero, M., X. Xu, C. Guo, and D. Poletti, 2019, Phys. Rev. E **100**, 022111.
Panda, R. K., A. Scardicchio, M. Schulz, S. R. Taylor, and M. Znidaric, 2019, Europhys. Lett. **128**, 67003.
Paredes, B., A. Widera, V. Murg, O. Mandel, S. Fölling, I. Cirac, G. V. Shlyapnikov, T. W. Hänsch, and I. Bloch, 2004, Nature (London) **429**, 277.
Parsons, M. F., F. Huber, A. Mazurenko, C. S. Chiu, W. Setiawan, K. Wooley-Brown, S. Blatt, and M. Greiner, 2015, Phys. Rev. Lett. **114**, 213002.
Parsons, M. F., A. Mazurenko, C. S. Chiu, G. Ji, D. Greif, and M. Greiner, 2016, Science **353**, 1253.
Pavlis, A., and X. Zotos, 2020, J. Stat. Mech. 013101.
Pereira, R., V. Pasquier, J. Sirker, and I. Affleck, 2014, J. Stat. Mech. P09037.
Peres, N. M. R., P. D. Sacramento, D. K. Campbell, and J. M. P. Carmelo, 1999, Phys. Rev. B **59**, 7382.
Peterson, M. R., S. Mukerjee, B. S. Shastry, and J. O. Haerter, 2007, Phys. Rev. B **76**, 125110.
Pidatella, A., A. Metavitsiadis, and W. Brenig, 2019, Phys. Rev. B **99**, 075141.
Piroli, L., J. De Nardis, M. Collura, B. Bertini, and M. Fagotti, 2017, Phys. Rev. B **96**, 115124.
Piroli, L., and E. Vernier, 2016, J. Stat. Mech. 053106.
Polkovnikov, A., K. Sengupta, A. Silva, and M. Vengalattore, 2011, Rev. Mod. Phys. **83**, 863.
Popescu, S., A. J. Short, and A. Winter, 2006, Nat. Phys. **2**, 754.
Popkov, V., D. Karevski, and G. M. Schütz, 2013, Phys. Rev. E **88**, 062118.
Popkov, V., and R. Livi, 2013, New J. Phys. **15**, 023030.
Pottier, N., 2010, *Nonequilibrium Statistical Physics: Linear Irreversible Processes* (Oxford University Press, Oxford).
Pozsgay, B., 2020, Phys. Rev. Lett. **125**, 070602.
Pratt, F. L., S. J. Blundell, T. Lancaster, C. Baines, and S. Takagi, 2006, Phys. Rev. Lett. **96**, 247203.
Preiss, P. M., R. Ma, M. E. Tai, A. Lukin, M. Rispoli, P. Zupancic, Y. Lahini, R. Islam, and M. Greiner, 2015, Science **347**, 1229.
Prelovšek, P., and J. Bonča, 2013, in *Strongly Correlated Systems: Numerical Methods*, edited by A. Avella and F. Mancini (Springer, Berlin), pp. 1–30.
Prelovšek, P., S. ElShawish, X. Zotos, and M. W. Long, 2004, Phys. Rev. B **70**, 205129.
Prosen, T., 1999, Phys. Rev. E **60**, 3949.
Prosen, T., 2008, New J. Phys. **10**, 043026.
Prosen, T., 2010, J. Stat. Mech. P07020.
Prosen, T., 2011a, Phys. Rev. Lett. **107**, 137201.
Prosen, T., 2011b, Phys. Rev. Lett. **106**, 217206.
Prosen, T., 2014a, Phys. Rev. Lett. **112**, 030603.
Prosen, T., 2014b, Phys. Rev. E **89**, 012142.
Prosen, T., 2014c, Nucl. Phys. **B886**, 1177.
Prosen, T., 2015, J. Phys. A **48**, 373001.
Prosen, T., and E. Ilievski, 2013, Phys. Rev. Lett. **111**, 057203.
Prosen, T., and I. Pižorn, 2007, Phys. Rev. A **76**, 032316.
Prosen, T., and M. Žnidarič, 2007, Phys. Rev. E **75**, 015202.
Prosen, T., and M. Žnidarič, 2009, J. Stat. Mech. P02035.
Prosen, T., and M. Žnidarič, 2012, Phys. Rev. B **86**, 125118.
Prosen, T., and B. Zunkovic, 2010, New J. Phys. **12**, 025016.
Prosen, T., and B. Žunkovič, 2013, Phys. Rev. Lett. **111**, 040602.
Psaroudaki, C., J. Herbrych, J. Karadamoglou, P. Prelovšek, X. Zotos, and N. Papanicolaou, 2014, Phys. Rev. B **89**, 224418.
Psaroudaki, C., and X. Zotos, 2016, J. Stat. Mech. 063103.
Purkayastha, A., A. Dhar, and M. Kulkarni, 2016, Phys. Rev. A **93**, 062114.
Purkayastha, A., S. Sanyal, A. Dhar, and M. Kulkarni, 2018, Phys. Rev. B **97**, 174206.
Rabson, D. A., B. N. Narozhny, and A. J. Millis, 2004, Phys. Rev. B **69**, 054403.
Rakovszky, T., F. Pollmann, and C. W. von Keyserlingk, 2018, Phys. Rev. X **8**, 031058.
Rakovszky, T., C. W. von Keyserlingk, and F. Pollmann, 2020, arXiv:2004.05177.
Ramanathan, C., P. Cappellaro, L. Viola, and D. G. Cory, 2011, New J. Phys. **13**, 103015.
Redfield, A. G., 1965, in *Advances in Magnetic Resonance*, Advances in Magnetic and Optical Resonance Vol. 1, edited by J. S. Waugh (Academic Press, New York), pp. 1–32.
Reichental, I., A. Klempner, Y. Kafri, and D. Podolsky, 2018, Phys. Rev. B **97**, 134301.
Reimann, P., 2007, Phys. Rev. Lett. **99**, 160404.
Reimann, P., and J. Gemmer, 2019, Phys. Rev. E **99**, 012126.

Rezania, H., A. Langari, P. H. M. van Loosdrecht, and X. Zotos, 2014, Eur. Phys. J. B **87**, 173.
Ribeiro, G. A. P., N. Crampé, and A. Klümper, 2010, J. Stat. Mech. P01019.
Richter, J., N. Casper, W. Brenig, and R. Steinigeweg, 2019, Phys. Rev. B **100**, 144423.
Richter, J., F. Jin, H. De Raedt, K. Michielsen, J. Gemmer, and R. Steinigeweg, 2018, Phys. Rev. B **97**, 174430.
Richter, J., F. Jin, L. Knipschild, H. De Raedt, K. Michielsen, J. Gemmer, and R. Steinigeweg, 2020, Phys. Rev. E **101**, 062133.
Richter, J., F. Jin, L. Knipschild, J. Herbrych, H. De Raedt, K. Michielsen, J. Gemmer, and R. Steinigeweg, 2019, Phys. Rev. B **99**, 144422.
Richter, J., M. H. Lamann, C. Bartsch, R. Steinigeweg, and J. Gemmer, 2019, Phys. Rev. E **100**, 032124.
Richter, J., and R. Steinigeweg, 2019, Phys. Rev. B **99**, 094419.
Rigol, M., V. Dunjko, and M. Olshanii, 2008, Nature (London) **452**, 854.
Rigol, M., and A. Muramatsu, 2004, Phys. Rev. Lett. **93**, 230404.
Rigol, M., and B. S. Shastry, 2008, Phys. Rev. B **77**, 161101.
Ronzheimer, J. P., M. Schreiber, S. Braun, S. S. Hodgman, S. Langer, I. P. McCulloch, F. Heidrich-Meisner, I. Bloch, and U. Schneider, 2013, Phys. Rev. Lett. **110**, 205301.
Rosch, A., 2006, Ann. Phys. (Amsterdam) **15**, 526.
Rosch, A., and N. Andrei, 2000, Phys. Rev. Lett. **85**, 1092.
Rousochatzakis, I., S. Kourtis, J. Knolle, R. Moessner, and N. B. Perkins, 2019, Phys. Rev. B **100**, 045117.
Rozhkov, A. V., and A. L. Chernyshev, 2005, Phys. Rev. Lett. **94**, 087201.
Ruelle, D., 2000, J. Stat. Phys. **98**, 57.
Ruggiero, P., P. Calabrese, B. Doyon, and J. Dubail, 2020, Phys. Rev. Lett. **124**, 140603.
Sabetta, T., and G. Misguich, 2013, Phys. Rev. B **88**, 245114.
Sachdev, S., and K. Damle, 1997, Phys. Rev. Lett. **78**, 943.
Sachdev, S., and K. Damle, 2000, J. Phys. Soc. Jpn. **69**, 2712.
Saito, K., 2003a, Europhys. Lett. **61**, 34.
Saito, K., 2003b, Phys. Rev. B **67**, 064410.
Saito, K., and S. Miyashita, 2002, J. Phys. Soc. Jpn. **71**, 2485.
Saito, K., S. Takesue, and S. Miyashita, 1996, Phys. Rev. E **54**, 2404.
Saito, K., S. Takesue, and S. Miyashita, 2000, Phys. Rev. E **61**, 2397.
Sakai, K., and A. Klümper, 2003, J. Phys. A **36**, 11617.
Sakai, K., and A. Klümper, 2005, J. Phys. Soc. Jpn. Suppl. **74**, 196.
Salomon, G., J. Koepsell, J. Vijayan, T. A. Hilker, J. Nespolo, L. Pollet, I. Bloch, and C. Gross, 2019, Nature (London) **565**, 56.
Sánchez, R. J., and V. K. Varma, 2017, Phys. Rev. B **96**, 245117.
Sánchez, R. J., V. K. Varma, and V. Oganesyan, 2018, Phys. Rev. B **98**, 054415.
Sandvik, A. W., 2010, AIP Conf. Proc. **1297**, 135.
Santos, L. F., 2004, J. Phys. A **37**, 4723.
Santos, L. F., 2008, Phys. Rev. E **78**, 031125.
Santos, L. F., 2009, J. Math. Phys. (N.Y.) **50**, 095211.
Santos, L. F., and A. Mitra, 2011, Phys. Rev. E **84**, 016206.
Scalapino, D. J., S. R. White, and S. Zhang, 1992, Phys. Rev. Lett. **68**, 2830.
Scalapino, D. J., S. R. White, and S. Zhang, 1993, Phys. Rev. B **47**, 7995.
Scheie, A., N. E. Sherman, M. Dupont, S. E. Nagler, M. B. Stone, G. E. Granroth, J. E. Moore, and D. A. Tennant, 2021, Nat. Phys. (in press), https://doi.org/10.1038/s41567-021-01191-6.
Schemmer, M., I. Bouchoule, B. Doyon, and J. Dubail, 2019, Phys. Rev. Lett. **122**, 090601.
Scherg, S., T. Kohlert, J. Herbrych, J. Stolpp, P. Bordia, U. Schneider, F. Heidrich-Meisner, I. Bloch, and M. Aidelsburger, 2018, Phys. Rev. Lett. **121**, 130402.
Schiulaz, M., and M. Müller, 2014, AIP Conf. Proc. **1610**, 11.
Schmittmann, B., and R. K. P. Zia, 1995, in *Statistical Mechanics of Driven Diffusive Systems*, edited by C. Domb, and J. L. Lebowitz, Phase Transitions and Critical Phenomena Vol. 17 (Academic Press, London).
Schneider, U., L. Hackermüller, S. Will, T. Best, I. Bloch, T. A. Costi, R. W. Helmes, D. Rasch, and A. Rosch, 2008, Science **322**, 1520.
Schneider, U., *et al.*, 2012, Nat. Phys. **8**, 213.
Schollwöck, U., 2005, Rev. Mod. Phys. **77**, 259.
Schollwöck, U., 2011, Ann. Phys. (N.Y.) **326**, 96.
Schollwöck, U., J. Richter, D. Farnell, and R. Bishop, 2004, Eds., *Integrability of Quantum Chains: Theory and Applications to the Spin-1/2 Chain*, Vol. 645 (Springer, Berlin).
Schönhammer, K., 2004, in *Strong Interactions in Low Dimensions*, edited by D. Baeriswyl and L. Degiorgi (Springer Netherlands, Dordrecht), pp. 93–136 [arXiv:cond-mat/0305035].
Schulz, M., S. R. Taylor, C. A. Hooley, and A. Scardicchio, 2018, Phys. Rev. B **98**, 180201.
Schwarz, F., M. Goldstein, A. Dorda, E. Arrigoni, A. Weichselbaum, and J. von Delft, 2016, Phys. Rev. B **94**, 155142.
Shastry, B., and B. Sutherland, 1990, Phys. Rev. Lett. **65**, 243.
Shastry, B. S., 1986, Phys. Rev. Lett. **56**, 1529.
Shastry, B. S., 2006, Phys. Rev. B **73**, 085117.
Shevchuk, O., 2012, master's thesis (University of Amsterdam).
Shimshoni, E., N. Andrei, and A. Rosch, 2003, Phys. Rev. B **68**, 104401.
Shirai, T., and T. Mori, 2020, Phys. Rev. E **101**, 042116.
Sierant, P., D. Delande, and J. Zakrzewski, 2020, Phys. Rev. Lett. **124**, 186601.
Sirker, J., 2006, Phys. Rev. B **73**, 224424.
Sirker, J., 2020, SciPost Phys. Lect. Notes **17**.
Sirker, J., and A. Klümper, 2005, Phys. Rev. B **71**, 241101(R).
Sirker, J., R. G. Pereira, and I. Affleck, 2009, Phys. Rev. Lett. **103**, 216602.
Sirker, J., R. G. Pereira, and I. Affleck, 2011, Phys. Rev. B **83**, 035115.
Sologubenko, A. V., K. Berggold, T. Lorenz, A. Rosch, E. Shimshoni, M. D. Phillips, and M. M. Turnbull, 2007, Phys. Rev. Lett. **98**, 107201.
Sologubenko, A. V., E. Felder, K. Gianno, H. R. Ott, A. Vietkine, and A. Revcolevschi, 2000, Phys. Rev. B **62**, R6108.
Sologubenko, A. V., K. Gianno, H. R. Ott, U. Ammerahl, and A. Revcolevschi, 2000, Phys. Rev. Lett. **84**, 2714.
Sologubenko, A. V., K. Gianno, H. R. Ott, A. Vietkine, and A. Revcolevschi, 2001, Phys. Rev. B **64**, 054412.
Sologubenko, A. V., T. Lorenz, J. A. Mydosh, A. Rosch, K. C. Shortsleeves, and M. M. Turnbull, 2008, Phys. Rev. Lett. **100**, 137202.
Sologubenko, A. V., T. Lorenz, H. R. Ott, and A. Freimuth, 2007, J. Low Temp. Phys. **147**, 387.
Spohn, H., 1977, Lett. Math. Phys. **2**, 33.
Spohn, H., 2012, *Large Scale Dynamics of Interacting Particles* (Springer Science+Business Media, New York).
Spohn, H., 2018, J. Math. Phys. (N.Y.) **59**, 091402.
Spohn, H., 2020a, J. Stat. Mech. 044001.
Spohn, H., 2020b, Phys. Rev. E **101**, 060103.
Srednicki, M., 1994, Phys. Rev. E **50**, 888.
Stachura, S., and G. R. Kneller, 2015, J. Chem. Phys. **143**, 191103.
Stadler, D., S. Krinner, J. Meineke, J.-P. Brantut, and T. Esslinger, 2012, Nature (London) **491**, 736.

Steiner, M., J. Villain, and C. G. Windsor, 1976, Adv. Phys. **25**, 87.
Steinigeweg, R., 2011, Phys. Rev. E **84**, 011136.
Steinigeweg, R., and W. Brenig, 2011, Phys. Rev. Lett. **107**, 250602.
Steinigeweg, R., and W. Brenig, 2016, Phys. Rev. B **93**, 214425.
Steinigeweg, R., H.-P. Breuer, and J. Gemmer, 2007, Phys. Rev. Lett. **99**, 150601.
Steinigeweg, R., and J. Gemmer, 2009, Phys. Rev. B **80**, 184402.
Steinigeweg, R., J. Gemmer, and W. Brenig, 2014, Phys. Rev. Lett. **112**, 120601.
Steinigeweg, R., J. Gemmer, and W. Brenig, 2015, Phys. Rev. B **91**, 104404.
Steinigeweg, R., J. Gemmer, and M. Michel, 2006, Europhys. Lett. **75**, 406.
Steinigeweg, R., F. Heidrich-Meisner, J. Gemmer, K. Michielsen, and H. De Raedt, 2014, Phys. Rev. B **90**, 094417.
Steinigeweg, R., J. Herbrych, F. Pollmann, and W. Brenig, 2016, Phys. Rev. B **94**, 180401.
Steinigeweg, R., J. Herbrych, and P. Prelovšek, 2013, Phys. Rev. E **87**, 012118.
Steinigeweg, R., J. Herbrych, P. Prelovšek, and M. Mierzejewski, 2012, Phys. Rev. B **85**, 214409.
Steinigeweg, R., J. Herbrych, X. Zotos, and W. Brenig, 2016, Phys. Rev. Lett. **116**, 017202.
Steinigeweg, R., F. Jin, H. De Raedt, K. Michielsen, and J. Gemmer, 2017, Phys. Rev. E **96**, 020105.
Steinigeweg, R., F. Jin, D. Schmidtke, H. De Raedt, K. Michielsen, and J. Gemmer, 2017, Phys. Rev. B **95**, 035155.
Steinigeweg, R., A. Khodja, H. Niemeyer, C. Gogolin, and J. Gemmer, 2014, Phys. Rev. Lett. **112**, 130403.
Steinigeweg, R., S. Langer, F. Heidrich-Meisner, I. P. McCulloch, and W. Brenig, 2011, Phys. Rev. Lett. **106**, 160602.
Steinigeweg, R., M. Ogiewa, and J. Gemmer, 2009, Europhys. Lett. **87**, 10002.
Steinigeweg, R., and T. Prosen, 2013, Phys. Rev. E **87**, 050103.
Steinigeweg, R., and R. Schnalle, 2010, Phys. Rev. E **82**, 040103.
Steinigeweg, R., H. Wichterich, and J. Gemmer, 2009, Europhys. Lett. **88**, 10004.
Stolpp, J., J. Herbrych, F. Dorfner, E. Dagotto, and F. Heidrich-Meisner, 2020, Phys. Rev. B **101**, 035134.
Stolpp, J., S.-S. Zhang, F. Heidrich-Meisner, and C. D. Batista, 2019, Phys. Rev. B **99**, 134413.
Stone, M., and P. Goldbart, 2009, *Mathematics for Physics* (Cambridge University Press, Cambridge, England).
Stoudenmire, E., and S. R. White, 2010, New J. Phys. **12**, 055026.
Sugiura, S., and A. Shimizu, 2012, Phys. Rev. Lett. **108**, 240401.
Sugiura, S., and A. Shimizu, 2013, Phys. Rev. Lett. **111**, 010401.
Šuntajs, J., J. Bonča, T. Prosen, and L. Vidmar, 2020, Phys. Rev. E **102**, 062144.
Suzuki, M., 1971, Physica (Amsterdam) **51**, 277.
Suzuki, M., and M. Inoue, 1987, Prog. Theor. Phys. **78**, 787.
Syljuåsen, O. F., and A. W. Sandvik, 2002, Phys. Rev. E **66**, 046701.
Szasz, A., R. Ilan, and J. E. Moore, 2017, Phys. Rev. B **95**, 085122.
Tai, M. E., A. Lukin, M. Rispoli, R. Schittko, T. Menke, D. Borgnia, P. M. Preiss, F. Grusdt, A. M. Kaufman, and M. Greiner, 2017, Nature (London) **546**, 519.
Takahashi, M., 1971, Prog. Theor. Phys. **46**, 401.
Takahashi, M., 1973, Prog. Theor. Phys. **50**, 1519.
Takahashi, M., 1999, *Thermodynamics of One-Dimensional Solvable Models* (Cambridge University Press, Cambridge, England).
Tal-Ezer, H., and R. Kosloff, 1984, J. Chem. Phys. **81**, 3967.
Tang, B., E. Khatami, and M. Rigol, 2013, Comput. Phys. Commun. **184**, 557.
Tarruell, L., and L. Sanchez-Palencia, 2018, C.R. Phys. **19**, 365.
Thurber, K., A. Hunt, T. Imai, and F. Chou, 2001, Phys. Rev. Lett. **87**, 247202.
Tiegel, A. C., S. R. Manmana, T. Pruschke, and A. Honecker, 2014, Phys. Rev. B **90**, 060406.
Torres-Herrera, E. J., and L. F. Santos, 2014, Phys. Rev. E **89**, 062110.
Toskovic, R., R. van den Berg, A. Spinelli, I. S. Eliens, B. van den Toorn, B. Bryant, J.-S. Caux, and A. F. Otte, 2016, Nat. Phys. **12**, 656.
Trotzky, S., Y.-A. Chen, A. Flesch, I. P. McCulloch, U. Schollwöck, J. Eisert, and I. Bloch, 2012, Nat. Phys. **8**, 325.
Tsvelick, A., and P. Wiegmann, 1983, Adv. Phys. **32**, 453.
Turner, C. J., A. A. Michailidis, D. A. Abanin, M. Serbyn, and Z. Papić, 2018, Nat. Phys. **14**, 745.
Urichuk, A., Y. Oez, A. Klümper, and J. Sirker, 2019, SciPost Phys. **6**, 5.
Vanicat, M., L. Zadnik, and T. Prosen, 2018, Phys. Rev. Lett. **121**, 030606.
Varma, V. K., C. de Mulatier, and M. Žnidarič, 2017, Phys. Rev. E **96**, 032130.
Varma, V. K., and M. Žnidarič, 2019, Phys. Rev. B **100**, 085105.
Vasseur, R., C. Karrasch, and J. E. Moore, 2015, Phys. Rev. Lett. **115**, 267201.
Vasseur, R., and J. E. Moore, 2016, J. Stat. Mech. 064010.
Verstraete, F., J. J. García-Ripoll, and J. I. Cirac, 2004, Phys. Rev. Lett. **93**, 207204.
Vidal, G., 2004, Phys. Rev. Lett. **93**, 040502.
Vidmar, L., D. Iyer, and M. Rigol, 2017, Phys. Rev. X **7**, 021012.
Vidmar, L., S. Langer, I. P. McCulloch, U. Schneider, U. Schollwöck, and F. Heidrich-Meisner, 2013, Phys. Rev. B **88**, 235117.
Vidmar, L., and M. Rigol, 2016, J. Stat. Mech. 064007.
Vidmar, L., J. P. Ronzheimer, M. Schreiber, S. Braun, S. S. Hodgman, S. Langer, F. Heidrich-Meisner, I. Bloch, and U. Schneider, 2015, Phys. Rev. Lett. **115**, 175301.
Vijayan, J., P. Sompet, G. Salomon, J. Koepsell, S. Hirthe, A. Bohrdt, F. Grusdt, I. Bloch, and C. Gross, 2020, Science **367**, 186.
Viti, J., J.-M. Stéphan, J. Dubail, and M. Haque, 2016, Europhys. Lett. **115**, 40011.
Volokitin, V., I. Vakulchyk, E. Kozinov, A. Liniov, I. Meyerov, M. Ivanchenko, T. Laptyeva, and S. Denisov, 2019, J. Phys. Conf. Ser. **1392**, 012061.
Vu, D.-L., and T. Yoshimura, 2019, SciPost Phys. **6**, 23.
Weimer, H., A. Kshetrimayum, and R. Orus, 2021, Rev. Mod. Phys. **93**, 015008.
Weiner, F., P. Schmitteckert, S. Bera, and F. Evers, 2020, Phys. Rev. B **101**, 045115.
Weiße, A., G. Wellein, A. Alvermann, and H. Fehske, 2006, Rev. Mod. Phys. **78**, 275.
Werner, M. A., C. Moca, O. Legeza, M. Kormos, and G. Zaránd, 2019, Phys. Rev. B **100**, 035401.
White, S., 1992, Phys. Rev. Lett. **69**, 2863.
White, S., 2009, Phys. Rev. Lett. **102**, 190601.
White, S. R., and A. E. Feiguin, 2004, Phys. Rev. Lett. **93**, 076401.
Wichterich, H., M. J. Henrich, H.-P. Breuer, J. Gemmer, and M. Michel, 2007, Phys. Rev. E **76**, 031115.
Wietek, A., P. Corboz, S. Wessel, B. Normand, F. Mila, and A. Honecker, 2019, Phys. Rev. Research **1**, 033038.
Wu, J., and M. Berciu, 2010, Europhys. Lett. **92**, 30003.
Wurtz, J., and A. Polkovnikov, 2020, Phys. Rev. E **101**, 052120.
Xia, L., L. A. Zundel, J. Carrasquilla, A. Reinhard, J. M. Wilson, M. Rigol, and D. S. Weiss, 2015, Nat. Phys. **11**, 316.
Xiao, F., J. S. Möller, T. Lancaster, R. C. Williams, F. L. Pratt, S. J. Blundell, D. Ceresoli, A. M. Barton, and J. L. Manson, 2015, Phys. Rev. B **91**, 144417.

Xu, X., J. Thingna, C. Guo, and D. Poletti, 2019, Phys. Rev. A **99**, 012106.
Yamaji, Y., T. Suzuki, and M. Kawamura, 2018, arXiv:1802.02854.
Yan, Y., F. Jiang, and H. Zhao, 2015, Eur. Phys. J. B **88**, 11.
Yang, C., and C. Yang, 1969, J. Math. Phys. (N.Y.) **10**, 1115.
Yang, C. N., 1967, Phys. Rev. Lett. **19**, 1312.
Yao, N. Y., C. R. Laumann, J. I. Cirac, M. D. Lukin, and J. E. Moore, 2016, Phys. Rev. Lett. **117**, 240601.
Ye, B., F. Machado, C. D. White, R. S. K. Mong, and N. Y. Yao, 2020, Phys. Rev. Lett. **125**, 030601.
Yoshimura, T., and H. Spohn, 2020, SciPost Phys. **9**, 040.
Zamolodchikov, A. B., and V. A. Fateev, 1980, Sov. J. Nucl. Phys. **32**, 298.
Zemljič, M. M., and P. Prelovšek, 2005, Phys. Rev. B **71**, 085110.
Zhang, C., E. Jeckelmann, and S. R. White, 1998, Phys. Rev. Lett. **80**, 2661.
Žnidarič, M., 2010a, New J. Phys. **12**, 043001.
Žnidarič, M., 2010b, J. Phys. A **43**, 415004.
Žnidarič, M., 2011a, Phys. Rev. Lett. **106**, 220601.
Žnidarič, M., 2011b, J. Stat. Mech. P12008.
Žnidarič, M., 2013a, Phys. Rev. Lett. **110**, 070602.
Žnidarič, M., 2013b, Phys. Rev. B **88**, 205135.
Žnidarič, M., 2015, Phys. Rev. E **92**, 042143.
Žnidarič, M., 2019, Phys. Rev. B **99**, 035143.
Žnidarič, M., and M. Ljubotina, 2018, Proc. Natl. Acad. Sci. U.S.A. **115**, 4595.
Žnidarič, M., T. Prosen, G. Benenti, G. Casati, and D. Rossini, 2010, Phys. Rev. E **81**, 051135.
Žnidarič, M., A. Scardicchio, and V. K. Varma, 2016, Phys. Rev. Lett. **117**, 040601.
Žnidarič, M., B. Žunkovič, and T. Prosen, 2011, Phys. Rev. E **84**, 051115.
Zotos, X., 1999, Phys. Rev. Lett. **82**, 1764.
Zotos, X., 2002, J. Low Temp. Phys. **126**, 1185.
Zotos, X., 2004, Phys. Rev. Lett. **92**, 067202.
Zotos, X., 2005, J. Phys. Soc. Jpn. Suppl. **74**, 173.
Zotos, X., 2017, J. Stat. Mech. 103101.
Zotos, X., F. Naef, and P. Prelovšek, 1997, Phys. Rev. B **55**, 11029.
Zotos, X., and P. Prelovšek, 1996, Phys. Rev. B **53**, 983.
Zotos, X., and P. Prelovšek, 2004, in *Strong Interactions in Low Dimensions* (Kluwer Academic Publishers, Dordrecht), Chap. 11 [arXiv:cond-mat/0304630].
Zwanzig, R., 1965, Annu. Rev. Phys. Chem. **16**, 67.
Zwolak, M., and G. Vidal, 2004, Phys. Rev. Lett. **93**, 207205.